OPEN ACCESS

University of BRISTOL

This electronic thesis or dissertation has been downloaded from Explore Bristol Research, http://research-information.bristol.ac.uk

Author:
Hawley, Bethan R

Title:
Identification of an Epithelial Cell Line for Two- and Three- Dimensional Studies of Intestinal Ion Transport

General rights
Access to the thesis is subject to the Creative Commons Attribution - NonCommercial-No Derivatives 4.0 International Public License. A copy of this may be found at https://creativecommons.org/licenses/by-nc-nd/4.0/legalcode This license sets out your rights and the restrictions that apply to your access to the thesis so it is important you read this before proceeding.

Take down policy
Some pages of this thesis may have been removed for copyright restrictions prior to having it been deposited in Explore Bristol Research. However, if you have discovered material within the thesis that you consider to be unlawful e.g. breaches of copyright (either yours or that of a third party) or any other law, including but not limited to those relating to patent, trademark, confidentiality, data protection, obscenity, defamation, libel, then please contact collections-metadata@bristol.ac.uk and include the following information in your message:

• Your contact details
• Bibliographic details for the item, including a URL
• An outline nature of the complaint

Your claim will be investigated and, where appropriate, the item in question will be removed from public view as soon as possible.

Identification of an Epithelial Cell Line for Two- and Three-Dimensional Studies of Intestinal Ion Transport

Bethan R Hawley

A dissertation submitted to the University of Bristol in accordance with the requirements for the award of the degree of Doctor of Philosophy in the Faculty of Life Sciences, School of Physiology, Pharmacology and Neuroscience.

September 2021

Word Count: 46,545

Abstract

Cystic fibrosis (CF) is an inherited disease caused by mutations in the epithelial anion channel cystic fibrosis transmembrane conductance regulator (CFTR). Many individuals with CF experience gastrointestinal tract complications, caused by impaired salt and water secretion across the intestinal epithelium. Intestinal organoids provide a powerful tool to investigate CFTR dysfunction in CF, aiding the identification of small molecule CFTR modulators for personalised medicine. The work in this thesis sought to identify an intestinal epithelial cell line suitable for studies of CFTR-mediated ion transport in the intestine, as an alternative to primary organoid models. The cell line should grow both as a 2D epithelium for electrical measurements of ion transport with the Ussing chamber technique, and as 3D spheroids to optically measure lumen expansion driven by fluid secretion.

Studies using the human colonic cell line LIM1863, which expresses CFTR and forms spheroids that swell in response to cAMP-mediated salt and water secretion, revealed that this cell line was unable to form polarised epithelia with a transepithelial resistance. Subsequently a panel of 15 human colorectal adenocarcinoma cell lines was screened to identify a cell line suitable for Ussing chamber and spheroid swelling studies.

Immunoblotting revealed CFTR expression in 7 of the 15 cell lines screened. When the CFTR-expressing cell lines were seeded onto permeable filter supports, only HCA7 cells developed a transepithelial resistance. To investigate transepithelial ion transport by HCA7 cells, Ussing chamber experiments were performed. Forskolin stimulated a small increase in current that was potentiated by genistein and inhibited by $CFTR_{inh}$-172. Complementary to these studies, when HCA7 cells were grown in Matrigel they formed spheroids with a lumen; lumen expansion was stimulated by forskolin and reduced by $CFTR_{inh}$-172. Thus, HCA7 cells are a useful model of CFTR-mediated ion transport, which might be used to identify new modulators of intestinal ion transport.

Acknowledgements

The work carried out in this thesis was performed in the School of Physiology, Pharmacology and Neuroscience, University of Bristol between September 2017 and September 2021. I would like to thank the Cystic Fibrosis (CF) Trust for providing me with the funding and opportunity to complete this research, and for the ongoing work the CF Trust does to support, and campaign on behalf of, the CF community. I would also like to thank members of the CF Trust-funded Strategic Research Centre, led by Professor Soraya Shirazi-Beechey, to which my research contributes, for their collaboration and support. In particular, I would like to thank Professor Hugo de Jonge and members of his laboratory for supplying primary intestinal organoids, in addition to much expertise and advice. I would like to thank the staff of the Wolfson Bioimaging Facility, University of Bristol, for their assistance with bioimaging studies, as well as the development of the image analysis programmes used in this thesis.

I would like to give particular thanks to my PhD supervisor, Professor David Sheppard, firstly for affording me the opportunity to complete this PhD thesis in his laboratory, and secondly for the support, motivation, and encouragement he has shown me throughout the time I have spent working in his lab. I have learnt so much from David, not only relating to the fields of electrophysiology, epithelial ion transport, and cystic fibrosis, but also the importance of maintaining enthusiasm and a positive outlook, attention to detail, and also a sense of perspective.

Thank you to the members of my progression panel, Professor Ann Williams, and Professor Ashley Toye for their guidance, encouragement and for letting me use their labs! Particular thanks to Ann for access to her cell lines, for moral support, and for keeping me going when PhD joy was lacking. I would also like to thank Tracey Collard, not only for accommodating me so kindly into the lab and her busy schedule, but for training me, keeping me organised, and sharing her wealth of experience and knowledge.

A huge thank you to the members of the Sheppard laboratory, past and present! You have made my PhD such a memorable experience! I would particularly like to thank Dr Hongyu Li, Dr Caroline Wang, Dr Sam Bose, Bart Harvey, and Demi Ng, who became good friends over the course of my PhD. I hope we stay in touch, and for those that are still members of the lab, I will be popping in to say Hi frequently.

Lastly, but by no means least, I would like to thank my friends and family. Thank you, Charlie, for being such a good friend over the many years we've known one another, for not minding when lab work made me late for our plans, and for putting up with my disappearance off the face of the earth during the last few months of writing up. Thank you to my family for their support, encouragement, and frequent reminders to write my thesis. Finally, thank you to my partner, who has provided endless emotional support and biscuits!

Thank you.

COVID-19 Statement

As outlined in the 'Future Work' sections of Chapters 4 and 5, COVID-19 restrictions disrupted planned research that was expected to contribute to the work presented in this thesis. However, the most significant disruption caused by COVID-19 was the cancellation of a 3-month research visit to the laboratory of Prof. H. R. de Jonge (Erasmus Medical Centre, Rotterdam). Prof. de Jonge's laboratory specialises in the culture of cystic fibrosis (CF) and non-CF primary organoids from rectal and small intestinal biopsies and are leading experts in the use of said organoids in studies of intestinal ion transport, including 3D forskolin-induced swelling (FIS) assays, 2D Ussing chamber studies, transepithelial pH studies, and epithelial imaging techniques.

It was anticipated that during my visit to Prof. de Jonge's laboratory I would learn the protocol for stem cell isolation from intestinal tissue biopsies, the technique for culturing intestinal stem cells as organoids, and the protocol for the ongoing maintenance of intestinal organoids in culture. I would then perform FIS assays using non-CF organoids and organoids homozygous for the most common CF mutation, F508del, allowing me to quantify the loss of cystic fibrosis transmembrane conductance regulator (CFTR)-mediated fluid secretion in these CF organoids. Initially, FIS assays would be performed using rectal organoids before moving onto organoids derived from rare ileal biopsies.

Once initial characterisation of FIS was performed in both rectal and ileal, CF and non-CF organoids, I would investigate the effects of Na^+/H^+ exchanger 3 (NHE3) inhibition by the clinically-approved drugs tenapanor, lubiprostone and linaclotide on intestinal fluid secretion. Of note, it would have been of special interest to determine whether inhibition of NHE3 in CFTR-F508del organoids, alongside treatment with the clinically-approved CFTR-targeting drugs lumacaftor (VX-809) or lumacaftor-ivacaftor (VX-770) combination therapy (Orkambi) restored FIS in these organoids to levels observed in organoids containing wild-type (wt) CFTR. These studies would demonstrate whether NHE3 inhibition has therapeutic potential as a CFTR mutation-independent treatment of intestinal disease in CF.

To complement FIS assays, I would culture rectal and ileal epithelia for 2D Ussing chamber studies. Performing Ussing chamber studies would allow me to characterise forskolin (FSK)-stimulated CFTR-mediated short-circuit current (I_{sc}) by epithelia derived from CFTR-wt and homozygous CFTR-F508del rectal and ileal biopsies. CFTR-mediated I_{sc} by these epithelia would be measured in response to linaclotide and

lubiprostone, both capable of stimulating cAMP/cGMP-mediated I_{sc}. Tenepanor, linaclotide and lubiprostone would be used alongside FSK, FSK + VX-770, and FSK + VX-809 + VX-770 to evaluate how these drug combinations effect, and potentially, restore I_{sc} in CFTR-F508del organoids, with CFTR-wt organoids as a reference.

Measures to circumvent the disruption to planned work caused by COVID-19 restrictions were taken. It was arranged for non-CF and homozygous CFTR-F508del organoids derived from both rectal and ileal biopsies to be shipped to Prof. Sheppard's laboratory from Prof. de Jonge's laboratory. Unfortunately, attempts to culture these organoids at the University of Bristol were unsuccessful with the failed passage of organoids and gradual decline of cultures. One likely reason for the difficulties experienced with the translation of the organoid culture method to the University of Bristol was the necessity to replace conditioned media, containing secreted noggin, r-spondin, and Wnt3A, with commercial growth factors. This substitution was necessary as a result of the limited resources available to produce and store the conditioned media required for organoid culture. Whilst the de Jonge laboratory kindly arranged for the shipment of small amounts of conditioned media, it was not feasible for the quantity of conditioned media required for continual organoid culture to be sourced from Prof. de Jonge.

The work I would have performed during my visit to Prof. de Jonge's laboratory would have formed an additional results chapter to this thesis. The work described above would also have allowed me to translate the techniques and skills I had developed using the LIM1863 and HCA7 cell line models to human derived CF and non-CF organoids. In addition, the work with human primary organoids would have provided an excellent reference of intestinal fluid secretion to compare with the HCA7 cell line model of intestinal fluid secretion. Finally, if the work in Prof. de Jonge's laboratory was successful it was hoped that the ensuing data alongside data gathered from other collaborative laboratories would have guided clinical trials of drugs that inhibit NHE3 in individuals with CF gastrointestinal disease.

Author's declaration

I declare that the work in this dissertation was carried out in accordance with the requirements of the University's Regulations and Code of Practice for Research Degree Programmes and that it has not been submitted for any other academic award. Except where indicated by specific reference in the text, the work is the candidate's own work. Work done in collaboration with, or with the assistance of, others, is indicated as such. Any views expressed in the dissertation are those of the author.

SIGNED: Bethan Hawley DATE: 10.11.2022

Table of Contents

List of Figures

List of Tables

List of Abbreviations

2D	Two dimensional
3D	Three dimensional
AM	Acetoxymethyl
APS	Ammonium persulphate
ASL	Airway surface liquid
ATP	Adenosine triphosphate
cAMP	Cyclic adenosine monophosphate
cDNA	Complementary deoxyribose nucleic acid
CaCC	Calcium-activated chloride channel
CF	Cystic fibrosis
CFTR	Cystic fibrosis transmembrane conductance regulator
cGMP	Cyclic guanosine monophosphate
ClCa1	Calcium-dependent chloride channel 1
CRISPR	Clustered regularly interspaced short palindromic repeats
DMEM	Dulbecco's Modified Eagle's Medium
DMSO	Dimethyl sulfoxide
dNTP	deoxyribonucleotide triphosphate
EDTA	Ethylenediaminetetraacetic acid
ENaC	Epithelial sodium channel
EP1	Prostaglandin E_1 receptor
EP4	Prostaglandin E_4 receptor
ER	Endoplasmic reticulum
FEV_1	Forced expiratory volume in 1 second
FIS	Forskolin-induced swelling
FSC-A	Forward scatter - area
FSC-H	Forward scatter - height
FSK	Forskolin
GCC	Guanylyl cyclase-C
GI	Gastrointestinal
HAC	Human artificial chromosome
HEPES	4-(2-hydroxyethyl)-1-piperazineethanesulfonic acid
I-172	$CFTR_{inh}$-172
I_{sc}	Short-circuit current
kDa	Kilodalton

LB	Luria broth
Lgr5+	Leucine-rich repeat-containing G-protein coupled receptor 5
MCC	Mucociliary clearance
MIA	Modular image analysis
mRNA	messenger ribonucleic acid
NHE	Sodium/hydrogen exchanger
NKCC1	Sodium-potassium-chloride cotransporter 1
PBS	Phosphate buffered saline
PEG	Polyethylene glycol
PERT	Pancreatic enzyme replacement therapy
PI	Propidium iodide
PI	Pancreatic insufficiency
PI-A	Propidium iodide-area
P_o	Open probability
PS	Pancreatic sufficiency
PVDF	Polyvinylidene fluoride
Q-RT-PCR	Quantitative real-time polymerase chain reaction
RNA	Ribonucleic acid
RPMI	Roswell Park Memorial Institute
R_t	transepithelial resistance
RT-PCR	Real-time polymerase chain reaction
S.E.M.	Standard error of the mean
SDS-PAGE	Sodium dodecyl-sulfate polyacrylamide gel electrophoresis
SIBO	Small intestinal bacterial overgrowth
siRNA	Small interfering ribonucleic acid
S-MEM	Spinner-modification minimum essential medium
SSC-H	Side scatter - height
TBP	TATA- binding protein
TMED	N,N,N,N-tetramethylene-diamine
UTP	Uridine-5’-triphosphate
VSORC	Volume-sensitive outwardly rectifying Cl^- conductance
wt	Wild-type

Chapter 1. Introduction

1.1. Cystic Fibrosis

Cystic fibrosis (CF) is an autosomal recessive disease caused by mutations in the *CFTR* gene, which encodes a cAMP-regulated anion channel known as the cystic fibrosis transmembrane conductance regulator (CFTR) (Riordan *et al.*, 1989). CFTR mediates the secretion of chloride (Cl^-) and bicarbonate (HCO_3^-) across the apical membrane of secretory epithelium, playing an important role in salt and fluid homeostasis (Frizzell and Hanrahan, 2012; Ratjen *et al.*, 2015). In the UK alone, CF is estimated to affect 10,500 people, with a prevalence at birth of 1:2,500 (CF Trust UK). Despite significant advances in CF therapy, individuals with CF have a limited lifespan [a median survival age of 47 years for individuals born with CF between 2014-2018 (Charman *et al.*, 2018)]. CF is a multi-organ disease with lung disease being the most severe consequence, however some individuals with CF also experience gastrointestinal (GI) symptoms (Sabharwal, 2016), with a reported prevalence in adults with CF of 65% (Hayee *et al.*, 2019). It is anticipated that with better understanding of CFTR function and the mechanisms regulating salt and fluid transport in the intestines, new therapeutic strategies will become available to alleviate GI disease in individuals with CF.

1.2. The cystic fibrosis transmembrane conductance regulator

1.2.1. CFTR structure-function

The *CFTR* gene, mutations in which cause CF, was identified in 1989 (Riordan *et al.*, 1989; Rommens *et al.*, 1989), after previous observations that cAMP-induced chloride ion (Cl^-) conductance was reduced across the apical membrane of certain epithelial cells in CF (Widdicombe, Welsh and Finkbeiner, 1985).

The CFTR protein is a member of the ATP-binding cassette (ABC) transporter family of proteins. Unique among ABC transporters, CFTR is an ion channel mediating chloride (Cl^-) and bicarbonate (HCO_3^-) flow across the apical membrane of secretory epithelia (Riordan, 2008; Borowitz, 2015). Like other members of the ABC superfamily, CFTR demonstrates structural modularity, namely two repeated homologous units each containing a membrane-spanning domain (MSD), and a cytoplasmic nucleotide-binding domain (NBD) (Riordan *et al.*, 1989; Liu *et al.*, 2017). Unique to CFTR however, is the presence of a 241 amino acid regulatory domain (RD) located intracellularly and linking the two MSD-NBD motifs between NBD1 and MSD2 (Riordan *et al.*, 1989; Mornon, Lehn and Callebaut, 2008). Arrangement of the protein within the cellular membrane is such

that the two MSDs form a membrane pore which is closed during the resting state (Hwang and Sheppard, 2009). Conformational change from an inward-facing closed channel to an outward-facing open channel is driven by cycles of ATP binding and hydrolysis at ATP-binding sites located on the NBDs. In the inward-facing closed state the dephosphorylated RD is wedged between the two NBDs, preventing NBD dimerization and so phosphorylation of the RD and subsequent exposure of the ATP-binding domains of the NBDs is a prerequisite for channel opening (Chong *et al.*, 2013; Zhang and Chen, 2016; Liu *et al.*, 2017).

Like many ABC proteins, each MSD of CFTR consists of 6 α-helical transmembrane segments (TMs) which form an anion selective channel pore (Hwang *et al.*, 2018). As is typical of ABC transporters the MSDs are continuous helices, with the exception of TM8 which is formed of two α-helices separated by an unstructured region (Zhang, Liu and Chen, 2018). The channel pore itself resembles an hourglass, asymmetric in shape, with a larger intracellular vestibule and smaller extracellular vestibule on either side of a transmembrane pore constriction (Sheppard and Welsh, 1999). Positioned towards the extracellular side of the plasma membrane, the pore constriction not only acts a selectivity filter, determining which ions can pass through the channel, but it is within this constriction that the single CFTR channel gate is located (Liu *et al.*, 2017).

Early structure-function studies indicated that TMs contribution towards lining the channel pore is not equally divided between MSD1 and 2, highlighting the important role TM6 plays in determining CFTR permeation properties (McDonough *et al.*, 1994; Linsdell, Tabcharani and Hanrahan, 1997). The atomic-resolution structure of human CFTR in both dephosphorylated and phosphorylated (Liu *et al.*, 2017, 2019), as well as drug bound (Zhang, Liu and Chen, 2018) forms were solved using cryo-electron-microscopy, and added further insight into the contribution of the TMs to the CFTR channel pore. These structural and functional studies propose that the channel pore is composed of TM1, 3, 4, 5, 6, 9, 10, 11 and 12 with amino acid residues belonging to TMs 6 and 12 contributing greatly to the ion permeability of the pore (Hwang *et al.*, 2018). Based on these data it can be reasoned that MSD1 has a dominant role in defining the channel pore properties of the CFTR protein.

These studies also gave insight into the amino acid residues that line both the channel pore, and the intracellular and extracellular vestibules. Unlike many other membrane proteins, the TMs of CFTR and their intracellular loops (ICLs) are rich in positively

charged arginine and lysine residues (Linsdell, 2017; Al Salmani *et al.*, 2020). The proposed role of these positive residues is to attract and guide anions such as Cl^- toward the channel pore and subsequently maximise the conductance of the channel itself (Liu *et al.*, 2017). Support for this role comes from multiple studies in which arginine and lysine residues lining the pore and ICLs were neutralised, resulting in a reduction of channel Cl^- conductance (Smith *et al.*, 2001; St. Aubin and Linsdell, 2006; Zhou *et al.*, 2010; El Hiani and Linsdell, 2015). Of particular importance in determining pore conductance properties are the TMs that form the pore constriction, also described as the "pore gate". Functional evidence highlight TM1, 6 and 11 as those that line the narrowest region of the pore, with residues F337, T338 and S341 of TM6 having the largest influence on pore properties (Linsdell, Zheng and Hanrahan, 1998; Linsdell, Evagelidis and Hanrahan, 2000; Beck *et al.*, 2008; Bai, Li and Hwang, 2010; Gao, Bai and Hwang, 2013; W. Wang *et al.*, 2014).

Interestingly, the intracellular entry point for anions entering the pore is located to the side of the protein, not directly below the central axis of the channel (a region likely obstructed by NBD dimerization) (Hwang *et al.*, 2018). ICLs form lateral funnels, guiding anions towards the channel pore. A major lateral anion entry port is located between TM4 and 6, whereas a secondary entry port is located between TM11 and 12 (Corradi, Vergani and Tieleman, 2015; Mornon *et al.*, 2015; El Hiani, Negoda and Linsdell, 2016).

CFTR's NBDs are arranged in a head-to-tail dimer with ATP-binding sites located on the dimer interface (Lewis *et al.*, 2004). They are in many ways typical of all ABC proteins and possess characteristic structural architecture: an ATP-binding core subdomain forming the head region, and an ABC α- and β- subdomain forming the NBD tail region (Lewis *et al.*, 2004). Located within the ATP-binding head region are a) an A loop, containing specific amino acid residues which interact with ATP; b) the Walker A and B motifs; and c) Q-loop and H-loop switch regions (Hwang *et al.*, 2018). The tail region of the NBD contains conserved amino acid sequences, one unique to NBD1 (LSGGQ) and another unique to NBD2 (LSHGH) (Lewis *et al.*, 2004; Hwang *et al.*, 2018).

ATP binding to the NBDs occurs between the Walker A/B motif of one NBD and the LSGGQ/LSHGH motifs within the tail region of the other NBD (Hwang and Sheppard, 2009). Whilst both ATP-binding sites within the NBDs bind ATP, only the binding site formed by the Walker A/B motif in NBD2 and LSGGQ sequence in NBD1 is enzymatically active (ATP-binding site 2), hydrolysing ATP rapidly after binding. The other ATP-binding

site (ATP-binding site 1) is enzymatically redundant (Hwang *et al.*, 1994, 2018; Callebaut *et al.*, 2004).

Upon ATP binding, NBDs dimerization results in an inward-facing to outward-facing conformational change in the CFTR channel and opening of the pore gate (Hwang *et al.*, 2018). MSD-NBD interfaces (interactions between the NBDs and MSDs) facilitate the translation of NBD dimerization to conformational changes in the channel pore. These interfaces are formed from the intracellular helices of the MSDs, extensions of which protrude into the cytoplasm, forming long ICLs. ICL2 (joining TM4 and 5), and ICL4 (joining TM10 and 11) dock tightly into clefts in NBD2 and NBD1, respectively (Mornon, Lehn and Callebaut, 2008; Serohijos *et al.*, 2008; Hwang *et al.*, 2018). The MSD-NBD interfaces at ICL2 and 4 behave like ball and socket joints, allowing for a pivoting motion to occur during inward-facing to outward-facing conformation change (Oldham, Davidson and Chen, 2008).

As stated previously, phosphorylation of the CFTR RD is a prerequisite for ATP-binding and CFTR opening. The RD located between NBD1 and MSD2, is disordered, having no stable secondary or tertiary structure (Ostedgaard *et al.*, 2000; Hwang *et al.*, 2018). In its dephosphorylated form, RD orientation is such that it is wedged between TMs 9, 10 and 12, extending into the cytoplasm between NBD1 and 2, preventing NBD dimerization (Zhang, Liu and Chen, 2018). Upon phosphorylation, the RD changes conformation moving from between the NBDs allowing NBD dimerization (Zhang, Liu and Chen, 2018). Multiple phosphorylation sites have been identified within the RD, predominantly serine residues requiring cAMP-dependent protein kinase A (PKA) phosphorylation. However, phosphorylation sites for kinases such as protein kinase C (PKC) and cGMP-dependent protein kinase (cGK) type II are also located here (Riordan *et al.*, 1989; Vaandrager *et al.*, 1997; Hegedus *et al.*, 2009; Chong *et al.*, 2013). Figure 1-1 shows a schematic of CFTR structure, including the proposed position of the channel pore.

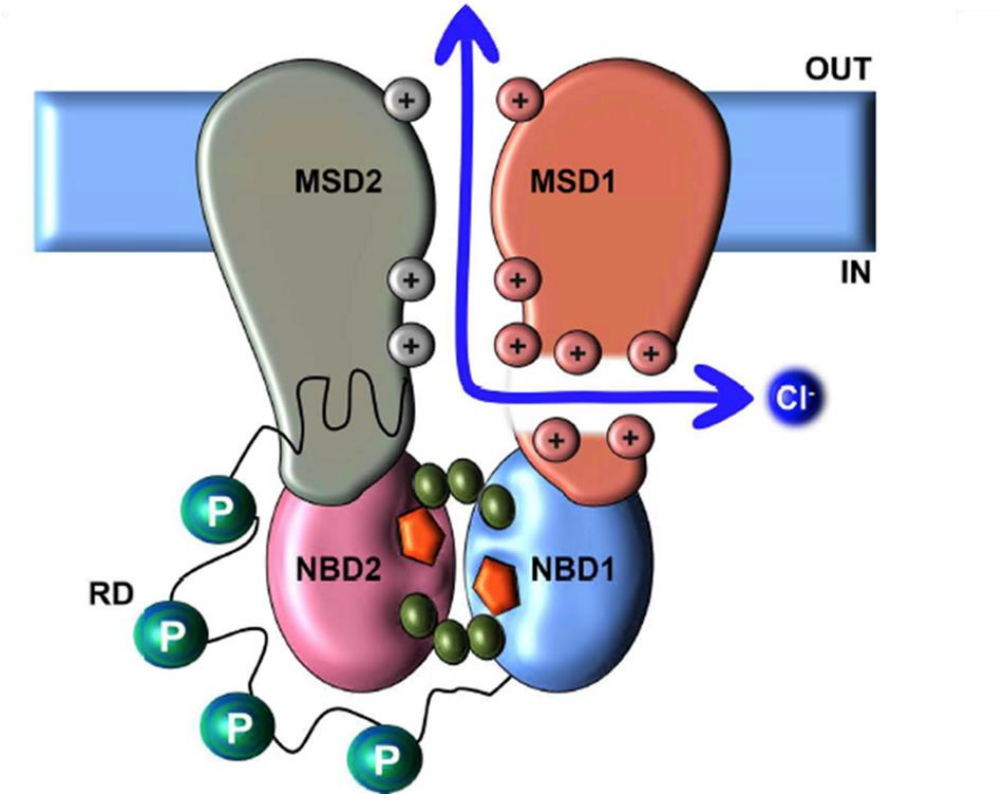

Figure 1-1: A schematic representation of the cystic fibrosis transmembrane conductance regulator channel.

The ABC transporter CFTR is a modular protein composed of two membrane-spanning domains (MSD1 and 2), two cytoplasmic nucleotide-binding domains (NBD 1 and 2), and an intracellular regulatory domain (RD). PKA-dependent phosphorylation of the RD along with ATP (represented by three green circles attached to an orange pentagon) binding to the NBDs mediates channel pore gating. Anions enter the channel pore intracellularly through a lateral opening beneath MSD1, exiting from the extracellular vestibule. The channel pore itself is lined with positively charged lysine and arginine residues facilitating the transport of anions across the membrane. Figure reproduced with permission from Al Salmani et al. (2020).

1.2.2. *CFTR* mutations

To date, over 2,000 variants have been identified within the *CFTR* gene, with missense mutations accounting for the highest frequency of mutation type (39% of mutations). Frameshift, splicing, and nonsense mutations also occur as do sequence variations (http://www.genet.sickkids.on.ca). Mutations occur throughout the CFTR protein and typically reduce protein number and/or protein function (Ratjen *et al.*, 2015). Whilst not all *CFTR* mutations cause CF, for those that do, establishing a correlation between

genotype and phenotype is not straight forward (Bombieri *et al.*, 2011; Johns *et al.*, 2013; Cutting, 2015). Variability in disease severity amongst individuals with the same *CFTR* genotype can be exacerbated by environmental factors such as exposure to environmental pathogens, and modifier genes such as transforming growth factor-β (TGF-β) and mannose-binding lectin 2 (MBL2) (Accurso and Sontag, 2008; Bombieri *et al.*, 2011; Cutting, 2015).

To lend organisation to the vast number of variations identified within the *CFTR* gene, mutation types have been grouped into 6 classes based on their resultant molecular mechanism of CFTR dysfunction (Welsh and Smith, 1993; Zielenski, 1995; Haardt *et al.*, 1999; Rowe, Miller and Sorscher, 2005). More recently it has been proposed that the 6 classes of *CFTR* mutation be further updated to reflect molecular and cellular phenotypes associated with *CFTR* mutations, resulting in a total of 31 mutation classes (Veit *et al.*, 2016).

The 6 mutation classes are discussed briefly below and summarised in Figure 1-2.

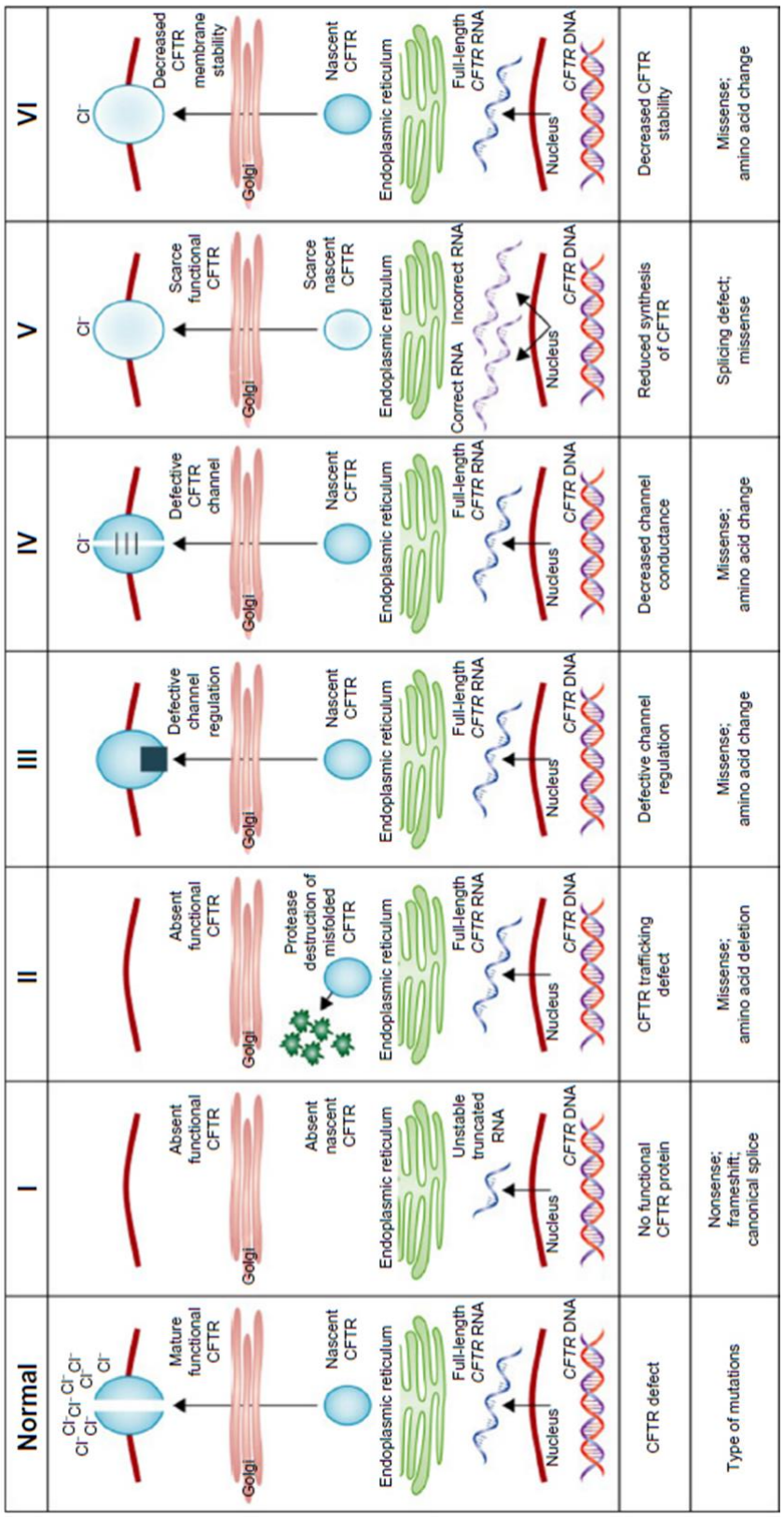

Figure 1-2: Summary of the six classes of CFTR mutation, and the mutation types that typically cause them.

Figure 1-2: Summary of the six classes of CFTR mutation, and the mutation types that typically cause them

Mutations in the CFTR gene fall into six classes depending on their subsequent molecular mechanism of CFTR dysfunction. Class I mutations are those which prevent the synthesis of CFTR protein, class II mutations are characterised by incorrect protein folding and processing, class III mutations result in incorrect channel gating, class IV mutations result in incorrect channel conductance, class V mutations reduce CFTR expression within the membrane, and class VI mutations result in reduced protein stability within the plasma membrane. Figure adapted with permission from Elborn and Vallieres (2014).

Class I mutations: defective protein production

Class I mutations introduce in-frame stop codons, also referred to as premature termination codons (PTCs) into the *CFTR* gene, preventing the synthesis of full length, functional CFTR protein (Welsh and Smith, 1993). PTCs arise within the DNA as a result of splice site abnormalities, nonsense and indel mutations which cause a frameshift in the reading frame of the gene, therefore disrupting correct translation of mRNA (Welsh and Smith, 1993). In cases such as R553X, the introduction of PTCs results in the production of unstable mRNA and no protein product (Welsh and Smith, 1993). Conversely, the nonsense mutation W1282X [the 5th most common *CFTR* mutation with ~45% prevalence within Ashkenazi Jews (Shoshani *et al.*, 1992; Watson *et al.*, 2004; Haggie *et al.*, 2017)], results in a protein truncated at NBD2. *In vitro* experiments have identified both classical and novel corrector-potentiator/co-potentiator combination therapies (See section 1.6.2) effective in rescuing W1282X truncated protein function, suggesting the possibility of small molecule therapies for a wider range of *CFTR* mutations in the future (Haggie *et al.*, 2017; Phuan *et al.*, 2019).

Class II mutations: defective protein processing

CFTR mutations that result in defective maturation and trafficking of functional CFTR protein to the plasma membrane characterise class II mutations (Welsh and Smith, 1993; Zielenski, 1995). Throughout CFTR synthesis, the evolving protein undergoes several endoplasmic reticulum (ER)-mediated 'quality control' checkpoints before ultimately being expressed within the plasma membrane (Amaral, 2004). The failure of class II mutated proteins to progress correctly through the biosynthetic pathway and intracellular

quality control mechanisms is likely due to polypeptide misfolding and incorrect glycosylation (Welsh and Smith, 1993; Y. Wang *et al.*, 2014).

Newly assembled CFTR polypeptides are cotranslationally inserted into the ER where N-glycosylation occurs giving rise to core-glycosylated immature protein, known as band B protein (~150 kDa) (Cheng *et al.*, 1990; Farinha, Matos and Amaral, 2013). Core-glycosylation of the protein provides both stabilisation to the protein as well as "self" recognition sites for immune response modulators (Farinha, Matos and Amaral, 2013). Following N-glycosylation, CFTR transiently interacts with molecular chaperone complexes, also known as molecular folders, namely heat-shock cognate (Hsc) 70/heat-shock protein (Hsp) 70, Hsp90 and human DnaJ 2 (Hdj-2) which facilitate correct protein folding (Yang *et al.*, 1993; Loo *et al.*, 1998; Meacham, 1999; Farinha *et al.*, 2002). Subsequent cycles of binding and release of the protein to the ER chaperone calnexin and further post-translational modifications results in fully folded CFTR (Pind, Riordan and Williams, 1994). At this stage CFTR protein undergoes ER-mediated quality control, and if correctly core-glycosylated and folded, leaves the ER (Farinha *et al.*, 2002). Prior to protein expression within the plasma membrane further post-Golgi glycosylation and post-translational modifications occur giving rise to fully glycosylated mature protein, also known as band C (~170-180 kDa) (Cheng *et al.*, 1990; Amaral, 2004).

The most common CF causing *CFTR* mutation, F508del (a deletion of a phenylalanine residue at position 508 in NBD1) is an example of a class II mutation resulting in protein misfolding (Cheng *et al.*, 1990; Y. Wang *et al.*, 2014). Evidence suggests that the majority of F508del protein is retained within the ER before degradation through the ubiquitin-proteasome pathway (Farinha, Matos and Amaral, 2013).

Class III mutations: defective channel regulation

CFTR protein affected by class III mutations are correctly synthesised and stably expressed within the plasma membrane, however regulation of channel gating is defective, often resulting in severe loss of channel function (Welsh and Smith, 1993; Zielenski, 1995). Many class III mutations occur within the NBDs and interfere with ATP-binding and hydrolysis. In contrast, missense mutations occurring within the RD are less frequently recorded and have minimal effect of channel gating. This is perhaps owing to the presence of multiple phosphorylation sites within the RD, phosphorylation of which can initiate channel opening (Welsh and Smith, 1993). The missense mutation G551D is a class III mutation and the 3rd commonest CF causing *CFTR* mutation with ~5% of

individuals with CF having the G551D mutation on at least one *CFTR* allele (Bompadre *et al.*, 2007; Ramsey *et al.*, 2011). The G551D mutation is associated with significant reduction in ATP-mediated channel opening and a severe clinical phenotype. The location of the G551D mutation and consequent glycine to aspartate residue change within the LSGGQ motif of NBD1 interferes with ATP-binding and hydrolysis at ATP-binding site 2 (Bompadre *et al.*, 2007). Incidentally, the G551D mutation was the first CF causing mutation to be treated with the clinically approved CFTR potentiator Ivacaftor (Van Goor *et al.*, 2009; Ramsey *et al.*, 2011).

Class IV mutations: defective channel conduction

Class IV mutations are characterised by *CFTR* mutations which cause altered channel conductance. Typically, class IV mutations are located in regions that correspond to TM segments within the MSDs. As such class IV mutations do not affect channel regulation by intracellular ATP nor cAMP-dependent phosphorylation (Zielenski, 1995). The missense mutations R117H, R334W and R347P are all examples of class IV mutations in which an arginine residue is replaced by a histidine residue at position 117 (TM2), a tryptophan residue at position 334 (TM6) and a proline residue at 347 (TM6), respectively (Sheppard *et al.*, 1993). All three mutations result in correctly synthesised protein, however cAMP-stimulated Cl^- current through the channel is significantly reduced compared to wild-type CFTR protein: wild-type CFTR>R347P>R117H>R334W (Sheppard *et al.*, 1993). These data suggest that *CFTR* mutations occurring within the MSDs directly or indirectly impair the permeability of the channel pore to Cl^- ions (Y. Wang *et al.*, 2014).

Class V mutations: reduced protein synthesis

Two years after the above four *CFTR* mutation classes were proposed by Welsh and Smith (1993), a fifth class of mutations was introduced to include those which reduce protein synthesis (Zielenski and Tsui, 1995). Class V mutations includes promoter mutations, nucleotide changes and amino acid substitutions which result in altered transcription, alternative splicing of CFTR transcripts and inefficient protein maturation, respectively (Zielenski and Tsui, 1995; Y. Wang *et al.*, 2014). These mutations typically result in CFTR protein that individually achieve Cl^- transport comparable to wild-type CFTR levels, albeit with reduced plasma membrane CFTR expression. An example of a *CFTR* mutation in this class is the missense mutation A455E associated with pancreatic sufficiency and milder lung disease (Sheppard *et al.*, 1995). Functional and

immunohistochemistry experiments on A455E-CFTR reveal that whilst channel gating properties and ion conductance and permeation were similar to wild-type CFTR, the overall production of fully mature band C protein was reduced (Sheppard *et al.*, 1995). Features such as these may account for the milder disease phenotype often associated class V mutations.

Class VI mutations: reduced protein stability

The studies of Haardt *et al* (Haardt *et al.*, 1999) identified frameshift and nonsense *CFTR* mutations that result in truncation of the CFTR C-terminal. While C-terminal truncated proteins were observed to have normal biosynthesis, trafficking and channel function, their stability within the plasma membrane was reduced with degradation rates ~6 times higher than wild-type CFTR protein (Haardt *et al.*, 1999). The C-terminal domain contains residues which collectively form a postsynaptic density protein 95/discs large/zonula occludens-1 (PDZ) binding domain. The PDZ domain of CFTR interacts with various scaffolding proteins (see Section 1.4.3 for further discussion), including EBP50, which have important roles in anchoring CFTR protein to the actin cytoskeleton (Haggie *et al.*, 2006). Disruption of PDZ domain binding to scaffolding proteins leads to increased mobility of CFTR within the plasma membrane and increased protein degradation (Haardt *et al.*, 1999; Haggie *et al.*, 2006; Valentine *et al.*, 2012).

The classification of *CFTR* mutations is complex and it is often the case that one *CFTR* mutation can have multifaceted effects on protein synthesis, function and expression (Veit *et al.*, 2016). The *CFTR* mutation F508del, a class II mutation according to this classical method of mutation categorisation, also shares characteristics of class III and VI mutations. This is further complicated when one takes into account the relationship between CFTR genotype and disease phenotype (Bombieri *et al.*, 2011). A classification system, such as that developed by Veit *et al* (2016), that considers CFTR expression and function as well as mutation associated disease phenotype paves the way for more effective CF therapeutic strategy development.

1.3. The human gastrointestinal tract

The digestion and absorption of nutrients is the primary function of the intestinal tract, however, as a consequence of this, the epithelium lining the intestines is exposed to many antigens and pathogens (Snoeck, Goddeeris and Cox, 2005). As discussed in the sections below, the intestinal epithelium is well adapted to its function allowing permeability to water, nutrients and macromolecules whilst forming a protective barrier between harmful pathogens within the intestinal lumen and the body (van der Flier and Clevers, 2009). Successful performance of these functions is in no small part due to the diverse range of specialised cell types found within the intestinal epithelium.

1.3.1. Organisation of the intestinal epithelium

The arrangement of the epithelial lining of the small (duodenum, jejunum and ileum), and large intestine (colon) is highly specialised and adapted to perform both secretory and absorptive functions. Within the small intestine the presence of villi - epithelial protrusions into the intestinal lumen considerably increase the absorptive surface area of the epithelium (Yang *et al.*, 2016). Between villi the epithelium invaginates into the underlying tissue forming the crypts of Lieberkühn in which intestinal stem cells (ISCs) and transit-amplifying (TA) progenitor cells are located (van der Flier and Clevers, 2009). TA cells, the progeny of ISCs, migrate toward the villus, undergoing several rounds of division, before their terminal differentiation into the different cell types of the intestinal epithelium (Czerwinski, Shroyer and Spence, 2018). ISCs ultimately give rise to all differentiated cell types within the intestine, including but not limited to, antimicrobial secreting Paneth cells (small intestine), mucin secreting goblet cells, epithelial enterocytes, tuft cells, M-cells, and endocrine cells. With the exception of Paneth cells, all intestinal cell types migrate from the crypt to the tip of the villus (small intestine) or epithelial surface (colon). Conversely Paneth cells are unique in that they migrate downwards to the base of the crypts upon terminal differentiation. Crypt-villus modules are self-renewing due to the highly proliferative nature of the cells located within the crypts (Clevers, 2013). It is this proliferative capability that allows for the complete regeneration of the intestinal epithelial surface every 4-5 days (van der Flier and Clevers, 2009).

1.3.1.1. Intestinal stem cells

Two populations of ISCs have been identified in the intestinal crypt, the crypt base columnar (CBC) stem cells and the +4 (also known as position 4) stem cells (Cheng and Leblond, 1974; Potten, Kovacs and Hamilton, 1974; Li and Clevers, 2010; Clevers, 2013). During homeostasis CBC cells divide rapidly, ultimately giving rise to all differentiated cell types within the intestine (Clevers, 2013). These cells can be readily identified by Lgr5 (leucine-rich repeat containing G-protein coupled receptor 5), a target of the Wnt signalling pathway and a marker of CBCs (Barker *et al.*, 2007), and as such are often referred to as Lgr5+ stem cells (Takahashi and Shiraishi, 2020).

A second population of +4 stem cells, identifiable by the molecular marker Polycomb group protein Bmi1, are proposed to reside at position +4 within the crypts. Initial studies reported +4 stem cells as a quiescent population of stem cells, rarely dividing and eventually giving rise to more proliferative CBC stem cells (Czerwinski, Shroyer and Spence, 2018). More recent studies have demonstrated that both CBC cells and +4 stem cells are able to give rise to the various cell types of the intestinal epithelium (Takeda *et al.*, 2011). Evidence has also been reported suggesting that +4 cells are able to ultimately differentiate into Paneth and enteroendocrine cells, with the ability to re-acquire stemness converting to Lrg5+ cells during epithelial stress and regeneration (Buczacki *et al.*, 2013; Li *et al.*, 2016).

The organisation of the small intestinal crypt-villus axis, along with the cellular lineages arising from the differentiation of CBC stem cells is shown in Figure 1-3.

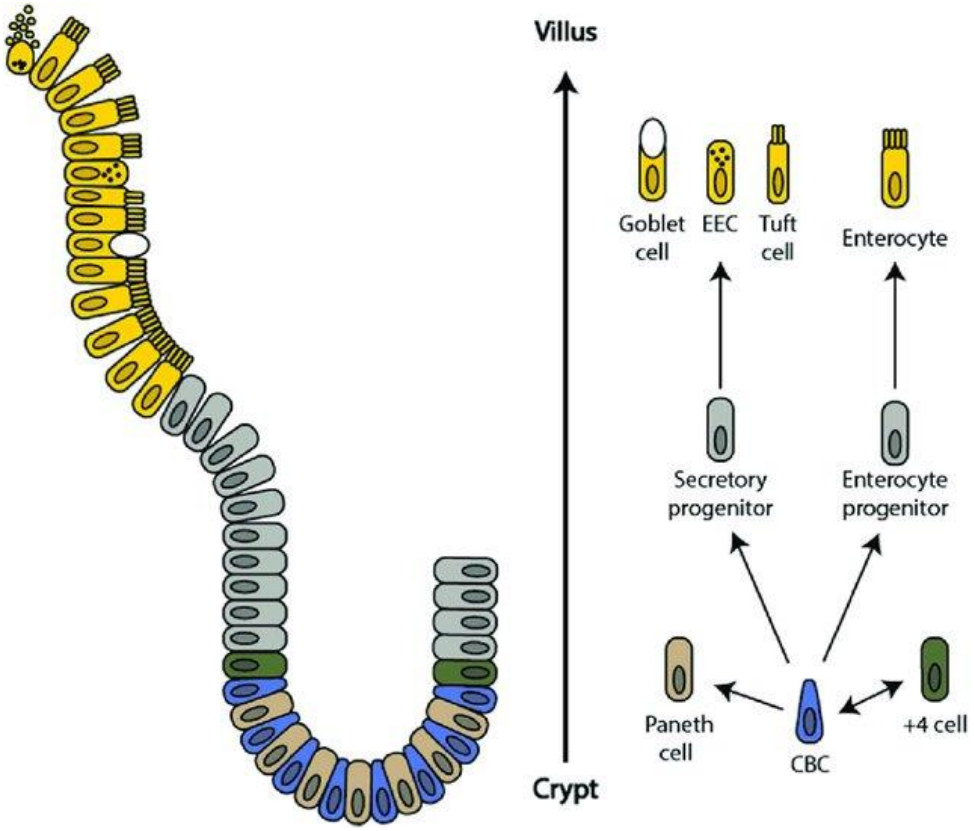

Figure 1-3: Schematic of the small intestinal crypt-villus axis.

The intestinal epithelium is maintained by Lgr5+ CBC and Bmi1+ +4 stem cells. Located at the bottom of the crypt these stem cells give rise to the differentiated cell populations of the intestinal epithelium including goblet cells, tuft cells, enteroendocrine cells, enterocytes, and Paneth cells. Figure reproduced with permission from Iismaa et al. (2018).

1.3.1.2. Secretory and absorptive cells

The differentiated cell types found within the intestine can broadly be categorised as either secretory or absorptive. Whilst most differentiated intestinal cells are present in both the small and large intestine, the prevalence of cell type in each can vary (Barker, Van Oudenaarden and Clevers, 2012).

Enterocytes are the most abundant cell of the intestinal epithelium, accounting for approximately 90% of total cells (Fre, 2015). Showing particular abundance in the small intestine, the primary function of these highly polarised columnar epithelial cells is the absorption of nutrients (Barker, Van Oudenaarden and Clevers, 2012). To facilitate the

absorption of nutrients in large volume, enterocytes have an apical brush border, maximising their surface area (van der Flier and Clevers, 2009). Neighbouring enterocytes are joined by tight junctions, restricting the paracellular transport of electrolytes and soluble compounds (Ikpa *et al.*, 2016). Passage of these molecules across the epithelium is facilitated by a number of transporters, channels and pumps each having expression specifically within either the apical or basolateral enterocyte membranes. Amongst these proteins are the apical CFTR channel and sodium/hydrogen exchanger NHE3. The activity of these two proteins is coordinated to regulate the transport of Cl^- and Na^+ across the epithelium, providing the underlying mechanism of water and pH homeostasis maintenance within the intestinal lumen (Montoro *et al.*, 2020). Intestinal enterocytes are also reported to produce antimicrobials and to have a role in antigen uptake and processing, therefore play a crucial part in intestinal barrier function (Snoeck, Goddeeris and Cox, 2005; Montoro *et al.*, 2020).

Advancements in single-cell RNA-sequencing (scRNS-seq) have recently revealed the existence of rare epithelial cells in mouse and human (*in vitro*) tracheal epithelia called ionocytes (Montoro *et al.*, 2018; Plasschaert *et al.*, 2018). Pulmonary ionocytes are characterised by the specific expression of forkhead box I1 (*FOXI1)* transcription factor, *CFTR*, and subunits of the vacuolar-type H^+-ATPase (V-ATPase) (Montoro *et al.*, 2018, 2020; Plasschaert *et al.*, 2018). Ionocytes express high levels of CFTR, providing the major source of CFTR RNA transcripts in the pulmonary epithelium, yet only accounting for <1% of epithelial cell types (Montoro *et al.*, 2018).

CFTR expression varies along the length of the intestines, with high levels of CFTR mRNA expressed in the duodenum, gradually decreasing to the ileum, and moderate expression in the colon (De Lisle and Borowitz, 2013). A gradient of CFTR mRNA expression is also found along the crypt-villus axis where highest levels can be detected within the crypts, decreasing to either the villi (small intestine) or lumen (large intestine) (De Lisle and Borowitz, 2013). Although cells possessing specific ionocyte defining characteristics have not as yet been identified within the intestinal epithelium, a population of villus cells expressing high levels of CFTR have been reported in rat and human small intestine (Ameen *et al.*, 1995).

Goblet cells account for approximately 4% of the cells of the duodenal epithelium, increasing to approximately 16% in the descending colon (van der Flier and Clevers, 2009). Goblet cells resemble a cup in shape with one end typically wider than the other due to the presence of cytoplasmic granules containing secreted Muc2 (the most

abundantly secreted intestinal mucin) along with other components of mucus secretion such as IgGFc-binding protein (FCGBP), chloride channel accessory 1 (CLCA1), and zymogen granule membrane protein 16 (ZG16) (Birchenough *et al.*, 2015). The main function of goblet cells is the secretion of mucins and trefoil proteins. Trefoil proteins act to stabilise secreted mucus and stimulate tissue repair at sites of injury (Playford, 1997).

Paneth cells were first described in the small intestine in 1872 by Gustav Schwalbe and Josef Paneth (Gassler, 2017). With expression largely restricted to the crypts of the small intestine, Paneth cells are readily identified by the presence of secretory granules throughout their cytoplasm (Barker, Van Oudenaarden and Clevers, 2012; Clevers and Bevins, 2013). Upon differentiation Paneth cells migrate downwards along the crypt-villus axis into the crypt (Gassler, 2017), and unlike other differentiated cells of the intestinal epithelium which turn over rapidly, Paneth cells reside in the crypts for up to 6 weeks (Barker, 2008; Clevers and Bevins, 2013). Paneth cells function as part of the innate immune system, producing and secreting large quantities of antimicrobial peptides and proteins such as α-defensins and lysozyme (van der Flier and Clevers, 2009). Secretion of these factors by Paneth cells is important in maintaining host-microbiome homeostasis and the correct flora of intestinal bacteria (Gassler, 2017). It has been demonstrated that Paneth cells, and to a lesser extent other cells of the secretory lineage, secrete the peptides guanylin (GN) and uroguanylin (UGN) (Ikpa *et al.*, 2016). These peptides act locally via the enzyme-receptor guanylyl cyclase C (GCC) and play an important role in maintaining intestinal fluid homeostasis (discussed further in Section 1.6.3).

Enteroendocrine cells (EECs) account for approximately 1% of the cells forming the intestinal epithelium, and can be grouped into subpopulations based on their endocrine secretions (van der Flier and Clevers, 2009; Shirazi-Beechey *et al.*, 2011). EECs play an important role in nutrient-sensing within the intestinal lumen, a function facilitated by luminal nutrient sensors expressed on their surface (Shirazi-Beechey *et al.*, 2011). These cells secrete hormonal peptides which can either act locally on neighbouring cells or systemically via the bloodstream. Peptides released by EECs have important roles in the regulation of metabolism, coordination of the digestion and absorption of food, the secretion of insulin and control of appetite (Gribble and Reimann, 2019). EECs are arranged into subtypes defined by their morphology and the hormones that they secrete (Clevers, 2013).

Chemosensory tuft cells reside at the base of the crypts and account for approximately 0.5% of the cells of the small and large intestinal epithelium (Banerjee, Coffey and Lau, 2018; Ting and von Moltke, 2019). Morphologically tuft cells are distinguishable from other intestinal epithelial cells by the presence of an apical brush border composed of microvilli (Banerjee, Coffey and Lau, 2018). Unlike other intestinal epithelial cells individual tuft cells poses 3-4 cytoplasmic projections, called cytospinules, that extend laterally from the cell and protrude through the neighbouring cells membrane to contact the nucleus (Hoover *et al.*, 2017). Tuft cells also contain filamentous actin, villin and fimbrin bundles that extend from the base of the microvilli through the cytoplasm to the ER which in turn are interspersed with vesicles (Hoover *et al.*, 2017; Banerjee, Coffey and Lau, 2018; Ting and von Moltke, 2019). These two structures collectively are termed the tubulovesicular network (Hoover *et al.*, 2017). It is suggested that this network, working alongside the cytospinules, provides a method of communication and the exchange of vesicular cargo between the gut lumen and the nuclei of neighbouring epithelial cells (Hoover *et al.*, 2017).

1.4. Intestinal electrolyte transport and fluid homeostasis

1.4.1. Basolateral membrane ion transport

The main driving force for the movement of fluid across the intestinal epithelium is the active transport of ions such as Cl^-, HCO_3^- and Na^+. A major source of cellular Cl^- uptake is via the basolateral membrane $Na^+/K^+/2Cl^-$ cotransporter NKCC1, leading to intracellular accumulation of Cl^- above its electrochemical equilibrium (Barrett and Keely, 2000). It has recently been hypothesised that activation of this co-transporter is sensitive to intracellular Cl^- concentration, a decrease in which leads to the activation of WNK (with no lysine) kinase, which via intracellular phosphorylation steps results in the phosphorylation and activation of NKCC1 (Frizzell and Hanrahan, 2012). In addition to this Cl^- dependent regulatory mechanism, a Cl^- independent, cAMP-mediated mechanism recruits NKCC1 to the basolateral membrane and increases its activity when the intracellular cAMP concentration is increased (Bachmann *et al.*, 2003; Reynolds *et al.*, 2007).

The electrochemical driving force needed to sustain Cl^- entry into the cell is maintained by cation recycling across the basolateral membrane. Na^+ is recycled via the Na^+/K^+ ATPase, maintaining an overall inward facing Na^+ concentration gradient (Julio-Kalajzić *et al.*, 2018). In the intestinal epithelium, it is thought that K^+ recycling occurs via small

conductance Ca^{+}-dependent K^{+} channels (KCNN4), cAMP-activated voltage dependent K^{+} channels (KCNQ1/KCNE3), and a pH-gated two-pore domain K^{+} channel TASK-2 (Schroeder *et al.*, 2000; Julio-Kalajzić *et al.*, 2018; Li, Rietmeijer and Brohawn, 2020). The requirement of both NKCC1 activity and K^{+} recycling for Cl^{-} transport is well documented. Inhibition of NKCC1 by the loop diuretic bumetanide greatly reduced apical chloride transport in several epithelial models including colorectal cancer LIM1863 cells (Currid, Ortega and Valverde, 2004) and NKCC1$^{-/-}$ mice (Flagella *et al.*, 1999; Gillie *et al.*, 2001). Similarly inhibition of KCNQ1 by both chromanol 293B and clofilium results in loss of Cl^{-} transport across the apical membrane (Bachmann, Quast and Russ, 2001; Currid, Ortega and Valverde, 2004).

An additional source of Cl^{-} influx across the basolateral membrane is the Cl^{-}/HCO_3^{-} exchanger (AE2), which along with the activity of the basolateral Na^{+}/H^{+} exchanger (NHE1) and Na^{+}/HCO_3^{-} co-transporter (NBC1) increases the intracellular net concentrations of Cl^{-}, Na^{+} and HCO_3^{-} (Gawenis *et al.*, 2010). The activity of these three transporters is closely linked as it is the efflux of H^{+} out of the cell in exchange for Na^{+}, and the subsequent increase in intracellular pH which activates the Cl^{-}/HCO_3^{-} exchanger and Cl^{-} influx (Yang *et al.*, 2016). The source of intracellular HCO_3^{-}, for recycling by the Cl^{-}/HCO_3^{-} exchanger, originates from the activity of NBC1 which co-transports Na^{+} and $2HCO_3^{-}$ across the basolateral membrane (Frizzell and Hanrahan, 2012). A summary of transporters, channels and pumps located within the basolateral membrane of intestinal epithelia is shown in Figure 1-4.

1.4.2. Apical membrane ion transport

The channel responsible for the majority of Cl^{-} secretion across the apical membrane of intestinal epithelial cells is the cAMP/cGMP regulated CFTR channel, capable of transporting both Cl^{-} and HCO_3^{-} across the apical membrane. Stimulation and inhibition of CFTR by modulators such as forskolin [increases intracellular cAMP (Dekkers *et al.*, 2013)] and $CFTR_{inh}$-172 [allosteric inhibitor of CFTR (Taddei *et al.*, 2004)] increase and decrease Cl^{-} secretion, respectively (Dekkers *et al.*, 2013). In the early 1990s, a second mechanism of apical Cl^{-} secretion was identified in epithelial cells, a mechanism that in 2008 was revealed to be the Ca^{2+}-dependent Cl^{-} channel TMEM16A (Caputo *et al.*, 2008). TMEM16A [also known as anoctamin-1 (ANO1)], transports Cl^{-} and HCO_3^{-} across the apical membrane contributing to the net secretion of these anions. Marked reduction of Ca^{2+}-dependent Cl^{-} secretion is demonstrated in both TMEM16A$^{-/-}$ mice and TMEM16A null cell lines (Ousingsawat *et al.*, 2009; Mall and Galietta, 2015).

It is not only the secretion of Cl^- into the intestinal lumen that plays an important role in maintaining intestinal fluid homeostasis. The secretion and absorption of Na^+ is also closely regulated. The accumulation of secreted anions in the intestinal lumen drives the diffusion of Na^+ though paracellular spaces in accordance with the electrochemical gradient. During basal activity in the intestine, Cl^- secretion via CFTR ceases and Na^+ is absorbed across the apical membrane of epithelial cells by Na^+ channels, transporters and pumps (Gawenis *et al.*, 2004). Although Na^+ absorption is largely via the sodium/hydrogen exchanger NHE3 in the small intestine, and the epithelial sodium channel (ENaC) in the colon, both transport proteins are found along the length of the intestinal tract (Zachos, Kovbasnjuk and Donowitz, 2009; Yang *et al.*, 2016). Activation of cAMP-mediated Cl^- secretion via CFTR occurs alongside inhibition of NHE3 activity, resulting in an accumulation of NaCl within the intestinal lumen and the subsequent transport of H_2O into the intestinal lumen down the transepithelial osmotic gradient. Figure 1-4 summarises the transporters, channels and pumps associated with the apical membrane of intestinal epithelia.

1.4.3. Regulation of NaCl and fluid secretion

The movement of fluid across the intestinal epithelium is secondary to, and therefore governed by, the electrogenic movement of ions (Julio-Kalajzić *et al.*, 2018). Of particular importance in the maintenance of fluid homeostasis is the regulation of luminal NaCl concentration, which in turn is regulated by coordinated Cl^- secretion by CFTR and Na^+ absorption by NHE3 (Gawenis *et al.*, 2002). The regulation of both CFTR and NHE3 is complex. While the activity of both is known to be mediated by cAMP/cGMP-dependent phosphorylation, it is becoming increasingly apparent that intracellular signalling and protein-protein interactions also play a significant role.

Much research has addressed the regulation of CFTR activity. As already discussed, a pre-requisite for CFTR activation is the cAMP- or cGMP-dependent phosphorylation of the RD, allowing regulation of channel gating by cycles of ATP binding to the NBDs (Winter and Welsh, 1997; Hwang and Sheppard, 2009; Hwang and Kirk, 2013). Similarly cAMP- and forskolin-dependent phosphorylation of the C-terminal cytoplasmic domain of NHE3 by protein kinases such as PKA has been shown to be important for NHE3 modulation, whereby mutation of key phosphorylation sites within the NHE3 protein prevent cAMP-mediated inhibition of NHE3 activity (Moe, Amemiya and Yamaji, 1995; Zhao *et al.*, 1999; Bagorda *et al.*, 2002). Additionally, cGMP-mediated phosphorylation

of NHE3 at key sites has been shown to inhibit NHE3 activity and alter protein trafficking, reducing its surface expression (Chen *et al.*, 2015).

Evidence also suggests an important role of protein-protein interactions not only in the regulation of CFTR and NHE3 activity, but in the modulatory role CFTR has over other proteins and ion channels, such as ENaC, calcium-activated chloride channels (CaCC), Cl^-/HCO_3^- exchangers and Na^+/H^+ exchangers, as well as CFTR interactions with the cytoskeleton (Stutts *et al.*, 1995; Ahn *et al.*, 2001; Wei *et al.*, 2001; Ko *et al.*, 2002; Li and Naren, 2010). The most commonly reported mechanism by which CFTR and NHE3 interact structurally with other proteins is via a protein binding motif located within the C-terminal domain of CFTR and intermediary PDZ (presynaptic density 95, Drosophila disc large tumour suppressor, zonula occludens-1) domain containing scaffolding proteins (Li and Naren, 2010). PDZ domains form peptide-binding clefts, typically 80-90 amino acids in length, where corresponding PDZ-binding motifs, located within the C-terminal domain of target proteins, interact (Harris and Lim, 2001; Hung and Sheng, 2002). It is common for proteins that contain a PDZ domain to contain more than one, allowing for a role of PDZ domain binding in the formation of multi-protein complexes. Evidence to support this comes from the reported dimerization of PDZ domains, and the observation that PDZ domain interactions in epithelial apical membranes occurs between functionally related protein groups (Bezprozvanny and Maximov, 2001; Chang *et al.*, 2011).

The PDZ motif of CFTR has been reported to have binding affinity for the PDZ scaffolding proteins NHE-regulatory factor-1 and -2 (NHERF1 and NHERF2), PDZ domain containing protein 1 and 2 (PDZK 1 and 2), CFTR-associated ligand (CAL), and Shank2 (Li and Naren, 2010). Some reports suggest that the interactions between NHERF1/NHERF2 FERM (protein 4.1, ezrin, radixin, moesin) domains and ezrin play a crucial role in localising and anchoring CFTR to the cortical cytoskeleton of the apical membrane (Short *et al.*, 1998; Bosanquet *et al.*, 2014). However this hypothesis has been contested by research whereby expression of CFTR lacking the C-terminus (site of the PDZ motif) had no effect on correct protein localisation in intestinal, tracheal, pancreatic and CF airway epithelium (Benharouga *et al.*, 2003; Ostedgaard *et al.*, 2003).

The association of CFTR to ezrin via PDZ scaffolding proteins has been suggested to have an additional function. Not only is ezrin a cytoplasmic linking protein with key roles in membrane structure and organisation, ezrin acts as an A kinase anchoring protein (AKAP), binding PKA and PKA type II (Dransfield *et al.*, 1997; Lamprecht, Weinman and Yun, 1998). Research suggests that CFTR exists within a multiprotein complex formed

of CFTR, NHERF2, ezrin and PKA (Sun, Hug, Bradbury, *et al.*, 2000; Sun, Hug, Lewarchik, *et al.*, 2000). In this way, PKA and CFTR are localised to facilitate cAMP-dependent phosphorylation of CFTR by PKA. The data demonstrate that CFTR co-immunoprecipitates with each of NHERF2, ezrin and PKA, and colocalised with NHERF2 and ezrin at the apical surface of Calu-3 airway epithelial cells. Moreover, blocking of PKA binding to AKAPs prevented CFTR activation by cAMP agonists (Li and Naren, 2010).

Like CFTR, NHE3 can interact with a variety of other proteins, including PDZ scaffolding proteins, such as NHERF1 and NHERF2 (also referred to as NHE3 kinase A regulatory protein (E3KARP)) (Lamprecht, Weinman and Yun, 1998; He and Yun, 2010). Moreover, the presence of either NHERF1 or NHERF2 is necessary for cAMP-mediated inhibition of NHE3 (Yun *et al.*, 1997). Although not well defined these scaffolding proteins are proposed to form part of a larger protein complex, acting as adapters between NHE3 and ezrin. Such complexes allow for localisation of PKA type II in proximity to NHE3, facilitating cAMP-mediated NHE3 inhibition by PKA (Lamprecht, Weinman and Yun, 1998; Weinman, Steplock and Shenolikar, 2001; Donowitz and Li, 2007; He and Yun, 2010).

Whilst much research has explored the regulation and protein binding partners of NHE3 and CFTR individually, some evidence suggests coordinated regulation of cAMP-mediated Cl^- secretion and Na^+ absorption. For example, in the small intestine of NHE3 knockout mice not only was cAMP-mediated Cl^- secretion decreased compared to control levels, but CFTR mRNA and protein expression were also reduced (Gawenis *et al.*, 2004). Similarly, Na^+ absorption and NHE3 protein expression were reduced in the small intestine of CFTR knockout mice (Clarke and Harline, 1996; Gawenis *et al.*, 2003, 2004).

It has been hypothesised that CFTR may regulate NHE3 activity (Donowitz and Li, 2007; He and Yun, 2010). One hypothesis proposes a direct interaction between the two proteins via NHERF proteins, known to associate with both CFTR and NHE3 (Donowitz and Li, 2007). An alternative hypothesis proposes an indirect functional interaction between the two proteins, possibly mediated by changes in cell volume (Donowitz and Li, 2007). In support of this latter idea, crypts are the site of Cl^- secretion and villi are the site of Na^+ absorption, such that CFTR and NHE3 are not typically found in the same cell (Strong, Boehm and Collins, 1994; Donowitz and Li, 2007). However, new research has challenged the segregation of Cl^- secretion to crypts and Na^+ absorption to villi,

suggesting instead a continuum of expression of CFTR and NHE3 in cells along the crypt-villus axis (Barret, 2018; Yin *et al*, 2018). For further discussion of the distribution of NHE3 and CFTR along the crypt villus axis please refer to Section 5.1. Thus, to date the mechanisms underpinning the coordinated regulation of CFTR and NHE3, linking their expression and function in the small intestine are not fully understood.

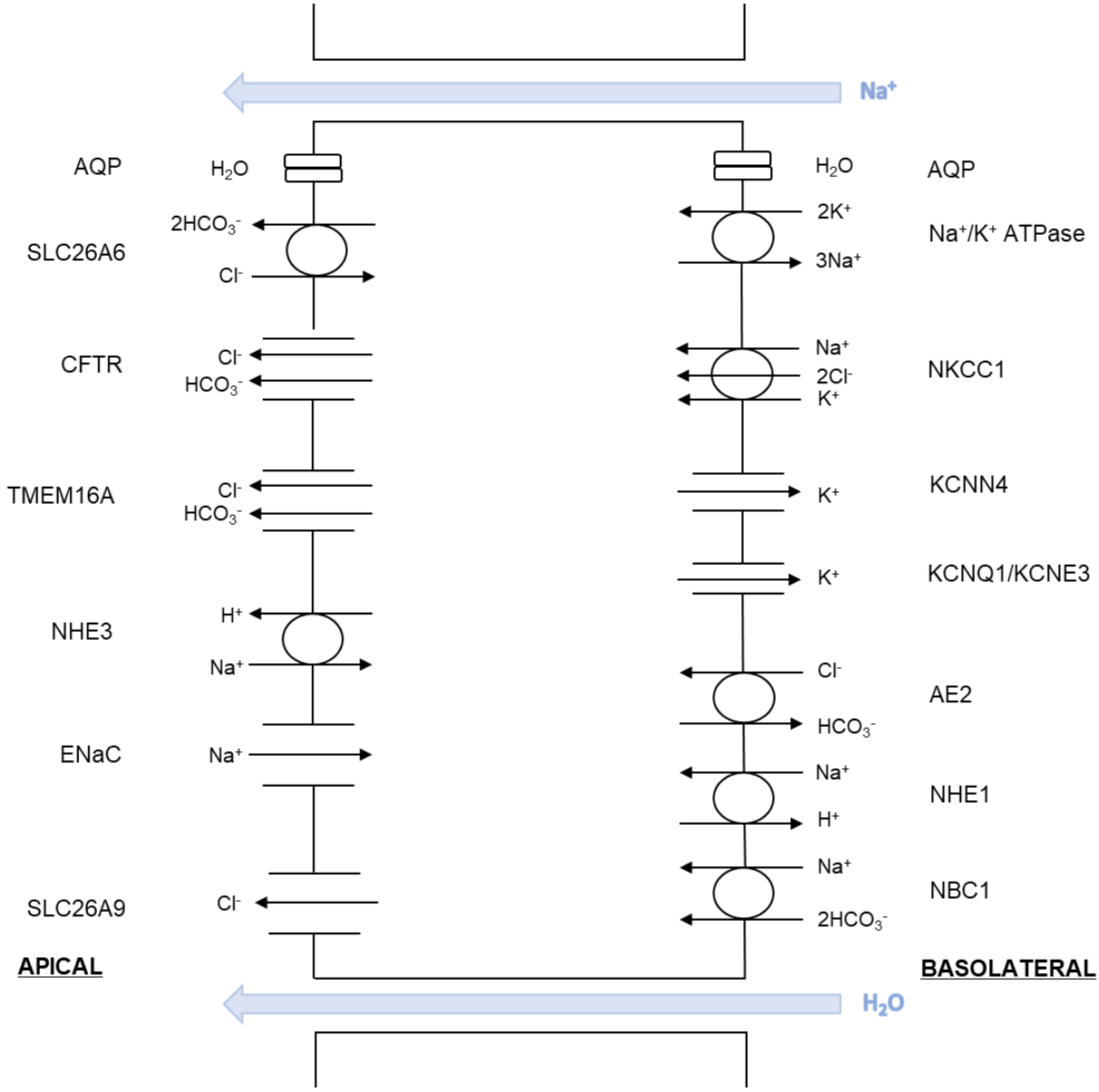

Figure 1-4: Schematic representation of channels, transporters, and pumps found within the intestinal epithelium.

A composite representation of ion channels, transporters and pumps located within the basolateral and apical surfaces of the intestinal epithelium. Secretory and absorptive epithelial cells occupy distinct regions along the crypt-villus axis, and as such will express a sub-set of the transporters shown. NHE3 function dominates in the small intestine, whereas ENaC function dominates within the colon. Aquaporin (AQP); cystic fibrosis transmembrane conductance regulator (CFTR); Transmembrane member 16A (TMEM16A); Sodium-hydrogen exchanger 1 and 3 (NHE1 and NHE3); Epithelial sodium channel (ENaC); Sodium-potassium-chloride cotransporter 1 (NKCC1); Intermediate conductance calcium-activated potassium channel protein 4 (KCNN4); Potassium voltage-gated channel subfamily Q member 1 (KCNQ1); Potassium voltage-gated channel subfamily E regulatory subunit 3 (KCNE3); anion exchange protein 2 (AE2); Electrogenic sodium bicarbonate transporter 1 (NBC1).

1.4.4. pH homeostasis

The maintenance of acid-base homeostasis within the intestines is vital for processes such as enzymatic function, correct mucin secretion, microbial normobiosis and host pathogenic defences (Gustafsson *et al.*, 2012; Borowitz, 2015). Coordination of HCO_3^- secretion by CFTR and NHE3 mediated HCO_3^- absorption has a significant role in correct intestinal pH buffering (Praetorius *et al.*, 2000; Chen, Cai and Sheppard, 2009). The pH buffering capacity, and therefore HCO_3^- secretory capacity of the intestinal epithelium must meet the requirements of the different sections of the intestinal tract lumen (De Lisle and Borowitz, 2013). High levels of *CFTR* are expressed in the duodenum, reflecting the need for large amounts of HCO_3^- for gastric acid (pH1-3) neutralisation (Strong, Boehm and Collins, 1994). CFTR is also found in high abundance in the epithelium of the pancreatic ducts (Wilschanski and Novak, 2013). Secretion of HCO_3^- rich pancreatic fluid contributes to pH buffering in the small intestine, with secretion volumes of up to 3 litres of fluid per day (Borowitz, 2015). Secretion of this large volume of HCO_3^- rich fluid is also crucial for passage of pancreatic enzymes to the intestine for later use in digestion, protection of the pancreatic ducts from enzyme activity, and providing optimal intestinal pH for enzyme activity (De Lisle and Borowitz, 2013; Wilschanski and Novak, 2013; Zhou and Melton, 2018).

Degradation and reabsorption of HCO_3^- is mediated by NHE3. The electroneutral exchange of Na^+ and H^+ ions across the apical membrane by NHE3 results in an accumulation of luminal H^+ which bind to HCO_3^- giving rise to intermediary H_2CO_3. This in turn is degraded to CO_2 and H_2O (Rector, Carter and Seldin, 1998). The coordination of CFTR and NHE3 activity, along with the distribution of these proteins along the length of the intestinal tract means that the pH buffering requirements of different regions of the intestines can be met, and acid-base homeostasis maintained.

1.5. The CF intestine

Despite the major developments in range and availability of therapeutics for the treatment and management of CF, the predominant cause of mortality for individuals with CF remains repeated episodes of chronic infection and inflammation of the respiratory tract (Kuk and Taylor-Cousar, 2015). As such, CF is commonly considered as primarily a respiratory disease, and the GI symptoms associated with CF have historically gone under reported despite a prevalence of GI symptoms in adults with CF of 65%

(Sabharwal, 2016; Hayee *et al.*, 2019). Many individuals with CF report that the CF-associated GI symptoms they experience have a significant impact on their quality of life, with commonly experienced GI symptoms, including bloating, stomach pains and cramps, wind and gas, constipation and diarrhoea (Smith *et al.*, 2020).

1.5.1. Clinical manifestations

The implications of CF on the GI tract are not limited to the reported physical symptoms. Clinical manifestations of CF include malnutrition, pancreatic insufficiency (PI), intestinal blockage, acidification of the intestinal lumen, and small intestinal bacterial overgrowth (SIBO) (Sabharwal, 2016; Hayee *et al.*, 2019). The occurrence of these complications is multifactorial and complex, often arising from the overlapping failure of several systems.

Certain *CFTR* mutations are associated with CF-associated PI, with 85% of individuals with CF reported as having PI by age 2 years (Wilschanski and Novak, 2013). Not only does the loss of pancreatic function contribute to the acidification of the intestinal lumen as a result of reduced secretion of HCO_3^- rich fluid, secretion of pancreatic enzymes into the small intestine is also lost (De Lisle and Borowitz, 2013). The impacted delivery of digestive enzymes from the pancreas to the duodenum results from both blockage of pancreatic ducts by viscose secretions and the lack of adequately hydrated pancreatic fluid for delivery of the enzymes to the intestine (Strong, Boehm and Collins, 1994). Consequently, individuals with CF can experience malabsorption of essential nutrients, fats and proteins, which in combination with the increased calorific demands of successive bouts of infection and inflammation, plus increased work breathing, leads to nutritional failure and difficulty maintaining weight (Sabharwal, 2016). In fact 22% of adults with CF have a body mass index (BMI) of less than 18.5 and so are classed as underweight (Stallings *et al.*, 2008).

1.5.2. Intestinal blockage

The most life threatening of intestinal complications associated with CF is intestinal blockage. In the CF intestine, reduced Cl^- secretion via CFTR, combined with dysregulated Na^+ absorption by NHE3 leads to a marked reduction of $NaCl^-$ in the intestinal lumen and consequently loss of the osmotic gradient required to drive H_2O into the intestinal lumen. As a result, the mucus lining the intestine is insufficiently hydrated,

becoming thickened and viscous. Loss of intestinal fluid volume as a result of PI, alongside the dehydration of mucus lining the intestinal epithelium results in inadequate lubrication of the intestinal lumen. Incorrectly managed this leads to the accumulation of mucus and faecal matter, ultimately partially or fully blocking the intestine (Groves *et al.*, 2017). Known as meconium ileus (MI) in neonates and distal intestinal obstructive syndrome (DIOS) in non-neonates, obstruction of the small intestine can cause extreme pain, and if left untreated, rupture and sepsis (De Lisle and Borowitz, 2013). The estimated prevalence of DIOS in individuals with CF varies extensively, with some reports suggesting 2.4% - 41% (Blackman *et al.*, 2006; Groves *et al.*, 2017). The disparity in prevalence historically reported likely occurred as a result of a lack of standardised diagnostic criteria, ranging severity of DIOS experienced, and a misdiagnosis of constipation as DIOS (Blackman *et al.*, 2006). During 2005, the European Society for Paediatric Gastroenterology, Hepatology and Nutrition (ESPGHAN) sought to standardise the criteria for DIOS diagnosis, define different levels of DIOS severity and distinguish DIOS from constipation in CF patients (Houwen *et al.*, 2010). Tables 1-1 and 1-2 outline the definitions for DIOS and constipation in CF patients, respectively.

No.1	Complete intestinal obstruction as evidenced by vomiting of bilious material and/or fluid levels in small intestine on an abdominal radiography.
No.2	Faecal mass in ileo-caecum.
No.3	Abdominal pain and/or distension.
Complete DIOS: No.1, No.2 and No.3	
Incomplete DIOS: No.2 and No.3, without No.1	

Table 1-1: ESPGHAN definition for DIOS in CF.

The diagnostic criteria for distal intestinal obstructive syndrome (DIOS), defining different levels of disease severity. Adapted with permission from Houwen et al. (2010).

No.1	Abdominal pain and/or distension.
No.2a	Reduced frequency of bowel movements in the last few weeks or months.
No.2b	Increased consistency of stools in the last few weeks or months.
No.3	Symptoms 1 and 2 are relieved by the use of laxatives.
Constipation: No.1 or No.2a or No.2b and No.3	

Table 1-2: ESPGHAN definition for constipation in CF.
The criteria from the diagnosis of constipation, distinguishing constipation from DIOS. Adapted with permission from Houwen et al. (2010).

These standard definitions clearly differentiate between DIOS and constipation and highlight the localisation of DIOS within the small intestine and constipation to the colon. Since the development of these diagnosis criteria, the reported incidence of DIOS in Europe is 6.2 episodes of intestinal obstruction per 1000 individuals with CF, per year (Houwen *et al.*, 2010), and in the UK 5% of individuals with CF are reported to suffer with DIOS per year (Smith *et al.*, 2020).

1.6. Current therapeutic approaches for GI complications associated with CF

The advancement of treatment options for CF has seen what was once considered a childhood disease become a disease with a median life expectancy for those born in 2019 of 49 years (Cystic Fibrosis Trust UK, 2019). Whilst the focus of therapy for CF remains the treatment of respiratory disease, a much-improved life expectancy for those born with CF has gone hand in hand with the requirement for therapeutic support for other complications associated with CF. One such area of CF therapy which it may be argued has been historically overlooked is the treatment of GI complications. The GI symptoms experienced by those with CF have a profoundly negative impact on quality of life and as such treatments to alleviate these are becoming sought as a priority (Hayee *et al.*, 2019; Smith *et al.*, 2020).

1.6.1. Symptomatic therapy

Many GI complications associated with CF are managed using symptomatic therapies. Pancreatic enzyme replacement therapy (PERT) administered alongside fat-soluble vitamin supplements is a therapeutic strategy for individuals with CF and PI (Anthony *et al.*, 1999; Sabharwal, 2016). PERT aims to replace lipase, protease and amylase enzymes secreted from the pancreas in the non-CF GI tract, by an oral tablet taken with meals. Administration of PERT requires careful management as high doses of PERT taken over a long period causes fibrosing colonopathy (Smyth *et al.*, 1994; Pawel, de Chadarévian and Franco, 1997; Stevens *et al.*, 1998). To prevent the occurrence of fibrosing colonopathy in individuals receiving PERT, the UK Committee on Safety of Medicines (CSM) recommend that individuals with CF receiving PERT do exceed a daily dose of enzymes equivalent to 10,000 units lipase/kg body weight (Borowitz *et al.*, 2013).

Other common symptomatic therapies prescribed for the management of GI symptoms associated with CF include painkillers, antacid medication, anti-sickness medication, and laxatives. However the reported effectiveness of these therapies varies with one study concluding that whilst 94% of healthcare professionals felt medications helped relieve CF associated GI symptoms, only 58% of individuals with CF believed the same (Smith *et al.*, 2020). Interestingly the same study found that 48% of individuals with CF considered that non-medicated treatments such as exercise, changes in diet, massage and heat were effective in relieving their GI symptoms.

Arguably the most serious acute complication of CF in the intestine is intestinal blockage. Treatment of MI and DIOS is often tailored to the individual episode, however both are often successfully treated with enemas using osmotic agents containing polyethylene glycol (PEG) (De Lisle and Borowitz, 2013; Groves *et al.*, 2017). For individuals presenting with incomplete blockage, initial approaches to therapy typically involve oral rehydration and laxatives containing PEG (Houwen *et al.*, 2010; Subhi *et al.*, 2014). Cases of MI and DIOS that cannot be resolved using the above treatments require surgical intervention and, in most cases, if caught before intestinal rupture and sepsis occurs, a successful outcome is achieved.

1.6.2. Small molecule CFTR modulators

The aim of small molecule CFTR modulators is to increase CFTR-mediated Cl^- secretion by increasing either the expression or function of CFTR at the plasma membrane (Hadida *et al.*, 2014). Although CFTR modulators can broadly be classed as either correctors, potentiators, stabilisers or read through molecules, currently only correctors and potentiators are licenced for use in humans and will be discussed here. CFTR correctors repair defects in protein folding and trafficking to the plasma membrane, thereby increasing the amount of CFTR protein at the cell surface, whereas CFTR potentiators increase channel open probability (P_o), therefore increasing Cl^- flow through the channel (Hanrahan *et al.*, 2017; Jih *et al.*, 2017; Mijnders, Kleizen and Braakman, 2017). Given the differing ways CFTR correctors and potentiators work to rectify loss of function associated with *CFTR* mutations, certain drugs have higher efficacy when used with specific mutation classes. For example, CFTR correctors are of particular use for class II mutations, such as F508del, where mutations cause defects in protein trafficking. By contrast, CFTR potentiators are only effective for mutation classes where CFTR protein is correctly trafficked to the plasma membrane and is capable of endogenous activation, such as the G551D mutation (Kuk and Taylor-Cousar, 2015).

The CFTR potentiator VX-770 (Ivacaftor; Kalydeco), developed by Vertex Pharmaceuticals, was licenced for use in individuals with CF in 2012 (Hadida *et al.*, 2014), and first made available on the NHS to individuals with CF in 2016 (CF Trust UK). During phase 3 clinical trials VX-770 was found to be of significant benefit to individuals with at least one copy of the G551D gating mutation (Hadida *et al.*, 2014), but demonstrated negligible benefit for those homozygous for the F508del mutation, most likely a result of reduced CFTR expression at the plasma membrane (Flume *et al.*, 2012). One study published in 2017 hypothesised that the beneficial effects of Ivacaftor therapy in CF patients with the G551D *CFTR* mutation were a result of increased HCO_3^- secretion. Using an ingested capsule to measure gastric and intestinal pH, it was observed that, following one month of Ivacaftor therapy, patients exhibited an increased pH level in the small intestine after gastric emptying (Gelfond *et al.*, 2017). Currently in the UK VX-770 is available for individuals over 4 months of age with the gating mutations G551D (the most common gating mutation), G178R, S549N, S549R, G551S, G1244E, S1251N, S1255P and G1349D, and over 6 months of age with the R117H mutation (Guigui, Wang and Cohen, 2016; CF Trust UK).

To address the fact that VX-770 exhibits limited therapeutic benefit to those individuals with the F508del mutation [the most common *CFTR* mutation in Europe (Burgel *et al.*, 2015)] Vertex Pharmaceuticals developed the small molecule corrector VX-809 (Lumacaftor) (Jaques, Shakeel and Hoyle, 2020). However, whilst VX-809 was shown to increase plasma membrane expression of CFTR-F508del in bronchial epithelial cells, as a monotherapy VX-809 was found to have little clinical benefit in individuals homozygous for the F508del mutation (Van Goor *et al.*, 2011; Clancy *et al.*, 2012).

The combination therapy of VX-770 and VX-809, sold under the brand name Orkambi is available on the NHS in the UK for individuals with CF over the age of 2 years and homozygous for the F508del mutation (CF Trust UK). Prescribed in combination VX-770 and VX-809 correct the underlying folding defect in CFTR-F508del allowing for trafficking and expression within the cell membrane, and subsequently increase channel P_o. Despite promising data which emerged from *in vitro* studies where combined use of VX-770 and VX-809 restored CFTR-mediated Cl^- current to 25% of CFTR-wt levels in CFTR-F508del human bronchial epithelial cells (Van Goor *et al.*, 2011), the efficacy of Orkambi in Phase III patient trials was variable. In some reports, Orkambi achieved a significant improvement in lung function as measured by FEV_1 (forced expiratory volume in one second) (Elborn *et al.*, 2016; Konstan *et al.*, 2017; Ratjen *et al.*, 2017), however this was not found to be the case in others (Milla *et al.*, 2017; McNamara *et al.*, 2019).

More recently, new combination therapies have been licenced for use in individuals with CF, utilising the new corrector molecules VX-661 (tezacaftor) and VX-445 (elexacaftor). These include the VX-770/VX-661 (ivacaftor/tezacaftor; brand name Symkevi) combination therapy, and the VX-770/VX-661/VX-445 [ivacaftor/tezacaftor/elexacaftor; brand name Kaftrio (EU) or Trikafta (US)] triple therapy (Jaques, Shakeel and Hoyle, 2020). Symkevi was found to increase FEV_1 by 6.5% after 8-weeks treatment in individuals with one copy of the F508del mutation and one residual function mutation, and by 3.4% after 24-weeks treatment in individuals homozygous for the F508del mutation, in two phase III trials (EXPAND and EVOLE, respectively) (Rowe *et al.*, 2017; Taylor-Cousar *et al.*, 2017). The most recent drug to be licenced for use in individuals with CF and subsequently made available on the NHS is Kaftrio. Whilst not currently licenced for use in those under the age of 12 years in the UK, Kaftrio is available for individuals over 12 years of age with one copy of the F508del mutation combined with any other mutation type, and for those with gating or residual function mutation types (CF Trust UK). During phase III clinical trials, Kaftrio was found to increase FEV_1, reduce

lung exacerbation, and improve quality of life compared to placebo, Orkambi, and Symkevi (Keating *et al.*, 2018; Middleton *et al.*, 2019; Becq *et al.*, 2021).

1.6.3. Mutation independent therapy

Despite the clear progress made in CFTR modulator therapy over the last decade, these drug therapies are only effective for individuals with certain *CFTR* mutation types. Whilst these are the most common mutation types and therefore many individuals with CF have benefitted from these treatments, for individuals with rare mutations or class I mutations where no protein is made, the development of mutation-independent therapies provide a more likely source of CF therapy.

One approach to mutation-independent therapy is gene therapy, made possible by the sequencing and subsequent cloning of the *CFTR* gene in 1989 (Riordan *et al.*, 1989). Shortly after, viral vectors were used to express the *CFTR* gene in airway and pancreatic epithelial cells, resulting in functional CFTR at the plasma membrane (Drumm *et al.*, 1990; Rich *et al.*, 1990). However, the initial promise of this proof-of-concept work has to date not translated into effective gene therapies for CF. Initial worked focused on delivering CFTR cDNA directly to airway epithelia via aerosolized packaging vectors such as adenovirus and adeno-associated virus, however early work in this field was met by several hurdles including host defence reactions and inefficient targeted gene delivery (Zabner *et al.*, 1993; Harvey *et al.*, 1999; Khamsi, 2020). To overcome these hurdles, alternative non-viral delivery systems, such DNA-lipid/protein complexes and human artificial chromosome (HAC) delivery, have been developed, although to date clinical trials have not shown these methods to provide long term therapeutic benefit (Alton *et al.*, 2015; Colemeadow, Joyce and Turcanu, 2016). More recently attempts have been made by pharmaceutical companies such as Translate Bio and ReCode Therapeutics to deliver aerosolised mRNA and tRNA, respectively, to patients as an alternative to cDNA. However, despite early promise, a recent press release from Translate Bio reports that whilst inhaled mRNA has been delivered safely and in a well-tolerated fashion to individuals with CF, no increase in FEV_1 was observed (Translate Bio press release, March 2021).

The relatively recent discovery and application of the CRISPR/Cas9 gene editing system to *CFTR* gene correction has shown promise with publication of CRISPR/Cas9 homologous repair being used to correct the F508del allele in functional organoids derived from CF patient intestinal stem cells (Schwank *et al.*, 2013). However, 'traditional'

CRISPR/Cas9 gene editing is not only inefficient but also poses the risk of off-target double strand DNA breaks. New developments in gene editing, including alternate CRISPR-nucleases and Cas-9 fusion proteins have led to more efficient and accurate correction of *CFTR* mutations in patient derived airway epithelial cells and intestinal organoids (Maule *et al.*, 2019; Geurts *et al.*, 2020).

An alternative approach to restoring epithelial fluid secretion is to target the activity of channels and transporters within the epithelium other than CFTR, removing the challenges posed by rescuing CFTR, itself. This type of mutation-independent therapy is known as bypass therapy and poses the advantage of working for all individuals with CF, regardless of their *CFTR* mutation (Li *et al.*, 2017). Typically bypass therapies aim to compensate for the loss of CFTR-mediated Cl^- section by activating or upregulating alternate Cl^- channels such as CaCC, and/or preventing unregulated Na^+ absorption by proteins such as ENaC and NHE3 (Becq *et al.*, 2011).

The inhibition of Na^+ absorption by NHE3 has become a focus of intestinal bypass therapy in recent years with the aim of preventing DIOS in individuals with CF. Inhibition of NHE3-mediated Na^+/H^+ exchange would not only help to maintain the luminal concentration of Na^+ and therefore the osmotic gradient required to drive H_2O across the intestinal epithelia, it would also prevent unregulated H^+ transport across the epithelium helping to prevent acidification of the small intestine. This therapeutic approach is particularly attractive as NHE3 inhibiting drugs are already licensed for use in humans to treat constipation and if found to be effective could be repurposed for use in treating GI symptoms associated with CF. Studies in $CFTR^{-/-}$ $NHE3^{-/+}$, and $CFTR^{-/-}$ $NHE3^{-/-}$ mice provide supportive evidence for this novel approach as both $CFTR^{-/-}$ $NHE3^{-/+}$, and $CFTR^{-/-}$ $NHE3^{-/-}$ mice demonstrate increased luminal fluidity and increased survival compared to $CFTR^{-/-}$ $NHE3^{+/+}$ mice (Bradford *et al.*, 2009). Tenapanor, linaclotide and lubiprostone are licensed drugs which all act to inhibit the activity of NHE3. Tenapanor is a direct inhibitor of NHE3, and has demonstrated efficacy in relieving intestinal symptoms and constipation in individuals with constipation-predominant irritable bowel syndrome (Chey, Lembo and Rosenbaum, 2017; Chey *et al.*, 2021). Linaclotide is a ligand for the transmembrane receptor GCC, increasing intracellular levels of cGMP and ultimately inhibiting NHE3 activity (Steinbrecher, 2014; Ahsan *et al.*, 2017), whereas the synthetic eicosanoid lubiprostone, is a ligand for EP1 and EP4 prostaglandin receptors, activating CFTR and inhibiting NHE3 via the cAMP/PKA pathway (Bassil *et al.*, 2008; Bijvelds *et al.*, 2009). Originally used to treat chronic constipation, lubiprostone is also a PKA-independent activator of ClC-2 channels (Cuppoletti *et al.*, 2004; O'Brien, Anderson

and Stowe, 2010). Studies using these drugs in *CFTR* null and homozygous CFTR-F508del mice concluded that tenapanor, linaclotide and lubiprostone all reduced fluid absorption in the jejunum, and, with the exception of linaclotide, in the colon (Tan *et al.*, 2021).

1.7. Organoids as models for studying intestinal ion transport in CF

The availability of models for the study of the multicellular, multifunctional, and complex intestinal environment has until relatively recently been limited to *in vitro* 2D cellular models and *in vivo* animal models. While both models possess their own merits and have undoubtedly contributed to advancements in many fields of research, the use of these models each has a unique set of limitations. Animal models recapitulate the complex cellular architecture and micro-environment found within the intestines, which is extremely difficult to reproduce *in vitro* using traditional 2D intestinal cell models, typically comprising a single cell type. This renders animal models of particular use in drug development, as well as the pathophysiology of gastrointestinal disease and cellular differentiation and stem cell renewal (Simon-Assmann *et al.*, 2007). However, experimental conditions using *in vivo* models are often hard to control and reproduce. Additionally, it can be challenging to study simplified elements of otherwise complex processes in whole animal models (Costa and Ahluwalia, 2019). *In vitro* 2D human intestinal cell models, although lacking the tissue level complexity of *in vivo* animal models, overcome many of their limitations, as well as the associated ethical and financial considerations and importantly allow for study using a human derived model.

Attempts to develop cell lines derived from healthy colon have historically been unsuccessful, however in the 1960s the first of many human colonic carcinoma cell lines was established, the HT-29 cell line (Simon-Assmann *et al.*, 2007). Since then, the application of established human colonic cell lines had been wide reaching, especially in cancer biology and developmental biology. Isolated human adenocarcinoma cells lines, such as the Caco-2, HT29, and T84 cell lines, differentiate and form polarised epithelia when cultured under the correct conditions, and in the case of the Caco-2 and HT-29 cell lines, the formation of 3D spheroids too (Samy *et al.*, 2019; Gheytanchi *et al.*, 2021). When grown to confluency, the Caco-2 cell line form polarised epithelia, with cells demonstrating apical microvilli, neighbouring cells joined by tight junctions, and the secretion of intestinal hydrolases (Sambuy *et al.*, 2005). Similarly, the T84 cell line, when

grown to confluency, produces polarised epithelia joined by tight junctions, and has been demonstrated to secrete Cl^- via apical membrane channels (McCool *et al.*, 1990). It is also reported that T84 epithelia contain discrete populations of Cl^- secreting and mucin secreting cells (McCool *et al.*, 1990). Unlike the Caco-2 and T84 cell lines, HT-29 cell line differentiation relies on the manipulation of culture medium, with different culture medium compositions resulting in differentiation into epithelia displaying different differentiated cell populations (Simon-Assmann *et al.*, 2007).

Derived from stem cells, intestinal organoids are 3D self-organising populations of cells which maintain the cellular heterogeneity and function of the intestinal epithelium (Rahmani *et al.*, 2019). The optimisation of intestinal organoid technology initiated their use in an extensive range of applications including drug development, disease modelling, regenerative medicine, and cellular proliferation studies (Costa and Ahluwalia, 2019). It is possible to produce intestinal organoids from both Lgr5+ stem cells isolated from human intestinal biopsies, and from pluripotent stem cells [either induced pluripotent stem cells (iPSCs) or embryonic stem cells (ESCs)] (Sato *et al.*, 2009, 2011; McCracken *et al.*, 2011; Date and Sato, 2015; Aurora and Spence, 2016). However, most work using intestinal organoids for the purpose of CF research utilise Lgr5+ stem cell derived organoids in order to capture the genotypes of the individuals the biopsies were collected from. Figure 1-5 shows an overview of the method used to produce intestinal organoids from Lgr5+ stem cells.

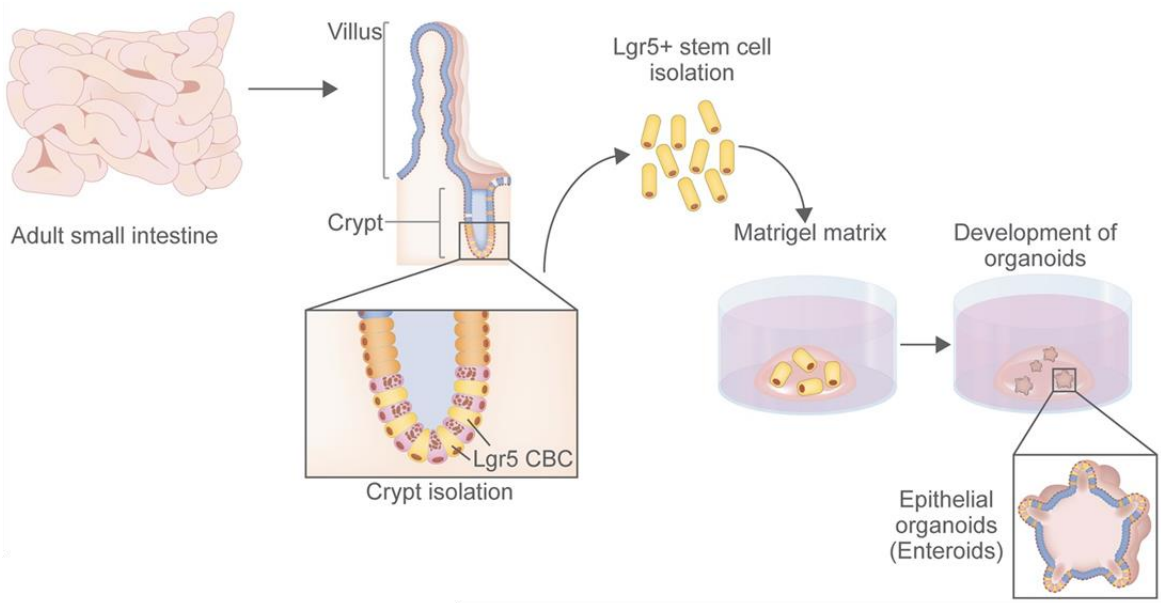

Figure 1-5: Human intestinal spheroids cultured using Sacrificial Micromolding as a model system for studying drug transport.

Lgr5+ stem cells are isolated from biopsied intestinal tissue before seeding into extracellular support matrix (ECM) and bathed in culture medium containing specific growth factors to promote stem cell proliferation and differentiation. Key growth factors in the culture of intestinal organoids are Wnt-3a, EGF, noggin and r-spondin. Figure adapted with permission from Rahmani et al. (2019).

Intestinal organoids have been shown to demonstrate CFTR-dependent luminal ion and fluid secretion when stimulated with secretagogues such as forskolin (FSK), which in turn leads to the quantifiable swelling of organoids. This phenomenon led to the development of forskolin-induced swelling (FIS) assay, whereby the degree of FIS relates to cAMP-mediated CFTR-dependent ion and fluid secretion (Dekkers *et al.*, 2013; Boj *et al.*, 2017). Organoids derived from the colon and small intestine of individuals with CF have been used to study the effect different *CFTR* mutations have on intestinal ion and fluid secretion, and therefore extent of FIS (Dekkers *et al.*, 2013). Patient derived organoids have also been used to screen CFTR modulators to determine which drug therapies are most effective at restoring correct ion and fluid homeostasis to the CF intestine (Dekkers, Berkers, *et al.*, 2016; Dekkers, Van Mourik, *et al.*, 2016). As discussed in Section 1.6.2 CFTR modulators demonstrate differing efficacy in restoring CFTR-mediated Cl^- secretion depending on the class of CFTR mutation and mechanism of drug action. While current drug therapies effectively restore CFTR function to many individuals with CF, for those individuals with rarer mutation types, the costly and time-consuming nature of clinical trials renders conventional methods of identifying effective drugs unfeasible

(Boj *et al.*, 2017). For these individuals, organoids generated from their intestinal stem cells provide a unique tool for the development of personalised medicines. A library of intestinal organoids expressing differing CFTR genotypes would also be of great use in the screening of future drug treatments, as well as in the development of mutation-independent therapeutics for intestinal disease in CF.

The potential of intestinal organoids as a tool for the study of intestinal ion transport and the development of novel and personalised drug treatments for CF are clear. However, intestinal organoid technology is not without limitations, as organoid cultures are expensive to maintain and require more complex tissue culture methodologies than many 2D cellular models. Additionally, biopsies of small and large intestinal tissue, necessary to harvest stem cells from individuals with CF, are painful and invasive. This is particularly true for small intestinal biopsies, which are also difficult to acquire.

Some isolated adenoma and carcinoma cell lines, such as the colonic adenocarcinoma LIM1863, Caco-2 and HT-29 cell lines, are reported to grow as 3D spheroids (Whitehead *et al.*, 1987; Gheytanchi *et al.*, 2021). The LIM1863 cell line expresses epithelial ion channels and transporters such as CFTR, ENaC, NKCC1, and NHE1-3 (Currid, Ortega and Valverde, 2004). What's more, the lumen of LIM1863 spheroids have been shown to swell in response to secretagogues such as forskolin, as a result of Cl^--mediated fluid secretion (Currid, Ortega and Valverde, 2004). While human carcinoma colonic cell lines grown as 3D spheroids provide an *in vitro* environment similar to that of the *in vitro* intestinal organoid, the cell populations do not originate from intestinal stem cells. Instead, cell populations are maintained by standard cell division and influenced by growth factors contained within culture medium, therefore the capacity of these cell lines to reflect all cell populations found within the intestinal epithelium is limited.

The use of colonic adenoma and carcinoma cell lines as 3D spheroid models for studying epithelial ion and fluid secretion has not been fully explored given the availability of primary intestinal organoids. However, it is possible that in addition to the LIM1863 cell line, one or more colonic cell lines could form 3D spheroids suitable for use in FIS assays, and 2D polarised epithelial monolayers suitable for Ussing chamber studies of epithelial ion channels. If this were found to be the case, novel cell line models of 2D and 3D intestinal ion transport could be used as alternative cost-effective and high-throughput screening tools to identify and develop new therapies for the treatment of GI disease in CF.

1.8. Hypotheses

- Cell lines derived from colonic epithelia will express ion channels, pumps and transporters associated with CFTR-mediated intestinal salt and fluid transport.
- One or more cell lines derived from colonic epithelia will provide a suitable model for the study of 2D and 3D intestinal ion and fluid transport.
- NHE3 will prove an effective CFTR mutation independent therapeutic target for the alleviation of gastrointestinal symptoms in the CF intestine.

1.9. Aims

- To identify an intestinal cell line for studies of intestinal ion transport.
- Ensure suitable cell line models expresses CFTR, and grow as 2D epithelia for Ussing chamber studies, and 3D spheroids for FIS assays.
- Optimise a FIS assay for use in 3D cell line models of intestinal ion transport, allowing for automated image acquisition and analysis.
- Determine the contribution of NHE3-mediated Na^+ absorption to intestinal salt and fluid transport.
- Assess the potential of NHE3 inhibition by three licenced NHE3 inhibitors, as a therapeutic strategy for alleviating GI disease associated with CF.

Chapter 2. Materials and Methods

The materials and methods described below are those that were used throughout this thesis. The methods described include tissue culture techniques, protein biochemistry methods, molecular biology techniques, and electrophysiology techniques.

2.1. Materials

2.1.1. Buffers and Solutions

Phosphate Buffered Saline (PBS): 1.1 mM KH_2PO_4, 155.2 mM NaCl, 3 mM $Na_2HPO_4 \cdot 7H_2O$ (Thermo Fisher Scientific)

0.05% Trypsin-EDTA: 0.05% (w/v) Trypsin with 0.48 mM EDTA $4Na \cdot 2H_2O$ (Thermo Fisher Scientific)

0.1% Trypsin EDTA: 0.1% (w/v) Trypsin (Difco, Becton Dickinson) with 0.1% (w/v) EDTA (Sigma-Aldrich)

Cell Lysis Buffer: 20 mM Tris-HCl (pH 7.5), 150 mM NaCl, 1 mM Na_2EDTA, 7 mM EGTA, 1% (v/v) Triton, 2.5 mM sodium pyrophosphate, 1 mM β-glycerophosphate, 1 mM Na_3VO_4, 1 µg/µl leupeptin (Cell Signalling Technology). One tablet of Protease Inhibitor Cocktail (Roche) per 10 ml cell lysis buffer.

Sample Buffer: 50 mM Tris-HCl, 2 mM EDTA, 12% (w/v) glycerol, 10% (v/v) SDS, 10% (v/v) β-mercaptoethanol, pH 6.8

Tris Buffered Saline (TBS) Tween: 25 mM Tris, 150 mM NaCl, 0.02% (v/v) TWEEN-20 (Sigma-Aldrich), pH 7.7

Isotonic Hanks Solution: 140 mM NaCl, 2.5 mM KCl, 1.2 mM $CaCl_2$, 0.5 mM $MgCl_2$, 10 mM HEPES, 5 mM glucose, pH 7.4, 300 mOsm

Basolateral (high Cl^-) Ussing Chamber Solution: 140 mM NaCl, 5 mM KCl, 0.5 mM $MgCl_2$, 0.36 mM K_2HPO_4, 0.44 mM KH_2PO_4, 1.3 mM $CaCl_2$, 10 mM HEPES, 4.2 mM $NaHCO_3$, pH 7.2

Apical (low Cl^-) Ussing Chamber Solution: 133.3 mM Na-gluconate, 5 mM K-gluconate, 0.5 mM $MgCl_2$, 0.36 mM K_2HPO_4, 0.44 mM KH_2PO_4, 5.65 mM $CaCl_2$, 10 mM HEPES, 4.2 mM $NaHCO_3$, pH 7.2

2.1.2. Bacterial strains and growth medium

One Shot® Stbl3™ chemically competent *Escherichia coli* (*E. Coli*, Thermo Fisher Scientific) were used to bacterially transform the XLG3-NHE3 construct (please refer to Section 2.1.3 for further detail). Liquid bacterial cultures were grown in Luria Broth (Sigma-Aldrich): 10 g/L Tryptone, 5 g/L yeast extract, 10 g/L NaCl, pH 7. For LB-agar: 1.6 g/100 ml agar (Lab M).
Ampicillin (Sigma-Aldrich) 0.1 mg/ml was used for selection of the XLG3-NHE3 construct.

2.1.3. Plasmid vectors

XLG3-GFP (XLG3eGFP lentiviral vector provided by Dr Giles Cory (University of Exeter) but with the addition of a modified multiple cloning site).
XLG3-NHE3 (modified XLG3eGFP with NHE3 cDNA).

2.1.4. siRNA sequences

ON-TARGETplus Human SLC9A3 (NHE3) siRNA – SMARTpool was ordered and produced by Dharmacon™ (Horizon Discovery).

ON-TARGETplus non-targeting control siRNA - control #3 – produced by Dharmacon™ (Horizon Discovery).

siRNA	Sequence ID	Sense (5'-3')	Anti-Sense (5'-3')
NHE3 (SLC9A3)	J-007624-05	GGACAGAUCGGGCACAAUU	AAUUGUGCCCGAUCUGUCC
NHE3 (SLC9A3)	J-007624-06	CCACAUCGCGUCCUUCACA	UGUGAAGGACGCGAUGUGG
NHE3 (SLC9A3)	J-007624-07	CCACGGAGGACGAGAAACA	UGUUUCUCGUCCUCCGUGG
NHE3 (SLC9A3)	J-007624-08	GCACCACCAUCAUCGUAGU	ACUACGAUGAUGGUGGUGC

Table 2-1: siRNA sequences.
Sequence ID and sequence of NHE3-targeting siRNA used in this thesis.

2.1.5. Drug treatments

Treatment	Solvent	Stock Concentration	Final Concentration	Supplier
Amiloride	DMSO	10 mM	10 µM	Sigma-Aldrich
Bumetanide	DMSO	100 mM	100 µM	Sigma-Aldrich
$CFTR_{inh}$-172 (I-172)	DMSO	10 mM	10 µM	Sigma-Aldrich
Forskolin	Methanol	10 mM	10 µM	Sigma-Aldrich
Genistein	DMSO	50 mM	50 µM	Sigma-Aldrich
Ionomycin	DMSO	1 mM	2 µM	Sigma-Aldrich
Linaclotide	DMSO	10 mM	10 nM – 300 µM	Cayman Chemical,
Lubiprostone	DMSO	10 mM	10 nM – 1 mM	Adooq Bioscience
Niflumic Acid	DMSO	100 mM	200 µM	Sigma-Aldrich
Ouabain	DMSO	100 mM	1 µM	Sigma-Aldrich
Tenapanor	DMSO	1 mM	10 nM - 10 µM	Adooq Bioscience
Uridine-5'-triphosphate	ddH_2O	100 mM	1 mM	Sigma-Aldrich

Table 2-2: Drug treatments.

Drug treatments used in this thesis along with their supplier. Final concentration refers to the concentration at which each compound was routinely used. For those drugs used in dose-response experiments, the range of concentrations used is indicated.

2.1.6. Primary antibodies

Antibody Name	Species	Protein Target	Type	Isotype	Source
α-Tubulin	Mouse	α-Tubulin	Monoclonal	IgG_1	Sigma- Aldrich
Calnexin	Rabbit	Calnexin (ER marker)	Polyclonal	IgG	Santa Cruz
CFTR-570	Mouse	CFTR R-domain aa 731-742	Monoclonal	IgG_1	JR Riordan (University of North Carolina)*
CFTR-596	Mouse	CFTR NBD2 aa 1204-1211	Monoclonal	IgG_{2b}	JR Riordan (University of North Carolina)*
CFTR-660	Mouse	CFTR NBD1 aa 576-585	Monoclonal	IgG_{2b}	JR Riordan (University of North Carolina)*
CFTR-769	Mouse	CFTR NBD2 aa 1204-1211	Monoclonal	IgG_1	JR Riordan (University of North Carolina)*
GAPDH	Mouse	Glyceraldehyde 3-phosphate dehydrogenase (GAPDH)	Monoclonal	IgG2b	Proteintech
Mr Pink	Rabbit	CFTR NBD1	Polyclonal		I Braakman (Utrecht University)
NHE3	Rabbit	Solute carrier family 9 (sodium/hydrogen exchanger) member 3.	Polyclonal	IgG	Proteintech

Table 2-3: Primary antibodies.

*Primary antibodies used throughout this thesis. CFTR (cystic fibrosis transmembrane conductance regulator), R-domain (regulatory-domain), NBD1 (nucleotide-binding domain 1), NBD2 (nucleotide-binding domain 2). * Distributed by Cystic Fibrosis Foundation Therapeutics.*

2.1.7. Secondary antibodies

Swine anti-rabbit, HRP conjugated (DAKO)
Rabbit anti-mouse, HRP conjugated (DAKO)

2.1.8. Q-RT-PCR primers

All primer sets were ordered and produced by Qiagen.

Primer Assay Set	Gene Symbol	Gene Product	Catalogue Number
CFTR	CFTR	Cystic fibrosis transmembrane conductance regulator	QT00070007
EP1	PTGER1	Prostaglandin E receptor 1	QT00210070
EP4	PTGER2	Prostaglandin E receptor 4	QT02288314
GCC	GUCY2C	Guanylyl cyclase 2C	QT00087619
HPRT	HPRT1	Hypoxanthine-guanine phosphoribosyltransferase	QT00059066
NHE3	SLC9A3	Solute carrier family 9 member 3	QT00095914
TBP	TBP	TATA-binding protein	QT00000721

Table 2-4: Qiagen QuantiTect® primer assay sets.
Primer assay sets used in this thesis along with corresponding gene targets and catalogue numbers.

2.1.9. Microscopes

Widefield microscopy: Leica LASX workstation (10x dry lens, 0.32 NA), with motorised stage, Wolfson Imaging Suite, University of Bristol

Spinning disk microscopy: Perkin Elmer UltraVIEW ERS 6FE confocal system attached to a Leica DM I6000 inverted epifluorescence microscope (10x dry lens, 0.4 NA), Wolfson Imaging Suite, University of Bristol
Tissue culture microscopy: Nikon TMS 10x lens

2.1.10. Ussing chamber

Warner Instrument Corp. Epithelial Voltage-Clamp (model EC-825; Warner Instruments).

Dual channel Ussing chamber system (model U2500; Warner Instruments).

2.1.11. Data processing

Swelling assay analysis:	Fiji/ImageJ software
Ussing chamber data acquisition	pCLAMP 10.7, Clampfit
Ussing chamber analysis:	AxoScope data acquisition and analysis software (version 8.2, Molecular Devices)
Flow cytometry analysis:	FlowJo software
Data analysis:	Microsoft Excel
	GraphPad Prism 8
Statistical Analysis:	GraphPad Prism 8
	SigmaPlot

2.2. Bacterial growth and isolation

2.2.1. Transformation of heat shocked *E. coli*

One Shot® Stbl3™ chemically competent *E. coli* were transformed with XLG3-NHE3. Briefly, *E. coli* were allowed to defrost on ice; 50 µl of cells were then added to a tube with 2 µg of plasmid DNA and left to incubate on ice for 1-hour. Following incubation, the cells were heat shocked in a 42 °C water bath for 40-seconds, before a further 2-minute incubation on ice. 250 µl of pre-warmed LB media was then added to the cells before they were incubated at 37 °C for 45-minutes in a rotary incubator (250 rpm). For selection, 100 µl of the transformed bacteria were then spread onto a pre-warmed LB agar plate containing ampicillin (0.1 mg/ml).

2.2.2. Large-scale DNA purification

The Qiagen Plasmid Maxi kit (Qiagen) was used for large-scale DNA purification (Maxipreps), according to the manufacturer's protocol. For each Maxiprep, a starter culture was produced by inoculating 5 ml of LB media containing ampicillin (0.1 mg/ml) with a single bacterial colony. The starter culture was incubated at 37 °C in a rotary incubator (250 rpm) for approximately 8-hours and then diluted 1 in 1000 into 250 ml LB media also containing 0.1 mg/ml ampicillin, which in turn was incubated overnight at 37 °C in a rotary incubator (250 rpm). Bacteria from the overnight culture were harvested the following morning by centrifugation at 6000 g for 15-minutes at 4 °C using either a Sorvall RC3Plus (rotor HLR-6) or a Sorvall RC6 (rotor SLA–1500) centrifuge. The concentration of isolated bacterial DNA was measured (see Section 2.2.3), and diluted to a concentration of 1 mg/ml for storage at –20 °C.

2.2.3. Measuring DNA concentration

DNA concentration was determined by measuring the absorbance at 260 nm using a NanoDrop ND-1000 spectrophotometer (Labtech International) and calculated according to the Beer Lambert Law for nucleic acids (Cammack *et al.*, 2008).

2.3. Tissue culture methods

2.3.1. BHK cell culture

BHK (baby hamster kidney) cells, both mock transduced (BHK-mock) and transduced with wild-type human CFTR (BHK-CFTR wt), were cultured in Dulbecco's Modified Eagle's Medium/F12 Medium (DMEM/F12 (1:1)) with GlutaMAX (Gibco) containing 5% (v/v) foetal calf serum (Thermo Fisher Scientific), 100 units/ml penicillin and 100 µg/ml streptomycin (Sigma-Aldrich). Culture medium for BHK cells transduced with wild-type human CFTR also contained the selection agent methotrexate (25 µg/ml) (Merck). All BHK cell lines were incubated at 37 °C in a humidified atmosphere of 5% CO_2. Cells were passaged for between 10 - 15 passages post thawing, at which point a new aliquot of cells was thawed and used for experiments.

2.3.2. HEK293T cell culture

HEK293T cells (human embryonic kidney 293 cell line) were cultured in Dulbecco's Modified Eagle's Medium (DMEM) with GlutaMAX (Thermo Fisher Scientific) containing 10% (v/v) foetal calf serum (Thermo Fisher Scientific). Cells were incubated at 37 °C in 5% CO_2. Cells were passaged for between 10 - 15 passages post thawing, at which point a new aliquot of cells was thawed and used for experiments.

2.3.3. LIM1863 spheroid culture

LIM1863 spheroids (sporadic colorectal cancer cell line) were cultured in suspension in Roswell Park Memorial Institute 1640 Medium (RPMI 1640) with GlutaMAX (Gibco) containing 5% (v/v) foetal calf serum (Thermo Fisher Scientific), 100 units/ml penicillin and 100 µg/ml streptomycin (Sigma-Aldrich), 1 µg/ml hydrocortisone (Sigma-Aldrich), 0.01 mM α-monothioglycerol (Sigma-Aldrich) and 1 µg/ml insulin (Sigma-Aldrich). LIM1863 spheroids were passaged every three days or as required by trituration to break large spheroids down into smaller ones. Spheroids were cultured at 37 °C in a humidified atmosphere of 5% CO_2. Cells were passaged for between 10 - 15 passages post thawing, at which point a new aliquot of cells was thawed and used for experiments.

For single cell LIM1863 cultures, spheroids were cultured in calcium free Minimum Essential Medium - Suspension (S-MEM) without GlutaMAX (Gibco) containing 1% (v/v) foetal calf serum (Thermo Fisher Scientific). Spheroids were incubated at 37 °C in 5% CO_2 for 48 hours at which point a single cell culture was achieved.

2.3.4. Adenoma and carcinoma cell line 2D culture

All human colonic adenoma and carcinoma cell lines were a generous gift from Prof. Ann Williams, School of Cellular and Molecular Medicine, University of Bristol, UK. All colonic adenoma and carcinoma cell lines were mycoplasma free. Caco-2, AN/C1, HCA7, HT29, SW1463, SW620, SW480, Lovo and LS174T cell lines were cultured in Dulbecco's Modified Eagle's Medium (DMEM) with 4500 mg/L glucose (Sigma-Aldrich), containing 10% (v/v) foetal calf serum (Thermo Fisher Scientific), 2 mM glutamine (Thermo Fisher Scientific), 100 units/ml penicillin and 100 µg/ml streptomycin (Sigma-Aldrich). The RG/C2, AA/C1 and AA/C1/SB/10C cell lines were cultured in Dulbecco's Modified Eagle's Medium (DMEM) with 4500 mg/L glucose (Sigma-Aldrich), containing 20% (v/v)

foetal calf serum (Thermo Fisher Scientific), 2 mM glutamine (Thermo Fisher Scientific), 1 µg/ml hydrocortisone (Sigma-Aldrich), 0.2 units/ml Insulin (Sigma-Aldrich), 100 units/ml penicillin and 100 µg/ml streptomycin (Sigma-Aldrich). HCT116 cells were cultured in McCoy's 5A Modified Medium with 3000 mg/L glucose (Thermo Fisher Scientific), containing 10% (v/v) foetal calf serum (Thermo Fisher Scientific), 2 mM glutamine (Thermo Fisher Scientific), 100 units/ml penicillin and 100 µg/ml streptomycin (Sigma-Aldrich).

All human colonic adenoma and carcinoma cell lines were incubated in a dry incubator at 37 °C in an atmosphere of 5% CO_2. Cell lines were routinely passaged once they had reached confluency using 0.1% Trypsin EDTA. Cells were passaged for between 10 - 15 passages post thawing, at which point a new aliquot of cells was thawed and used for experiments.

2.3.5. HCA7 3D spheroid culture

HCA7 (human adenocarcinoma, colon) cells from 2D culture were trypsinized (0.1% Trypsin-EDTA), washed in Dulbecco's Modified Eagle's Medium/Ham's F12 (Advanced DMEM/F12, Thermo Fisher Scientific) and resuspended in PBS. Remaining cell clumps were broken up by triturating using an 18G needle, the cell suspension was then passed through a 40 µm cell strainer to ensure a single cell suspension and the cells counted. 50 µl of thawed Matrigel (Growth Factor Reduced, lactose dehydrogenase elevating virus free, Corning), containing ~400 single HCA7 cells, was placed as a dome into wells of a pre-warmed 24 well plate which was subsequently incubated at 37 °C for 10-minutes to allow the Matrigel to solidify. Alternatively, 5 µl of thawed Matrigel containing ~40 single HCA7 cells, was placed as a dome into wells of a pre-warmed 96 well plate. Once solidified, 500 µl Advanced DMEM/F12 containing 0.1% BSA (w/v) (Sigma-Aldrich), 2 mM glutamine (Thermo Fisher Scientific), 10 mM HEPES (Sigma-Aldrich), 1 mM N-Acetyl-L-cysteine (Sigma-Aldrich), 1x N-2 supplement (Thermo Fisher Scientific), 1x B27 supplement (Thermo Fisher Scientific), 100 units/ml penicillin and 100 µg/ml streptomycin (Sigma-Aldrich) was added to each well containing Matrigel. For wells of a 96 well plate containing 5 µl Matrigel, 100 µl of the above medium was added. Wells that did not contain Matrigel were filled with sterile PBS; the plate was placed into a plastic container containing damp tissue and the spheroids incubated in a dry incubator at 37 °C in an atmosphere of 5% CO_2. Medium changes took place on days 7, 11 and 14 of culture after which point the spheroids were used for swelling assays (described in Section 2.6).

2.4. Transfection and transduction of cells

2.4.1. siRNA transient transfection of the colonic adenocarcinoma LS174T cell line

ON-TARGETplus Human SLC9A3 SMARTpool siRNA and ON-TARGETplus non-targeting control siRNA - control #3 were prepared to a final concentration of 100 µM in nuclease free water and stored at –20 °C. Transfections were performed using Lipofectamine RNAiMax (Thermo Fisher Scientific) according to the manufacturer's instructions.

24-hours before transfection, LS174T cells that had reached ~70% confluency in T25 tissue culture flasks (Corning) were medium changed into appropriate DMEM (see Section 2.3.4) without the addition of antibiotics.

On the day of transfection two microcentrifuge tubes per transfection were set up as follows:

Tube A		**Tube B**		**Final seeding volume**	**Final siRNA concentration**
Optimem*	Lipofectamine RNAiMax	Optimem	siRNA (100 µM stock)**	2 ml	50 nM
250 µl	5 µl	250 µl	1 µl		

Table 2-5: Preparation of siRNA transfection mix.

Details of tube A and tube B transfection mix preparations, prior to combination and addition to cells.
** Optimem Reduced-Serum Medium (Thermo Fisher Scientific)*
*** siNHE3 or non-targeting control siRNA*

After incubation at room temperature for 5-minutes, tube A was added dropwise to tube B whilst tube B was gently agitated, and the combined mix allowed to incubate at room temperature for a further 20-minutes. During incubation of this transfection mixture, LS174T cells that had been cultured in antibiotic-free culture medium were trypsinised,

washed in PBS, resuspended in antibiotic free culture medium and counted. For each transfection, $2x10^6$ cells, in antibiotic free DMEM (not exceeding a maximum volume of 1.5 ml), were added to a T12.5 tissue culture flask (Corning). To each flask of LS174T cells, 500 µl of siRNA complex was added and the final volume of each flask was made up to 2 ml. Cells were incubated at 37 °C for 24-hours before the medium was changed to DMEM containing antibiotics as described in Section 2.3.4. Cells were prepared for protein lysate samples at 24-, 48-, 74- and 168-hours post transfection.

2.4.2. Transfection of HEK cells to produce Lentivirus

For each transfection, 20 µg XLG3-NHE3, 5 µg envelope plasmid pMD2.VSVG, 15 µg packaging plasmid pPAX in 250 µl H_2O, along with 250 µl 0.5 M $CaCl_2$ was added to a microcentrifuge tube at room temperature. 500 µl of 2x HBSS (HEPES-buffered saline solution) was then added whilst the mixture was vortexed vigorously for a minimum of 1 minute. After precipitation at room temperature for 25 minutes, the transfection mix was added dropwise to a plate of confluent HEK293T cells in 5 ml DMEM containing 10% (v/v) foetal calf serum. After 24 hours incubation at 37 °C in 5% CO_2, the DMEM was removed from the adherent HEK293T cells and replaced with 5 ml of HCA7 medium (see Section 2.3.4), and the cells incubated at 37 °C in 5% CO_2 for a further 48 hours. Lentivirus containing XLG3-NHE3 was isolated from the medium and concentrated using Lenti-X Concentrator (Clontech) according to the manufacturer's protocol. Concentrated virus was resuspended in 50 µl HCA7 medium and stored at –80 °C.

2.5. LIM1863 swelling assay

2.5.1. Calcein green staining

Calcein green staining is commonly used to label viable cells. During initial swelling assays calcein green staining was used to differentiate live cells forming the LIM1863 spheroid epithelium from both the spheroid lumen and unoccupied spaces between spheroids. It was anticipated that this would aid the automation of FIS assay analysis. For calcein green staining, LIM1863 spheroids were incubated with 10 µM CellTrace™ Calcein Green, AM (Thermo Fisher Scientific) in RPMI 1640 for 30-minutes at 37 °C and protected from light. Spheroids were then centrifuged at 180 g for 1-minute at RT and resuspended in RPMI 1640 before seeding onto Matrigel coated plates for use in swelling assays.

2.5.2. LIM1863 seeding

24-hours prior to use, 24 or 96 well tissue culture plates were coated with 0.16 mg/ml Matrigel in RPMI 1640 with GlutaMAX, incubated at room temperature for 1-hour and then stored at +4 °C until required. Immediately prior to use, Matrigel coated plates were incubated at 37 °C for 1-hour and excess Matrigel removed. An appropriate amount of LIM1683 spheroids, suspended in RPMI 1640 with GlutaMAX, were seeded into coated wells and allowed to settle for 30-minutes, after which excess media was removed and 200 µl isotonic Hanks solution added to each well.

2.5.3. Image acquisition

For image acquisition using a spinning disk microscope, wells containing LIM1863 spheroids were treated and imaged one at a time to prevent pre-seeded wells from drying out. For each well, an appropriate field of view was selected, and z-stack limits defined (7 µm intervals) before the addition of 50 µl of the desired drug stock to give the final drug concentration detailed in Section 2.1.5. Image acquisition began immediately, and z-stacks were obtained every 2-minutes for a total of 30 minutes. During initial experiments, both phase contrast and calcein green images were acquired, however during subsequent experiments only phase contrast images were acquired. For calcein green image acquisition, an argon laser was used with an excitation filter of 540-552 nm and an emission filter of 580-620 nm. All imaging took place at 37 °C.

For image acquisition using a widefield microscope, multiple well positions were imaged simultaneously using a motorised stage. For each well, the x and y coordinates of one or more fields of view were saved, and for each field the z-stack limits defined (7 µm intervals). Drug addition and image acquisition took place as described for spinning disk microscopy; however only phase contrast images were acquired. All data were acquired at 37 °C.

2.5.4. Manual Image analysis

Fiji/ImageJ was used to manually measure the area in pixels (px^2) of each selected spheroid lumen or total spheroid area at desired timepoints. To reduce experimenter bias, spheroids to be analysed were picked at random from the final timepoint image before any measurements took place.

For quantification of spheroid area change, LIM1863 spheroid area in px^2 was obtained from Fiji/ImageJ and normalised to time t = 0 minutes (hereafter referred to as T0; T0 = 100%).

For quantification of epithelial area change, lumen area (px^2) was subtracted from spheroid area (px^2), and this in turn was normalised to epithelial area at T0 (T0 = 100%).

For quantification of lumen area change, LIM1863 spheroid lumen area (px^2) was calculated and normalised to T0 (T0 = 100%).

For quantification of normalised spheroid lumen area, LIM1863 spheroid lumen area (px^2) was normalised to radius of corresponding spheroid (px) at T0, this was then normalised to that at T0 (T0 = 100%).

2.5.5. Automated Image Analysis

For automated image analysis of LIM1863 spheroids a Lumina tracking plugin was designed by Dr Stephen Cross (Wolfson Bioimaging, University of Bristol) in MATLAB® for use in Fiji/ImageJ. For each field of view to be analysed the user selected an image from the appropriate z-stack, that represented a plane with the widest cross-section through multiple spheroids. As spheroids rested on the bottom of multi-well plates, several spheroids could be analysed from one image. The software then used pixel intensity to distinguish between spheroid lumen and epithelial cells, to quantify lumen area in $pixel^2$ (px^2). As LIM1863 spheroids were not securely attached to the multi-well plate, spheroids often drifted over the duration of the assay, and as such automated spheroid tracking between timepoints was not possible. Matching of spheroid data between timepoints required manual input.

2.6. HCA7 swelling assay

2.6.1. Image acquisition

Swelling assays took place using HCA7 spheroids grown for 14 days as described in Section 2.3.4. All drugs were added to spheroids in medium to a final concentration given in Table 2-2. Spheroids were imaged using a widefield microscope and phase

contrast image acquisition (10x magnification) on day 14 (24 hours before drug treatments). For the purpose of data analysis, this time point will be referred to as –24 hours (refer to Figure 2-1 for a schedule of spheroid drug treatment and imaging). For each well containing spheroids, one or more fields of view were selected and the x and y coordinates saved. A z-stack image was acquired (7 µm intervals) through multiple spheroids per field of view. After imaging at –24 hours was completed, the medium bathing the spheroids was replaced with fresh medium.

For treatment conditions which included the inhibitor I-172 (Table 2-2), cells were pre-treated with I-172 for 2 hours prior to the addition of forskolin, and all other wells received fresh medium (Figure 2-1). At 0-hours, all wells received fresh medium containing final drug conditions. At 2-, 24-, and 48- hours post treatment, spheroids were imaged using the x,y coordinates saved during –24 hour imaging (Figure 2-1). All spheroids received fresh medium containing relevant drugs directly after imaging at 24-hours. All data were acquired at 37 °C.

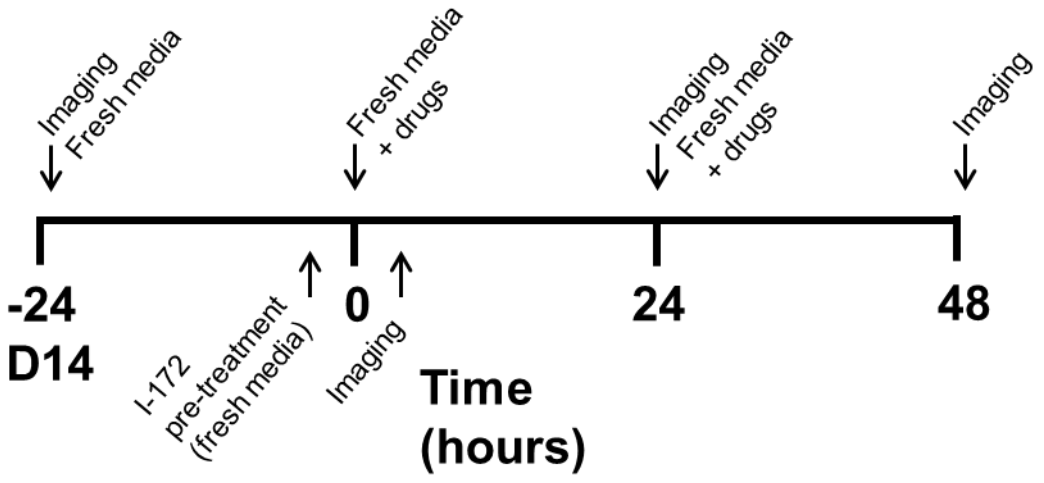

Figure 2-1: Timeline of HCA7 spheroid treatment and imaging during swelling assays.

HCA7 spheroids were cultured according to the protocol outlined in Section 2.3.5, until day 14 of culture (D14). D14 of spheroid culture corresponded with the initial –24 hour (–24) imaging timepoint of HCA7 spheroid FIS assays. For conditions involving $CFTR_{inh}$-172 (I-172, 10 µM) pre-treatment occurred 2 hours before the addition of FSK (10 µM). Imaging took place at –24, 2-, 24- and 48-hour timepoints.

2.6.2. Manual image analysis

Fiji/ImageJ was used to measure both spheroid area and lumen area in pixels (px^2) at –24, 2-, 24- and 48- hours. For each analysed spheroid, a z-plane was selected that represented the widest cross section through the spheroid and its lumen.

For quantification of HCA7 lumen area increase, lumen area was obtained from Fiji/Image J (px^2) and normalised to that at –24 hours (–24 = 100%).

For quantification of normalised lumen area, HCA7 spheroid lumen area (px^2) was calculated and normalised to the corresponding spheroid area (px^2) at each timepoint, these values were normalised to –24 hours (–24 hours = 100%).

For quantification of HCA7 spheroid area increase, spheroid area was obtained (px^2) and normalised to that at –24 hours (–24 hours = 100%).

For the purpose of normalisation of lumen area to the –24 hour timepoint, spheroids with no visible lumen at –24 hours were allocated a –24 hour lumen area of 1 px^2.

2.6.3. Automated image analysis

For automated image analysis of HCA7 spheroids, a Modular Image Analysis (MIA) plugin designed by Dr Dominic Alibhai (Wolfson Bioimaging, University of Bristol) in MATLAB® for use in Fiji/ImageJ. For each field of view to be analysed, the software compiled z-stack images and determined the widest cross section through each spheroid. The plugin identified spheroids as circles within the image, the thresholds of which were defined by the user. The thresholds defined by the user included the image set to be analysed, the degree of circularity imposed on spheroid detection, and the minimum and maximum spheroid area detection limits. Once suitable thresholding had been achieved, an output of area (both $pixels^2$ and μm^2) for each spheroid was generated and saved as an Excel file. An accompanying circle overlay image, in which each circle/spheroid is assigned a numerical identification, linked the image to the numerical output, an example of which is given in Figure 2-2. Data generated by the plugin were checked against the circle overlay image before being used to generate figures, eliminating false readings and incorrectly identified spheroids. This analysis was performed on images from each experimental time point and using the identification number assigned to each spheroid, it was possible to link corresponding measurements.

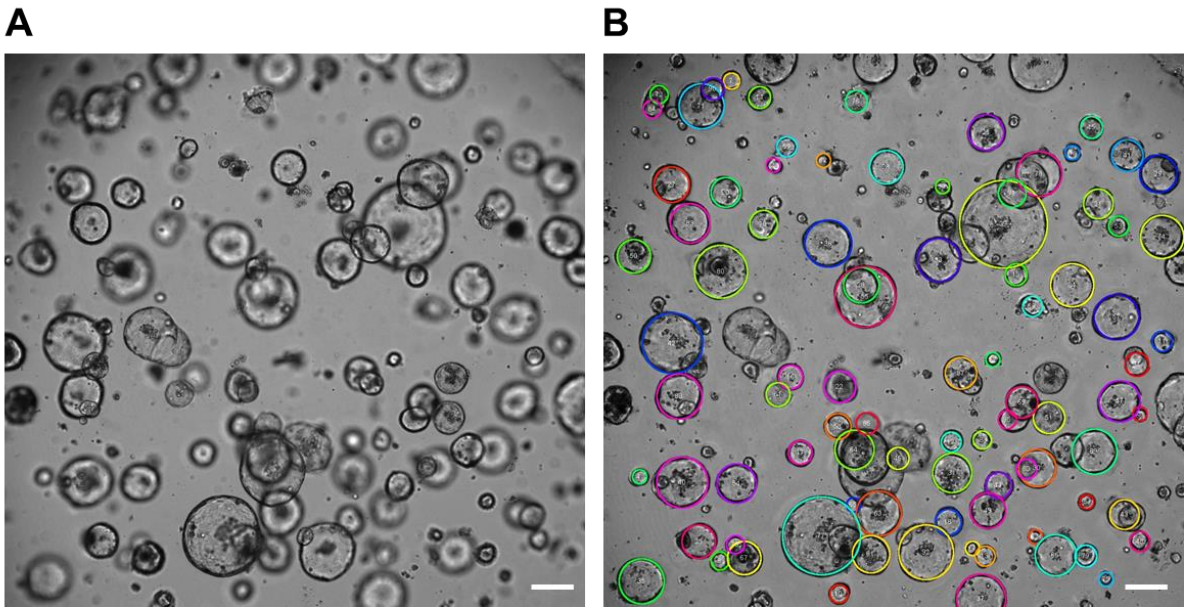

Figure 2-2: Automated image analysis of spheroid area using a Modular Image Analysis plugin for Fiji/ImageJ.

*(**A**) Representative phase contrast image of HCA7 spheroids selected from a defined range of acquired z-stack images. The MIA plugin compiled all z-stack images from each individual field of view to give a final image representing the widest cross section of all spheroids. (**B**) Circle overlay image generated by the MIA plugin image for (**A**). Each spheroid was assigned a numerical identification linked to corresponding Excel data output file. For **A** and **B**, HCA7 spheroids are 2-hours post treatment with FSK (10 µM). Images were acquired using a widefield microscope. Scale bars = 200 µm.*

2.7. Flow cytometry

For flow cytometry, $2x10^5$ single LIM1863 cells were resuspended in 200 µl calcium free S-MEM without GlutaMAX and propidium iodide (PI, Miltenyi Biotech) was added to a final concentration of 1 µg/ml. Fluorescence was detected using a Novocyte® Flow Cytometer (ACEA Biosciences) to distinguish between live (PI negative) and dead cells (PI positive). All data were analysed using Novocyte Express software 1.2.5.

2.8. Protein biochemistry methods

2.8.1. Cell lysis

All adherent cells were lysed *in situ*. Cells were washed once in +4 °C PBS before the addition of 100 µl 1x cell lysis buffer per T25 flask. Cells were incubated with lysis buffer for 15-minutes on ice whilst rocking. After incubation, cells were scraped from the flask and the lysate transferred into microcentrifuge tubes, which were then centrifuged at 18,500 g for 15-minutes at +4 °C to remove cellular debris and DNA. Cleared cell lysates were stored at –80 °C before protein concentrations were determined.

2.8.2. Protein concentration

The Bio-Rad DC protein assay, based on the Lowry Assay (Shen, 2019), was used to determine the protein concentration of whole cell lysates. It was carried out according to the manufacturer's protocol following detergent solubilisation of lysates.

Cell lysates were diluted 1 in 10 in cell lysis buffer, added to 25 µl Reagent A' (Reagent A containing 2% (v/v) Reagent S) in a 96 well plate, and then 200 µl Reagent B was added. Samples were allowed to incubate at room temperature for 15-minutes. The absorbance of each sample was measured in triplicate at 750 nm using a plate reader (Spectramax M2, Molecular Devices). The mean absorbance for each sample was compared to a standard curve generated using the same method and known concentrations of bovine serum albumin (BSA). Known concentrations of BSA used to generate a standard curve were: 0.025, 0.125, 0.25, 0.5, 0.75, 1, 1.5, and 2 µg/µl.

2.8.3. SDS-PAGE gel electrophoresis

A BioRad Mini PROTEAN® Tetra gel electrophoresis system was used for separation of proteins by sodium dodecyl sulphate polyacrylamide gel electrophoresis (SDS-PAGE). Resolving gels of varying dilutions (8 and 10% acrylamide) were prepared using a stock of 30% (w/v) acrylamide (Severn Biotech), Tris-HCl (final concentration 0.4 M, pH 8.8), SDS (final concentration 0.1% (v/v), 0.4% N,N,N,N-tetramethylene-diamine (TMED) and 0.1% (w/v) ammonium persulphate (APS). The stacking gel was made using 5% (w/v) acrylamide, 0.13 M Tris-HCl (pH 6.8), 0.1% (w/v) SDS, 0.1% (w/v) APS and 0.1% (v/v) TEMED. Sample buffer (50 mM Tris-base pH 8, 12% (v/v) glycerol, 10% (w/v) SDS, 2 mM EDTA, 10% (v/v) β-mercaptoethanol) was used to load lysates into the gel after

incubation of lysates in sample buffer at 95 °C for 30 seconds. Initial electrophoresis took place at 60 volts and increased to 90-180 volts once all loading dye had entered the resolving gel.

2.8.4. Transfer of proteins to PVDF (Western blotting)

After SDS-PAGE separation, proteins were transferred to polyvinylidene difluoride (PVDF) membrane (Millipore Immobilon®-P, Merck) using a semi-dry blotter (model: TE77 PWR, Amersham, GE Healthcare). Gels containing resolved proteins were placed on top of a PVDF membrane which was in turn sandwiched between layers of 3MM Whatman paper pre-socked in transfer buffer (39 mM glycine, 48 mM Tris-base, 1.3 mM SDS in 20% (v/v) methanol). Prior to use the PVDF membrane was soaked in methanol (1-minute) and transfer buffer (1-minute, room temperature). Proteins were transferred for a minimum of 90-minutes at 45 mA per gel.

2.8.5. Antibody probing of Western blots

The blocking of Western blots took place overnight at +4 °C using 5% (w/v) milk solution made in Tris buffered saline using TBS TWEEN (listed in Section 2.1.1). All subsequent washes and antibody incubations took place at room temperature with gentle rocking. Primary antibodies (refer to Table 2-3) were diluted in 5% (w/v) milk solution to the desired concentration, added to the PVDF membrane and allowed to incubate for 1-hour, followed by four 5-minute washes of the membrane in TBST. Secondary antibodies (refer to Section 2.1.7), conjugated to horseradish peroxidase were diluted in 5% (w/v) milk solution as required and incubated with the membrane for 1-hour and the wash step repeated. Secondary antibodies were detected using Amersham ECL™ Western blotting reagents, and imaged using an Amersham Imager 600 (Amersham, GE Healthcare). The Western blots shown in Figure 4-2 were kindly performed by Tracey Collard, School of Cellular and Molecular Medicine, University of Bristol, UK.

2.9. Molecular biology techniques

2.9.1. RNA extraction and purification

For RNA extraction from human colonic adenoma and carcinoma cell lines, culture medium was removed from cells, and cells washed twice in PBS before the addition of 1 ml TRI reagent (Sigma-Aldrich) to lyse cells. After 5-minutes incubation at room temperature, cell lysates were collected in Eppendorf tubes and allowed to incubate at room temperature for a further 5-minutes. After incubation, 200 µl chloroform (VWR) was added to each tube, the tube contents mixed thoroughly by inversion for 15-seconds, and the mix incubated for 10-minutes at room temperature before centrifugation at 11,500 rpm for 10-minutes at +4 °C. After centrifugation, tube contents were separated into three distinct phases: a pink bottom phase containing protein, a white middle phase containing DNA, and a colourless upper phase containing RNA. The colourless RNA-containing phase was carefully removed and placed into a sterile Eppendorf tube containing 500 µl isopropanol (VWR), inverted to mix, and incubated at room temperature for 10-minutes for the RNA to precipitate. RNA was pelleted by centrifugation at 11,500 rpm for 10-minutes at +4 °C, the pellet washed in 500 µl of 70% ethanol, and centrifuged again at 8,500 rpm for 5-minutes at +4 °C. Following this final centrifugation, the supernatant was removed, and the pellet air dried before re-suspension in 100 µl molecular grade water.

To eliminate potential chemical and genomic contamination of RNA, RNA clean-up was performed using the Qiagen RNeasy MINI kit (Qiagen) according to the manufacturer's protocol. The RNA concentration of each sample was determined using a NanoDrop (ThermoScientific) before storage at –80 °C until required.

2.9.2. Synthesis of cDNA

Synthesis of complementary DNA (cDNA) from an mRNA template, by reverse transcription, was performed using Moloney murine leukaemia virus (M-MLV) reverse transcriptase, an RNA-dependent DNA-polymerase. For each sample of RNA, 0.5 µg Oligo dT primer (Promega) was added to a pair of PCR tubes each containing 2 µg RNA and the tubes were incubated at 70 °C for 5-minutes. This incubation phase permitted the melting of RNA secondary structures and the annealing of Oligo dT primer to the RNA template. Following incubation, all tubes were transferred to an ice bucket to prevent re-formation of secondary structures and to each tube 5 µl 5x M-MLV reaction

buffer, 5 µl deoxyribonucleotide triphosphate (dNTPs, 10 mM stock), and 25 units recombinant RNasin ribonuclease inhibitor were added. To one out of each pair of PCR tubes, 200 units of M-MLV reverse transcriptase was added, facilitating the synthesis of the first strand of cDNA from RNA. The second of the pair of PCR tubes, not containing M-MLV reverse transcriptase was a negative control, where the lack of enzyme prevented cDNA synthesis. The final volume of all PCR tubes was made up to 25 µl with molecular grade water, and the tubes were incubated at 40 °C for 1-hour for cDNA synthesis. After this incubation, a further 75 µl molecular grade water was added to each tube giving a final volume of 100 µl and concentration of 20 ng/µl (this assumes an efficiency of cDNA synthesis of 100%). Samples were stored at –20 °C until required.

2.9.3. Quantitative real-time PCR

Quantitative real-time PCR (Q-RT-PCR) is an assay used for the detection and monitoring of expression of a DNA product, using primers for a gene of interest (Foroni *et al.*, 2017). The detection and quantification of a DNA product relies on the detection of a fluorescence signal produced by the reporter molecule SYBR Green as a result of double stranded DNA synthesis. The emission of a fluorescence signal corresponds to the synthesis of DNA product, which in turn corresponds to the initial amount of cDNA template.

Q-RT-PCR was performed using SYBR Green PCR mix (Qiagen), cDNA template, and the primers detailed in section 2.1.8. The reaction mixture underwent thermal cycling using a Stratagene Mx3005P PCR System (Aligent Technologies) as illustrated in Figure 2.3.

Gene expression was normalised to both TBP (TATA-binding protein) and HPRT (hypoxanthine phosphoribosyl transferase) housekeeping genes interchangeably. Data were analysed using MxPro software 4.10 (Aligent Technologies).

Optimisation of primers and annealing temperatures was kindly carried out by Tracey Collard, School of Cellular and Molecular Medicine, University of Bristol, UK.

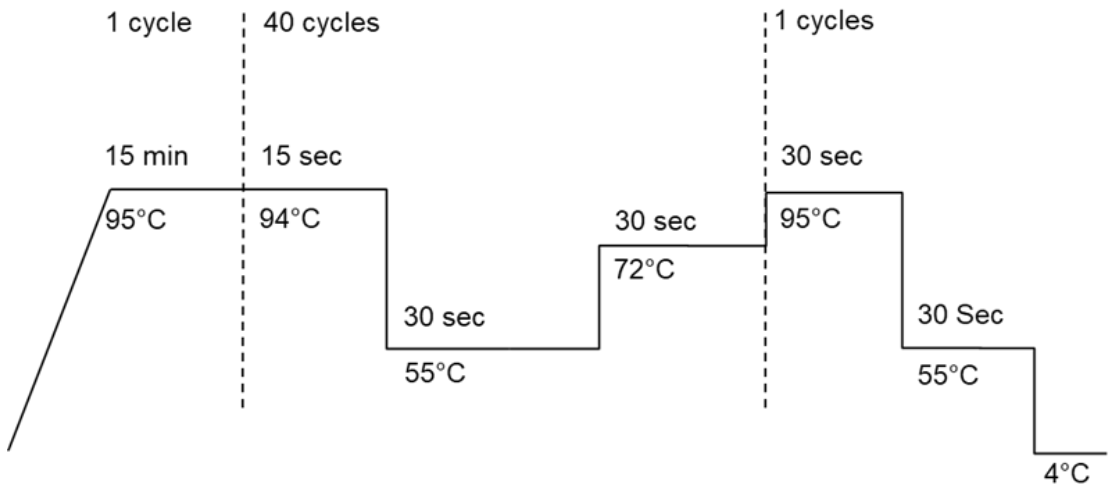

Figure 2-3: PCR thermal cycling parameters.

A PCR reaction mix containing cDNA template, SYBR Green PCR mix, and primer underwent thermal cycling to amplify DNA of interest.

2.10. Ussing chamber experiments

2.10.1. Seeding of Transwell Inserts

FRT cells, CFTR-expressing adenoma and carcinoma cell lines, and single LIM1863 cells were seeded onto 12 mm, 0.4 µm PCF cell culture Transwell inserts (Millicells, Merck) at a seeding density of $2.5x10^5$ cells per insert. For LIM1863 spheroids, the equivalent of 1/10 of 8 ml confluent spheroid suspension was used to seed Transwell inserts. Cells were added to the internal (apical) portion of the Millicell in 250 µl of medium. 500 µl of medium was added to the external (basolateral) area surrounding the Transwell insert. The medium bathing FRT, adenoma and carcinoma cells was changed every other day and the transepithelial electrical resistance (R_t) of the epithelial monolayer was monitored every 2 days using an epithelial volt/ohm meter (EVOM; World Precision Instruments) coupled to an STX2 electrode set (World Precision Instruments).

2.10.2. Ussing chamber experiments

For Ussing chamber studies using FRT and HCA7 cells, epithelia were cultured as described in Section 2.3. Once peak R_t values had been reached (approximately day 4 for FRT epithelia, and day 8 for HCA7 epithelia) epithelia were used for experiments. Epithelia were mounted in modified Ussing chambers and a large Cl^- concentration

gradient was imposed across the epithelium using the apical and basolateral solutions described in Section 2.1.1. The solution bathing the epithelial basolateral membrane contained (mmol/L): 140 NaCl, 5 KCl, 0.5 $MgCl_2$, 0.36 K_2HPO_4, 0.44 KH_2PO_4, 1.3 $CaCl_2$, 10 HEPES, 4.2 $NaHCO_3$. The composition of the solution bathing the apical membrane was as for the basolateral solution, however 140 mmo/L NaCl and 5 mmol/L KCl were replaced with 133.3 mmol/L Na gluconate + 2.5 mmol/L NaCl, and 5 mmol/L K gluconate, respectively, ($[Cl^-]_{basolateral}$, 149 mM; $[Cl^-]_{apical}$, 14.8 mM). The concentration of Ca^{2+} was increased to 5.7 mmol/L in the apical solution to compensate for the Ca^{2+} buffering capacity of gluconate. All solutions were maintained at 37 ºC and bubbled with 5% CO_2. Transepithelial voltage was clamped at 0 mV and short-circuit current (I_{sc}) was continuously recorded. The resistance of the filter and solutions, in the absence of cells, was subtracted from all measurements. A schematic of the Ussing chamber set up used during experiments is shown in Figure 2-4. Under these conditions, CFTR activation by the cAMP agonist forskolin induces flow of current from the basolateral solution to the apical solution causing an increase in I_{sc}. This increase in I_{sc} corresponds to the movement of Cl^- across the epithelium through open CFTR channels. I_{sc} is decreased when the flow of current is inhibited by the CFTR inhibitor I-172 and Cl^- transport ceases. For the purpose of illustration, basal I_{sc} (I_{sc} value recorded immediately before forskolin addition) was subtracted from all subsequent I_{sc} values. To this end, data are presented as ΔI_{sc} (μAcm^2).

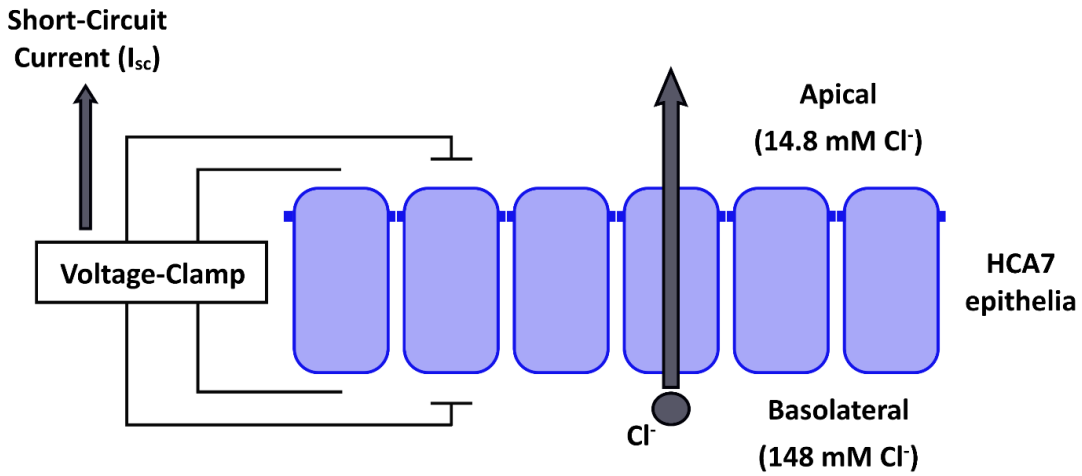

Figure 2-4: Schematic of Ussing chamber technique to measure epithelial ion transport.

Epithelia were mounted in Ussing chambers, a large Cl^- concentration gradient imposed across the epithelium ($[Cl^-]_{basolateral}$, 148 mM; $[Cl^-]_{apical}$, 14.8 mM), transepithelial voltage was clamped at 0 mV and short-circuit current (I_{sc}) recorded continuously.

2.11. Statistics

Results are expressed as means ± S.E.M of *n* observations. All data were tested for normal distribution using the Shapiro-Wilk normality test, and equal variance using the Brown Forsythe test. When $p < 0.05$ differences were considered significant. Throughout this thesis degree of significance is indicated as follows: *, $p < 0.05$, **, < 0.01.

For comparison of 3 or more discrete populations one-way ANOVA was used. Where data failed equal variance tests, for comparison of 2 discrete populations, two-tailed, un-paired t-tests with Welch's correction were used, and for comparison of 2 matched samples two-tailed, paired t-tests were used.

For data that failed both normality and equal variance tests, for comparison of 2 discrete populations Mann-Whitney tests were used, and for. comparison of 3 or more discrete populations the Kruskal-Wallis test was performed. For comparison of 2 matched samples the Wilcoxon matched-pair signed rank test was used.

2.12. List of Suppliers

- Aooq Bioscience - Irvine, California, United States
- Aligent Technologies - Santa Clara, California, United States
- Amersham (owned by GE Healthcare) - Amersham, Buckinghamshire, United Kingdom
- Becton Dickinson - Franklin Lakes, New Jersey, United States
- Calbiochem (owned by Merck) - Burlington, Massachusetts, United States
- Cell Signalling Technology - Danvers, Massachusetts, United States
- Cayman Chemical - Ann Arbor, Michigan, United States
- Clontech (Takara) - Kusatsu, Shiga, Japan
- Corning - New York, United States
- Dako (Aligent) - Las Vegas, Nevada, United States
- Gibco (owned by Thermo Fisher Scientific) - Waltham, Massachusetts, United States

- Horizon Discovery (owned by PerkinElmer) - Waltham, Massachusetts, United States
- Lab M - Heywood, United Kingdom
- Labtech International - Heathfield, East Sussex, United Kingdom
- Merck - Burlington, Massachusetts, United States
- Molecular Devices - San Jose, California, United States
- Promega - Madison, Wisconsin, United States
- Proteintech - Rosemont, Illinois, United States
- Qiagen - Hilden, Germany
- Roche - Basel, Switzerland
- Santa Cruz Biotechnology - Dallas, Texas, United States
- Sigma-Aldrich (owned by Merck) - Burlington, Massachusetts, United States
- Thermo Fisher Scientific - Waltham, Massachusetts, United States
- VWR (owned by Avantor) - Radnor, Pennsylvania, United States
- Warner Instruments - Hamden, Connecticut, United States

Chapter 3. Initial studies of intestinal ion transport using the colorectal carcinoma LIM1863 cell line.

3.1. Introduction

The LIM1863 cell line was first reported by Whitehead *et al* (1987), as spheroid forming cells expressing many characteristics typical of colonic crypts. Originally isolated from a 74-year old Caucasian female, LIM1863 spheroids maintain crypt-like morphology and express the epithelial Na^+ channel (ENaC), the ion channel responsible for a large proportion of colonic Na^+ absorption (Currid, *et al*, 2004; Yang *et al.*, 2016). These characteristics were novel when compared to earlier *in vitro* models of human colonic Cl^- secretion.

Previous studies have sought to further characterise the LIM1863 cell line both as an *in vitro* model of the colonic crypt, and as a model of colonic Cl^- secretion (Hayward and Whitehead, 1992; Currid, *et al*, 2004). They demonstrated that LIM1863 cells grow as free-floating spheroids composed of polarized epithelial cells arranged around a central lumen (Whitehead *et al.*, 1987; Hayward and Whitehead, 1992). The spheroids formed by the LIM1863 cell line are functionally and morphologically organised, possessing characteristics typical of colonic crypts, including a brush border, differentiated goblet cells, columnar enterocytes and tuft cells (Hayward and Whitehead, 1992). RT-PCR and Western blotting demonstrated that the LIM1863 cell line express mRNA and protein of several ion channels and transporters associated with transepithelial electrolyte transport in the colon. These include CFTR, Ca^{2+}-dependent Cl^- channel 1 (ClCa1), epithelial Na^+ channel (ENaC), Na^+-K^+-$2Cl^-$-cotransporter 1 (NKCC1), and Na^+/H^+ exchangers (NHE1-3) (Currid, *et al*, 2004).

Work performed by Currid *et al* (2004) demonstrates that LIM1863 spheroids provide a useful model to study colonic electrolyte and fluid secretion, and describes the basis of an assay that could be adapted for high-throughput screening of compounds with potential therapeutic benefit for patients with CF. In the forskolin-induced swelling (FIS) assays reported by Currid *et al* (2004), electrolyte and subsequent fluid secretion across the apical membrane into the enclosed spheroid lumen was quantified by morphometric analysis of lumen area in response to secretagogues. LIM1863 spheroids were seeded onto collagen-coated Petri dishes, bathed in isotonic Hanks solution containing the experimental compound(s) of interest and imaged over a period of time. Then, the acquired phase contrast images were analysed to give the initial area of each spheroid and the area of the lumen at each time point. Normalisation of lumen area, required to take into consideration the large distribution of spheroid sizes, was achieved by dividing

the lumen area at each time point by the radius of the corresponding spheroid at the beginning of each experiment (T = 0).

More recent work, utilising intestinal organoids derived from both mouse models and human subjects, has employed assays similar to that described by Currid *et al*. (2004), to characterise FIS in mouse and human CFTR-mutant and CFTR-wt intestinal organoids (Dekkers *et al.*, 2016; Dekkers *et al*., 2013). The FIS assay developed by Dekkers *et al* (2013), was initially optimised using CFTR-wt intestinal organoids derived from mice, and then used to characterise FIS in human intestinal organoids derived from both CF and non-CF individuals. Although the assay uses the same premise as that developed by Currid *et al*. (2004), organoids were labelled with calcein green prior to imaging, allowing for automated fluorescence image analysis, increasing the capacity of the assay (Dekkers *et al.*, 2013). Subsequently, the automated assay described by Dekkers *et al* (2013) was used to characterise the CFTR-mediated swelling response of organoids derived from the rectal epithelia of 71 participants expressing a total of 28 *CFTR* genotypes, to clinically approved CFTR-modulating drugs (Dekkers *et al.*, 2016).

Combined, these studies highlight the potential of the LIM1863 cell line as a model for studying colonic electrolyte and fluid secretion and suggest an assay that could be used for high-throughput screening of compounds which may possess therapeutic potential by restoring correct water homeostasis to the CFTR intestine.

3.2. Aims

This chapter aims to build on the work of Currid *et al* (2004) and determine the suitability of the LIM1863 cell line as both a 2D and 3D model of intestinal ion transport. To fulfil the required criteria, firstly LIM1863 spheroids should be capable of CFTR-mediated spheroid swelling, the extent of spheroid swelling must be quantifiable, and quantification must be such that it allows for high-throughput screening assays. Secondly, the LIM1863 cell line should be capable of forming polarised epithelia on Transwell inserts, allowing it to be used in epithelial ion transport studies utilising the Ussing chamber technique.

To assess whether the LIM1863 cell line met the criteria outlined above, LIM1863 spheroids will be seeded into multi-well tissue culture plates and subjected to forskolin-induced swelling (FIS) assays. CFTR-mediated spheroid swelling will be characterised in response to forskolin alone and inhibitors of ion channels and transporters important for epithelial Cl^- transport. Both LIM1863 spheroids and single LIM1863 cells will be seeded onto Transwell inserts and cultured in a selection of suitable growth media. Transepithelial resistance will be measured periodically to determine whether a polarised epithelium has formed. Upon successful formation of a polarised epithelium, the Ussing chamber technique will be used to characterise transepithelial ion transport by LIM1863 cells in response to forskolin

Secondly, this chapter aims to develop a high-throughput assay to screen compounds which may possess therapeutic potential to restore ion and water homeostasis in the CF intestine. The principle of this assay will be to measure CFTR-mediated spheroid swelling, occurring as a result of CFTR-mediated fluid secretion into the spheroid lumen, in response to the secretagogue forskolin. A desirable assay would allow the simultaneous screening of multiple compounds and controls, produce reliable and reproducible results, detect subtle changes in spheroid area, and allow for automated analysis.

3.3. Results

3.3.1. CFTR-mediated swelling of LIM1863 spheroids

To build on previous research (Currid *et al.*, 2004) and determine whether LIM1863 spheroids would be suitable for the development of a FIS assay to quantify CFTR-mediated spheroid swelling, LIM1863 spheroid swelling was assessed in response to forskolin (FSK). LIM1863 spheroids were cultured and seeded for FIS assays as outlined in Sections 2.3.3 and 2.5.2. FSK (10 μM) was added to isotonic Hanks solution bathing the spheroids immediately prior to image acquisition (T0). To confirm that any observed spheroid swelling was a result of CFTR-mediated fluid secretion into the spheroid lumen, control assays were performed using the CFTR inhibitor, $CFTR_{inh}$-172 (I-172). For I-172 assays, spheroids were incubated with 10 μM I-172 for 1 hour before image acquisition. Immediately prior to image acquisition, FSK (10 μM) and I-172 (10 μM) were added to the Hanks solution bathing the spheroids. Image acquisition took place as described in Section 2.5.4 and 2.5.5.

LIM1863 spheroids produced a visible lumen in response to stimulation with FSK, recapitulating previous findings (Currid *et al*, 2004). Spheroid lumens were visible 10-minutes post FSK addition. The observed FIS response was demonstrated to be the result of CFTR-mediated fluid transport using I-172, which dramatically decreased both the occurrence of lumen formation and overall lumen area increase. Representative images of LIM1863 spheroid swelling in response to 10 μM FSK, 10 μM FSK + 10 μM I-172, 10 μM I-172, and untreated are shown in Figure 3-1.

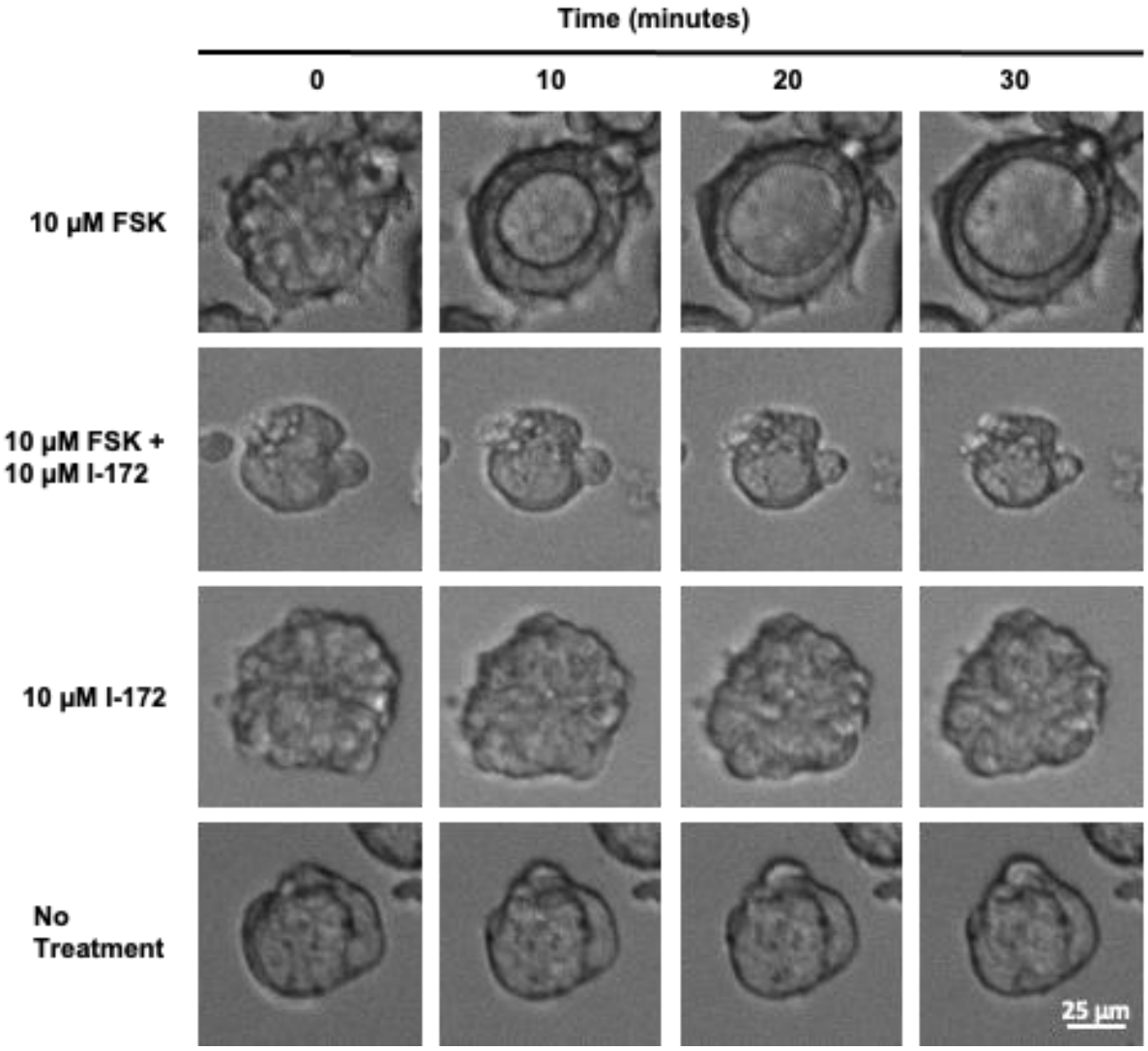

Figure 3-1: Representative images of CFTR-mediated swelling by LIM1863 spheroids.

Phase contrast images of LIM1863 spheroids were taken at 10-minute intervals over a 30-minute period. LIM1863 spheroids were treated with either 10 µM forskolin (FSK), 10 µM FSK + 10 µM $CFTR_{inh}$-172 (I-172), 10 µM I-172, or untreated. For conditions containing I-172 spheroids were incubated with 10 µM I-172 for 1 hour before image acquisition. Images were acquired using a spinning disk confocal microscope with 10x magnification. Scale bar = 25 µm.

3.3.2. Quantification of CFTR-mediated swelling by LIM1863 spheroids

To complement the representative images in Figure 3-1 demonstrating that FSK stimulates CFTR-mediated luminal fluid secretion and subsequent swelling by LIM1863 spheroids, this response was quantified. Several quantification methods were evaluated and their suitability and accuracy in evaluating the swelling response was assessed. The four quantification methods considered and the different ways each represents a single 30-minute LIM1863 spheroid FIS assay are shown in Figures 3-2 to 3-5. In these assays, spheroids were either stimulated with 10 μM FSK (n = 8 spheroids) or untreated (n = 8 spheroids). For all experiments outlined in Sections 3.3.2, 3.3.3 and 3.3.4, data were acquired using a spinning disk microscope and analysed manually in Fiji/ImageJ.

In Figure 3-2A, total spheroid area (px^2; x,y plane) measured at 2-minute intervals and normalised to spheroid area at T0 (T0 area = 100%) is shown for FSK stimulated and untreated spheroids. This approach to quantification of FIS assays has been previously used with human rectal organoids from individuals with CF (Dekkers *et al.*, 2013; Dekkers *et al.*, 2016). Whilst some fluctuation in spheroid area over the 30-minute period was observed, no significant difference in spheroid area was recorded between FSK stimulated and untreated spheroids after 30-minutes (Figure 3-2B). These data suggest that FSK-induced fluid secretion in LIM1863 spheroids does not result in spheroid area increase, therefore this method of quantification is unsuitable as it does not distinguish between FSK stimulated and untreated spheroids.

Figure 3-3A shows the change in area of the epithelium surrounding the spheroid lumen in the same FSK stimulated and untreated LIM1863 spheroids as analysed in Figure 3-2. The area of epithelium surrounding each spheroid was calculated by subtraction of the lumen area (px^2) from the spheroid area (px^2), and this in turn was normalised to epithelium area at T0 (T0 area = 100%). Whilst the area occupied by epithelium remained largely unchanged in untreated spheroids, the area occupied by epithelium in spheroids treated with 10 μM FSK gradually decreased over time, ultimately occupying an area 70% of that at T0. Figure 3-3B demonstrates that 30-minutes post FSK stimulation there was a significant difference ($p = 0.0035$) in epithelial area surrounding the spheroid lumen between spheroids treated with FSK and untreated spheroids.

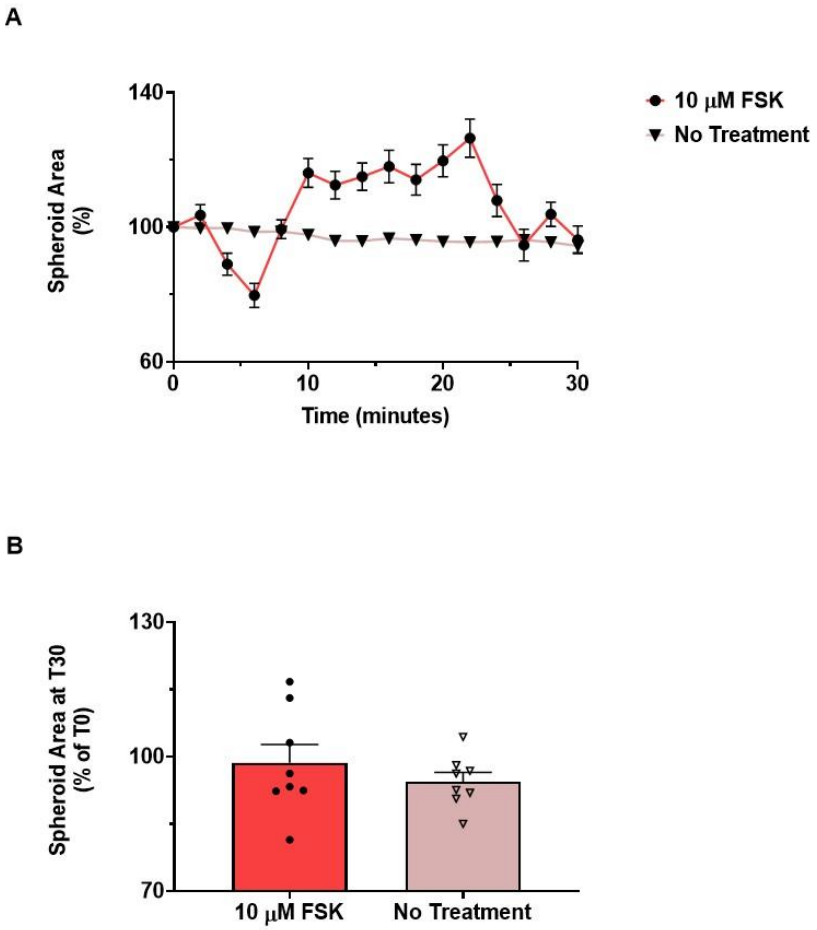

Figure 3-2: Quantification of spheroid area change during CFTR-mediated swelling in LIM1863 spheroids.

(A) *LIM1863 spheroid area (x,y plane) shown as percentage increase from T0 (100%) for both untreated spheroids and spheroids stimulated with 10 μM forskolin.* ***(B)*** *LIM1863 spheroid area 30-minutes post addition of forskolin for both untreated spheroids and spheroids stimulated with 10 μM forskolin. No significant difference in T30 spheroid area was observed between forskolin treated and untreated spheroids (p = 0.39, two-tailed, un-paired T-test with Welch's correction). In* ***A*** *and* ***B****, for untreated spheroids and forskolin stimulated spheroids data are means ± S.E.M (n = 8).*

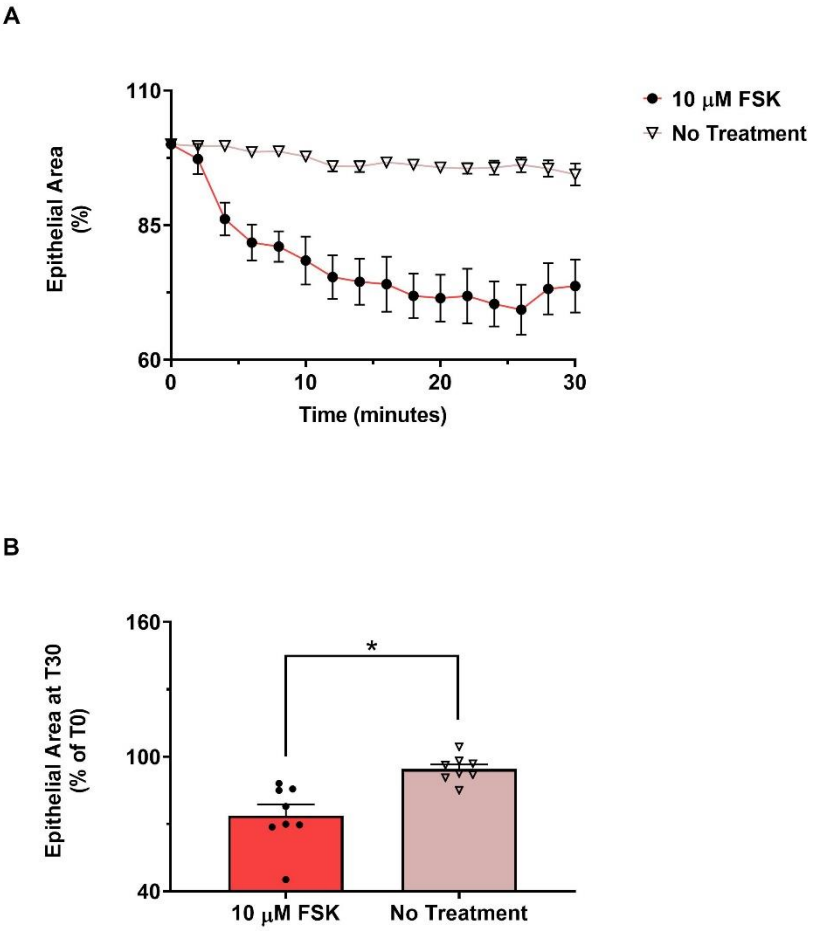

Figure 3-3: Quantification of epithelial area change during forskolin-induced swelling in LIM1863 spheroids.

(A) *LIM1863 epithelial area (x,y plane) shown as percentage increase from T0 (100%) for both untreated spheroids and spheroids stimulated with 10 μM forskolin. Epithelial area was calculated by the subtraction of the lumen area (μm^2) from the spheroid area (μm^2) and this in turn plotted as a percentage of epithelium area at T0 (T0 area = 100%).* ***(B)*** *LIM1863 epithelial area 30-minutes post addition of forskolin for both untreated spheroids and spheroids stimulated with 10 μM forskolin. In* ***A*** *and* ***B****, for untreated spheroids and forskolin stimulated spheroids, data are means ± S.E.M (n = 8); *, p < 0.05; two-tailed, un-paired T-test with Welch's correction.*

This method of quantification clearly distinguished between FSK-treated and untreated spheroids. However, a disadvantage of this approach is that it requires two parameters to be measured to calculate the area occupied by the epithelium. This additional measurement would slow data analysis in larger scale drug screening assays compared to quantification requiring only one measurement.

Both Figures 3-4 and 3-5 represent FIS in LIM1863 spheroids as a function of change in lumen area. In Figure 3-4A, total lumen area, measured at 2-minute intervals over a 30-minute period, was normalised to lumen area at T0 (T0 area = 100%) for LIM1863 spheroids stimulated with FSK and untreated spheroids. In Figure 3-5A, change in spheroid lumen area is also plotted over a 30-minute period. However, lumen area measurements taken every 2-minutes were normalised to the corresponding spheroid radius at T0. This method was previously used to quantify lumen formation in LIM1863 spheroids by known secretagogues (Currid et al., 2004). A significant difference in lumen area in FSK stimulated spheroids compared to untreated spheroids at T30 was found using both quantification methods ($p = 0.0002$ and $p = 0.0046$ for Figures 3-4B and 3-5B, respectively).

Considered together these data indicate that FSK-induced fluid secretion in LIM1863 spheroids results in an increase in lumen area significantly greater than that observed in untreated spheroids (Figures 3-4 and 3-5). The increase in lumen area is not associated with an overall increase in spheroid area (Figure 3-2), rather, the epithelium lining the spheroid lumen constricts to accommodate luminal fluid secretion (Figure 3-3). As briefly discussed in the proceeding paragraphs, the quantification methods used to produce Figures 3-2 and 3-3 are not suitable for this assay. Whilst the quantification methods used to generate Figures 3-4 and 3-5 are both appropriate for use with FIS assays, it was decided that the method previously used by Currid *et al.* (2004) would be selected for the analysis of LIM1863 spheroid swelling data going forward. Hereafter, normalised lumen area will be referred to as lumen area.

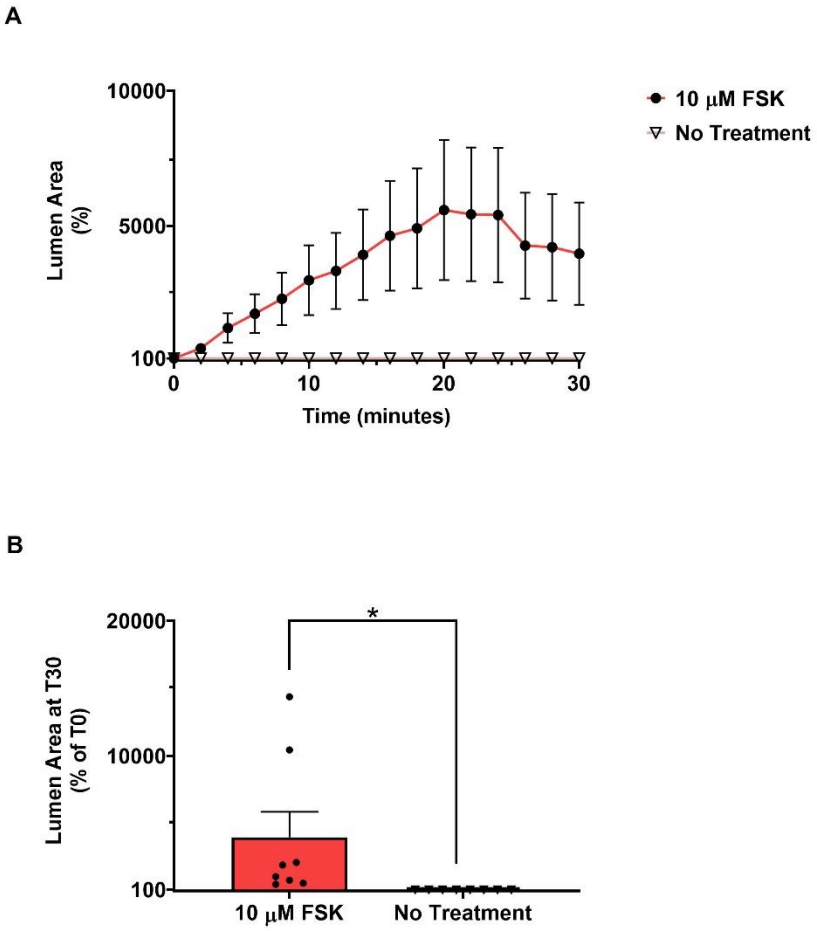

Figure 3-4: Quantification of lumen area change during forskolin-induced swelling in LIM1863 spheroids.

A) *LIM1863 lumen area (x,y plane) shown as percentage increase from T0 (100%) for both untreated spheroids and spheroids stimulated with 10 μM forskolin.* ***(B)*** *LIM1863 lumen area 30-minutes post addition of forskolin for both untreated spheroids and spheroids stimulated with 10 μM forskolin. In* ***A*** *and* ***B****, data are mean ± S.E.M. (n = 8);* *******, $p < 0.05$; Mann-Whitney test.*

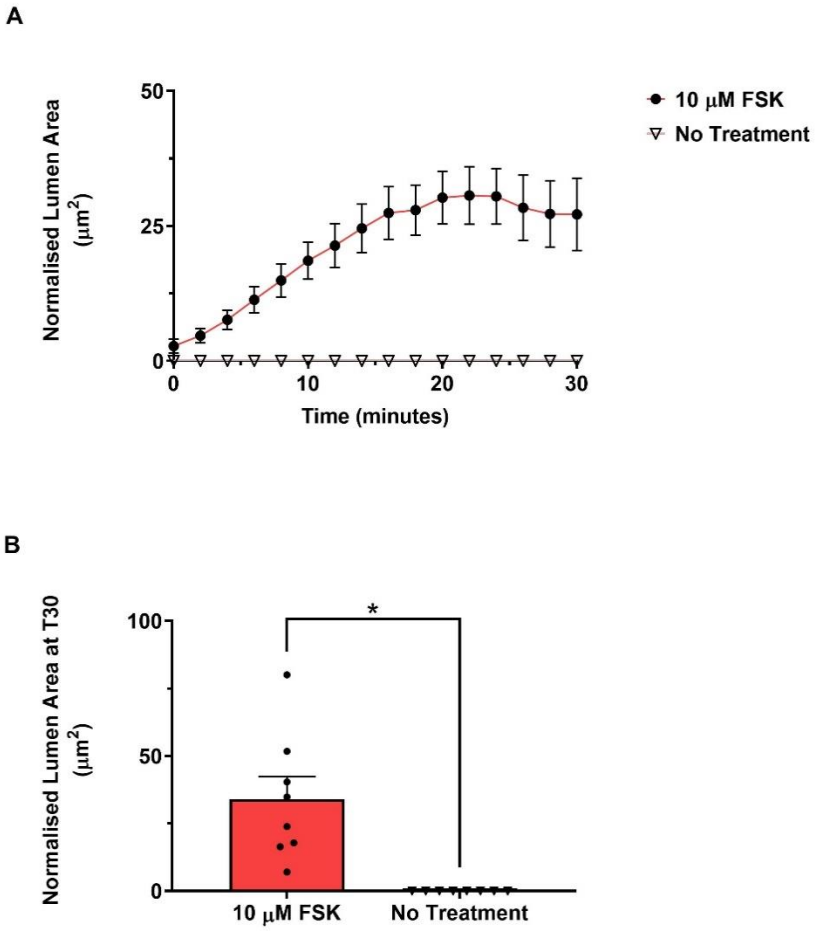

Figure 3-5: Quantification of lumen area change normalised to T0 spheroid radius during forskolin-induced swelling in LIM1863 spheroids.

(A) *LIM1863 lumen area increase normalised to spheroid radius at T0 shown for both untreated spheroids and spheroids stimulated with 10 μM forskolin.* ***(B)*** *Normalised lumen area 30-minutes post addition of forskolin for both untreated spheroids and spheroids stimulated with 10 μM forskolin. In* ***A*** *and* ***B****, data are mean ± S.E.M. (n = 8);* *******, p < 0.05; two-tailed, unpaired t-test with Welch's correction.*

3.3.3. Extent of LIM1863 lumen swelling in response to forskolin stimulation is reproducible.

Three independent FIS assays were performed using LIM1863 spheroids from separate passages in order to determine assay reproducibility. For all three repeats, spheroids were cultured and seeded for FIS assays as outlined in Sections 2.3.3 and 2.5.2. Spheroids were stimulated with FSK (10 µM) immediately prior to image acquisition. For experiment 1, n = 8, for experiment 2, n = 10 and for experiment 3, n = 10. Lumen area increase from T0 to T30 for all three FIS assay repeats are shown in Figure 3-6A. No significant difference in lumen area was observed between the three repeats at T0 ($p = 0.19$), and at T30 ($p = 0.66$) (Figures 3-6B and C). These data suggest that normalising lumen area to the corresponding spheroid radius at T0 accounted for variation in spheroid size and therefore lumen area. Typically, larger spheroids produced larger lumen over a 30-minute period upon stimulation with FSK. This trend is illustrated in Figure 3-4A where large error bars (S.E.M) illustrate the extent of variation in lumen area between spheroids when overall spheroid size is not taken into consideration. Interestingly, the data shown in Figures 3-6A and B suggest that the addition of FSK has an immediate effect on spheroids, driving fluid secretion into the spheroid lumen resulting in an increase in lumen area before the first image is acquired. Typically, experimental conditions that did not use FSK produced no visible lumen during the 30-minute-period.

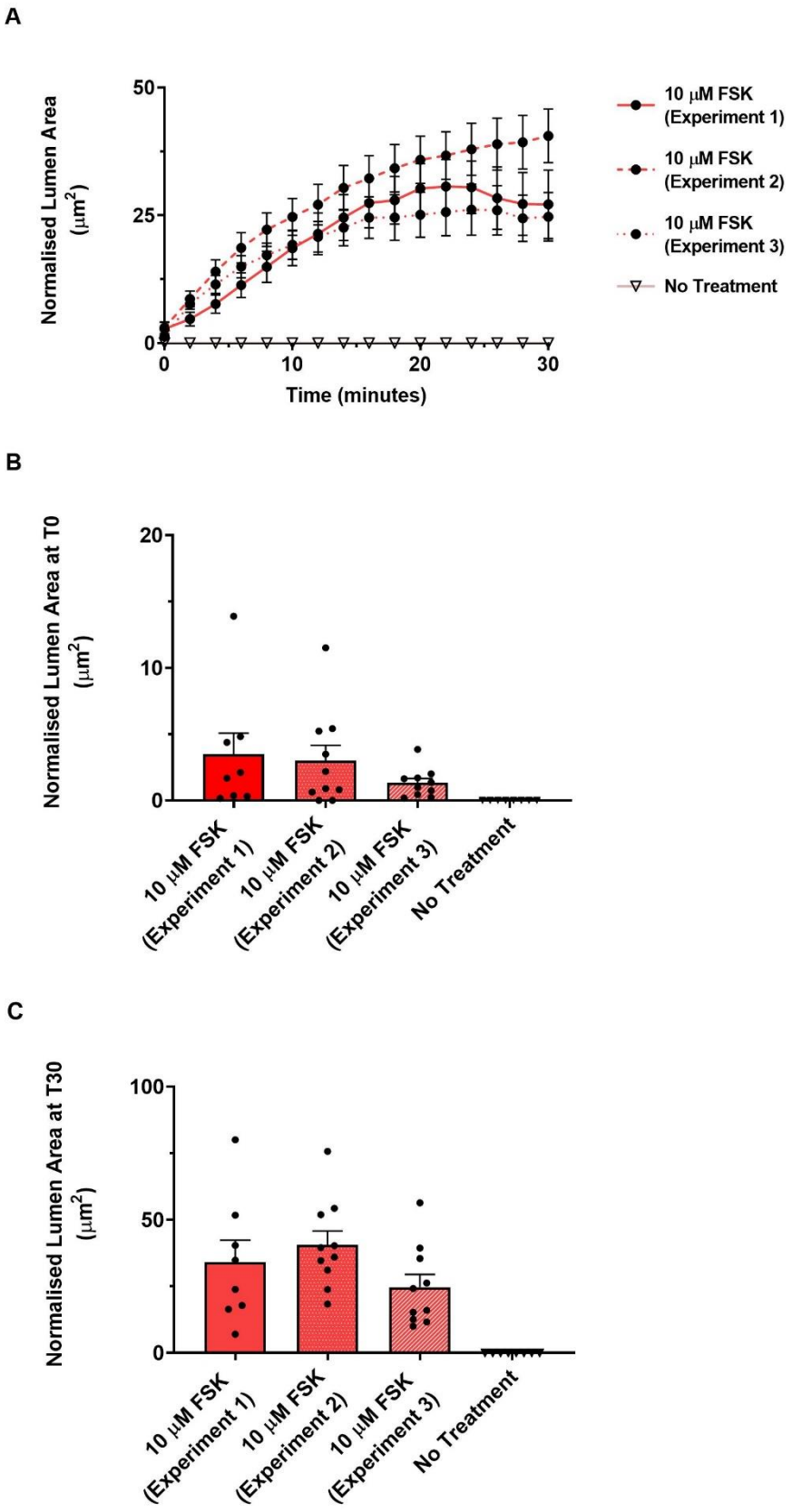

Figure 3-6: Quantification of lumen area change normalised to T0 spheroid radius allows for reproducible data comparison between experimental repeats.

Figure 3-6: Quantification of lumen area change normalised to T0 spheroid radius allows for reproducible data comparison between experimental repeats.

(A) *LIM1863 lumen area increase normalised to spheroid radius at T0 shown for both untreated spheroids and spheroids stimulated with 10 µM forskolin.* ***(B)*** *Normalised lumen area at T0, for both untreated spheroids and spheroids stimulated with 10 µM forskolin.* ***(C)*** *Normalised lumen area 30-minutes post addition of forskolin for both untreated spheroids and spheroids stimulated with 10 µM forskolin. In* ***A****,* ***B****, and* ***C****, data are means ± S.E.M. (n = 8-10). No significance was found, Kruskall-Wallis test* ***(A),*** *one-way ANOVA* ***(B and C)****.*

3.3.4. CFTR-mediated swelling of LIM1863 spheroids is reduced by the CFTR inhibitor $CFTR_{inh}$-172 and the NKCC1 inhibitor bumetanide.

Upon selection of a suitable quantification method of FSK-induced lumen swelling by LIM1863 spheroids further characterisation and quantification of the swelling response was performed. To support the conclusion that FSK-induced swelling of LIM1863 spheroids is the result of CFTR-mediated Cl^- transport, the reduction in swelling resulting from pre-treatment with the CFTR inhibitor $CFTR_{inh}$-172 (I-172) (Ma et al., 2002) was quantified. For both I-172 and FSK + I-172 conditions, spheroids were incubated with I-172 (10 µM) for 1-hour prior to FSK stimulation and image acquisition at T0. As shown in Figure 3-7A, LIM1863 spheroids pre-treated with 10 µM I-172 (n = 8 spheroids) demonstrated a quantifiable reduction in luminal swelling when stimulated with FSK compared to those treated with FSK only (n = 8 spheroids). Pre-treatment of spheroids with I-172 reduced the mean lumen area to 38% of that observed in FSK stimulated spheroids 30-minutes post FSK addition ($p = 0.04$) (Figure 3-7B).

The basolateral membrane $Na^+/K^+/2Cl^-$ co-transporter, NKCC1, provides an intracellular source of Cl^- ions, maintaining intracellular levels of Cl^- above its electrochemical equilibrium (Frizzell and Hanrahan, 2012) . Inhibition of NKCC1 by the loop diuretic bumetanide reduced LIM1863 spheroid swelling (Currid et al, 2004). To determine whether this result was reproducible in the current model, LIM1863 spheroids were incubated with 100 µM bumetanide for 5 minutes prior to the addition of 10 µM FSK and image acquisition.

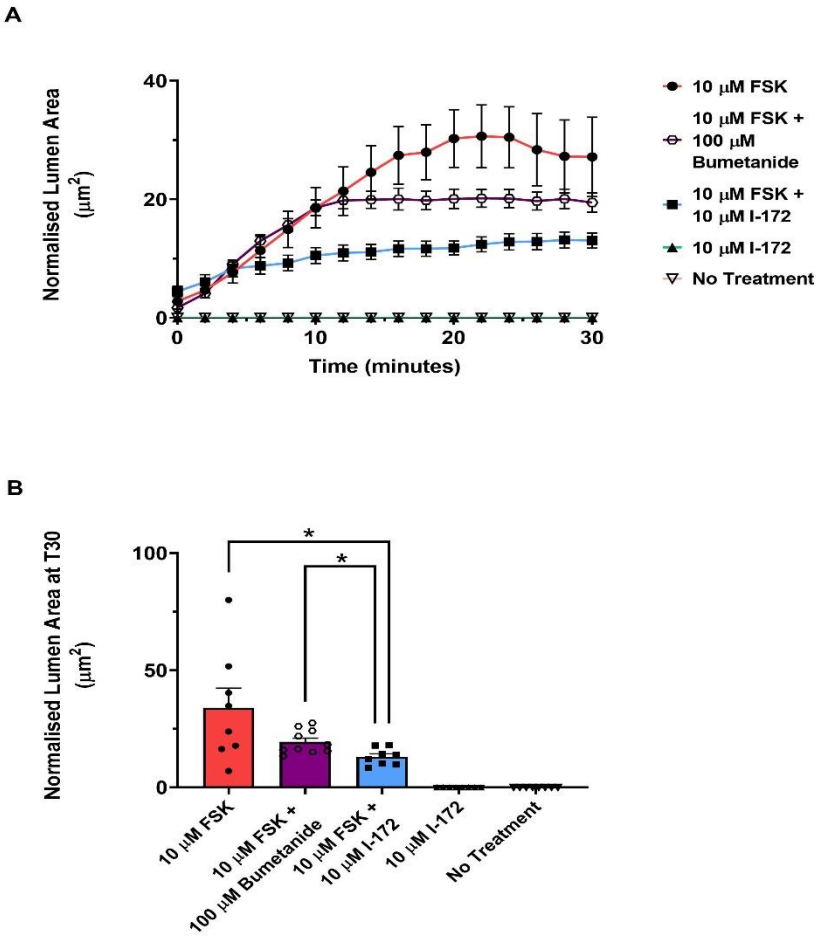

Figure 3-7: The CFTR inhibitor CFTR$_{inh}$-172 (I-172) and the NKCC1 inhibitor bumetanide reduce luminal swelling of LIM1863 spheroids in response to forskolin stimulation.

(A) *LIM1863 lumen area increase for spheroids treated with either 10 μM FSK, 10 μM FSK + 100 μM bumetanide, 10 μM FSK + 10 μM I-172, 10 μM I-172, or untreated.* ***(B)*** *LIM1863 lumen area 30-minutes post addition of forskolin for spheroids treated with either 10 μM FSK, 10 μM FSK + 100 μM bumetanide, 10 μM FSK + 10 μM I-172, 10 μM I-172, or untreated. For conditions containing I-172, spheroids were incubated with 10 μM I-172 for 1 hour before image acquisition. For conditions containing bumetanide spheroids were incubated with 100 μM bumetanide for 5 minutes before image acquisition. For all conditions, data are means ± S.E.M. (n = 8 – 10); *, p < 0.05; two-tailed unpaired Students t-test with Welch's correction.*

As shown in Figure 3-7A, pre-incubation with bumetanide (n = 10) reduced luminal swelling in response to FSK stimulation over a 30-minute period compared to that observed in spheroids treated with FSK alone (n = 8). At 30-minutes post FSK addition,

the lumen area increase in spheroids pre-treated with bumetanide was 57% of that observed in FSK stimulated spheroids.

Whilst the difference in T30 lumen area between spheroids treated with bumetanide prior to FSK stimulation and spheroids stimulated with FSK alone was not found to be significant ($p = 0.1265$), that between spheroids pre-treated with bumetanide and I-172 prior to FSK stimulation was significant ($p = 0.0066$) (Figure 3-7B). Neither pre-treatment of spheroids with I-172 nor bumetanide reduced luminal swelling to levels observed in untreated spheroids or those pre-treated with I-172 without subsequent addition of FSK. These data indicate that the FIS assay and quantification method discussed are suitable for studying CFTR-mediated fluid secretion into the lumen of LIM1863 spheroids. This assay can accurately quantify the effect of CFTR-mediated fluid secretion on lumen area as a direct result of FSK stimulation. Similarly, it can quantify more subtle changes in swelling induced by inhibitors of ion channels and transporters crucial to epithelial Cl^- transport.

Swelling assays were also performed using the vehicles detailed in Section 2.1.5, diluted as for drug treatments. In all vehicle control assays, no visible lumen formation was observed in LIM1863 spheroids (data not shown; for DMSO n = 10; for methanol n = 10).

3.3.5. Development of Automated FIS Assay Analysis

To increase the screening capacity of the FIS assay, allowing for simultaneous analysis of a larger number of LIM1863 spheroids, an automated analysis method was sought. An automated program termed Lumina Tracking, written in MATLAB as a plugin for Fiji/ImageJ, was developed (Lumina Tracking was developed by Dr S. Cross, Wolfson Bioimaging Facility, University of Bristol). Initial experiments conducted during the development of this program explored the use of the cell-permeant dye calcein green to stain LIM1863 spheroids prior to image acquisition. Upon entering live cells surrounding the LIM1863 spheroid lumen, nonfluorescent calcein-AM (acetoxymethyl) is converted to green fluorescent calcein by the removal of the acetomeoxy group by intracellular esterases (Bratosin *et al.*, 2005). This green fluorescence permits the identification and tracking of spheroid lumen based on the contrast between fluorescing epithelial cells and the dark luminal background. Cell labelling using calcein green prior to FIS assays has been previously reported to be a useful tool for automated image analysis of both murine and human primary organoids (Dekkers *et al.*, 2013; Dekkers *et al.*, 2016).

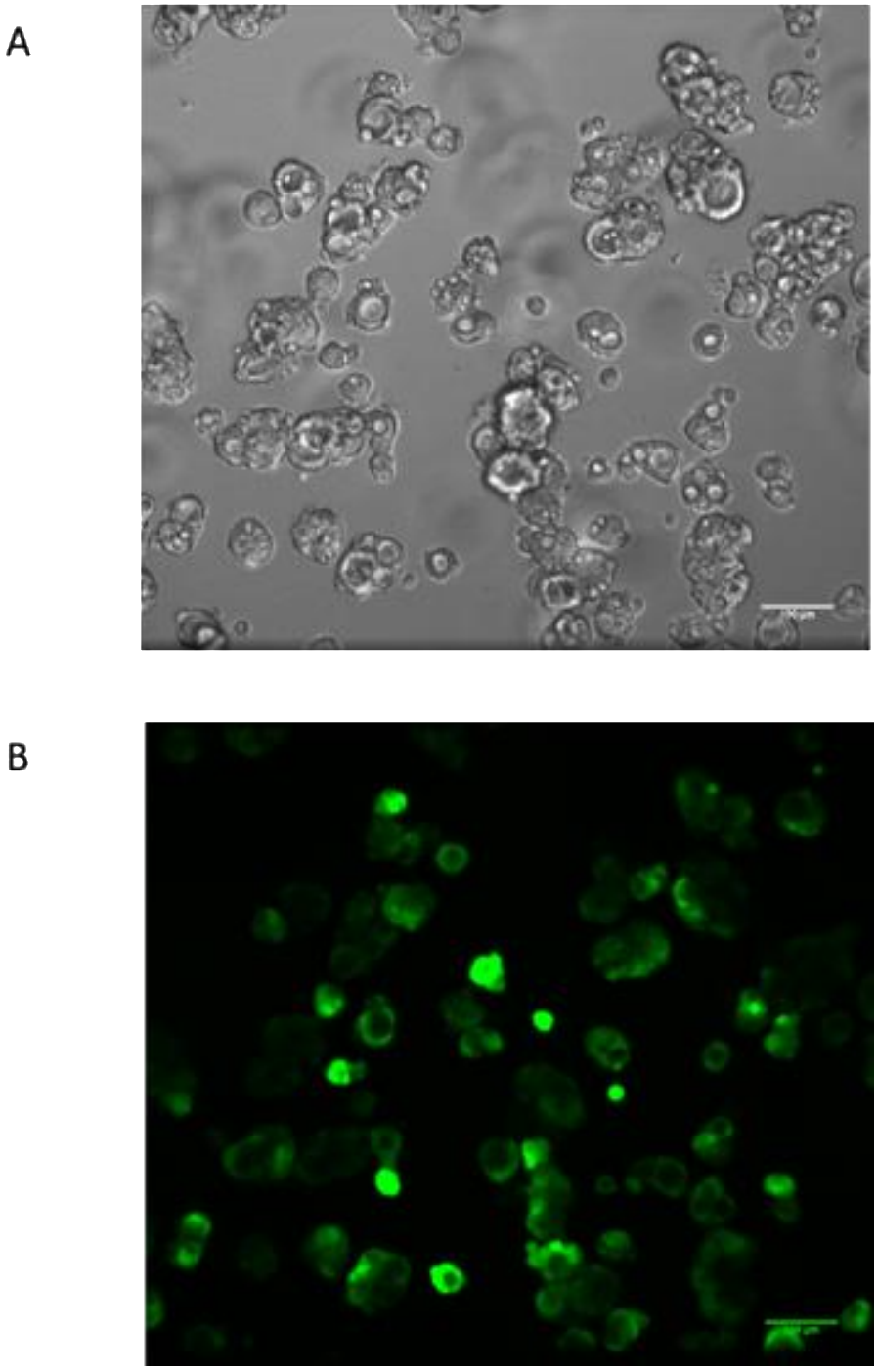

Figure 3-8: Calcein green staining of LIM1863 spheroids after stimulation with 10 µM forskolin.

*Phase contrast **(A)**, and calcein green fluorescence **(B)** images of LIM1863 spheroids 25-minutes post stimulation with 10 µM forskolin. LIM1863 spheroids were incubated with calcein green (10 µM) for 1-hour at 37 ℃, protected from light, prior to imaging. Images were acquired using a spinning disk confocal microscope with 10x magnification. Scale bars = 100 µm.*

It was observed that in LIM1863 spheroids staining with calcein green, (5 μM and 10 μM) for both 30-minute and 1-hour incubations at 37 °C while protected from light, failed to produce sufficient nor consistent staining for automated image analysis. Figure 3-8 shows a representative example of LIM1863 spheroids stained with 10 μM calcein green (1-hour, 37 °C and protected from light) and the corresponding phase-contrast image, 25-minutes post incubation with 10 μM FSK.

After concluding that calcein green staining was not suitable for automated image analysis of LIM1863 spheroids in FIS assays, attempts were made to overcome this by redesigning the Lumina Tracking plugin to use only phase contract images. The principle behind this approach was similar to that for calcein green staining of LIM1863 spheroids in that the Lumina Tracking plugin would differentiate between epithelial cells and spheroid lumen based on pixel intensity. Although at later time points the automated analysis software detected spheroid lumen using phase contrast images, it was not able to accurately detect spheroid lumen at early time points, and mis-identified lumen of spheroids in close proximity over the duration of the experiment. As a result, early time point measurements were required to be measured manually, and the plugin could not be used to accurately quantify more subtle changes in swelling induced by known inhibitors of channels and transports key to epithelial Cl^- transport.

3.3.6. LIM1863 spheroids dissociate giving rise to viable single cell populations.

For experiments to measure CFTR-mediated transepithelial Cl^- transport with the Ussing chamber technique, and potential experiments utilising gene editing, it was necessary to develop a tissue culture protocol to dissociate LIM1863 spheroids into viable single cell cultures. In order to generate a single cell population of LIM1863 cells, spheroids were cultured in calcium free S-MEM without GlutaMAX and containing 1% (v/v) foetal calf serum (see Section 2.3.3). After 48-hours of incubation at 37 °C in 5% CO_2 the resultant cellular population was passed through a 40 μm cell strainer to remove remaining cellular clumps, and the collected cells counted. $2x10^5$ single LIM1863 were resuspended in 200 μl calcium free S-MEM without GlutaMAX and propidium iodide (PI) was added to a final concentration of 1 μg/ml. Flow cytometry was used to assess single cell and viable cell populations. This experiment was performed on three independent cultures of LIM1863 spheroids. The flow cytometry gating strategy used along with representative data from culture 1 are shown in Figure 3-9.

Analysis of flow cytometry data for culture 1 of single LIM1863 cells showed that 84% of recorded events were singlets with 69% of singlets being live cells; from culture 2 of single LIM1863 cells, 84% of recorded events were singlets with 62% of singlets live cells; and from culture 3 of single LIM1863 cells, 80% of recorded events were singlets with 61% of singlets live cells. These data strongly support the use of this culture method to produce viable single cell populations of LIM1863 cells for Ussing chamber and gene editing studies.

3.3.7. Single LIM1863 cell populations can re-form spheroids capable of CFTR-mediated swelling.

To assess whether cultures of single LIM1863 cells were able to reform spheroids that swelled in response to FSK stimulation, single cells from cultures 1 to 3 were washed and resuspended in LIM1863 spheroid media (see Section 2.3.3) and then incubated for 2-weeks at 37 °C, 5% CO_2. Figure 3-10 shows a sequence of images capturing the dissociation of LIM1863 spheroids into single cells, and subsequent re-formation of spheroids. A FIS assay was performed on spheroids derived from all three cultures of single LIM1863 cells and corresponding original LIM1863 spheroid cultures used to produce the single LIM1863 cells. Figure 3-11 shows representative data from spheroids derived from single cell LIM1863 culture 1 and corresponding original spheroid culture. Control swelling assays using Hanks solution were also performed (data not shown) resulting in no visible lumen formation. These data demonstrate that LIM1863 spheroids derived from single cell cultures are capable of CFTR-mediated Cl^- transport in response to stimulation with FSK. Although Figure 3-11 suggests that control spheroids are capable of greater luminal swelling over a 30-minute period than those generated from single cell LIM1863 culture, further repeats would have to be performed and analysed to verify this observation.

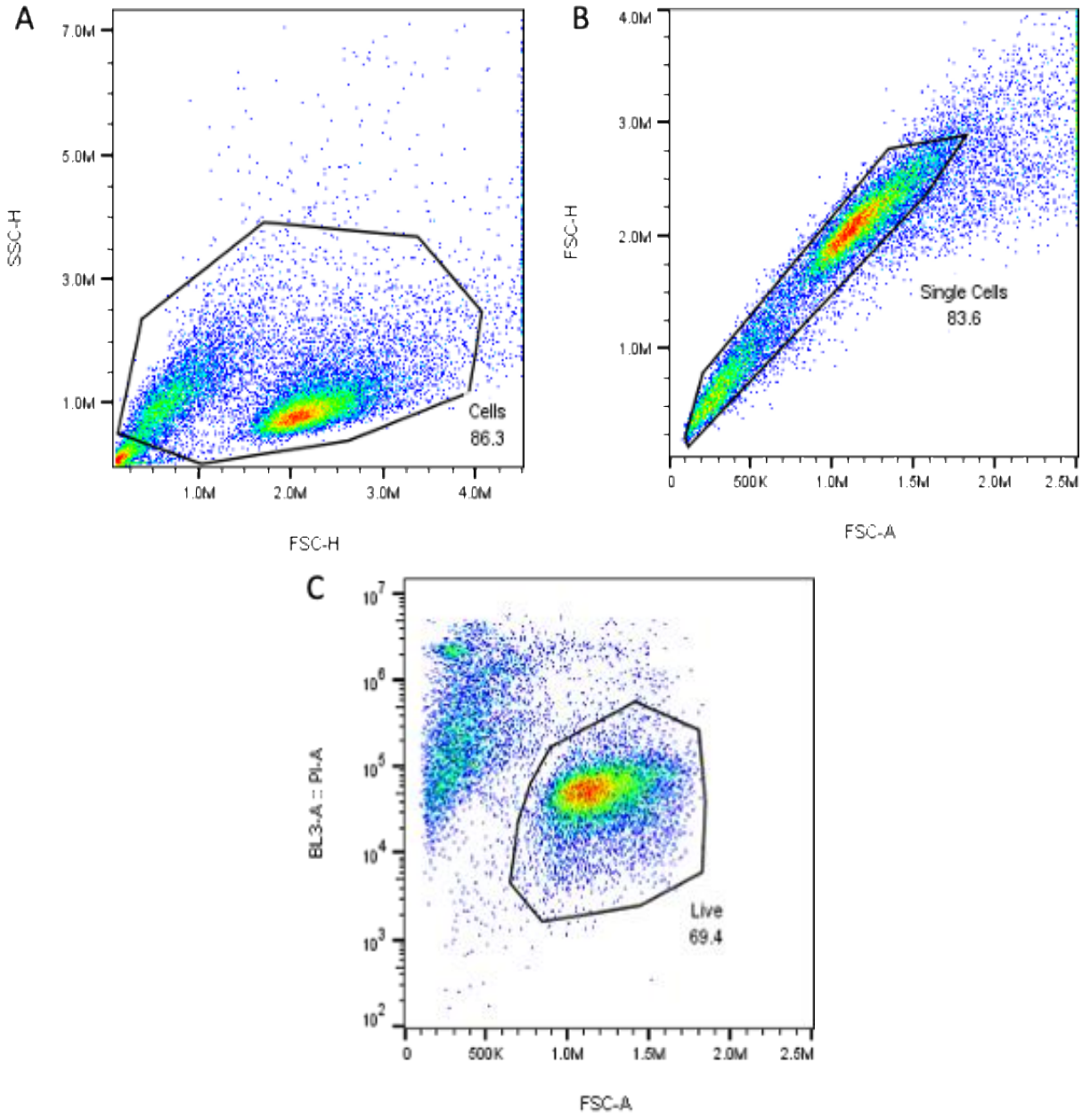

Figure 3-9: Culture of LIM1863 spheroids towards viable single cell cultures.

*$2x10^5$ single cells were stained with propidium iodide (PI) and flow cytometry used to detect single cell and live cell populations. Flow cytometry gates were designed to exclude debris **(A)**, isolate singlets (84% of cells) **(B)**, and among the singlets identify live (PI negative [69% of singlets]) and dead (PI positive) cells **(C)**. Abbreviations: SSC-H (side scatter-height), FSC-H (forward scatter-height), FSC-A (forward scatter-area), PI-A (PI-area). Data shown are for culture 1 of three independent experimental repeats.*

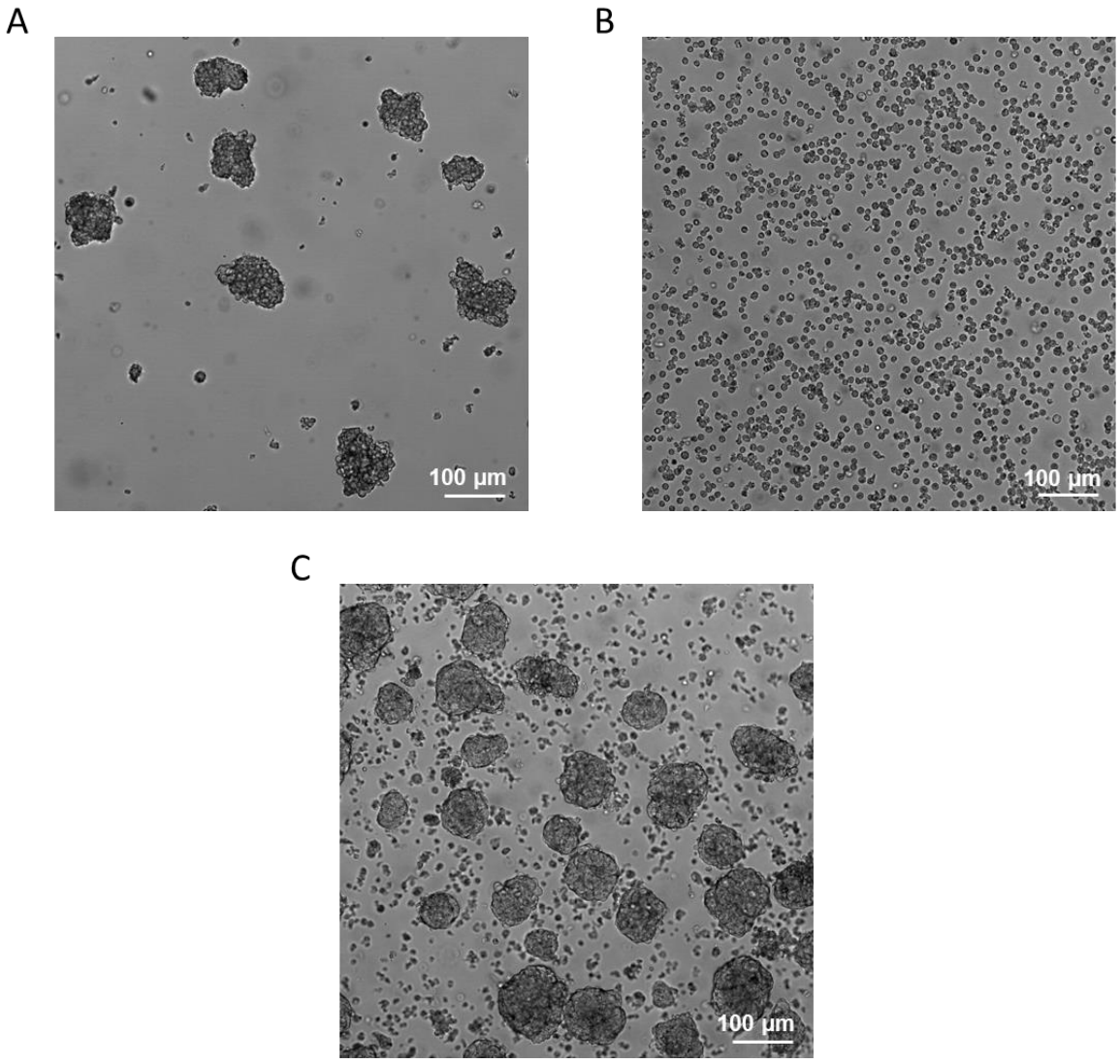

Figure 3-10: LIM1863 spheroids can dissociate to form a single cell culture and re-form morphologically organised spheroids.

Phase contrast images of the LIM1863 cell line are shown. ***(A)*** *Original spheroid population cultured in LIM1863 spheroid media.* ***(B)*** *Single cell LIM1863 population, after 48-hours cultured in calcium free S-MEM without GlutaMAX and containing 1% (v/v) foetal calf serum.* ***(C)*** *LIM1863 spheroids reformed from single cell populations, cultured in LIM1863 spheroid medium for 2-weeks. All images are of culture 1. They were acquired using a widefield microscope with 10x magnification. Scale bars = 100 μm.*

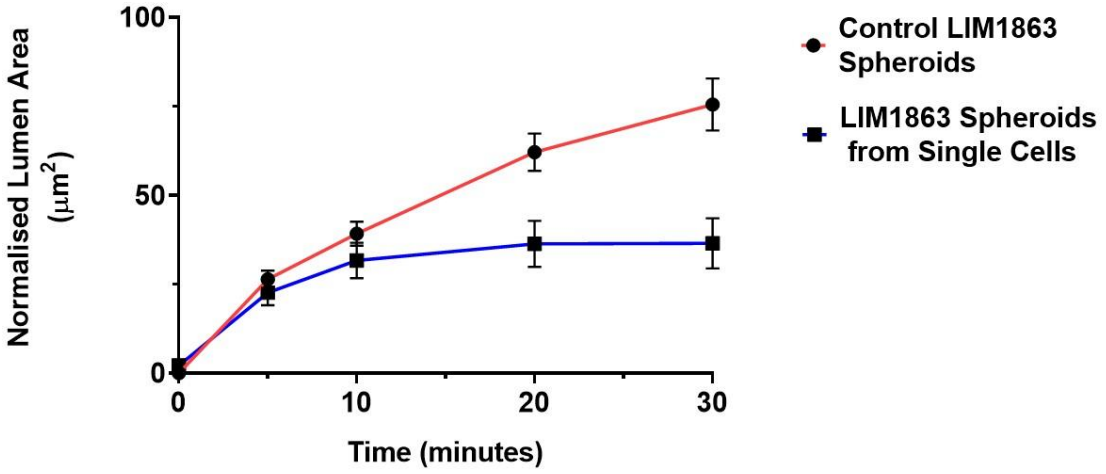

Figure 3-11: Spheroids derived from single cell LIM1863 culture demonstrate CFTR-mediated luminal swelling in response to FSK-stimulation.

Lumen area increase for both control LIM1863 spheroids, and spheroids derived from single cell culture upon stimulation with Forskolin (10 μM). LIM1863 lumen area is normalised to spheroid radius at T0 for both culture 1 control LIM1863 spheroids (n = 10) and spheroids derived from culture 1 of single LIM1863 cells (n = 10). Control swelling assays performed with Hanks resulted in no lumen area change (data not shown). Data plotted as mean ± S.E.M.

3.3.8. Transepithelial resistance of LIM1863 epithelia.

To further characterise CFTR-mediated transepithelial Cl^- transport, attempts were made to grow the LIM1863 cell line as polarised epithelia on Transwell inserts for Ussing chamber studies as described in Section 2.10.1. Transwell inserts were seeded with both LIM1863 spheroids and single LIM1863 cells. For LIM1863 spheroids, Transwell inserts were seeded with spheroids corresponding to 1/10 of 8 ml of a confluent tissue culture flask and incubated in LIM1863 spheroid media (see Section 2.10.1) for 14 days. For single cell LIM1863 cells, Transwell inserts were initially seeded with 5 x 10^5 cells. However, this seeding density proved to be too dense and so subsequently Transwell inserts were seeded with 2.5 x 10^5 cells and incubated in either LIM1863 spheroid media or calcium free S-MEM without GlutaMAX and containing 1 % (v/v) foetal calf serum.

The transepithelial resistance (R_t) was measured every other day for a maximum of 14 days. The R_t of a blank Transwell insert was also measured to provide control data. As illustrated in Figure 3-12, none of the experimental conditions tested generated an R_t above that of a blank Transwell insert. It was therefore concluded that the LIM1863 cell line was not able to grow as a polarised epithelium for Ussing chamber experiments to study transepithelial ion transport.

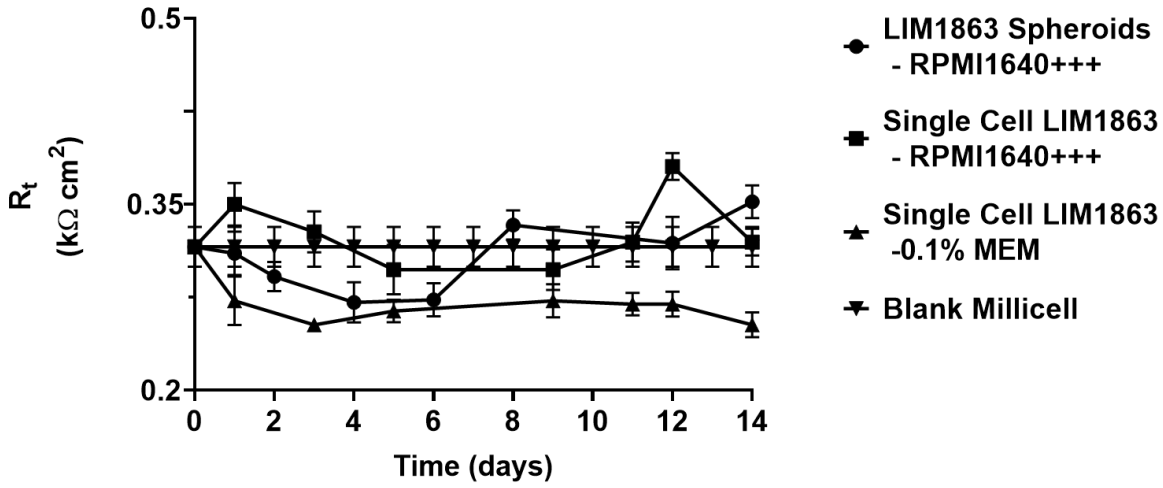

Figure 3-12: Transepithelial resistance of LIM1863 cells and spheroids.

Transepithelial resistance of LIM1863 cells and spheroids at a range of timepoints post seeding onto Transwell inserts are shown. For all experimental conditions n = 8, for blank Transwell insert control n = 46. Data are plotted as means ± S.E.M.

3.4. Discussion

The aims of this work were two-fold. Firstly, to evaluate the LIM1863 cell line as a model for studying intestinal ion transport, particularly that mediated by the apical membrane Cl^- channel CFTR. As outlined in Section 3.2, for the LIM1863 cell line to meet the criteria required LIM1863 spheroids must be capable of CFTR-mediated spheroid swelling, the extent of spheroid swelling must be quantifiable, and quantification must be such that it allows high-throughput screening. Secondly, to develop and optimise a high-throughput screen to identify compounds which may be of therapeutic use in the restoration of ion and water homeostasis to the CF intestine.

The work presented highlights some of the advantages and limitations of the LIM1863 cell line as a model for studying CFTR-mediated intestinal ion transport. This work also details preliminary studies to develop an automated high-throughput screening assay.

LIM1863 spheroids responded to stimulation with FSK as previously reported (Currid et al., 2004). This response was observed visually as the emergence of a central lumen within 10-minutes of spheroid stimulation with 10 μM FSK (Figure 3-1). Whilst in some LIM1863 spheroids a visible lumen was apparent before the addition of FSK, this was atypical. The measurable change in LIM1863 spheroid morphology associated with FIS provides the opportunity for quantifiable morphometric analysis, which in turn gives scope for the development of an automated screening assay.

Intestinal organoids derived from mouse models and human subjects demonstrate an overall increase in organoid area when stimulated with FSK (Dekkers *et al.*, 2013; Dekkers *et al.*, 2016; Boj *et al.*, 2017), which was quantified from total organoid area at selected time points post FSK stimulation, expressed as a percentage of organoids area (x,y plane) at T0 (T0 area = 100%). Initial approaches towards characterising the FIS response in LIM1863 spheroids revealed that the appearance of a visible spheroid lumen did not correspond to an overall increase in spheroid area (Figure 3-2). Interestingly, it was found that in LIM1863 spheroids the FIS response is more accurately portrayed as an increase in internal lumen area with a corresponding decrease in epithelial area (Figures 3-3, 3-4 and 3-5). When considering these findings, alongside the aim of developing a FIS assay high-throughput screen, it was decided to use lumen area normalised to T0 spheroid radius for FIS quantification (Figure 3-5). The justification for this decision arose from the following points. Firstly, although quantification of FIS as a

function of change in epithelial area (as used to produce Figure 3-3), clearly distinguished between untreated and FSK stimulated spheroids, the generation of data points required the measurement and subsequent data handling of two parameters. Analysis of data using this approach would therefore be more time consuming than possible alternatives and not conducive to high-throughput screening. Secondly, whilst representation of FIS response using lumen area increase as a percentage increase from that at T0 (100%) (as used to produce Figure 3-4), also clearly distinguished between untreated and FSK stimulated spheroids, this method does not take into account the wide distribution of spheroid size observed within and between cultures. Normalisation of lumen area to the radius of the corresponding spheroid radius at T0 accommodates for variation in spheroid size across cultures, allowing the comparison of experimental repeats from different LIM1863 spheroid cultures (Figure 3-6). Thirdly, when representing FIS using lumen area increase as a percentage increase from that at T0 (100%), the number of spheroids per assay which have a visible lumen at T0 can heavily influence the outcome of each assay. For spheroids with a visible lumen at T0 each subsequent lumen area will be normalised to a higher value than those normalised to a value of 1 (spheroids with no visible lumen). Whilst the occurrence of a visible lumen at T0 is a chance event, assays with a higher proportion of lumen assigned a value of 1 at T0 will be reported as having an average lumen area increase much greater than assays with fewer lumens assigned a value of 1 at T0. Representation of FIS as lumen area in μm, rather than as a percentage increase from T0 circumvents this issue.

An increase in LIM1863 spheroid lumen area post-stimulation with FSK suggests that CFTR-mediated Cl^- transport was occurring across the apical membrane of the epithelial cells lining the spheroid lumen. FSK increases intracellular cAMP, promoting cAMP-dependent phosphorylation and activation of CFTR (Dulhanty and Riordan, 1994; Csanády, Vergani and Gadsby, 2019). CFTR-mediated Cl^- transport, alongside the movement of Na^+ into the spheroid lumen down its concentration gradient draws H_2O from the Hanks solution bathing the spheroids into the spheroid lumen according to the osmotic gradient (Frizzell *et a*l., 1979; Henderson *et al.*, 1992; Moran and Zegarra-Moran, 2008; Boj *et al.*, 2017). LIM1863 spheroids treated with the CFTR inhibitor I-172 (Ma *et al.*, 2002) alone, and spheroids pre-treated with I-172 and then stimulated with FSK, produced no visible lumen, and reduced FIS respectively (Figure 3-7). These findings provide further supportive evidence that the FIS observed was a result of CFTR-mediated Cl^- transport. Incubation of LIM1863 spheroids with the NKCC1 inhibitor bumetanide, prior to stimulation with FSK, resulted in a marked reduction in luminal swelling, when compared to that observed in spheroids stimulated with FSK alone

(Figure 3-7), in agreement with previous data (Currid *et al*., 2004). The observations discussed support the proposition that the mechanism of fluid secretion into the LIM1863 spheroid lumen recapitulates that known to occur in the colonic epithelium (Barrett and Keely, 2000).

Considered together these observations corroborate previously findings (Currid *et al*., 2004), highlighting the LIM1863 cell line as a potential model for studying CFTR-mediated colonic ion transport, and identifying a measurable change in LIM1863 spheroid morphology associated with fluid secretion into the spheroid lumen. This morphological change provides the opportunity for quantifiable morphometric analysis, which in turn gives scope for the development of an automated screening assay.

Automated analysis of FIS in LIM1863 using calcein green staining was unsuccessful, unlike FIS assays analysed using this method reported by Dekkers *et al.* (2013, 2016), and Boj *et al.* (2017). In contrast to intestinal organoids derived from mouse and human intestine, calcein green staining of LIM1863 spheroids was inconsistent and did not differentiate clearly enough the LIM1863 spheroid epithelium from the surrounding media and internal lumen (Figure 3-8). Attempts to use this method of analysis were further complicated by the necessity to measure the internal lumen area, as opposed to the overall spheroid area. Automated analysis using phase contrast images was more successful, as the Lumina Tracking plugin was able to detect and track lumen over time. However, limitations were still apparent. At early time points, the plugin could not detect developing lumen. Similarly, the plugin was not able to distinguish the lumen of spheroids that were overlapping or in close proximity. As a result, a considerable amount of manual input was required making large scale screening and image analysis unfeasible.

Despite the limitations associated with the automation of image analysis, assay optimisation resulted in a LIM1863 FIS assay where multiple experimental conditions were investigated in a single experiment. Initial FIS assays were recorded using a spinning disk confocal microscope without a programable motorised stage. As a result of this the desired x,y coordinates for each field of view had to be recorded and located manually, and the upper and lower boundaries of the required z-plane defined, for each well at each time point. The time-consuming nature of this, combined with the desire to record both phase contrast and calcein green images at 2-minute intervals, restricted the experimental conditions that could be assayed at any one time. Later FIS assays were recorded using a widefield microscope with a programable motorised stage. For each

well, the x and y coordinates of one or more fields of view were saved, and for each field the z-stack limits defined (7 µm intervals). The ability to program the experimental settings beforehand, alongside the need to only acquire phase contrast images, allowed for multiple well positions and experimental conditions to be imaged in quick succession. These considerations lend themselves to high-throughput screening.

Viable cultures of single LIM1863 cells were sought to facilitate Ussing chamber experiments to study transepithelial ion transport by LIM1863 epithelia and allow future experiments utilising gene editing techniques. Disaggregation of LIM1863 spheroids, producing viable single cell cultures has been previously reported (Hayward and Whitehead, 1992). Work presented in this chapter successfully reproduced this method to produce three individual cultures of viable single LIM1863 cells as a proof of principle (Figure 3-9). Subsequently, it was demonstrated that populations of single LIM1863 cells, when cultured in LIM1863 spheroid media, could reform morphologically organised spheroids capable of CFTR-mediated swelling in response to FSK-stimulation (Figures 3-10 and 3-11).

The LIM1863 cell line expresses wild-type CFTR and NHE3, both proteins of interest in this thesis (Currid *et al*., 2004). Depletion of one or both of these proteins in LIM1863 cells using gene editing (e.g. via CRISPR-Cas9 or siRNA transfection) would create a valuable model system for studies of intestinal ion transport. It would allow the study of CFTR depletion on FIS, the rescue of luminal hydration by NHE3 inhibition, and validation of NHE3 inhibition studies. Recently optimised methods to deliver siRNA into 3D spheroids contained in Matrigel have been reported, where previously delivery of siRNA into 3D cultures has proved difficult (Morgan *et al.*, 2018). The ability to explore gene editing using siRNA transfection in both 3D spheroids and single cell cultures widens the scope of future work using LIM1863 spheroids, especially given that single cell LIM1863 populations can re-form functional 3D spheroids.

Ussing chamber studies would further aid characterisation of the ion channels and transporters associated with the LIM1863 cell line, and complement data acquired from FIS assays. Since its origins in 1950, the Ussing chamber technique has been widely used to assess ion transport across epithelial tissues (Ussing and Zerahn, 1951; Li, Sheppard and Hug, 2004; Clarke, 2009). Of particular relevance, this technique has been used to record short-circuit current (I_{sc}) across epithelia derived from intestinal cell lines, native intestinal tissue biopsies, and intestinal primary cell cultures (Cuthbert *et al.*, 1987; Travis, Berger and Welsh, 1997; Cuppoletti *et al.*, 2004; Bradford *et al.*, 2009;

Dekkers, Van Mourik, *et al.*, 2016). Combined these studies highlight the use of the Ussing chamber technique not only in the characterisation of epithelial ion channels, but also as a tool for identifying compounds that activate and inhibit epithelial ion channels which might have therapeutic potential for the treatment of CF. Despite the production of viable single cell LIM1863 populations, attempts to generate polarised epithelia on Transwell inserts seeded with single LIM1863 cells and LIM1863 spheroids were unsuccessful (Figure 3-12). It was therefore concluded that the LIM1863 cell line was not suitable for Ussing chamber studies.

3.5. Concluding Remarks

The LIM1863 cell line shows potential as a model for the study of CFTR-mediated Cl^- transport. When subject to FIS assays, LIM1863 spheroids demonstrated a quantifiable response to FSK-stimulation by way of an increase in lumen area. Although quantification of the FIS swelling response was sensitive enough to detect subtle changes in spheroid lumen area in response to known inhibitors of ion channels and transporters key to epithelial Cl^- transport, use of the assay for high-throughput screening was limited by difficulties automating image analysis. Viable single LIM1863 cells, which possessed the ability to re-form organised and functional spheroids, were successfully cultured, lending the LIM1863 cell line to future work utilising gene editing techniques. Despite previously reported use of intestinal cell lines, and primary intestinal tissue in Ussing chamber studies, LIM1863 cells failed to polarise and generate a R_t, thus rendering the cell line unsuitable for Ussing chamber studies. To this end, it was concluded that the LIM1863 cell line did not meet the criteria required and stated in Section 3.2, and an alternative cellular model for the study of intestinal ion transport was sought.

Chapter 4. Establishment of a cellular model for the study of intestinal ion transport.

4.1. Introduction

The intestine is a complex tissue of much interest due to its ability to self-renew from a pool of local stem cells, its multifaceted role in immunity, and its function as an absorptive and secretory epithelium (Greger, 2000; Simon-Assmann *et al.*, 2007; De Lisle and Borowitz, 2013). Cell line and animal models of the intestine have proved invaluable research tools, shedding light on cellular differentiation, furthering our understanding of gastrointestinal pathophysiology, and aiding the identification of drug targets and therapeutics (Kim, Koo and Knoblich, 2020). Owing to the complexity of the intestinal tissue structure and environment, experiments using *in vivo* models can prove difficult to control and reproduce (Costa and Ahluwalia, 2019). *In vitro* cell line models for studying the intestine overcome this hurdle and provide a simplified, well-controlled environment whilst avoiding the expense and ethical issues surrounding the use of animal models in research. However, *in vitro* cell line models, themselves, have limitations as it is rare, especially with 2D intestinal epithelial models, for a single cell line to recapitulate the complex tissue architecture and associated environment of the intestine.

Since the establishment of the human colonic HT-29 human cell line in the 1960s, colonic cancer cell lines have provided effective models to investigate the proliferation, differentiation, and regulation of intestinal cell populations (Simon-Assmann *et al.*, 2007). The human adenocarcinoma cell lines Caco-2 and T84 have been widely used for studies of intestinal ion transport, particularly epithelial Cl^- secretion (McCool *et al.*, 1990; Cuppoletti *et al.*, 2004; Zhu *et al.*, 2005; Sun *et al.*, 2008; Bijvelds *et al.*, 2009). Upon differentiation, both Caco-2 and T84 cells exhibit polarity and characteristics of enterocyte morphology and function (McCool *et al.*, 1990; Sambuy *et al.*, 2005; Simon-Assmann *et al.*, 2007). More recently, methods have been developed allowing for the culture of Caco-2 and HT-29 cell lines as 3D spheroids (Samy *et al.*, 2019; Gheytanchi *et al.*, 2021), however many 2D epithelial cell line models do not recreate the complex microenvironment of the intestine. This complex 3D microenvironment plays a significant role in intestinal function.

The identification of Lgr5-positive (Lgr5+) stem cells within colonic and small intestinal crypts (Barker *et al.*, 2007) initiated research leading to the culture of 3D intestinal organoids. In *in vitro* culture Lgr5+ stem cells have the capacity to differentiate into all cell populations of the intestinal epithelium and self-organise into 3D ‘mini-guts’ or organoids with characteristic crypt villi folding (Sato *et al.*, 2009, 2011). Since their

advent, intestinal organoids have been used extensively to study cellular proliferation and differentiation, as well as regenerative medicine, disease modelling and therapeutic development (Costa and Ahluwalia, 2019). For example, intestinal organoids derived from the small intestine and colon of individuals with CF have been used to study the impact of different disease-causing *CFTR* mutations on intestinal ion and fluid secretion (Dekkers *et al*., 2013). These patient-derived organoids have also been used to identify small molecule CFTR modulators and evaluate their efficacy in restoring ion and fluid transport to the CF intestine (Dekkers *et al*., 2016; Dekkers *et a*l., 2016; Dekkers *et al*., 2013), leading to personalised treatment based on patient genotype. Whilst initially used in 3D studies of intestinal ion and fluid transport, more recent methods allow the growth of 2D enterocyte monolayers from the same Lgr5+ stem cells (Thorne *et al.*, 2018).

Whilst the benefits of intestinal organoids as a research tool are clear, they also present their own unique set of limitations. Intestinal organoid cultures derived from primary human tissue are expensive to maintain and require more complex tissue culture techniques and conditions compared to traditional 2D cellular models (Vonk *et al.*, 2020). Moreover, biopsies to collect the primary intestinal tissue (both from the colon and small intestine) required to generate organoids can be an invasive and painful procedure. This is especially true for individuals with CF, who are already subject to an array of invasive treatments and tests, and for which a large proportion of patients are children and adolescents (Ratjen *et al.*, 2015). Biopsies derived from the small intestine are particularly difficult and painful to acquire.

To circumvent the limitations associated with primary intestinal organoids and 2D cell line models, a new cell line model of CFTR-mediated intestinal ion transport was sought. This cell line model should possess the ability to grow as 2D epithelial monolayers for Ussing chamber studies and as 3D spheroids for FIS assays, allowing the quantification of CFTR-mediated luminal Cl^- and fluid secretion.

4.2. Aims

This chapter aims to identify one or more cellular models of intestinal ion transport from a panel of adenoma and carcinoma colonic cell lines. As for LIM1863 spheroids, a suitable cellular model must grow as epithelial monolayers for 2D Ussing chamber studies and as 3D spheroids capable of CFTR-mediated spheroid swelling.

Cell lines will be screened for expression of CFTR mRNA and CFTR protein. Those that are found to express CFTR will be seeded onto Transwell inserts to promote the formation of epithelial monolayers, assessed by measurement of transepithelial resistance. Cell lines that successfully form epithelia will be used in 2D Ussing chamber studies to characterise the activity of ion channels and transporters associated with transepithelial Cl^- transport. Simultaneously, those cell lines forming epithelial monolayers will be assessed for their ability to grow as 3D spheroids capable of CFTR-mediated spheroid swelling in FIS assays. FIS assays will be evaluated to be quantifiable, reproducible, and image analysis conducive to automation.

This work also aims to build upon that in Chapter 3 towards the development of a high-throughput assay to screen compounds with the potential to restore fluid homeostasis to the CF intestine. The underlying principle of this assay remains the measurement of spheroid swelling driven by CFTR-mediated ion and fluid secretion into the spheroid lumen. As such, by the end of this chapter, it is anticipated that a suitable cellular model of intestinal ion transport will be identified and its use in a fully automated FIS assay optimised. This will pave the way for future experiments to determine the efficacy of novel therapeutic compounds in alleviating the gastrointestinal symptoms of CF.

4.3. Results

4.3.1. CFTR expression in a panel of colorectal adenoma and carcinoma cell lines.

A panel of human colonic adenoma and carcinoma cell lines (kindly donated by Professor A. Williams, University of Bristol), known to grow as both 2D cell suspensions, and 3D spheroids, were screened to identify those which express CFTR. Cell lines that express CFTR could potentially be used in 2D and 3D studies of CFTR-mediated epithelial ion transport. The panel of cell lines screened were AA/C1, AA/C1/15B/10C, AN/C1, RG/C2, HT-29, HCA7, HCT116, HCT15, SW480, SW620, LoVo, LS147T, SW1463, Caco-2 and RKO. SDS-PAGE protein separation followed by Western blotting was used to assess whole cell lysate CFTR protein, whereas Q-RT-PCR was used to identify CFTR mRNA.

Prior to screening cell lines for CFTR protein, a selection of antibodies against CFTR were tested for specificity (for antibody details see Section 2.1.6). CFTR antibody testing used SDS-PAGE protein separation and Western blotting of BHK-mock and BHK-CFTR wt whole cell lysates (lysate corresponding to $1x10^6$ BHK cells). For methodologies associated with cell lysis, SDS-PAGE electrophoresis, and Western blotting see Section 2.8. The results of this experiment are shown in Figure 4-1. It was anticipated that bands running at 150 kDa and 170-180 kDa, representing immature core-glycosylated and mature fully glycosylated CFTR, respectively (Cheng *et al.*, 1990), would be observed in the lane containing BHK-CFTR wt lysate, and absent in the lane containing BHK-mock lysate. With the exception of the antibody Mr Pink (Hoelen *et al.*, 2010), all CFTR antibodies demonstrated protein binding at molecular weights appropriate for antibody binding in BHK-CFTR wt lysates and reduced or no binding in BHK-mock lysates. CFTR-596 (Cui *et al.*, 2007) was confirmed to bind CFTR protein with little non-specific binding and was selected to screen the panel of human colonic cell lines for CFTR expression.

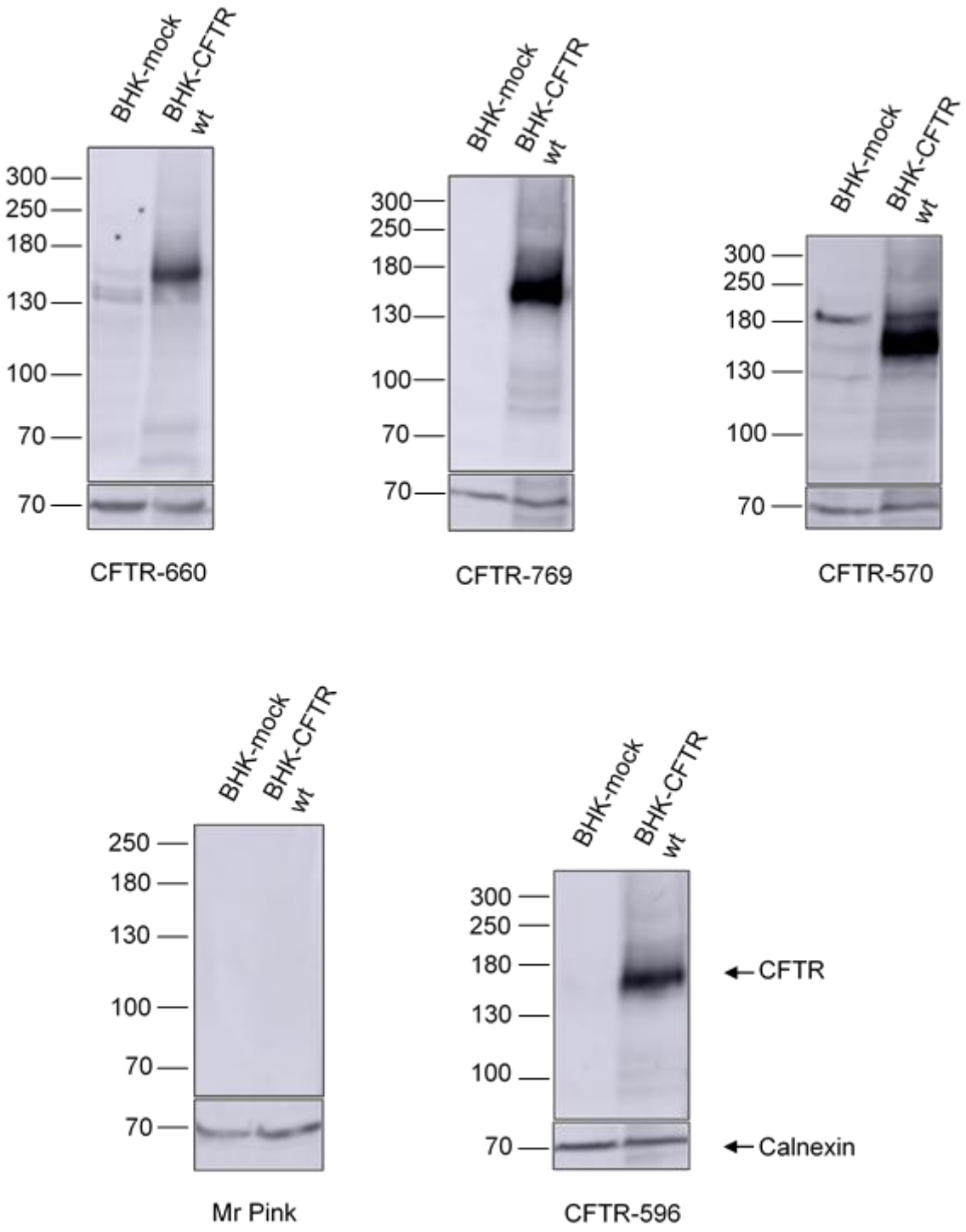

Figure 4-1: CFTR antibody testing in BHK-CFTR wt and BHK-mock whole cell lysates.

1x10^6 BHK-CFTR wt or BHK-mock whole cell lysates were separated by SDS-PAGE and immunoblotted with anti-CFTR antibodies. All primary antibodies were diluted 1/1000 in 5% (w/v) milk solution and all secondary antibodies were diluted 1/2000 in 5% (w/v) milk solution. An anti-calnexin antibody was used as a loading control. For Western blotting n = 1.

Once a suitable CFTR-antibody had been identified, SDS-PAGE protein separation and Western blotting was performed on 100 μg of total protein from the human adenoma and carcinoma cell lines studied. Protein concentration of whole cell lysates was determined using the Bio-Rad DC protein assay, following the manufacturer's protocol (see Section 2.8.2). Experimental samples were separated alongside whole cell lysate corresponding to 100 μg total protein from BHK-CFTR wt and BHK-mock cells, the positive and negative controls, respectively. Cell lines expressing CFTR protein corresponded to samples which demonstrated CFTR-596 antibody binding at 150 kDa and 170-180 kDa, (Figure 4-2).

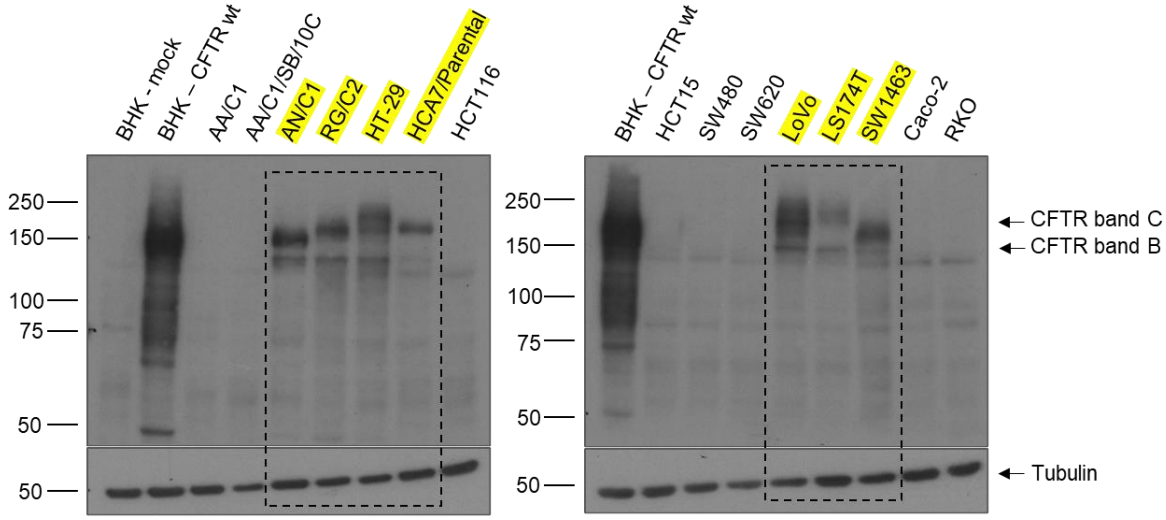

Figure 4-2: CFTR expression in human colonic adenoma and carcinoma cell lines.

100 μg of protein from human colonic adenoma and carcinoma whole cell lysates were separated by SDS-PAGE and immunoblotted with the anti-CFTR-596 antibody. An anti-tubulin antibody was used as a loading control. Cell lines identified as expressing CFTR were AN/C1, RG/C2, HT-29, HCA7 Parental, LoVo, LS174T and SW1463. These Western blots were performed by Tracey Collard, School of Cellular and Molecular Medicine, University of Bristol. For Western blotting n = 1.

The cell lines identified as expressing CFTR in Figure 4-2 were AN/C1, RG/C2, HT-29, HCA7/Parental, LoVo, LS147T and SW1463. Henceforth, the HCA7/Parental line will be referred to as the HCA7 cell line.

For the cell lines expressing CFTR protein, quantitative real-time PCR (Q-RT-PCR) was used to identify CFTR mRNA. Q-RT-PCR was also performed on AA/C1, AA/C1/SB/10C and Caco-2 cell lines. In brief, RNA was extracted from each cell line, purified and the resultant RNA concentration determined. With this RNA template, cDNA was synthesised and used alongside a CFTR primer in a Q-RT-PCR assay to determine the expression of a CFTR DNA product. The quantity of CFTR mRNA for each cell line was normalised to that detected in RG/C2 lysates. The RG/C2 cell line was selected for normalisation as it was found to express intermediate amounts mRNA compared to other cell lines investigated. With the exception of the Caco-2 cell line, CFTR mRNA was detected in all samples (Figure 4-3).

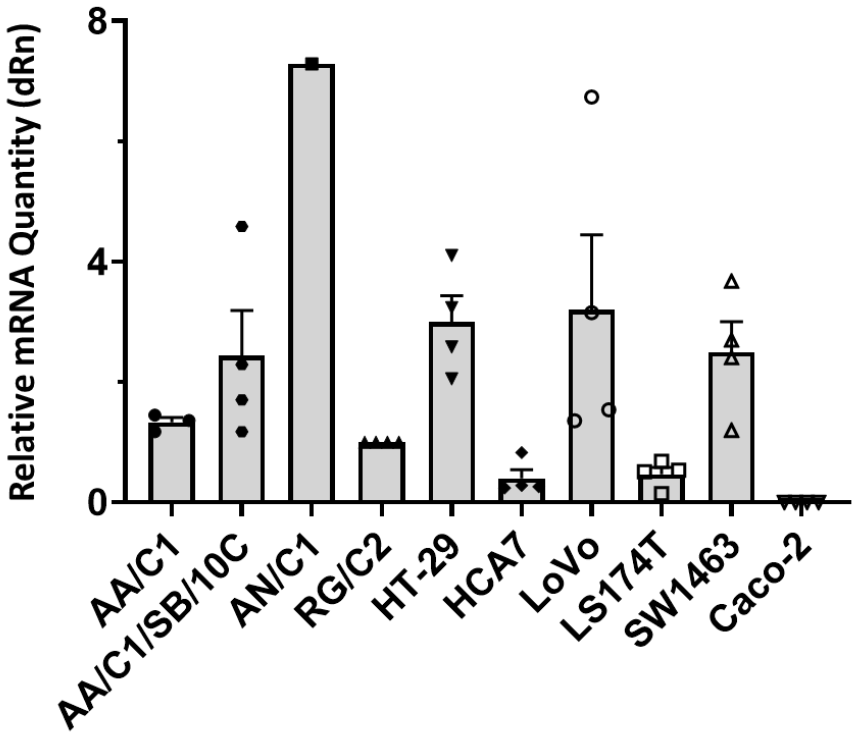

Figure 4-3: CFTR mRNA expression in human colonic adenoma and carcinoma cell lines.

Q-RT-PCR was performed on cell lines AA/C1, AA/C1/SB/10C, AN/C1, RG/C2, HT-29, HCA7, LoVo, LS174T, SW1463, and Caco-2. Results are presented as fold change in mRNA relative to negative control wells (no reverse transcriptase) and normalised to RG/C2. Data are means ± S.E.M. (n = 4).

4.3.2. Growth of CFTR-expressing colorectal adenoma and carcinoma cell lines as polarised epithelia.

Of the initial colonic carcinoma and adenoma cell line panel screened the HCA7, HT-29, LoVo, LS174T, RG/C2, SW1463 and Caco-2 cell lines were assessed for their ability to grow as polarised epithelia on polycarbonate Transwell inserts (see Section 2.10.1). Cell lines that produced polarised epithelia would generate a transepithelial resistance (R_t), measurable with a Volt/ohm meter and indicative of their suitability for Ussing chamber studies. Although the Caco-2 cell line studied did not express either CFTR protein or CFTR mRNA (Figures 4-2 and 4-3), it was included in this experiment because it has previously been reported to express CFTR, differentiate to form polarised epithelia, and grow on polycarbonate membranes (Sambuy *et al.*, 2005; Sun *et al.*, 2008; Jantarajit *et al.*, 2017). Figure 4-4 shows the R_t profiles for all cell lines tested, alongside that of a blank Transwell insert control. The R_t of FRT-CFTR wt and FRT-F508del epithelia are also displayed to illustrate the range of R_t achieved in alternative cell lines. The FRT cell line heterologously expressing exogenous CFTR-wt and F508del-CFTR, provides a model epithelium for studying Cl^- movement via CFTR (Sheppard *et al.*, 1994). Cell lines HT-29 (n = 8), LoVo (n = 8), LS174T (n = 8), RG/C2 (n = 8), SW1463 (n = 8) and Caco-2 (n = 8) did not generate R_t above that of a blank Transwell insert (Figure 4-4). Of the 7 cell lines seeded onto Transwell inserts, only the HCA7 cell line (n = 5-72), generated an R_t above that of a blank Transwell insert (Figure 4-4).

The screening of colonic adenoma and carcinoma cell lines outlined above revealed that only the HCA7 (human adenocarcinoma, colon) cell line expressed both CFTR mRNA and CFTR protein, grew in both 2D and 3D culture, and generated R_t when seeded onto Transwell inserts allowing for Ussing chamber experiments. As such, the HCA7 cell line was selected for use in all following functional studies described in this chapter.

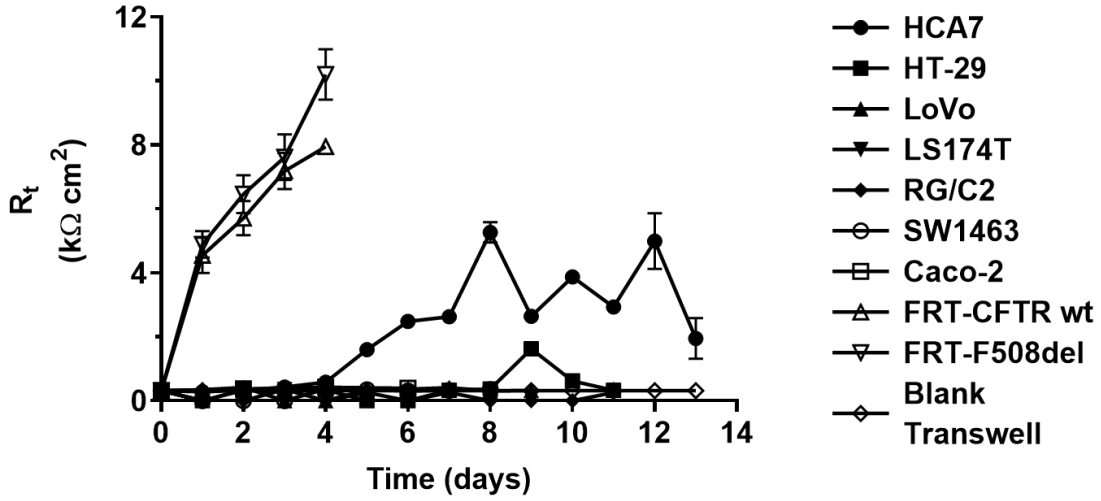

Figure 4-4: Transepithelial resistance of colonic cell lines.

Transepithelial resistance (R_t) of colonic cell lines expressing CFTR, FRT-CFTR wt cells and FRT-F508del cells at a range of time points post seeding onto Transwell inserts are shown. For FRT cells R_t was measured for 4-days until peak R_t was achieved and cells were used in experiments. All other cell lines were studied for 14-days. Data are means ± S.E.M. (HCA7: n = 5-72; HT-29: n = 8; LoVo: n = 8; LS174T: n = 8; RG/C2: n = 8; SW1463: n = 8; Caco-2: n = 5; FRT-CFTR wt: n = 11-25; FRT-F508del: n = 20-50; blank Transwell insert: n = 46.

4.3.3. Characterisation of ion transport across HCA7 epithelial monolayers.

The Ussing chamber technique allows for the net movement of ions across an epithelium to be studied. Experimental conditions can be manipulated so that the movement of a single ion of interest, for example Cl^-, can be assessed. Using known activators and inhibitors of ion channels and transporters involved in intestinal epithelial Cl^- transport, it is possible to both confirm the presence and characterise the activity of transport proteins associated with CFTR-mediated Cl^- transport in the HCA7 epithelium.

4.3.3.1. Forskolin induced and genistein potentiated I_{sc} by HCA7 epithelia.

To determine whether CFTR-mediated Cl^- current was generated by HCA7 epithelia, forskolin (FSK, 10 µM) was added to solution bathing the apical membrane. Figure 4-5A and B shows that 10 µM FSK increased I_{sc} (short-circuit current). Genistein (50 µM), a known potentiator of CFTR activity (Hwang and Sheppard, 1999; Wang *et al.*, 2002), significantly increased I_{sc} above that generated by FSK, (17.5% increase; $p = 0.048$). The I_{sc} generated by FSK and potentiated by genistein was significantly reduced (73% decrease) by the CFTR inhibitor I-172 (I-172; 10 µM; $p < 0.0001$). These data suggest that CFTR-mediated Cl^- current is generated by HCA7 epithelia.

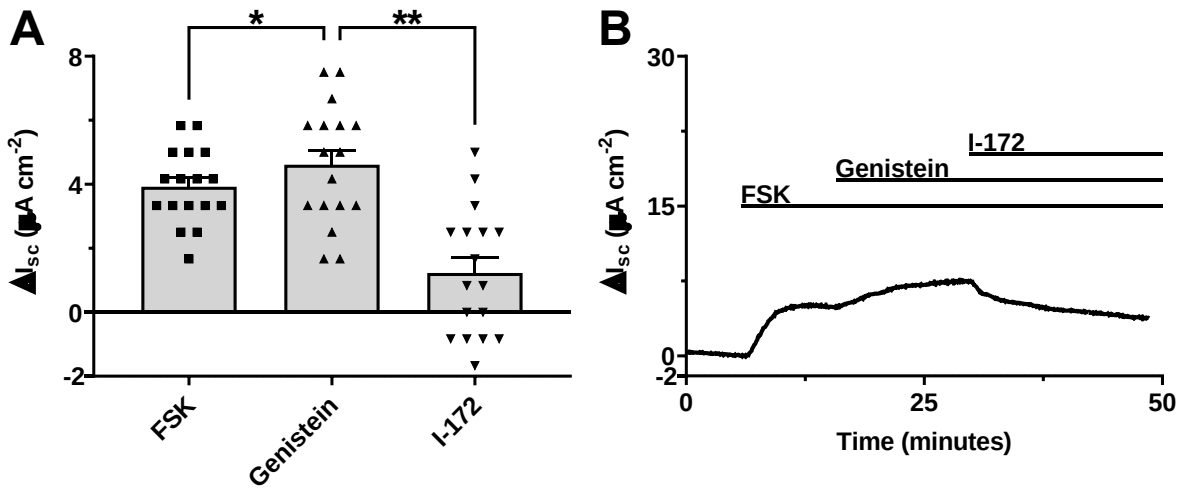

Figure 4-5: Representative Ussing chamber traces characterising FSK generated, and genistein potentiated I_{sc} by HCA7 epithelia.

(A) *Summary ΔI_{sc} data by HCA7 epithelia in response to CFTR activation by the cAMP agonist forskolin (FSK; 10 µM), and potentiation with genistein (50 µM). Currents were inhibited by the addition of $CFTR_{inh}$-172 (I-172; 10 µM). Data are means ± S.E.M. (n = 17); *, $p < 0.05$; Wilcoxon matched-pair signed rank test, **, $p < 0.01$; 2-tailed paired t-test.* ***(B)*** *Representative Ussing chamber trace for conditions quantified in* ***(A)****. The continuous lines indicate the presence of different compounds in the apical bathing solution. Data are displayed as change in short-circuit current (ΔI_{sc}) from baseline.*

4.3.3.2. Bumetanide decreases CFTR-mediated I_{sc} by HCA7 epithelia.

The majority of Cl^- uptake across the basolateral membrane into intestinal epithelia occurs via the basolateral membrane $Na^+/K^+/2Cl^-$ cotransporter, NKCC1 (Frizzell and Hanrahan, 2012). NKCC1 also has an important role in the recycling of Na^+ and K^+ ions across the basolateral membrane (Frizzell and Hanrahan, 2012). Ussing chamber experiments were performed to determine whether NKCC1 mediates the intracellular accumulation of Cl^- by the HCA7 cell line and quantify its activity if present. The NKCC1 inhibitor bumetanide (100 µM), was added to the solution bathing the basolateral membrane once a stable FSK (10 µM) induced and genistein (50 µM) potentiated Cl^- current had been established. Figure 4-6A and B reveal that bumetanide significantly reduced FSK induced, genistein potentiated I_{sc} by 47% ($p = 0.0003$). The bumetanide reduced I_{sc} was further inhibited (86% decrease) by I-172 (10 µM) ($p = 0.0039$). Combined, these data provide further evidence that CFTR-mediated Cl^- current is generated by HCA7 epithelia. The reduction of CFTR-mediated Cl^- current upon the addition of bumetanide strongly suggests the presence of NKCC1 within the basolateral membrane of HCA7 epithelia. Inhibition of NKCC1 activity reduces the intracellular concentration of Cl^- ions, diminishing the availability of Cl^- for CFTR-mediated transport.

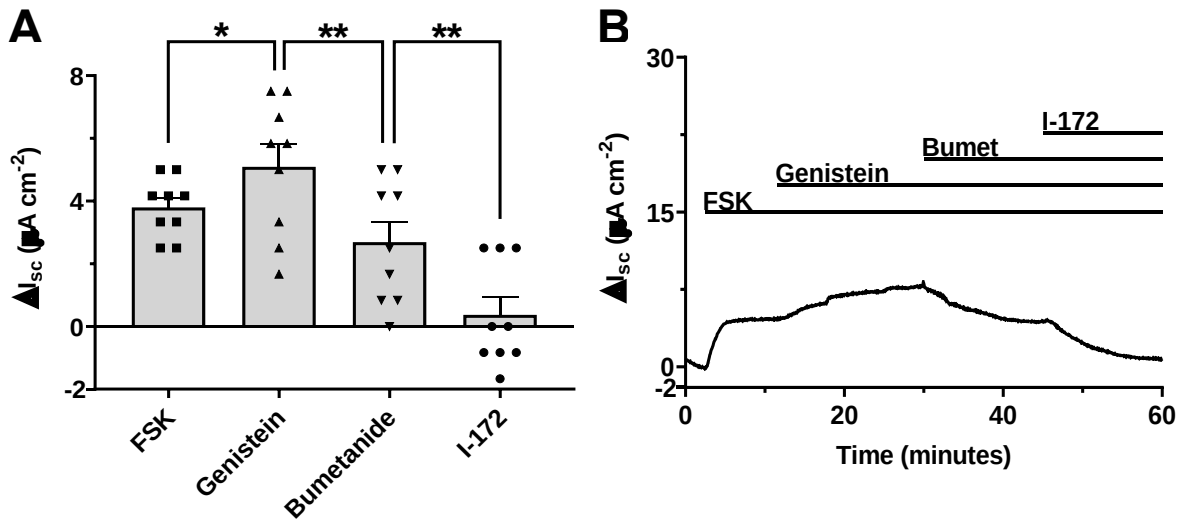

Figure 4-6: Representative Ussing chamber traces characterising bumetanide inhibition of FSK generated, and genistein potentiated I_{sc} by HCA7 epithelia.

(A) *Summary ΔI_{sc} data of HCA7 epithelia in response to CFTR activation by the cAMP agonist forskolin (FSK; 10 μM), potentiation with genistein (50 μM), and NKCC1 inhibition by bumetanide (Bumet; 100 μM). Currents were inhibited by the addition of $CFTR_{inh}$-172 (I-172; 10 μM) following bumetanide addition. Data are means ± S.E.M. (n = 9); *, p < 0.05; 2-tailed paired t-test, **, p < 0.01; 2-tailed paired t-test (genistein vs bumetanide) and Wilcoxon matched-pair signed rank test (bumetanide vs I-172).* ***(B)*** *Representative Ussing chamber trace for conditions quantified in* ***(A)****. The continuous lines indicate the presence of different compounds in the apical (FSK, genistein and I-172) and basolateral (bumetanide) bathing solutions. Data are displayed as change in short-circuit current (ΔI_{sc}) from baseline.*

4.3.3.3. CaCC-mediated I_{sc} across HCA7 epithelium.

Whilst a major route of Cl^- secretion, CFTR is not the only ion channel sited within the apical membrane of the intestinal epithelium by which Cl^- secretion occurs (Frizzell and Hanrahan, 2012). Calcium-activated chloride channels (CaCC), such as TMEM16A, also provide a mechanism for apical Cl^- secretion into the intestinal lumen (Frizzell and Hanrahan, 2012; Pedemonte and Galietta, 2014). Drugs such as ionomycin and uridine-5'-triphosphate (UTP) activate CaCC, generating transepithelial Cl^- current (Eggermont, 2004). Ionomycin is an ionophore, facilitating the transport of Ca^{2+} ions across the plasma membrane (Dedkova, Sigova and Zinchenko, 2000) to increase the intracellular Ca^{2+} concentration and activate CaCC. UTP is a P2Y2 (a G-protein coupled receptor) receptor agonist (Xu *et al.*, 2018). Activation of P2Y2 receptors by UTP instigates an

intracellular signalling pathway ultimately resulting in the mobilisation of Ca^{2+} from the ER, increasing intracellular Ca^{2+} concentrations and activating CaCC (Erb and Weisman, 2012).

Ussing chamber experiments utilising ionomycin and UTP were performed to determine the presence of CaCC in HCA7 epithelia. To ensure that ΔI_{sc} measured in response to either ionomycin or UTP to the solution bathing the apical membrane was CaCC-mediated, it was necessary to eliminate all CFTR-mediated I_{sc}. CFTR was activated by FSK (10 µM) and inhibited using I-172 (10 µM). Subsequently, ionomycin (2 µM) increased I_{sc} by 9.2 µA cm^{-2}, 514% above the residual CFTR-mediated I_{sc} ($p = 0.0001$; Figures 4-7A and C). As shown in Figures 4-7B and C, both FSK and ionomycin induced I_{sc} were inhibited when HCA7 epithelia were pre-treated with niflumic acid (200 µM; $p = 0.05$ and $p = 0.065$, respectively). Niflumic acid is a known inhibitor of CaCC and an open-channel blocker of CFTR (White and Aylwin, 1990; Scott-Ward *et al*, 2004). Addition of UTP (1 mM) to the solution bathing the apical membrane increased I_{sc} by 12.2 µA cm^{-2}, 183% above the residual CFTR-mediated I_{sc} ($p = 0.0015$; Figures 4-8A and B).

Together the data presented in Figures 4-7 and 4-8 provide compelling evidence to support of the presence of CaCC in the apical membrane of HCA7 epithelia.

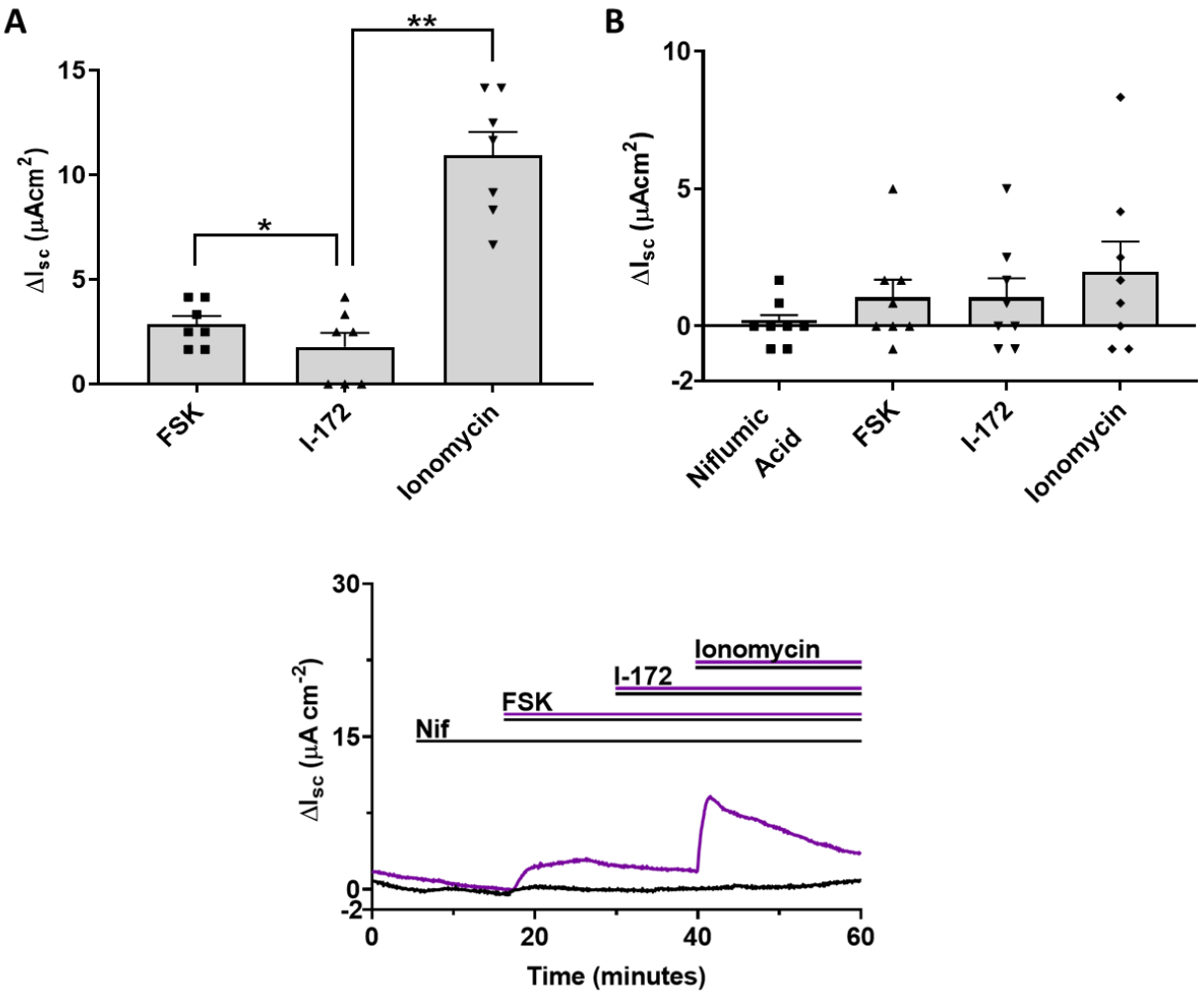

Figure 4-7: Representative Ussing chamber traces characterising Ionomycin induced, CaCC-mediated I_{sc} by HCA7 epithelia.

(A) *Summary ΔI_{sc} data by HCA7 epithelia in response to CaCC activation with the ionophore ionomycin (2 μM), following elimination of CFTR-mediated Cl^- current. CFTR-mediated current was activated by forskolin (FSK; 10 μM) and inhibited by $CFTR_{inh}$-172 (I-172; 10 μM). Data are means ± S.E.M. (n = 7); *, p < 0.05; 2-tailed paired t-test, **, p < 0.01; 2-tailed paired t-test.* ***(B)*** *Summary ΔI_{sc} data by HCA7 epithelia pre-treated with niflumic acid (200 μM) in response to CaCC activation by ionomycin (2 μM) following elimination of CFTR-mediated Cl^- current as described for* ***(A)****. Data are means ± S.E.M. (n = 8).* ***(C)*** *Representative Ussing chamber traces for conditions outlined in* ***(A)*** *and* ***(B)****. The continuous lines indicate the presence of different compounds in the solution bathing the apical membrane. Data are displayed as change in short-circuit current (ΔI_{sc}) from baseline.*

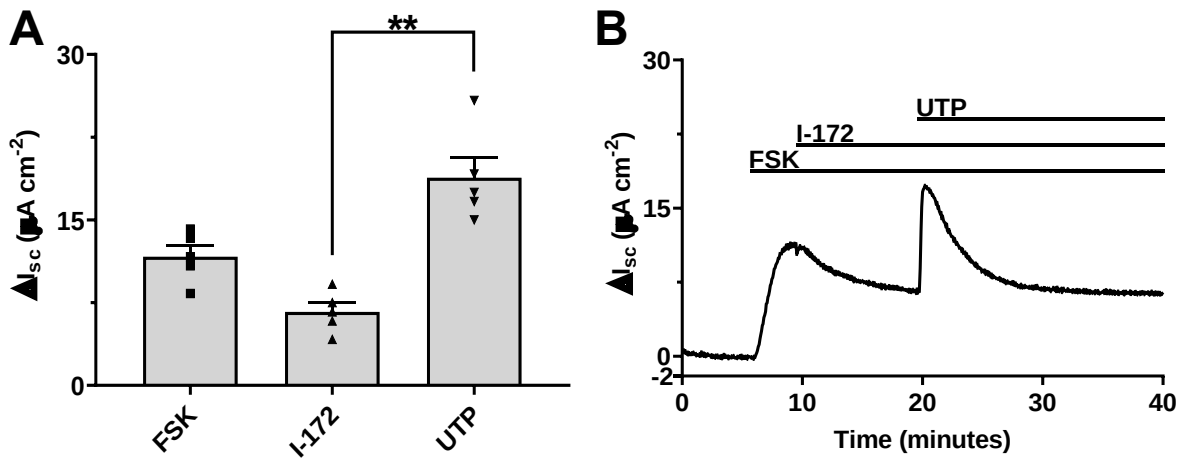

Figure 4-8: Representative Ussing chamber traces characterising UTP induced, CaCC-mediated I_{sc} by HCA7 epithelia.

(A) *Summary ΔI_{sc} data by HCA7 epithelia in response to CaCC activation by the P2Y2 receptor agonist UTP (1 mM), following elimination of CFTR-mediated Cl^- current. CFTR-mediated current was activated by forskolin (FSK; 10 μM) and inhibited by $CFTR_{inh}$-172 (I-172; 10 μM). Data are means ± S.E.M. (n = 5); **, p < 0.01; 2-tailed paired t-test.* ***(B)*** *Representative Ussing chamber trace for conditions outlined in* ***(A)****. The continuous lines indicate the presence of different compounds in the solution bathing the apical membrane. Data are displayed as change in short-circuit current (ΔI_{sc}) from baseline.*

4.3.3.4. Ouabain decreases CFTR-mediated I_{sc} across HCA7 epithelium.

The Na^+/K^+ ATPase plays a crucial role in maintaining Na^+ and K^+ gradients across the apical and basolateral membranes of secretory epithelia (Clausen, Hilbers and Poulsen, 2017). In intestinal epithelia, the initial gradients established by the Na^+/K^+ ATPase in the basolateral membrane ultimately provide the driving force required for apical Cl^- secretion. To determine whether the Na^+/K^+ ATPase was expressed in HCA7 epithelia, Ouabain (1 μM), a known inhibitor of Na^+/K^+ ATPase activity (Li, Findlay and Sheppard, 2004; Jansson *et al.*, 2015), was added to the solution bathing the basolateral membrane of HCA7 epithelia once a stable FSK (10 μM) induced Cl^- current had been established. As shown in Figure 4-9A and B, ouabain produced a rapid yet transient decrease in I_{sc} of ~2 μA cm^{-2} ($p = 0.0067$). The remaining Cl^- current was diminished by I-172 (10 μM; $p = 0.04$). These data support the presence of the Na^+/K^+ ATPase within the basolateral membrane of HCA7 epithelia and highlight the pump's crucial role in CFTR-mediated Cl^- transport.

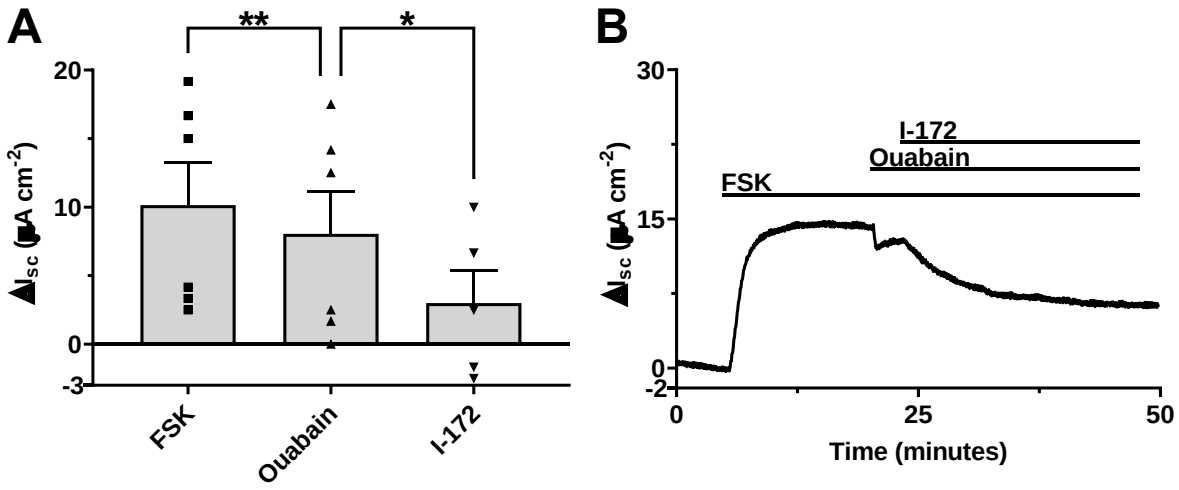

Figure 4-9: Representative Ussing chamber traces characterising ouabain inhibition of FSK generated I_{sc} by HCA7 epithelia.

(A) *Summary ΔI_{sc} data by HCA7 epithelia in response to Na^+/K^+ ATPase inhibition with ouabain (1 μM), following establishment of a stable FSK (10 μM) induced, CFTR-mediated current. The remaining current was inhibited by $CFTR_{inh}172$ (I-172; 10 μM). Data are means ± S.E.M. (n = 5-6); *, p < 0.05; 2-tailed paired t-test, **, p < 0.01; 2-tailed paired t-test.* ***(B)*** *Representative Ussing chamber trace for conditions outlined in* ***(A)****. The continuous lines indicate the presence of different compounds in the solutions bathing the apical (FSK and I-172) and basolateral (ouabain) membranes. Data are displayed as change in short-circuit current (ΔI_{sc}) from baseline.*

4.3.3.5. Amiloride has no effect on I_{sc} by HCA7 epithelia.

The closely regulated balance between Cl^- secretion and Na^+ absorption across the intestinal epithelium underpins the mechanism by which salt concentration determines water movements into and out of the intestinal lumen (Seidler *et al.*, 2009). In the colon, the primary route of Na^+ absorption is via the epithelial Na^+ channel (ENaC), although other routes such as those via the Na^+/H^+ exchanger family (NHE) also exist (Greger, 2000; Bijvelds *et al.*, 2009; Seidler *et al.*, 2009; He and Yun, 2010). Amiloride, an ENaC blocker (Mall *et al.*, 1998; Greger, 2000), was used to assess the presence of ENaC in HCA7 epithelia. Figure 4-10A and B shows that addition of amiloride (10 μM) to the solution bathing the apical membrane of HCA7 epithelia had little effect on I_{sc} ($p = 0.465$; 2-tailed paired t-test) and did not influence the subsequent I_{sc} increase generated by FSK (10 μM; $p = 0.0002$). Current was diminished by I-172 (10 μM). Consistent with previous findings (Roberts *et al.*, 1991), these data do not support the presence of amiloride-sensitive ENaC in HCA7 epithelia.

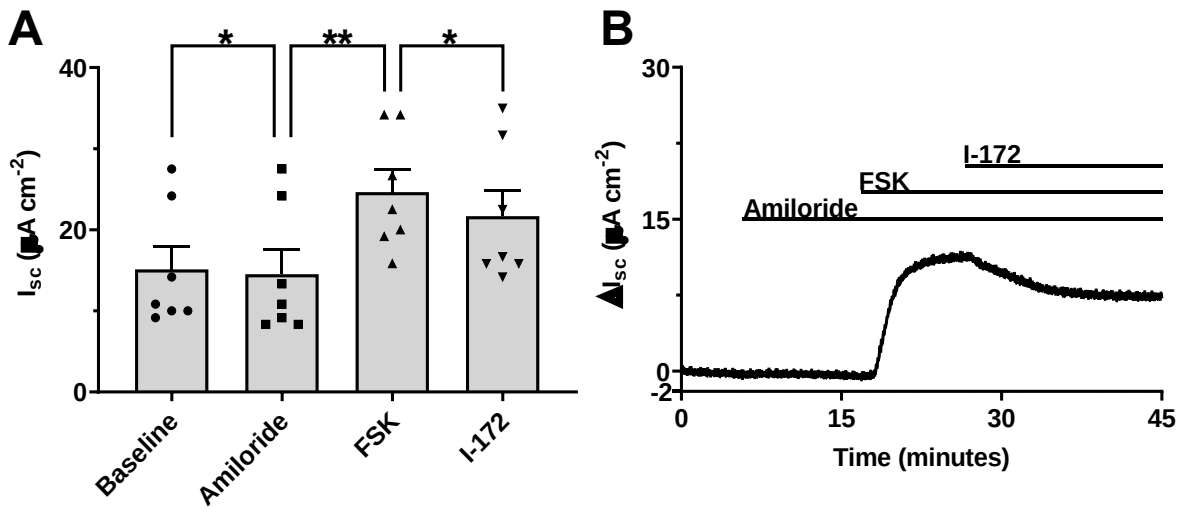

Figure 4-10: Representative Ussing chamber traces characterising the effect of amiloride on I_{sc} by HCA7 epithelia.

(A) *Summary ΔI_{sc} data by HCA7 epithelia in response to the ENaC blocker amiloride (10 μM). Subsequently, CFTR-mediated current was activated by forskolin (FSK; 10 μM) and inhibited by $CFTR_{inh}$-172 (I-172; 10 μM). Data are means ± S.E.M. (n = 7); *, p < 0.05; 2-tailed paired t-test; **, p < 0.01; 2-tailed paired t-test.* ***(B)*** *Representative Ussing chamber trace for conditions outlined in* ***(A)****. The continuous lines indicate the presence of different compounds in the solution bathing the apical membrane. Data are displayed as change in short-circuit current (ΔI_{sc}) from baseline.*

For all Ussing chamber experiments, relevant vehicle control experiments were performed using the solvents outlined in Section 2.1.5 (data not shown; n = 3-5). None of the solvents used in these control experiments demonstrated an effect on I_{sc} by HCA7 epithelia.

The work presented in Section 4.3.3 builds a thorough picture of the ion channels, transporters, and pumps crucial to CFTR-mediated Cl^- transport by HCA7 epithelia. To summarise, these data strongly suggest the presence of the apical membrane Cl^- channel CFTR, the apical membrane CaCC, the basolateral membrane NKCC1 co-transporter, and the basolateral membrane Na^+/K^+ ATPase. Ussing chamber studies do not support the presence of apical membrane amiloride-sensitive ENaC in HCA7 epithelia.

4.3.4. Development of an assay to measure CFTR-mediated swelling by HCA7 spheroids.

The Ussing chamber studies presented in Section 4.3.3 characterise the ion channels, transporters and pumps associated with CFTR-mediated Cl^- transport by 2D HCA7 epithelia. To complement this work, HCA7 cells were grown as 3D spheroids (as outlined in Section 2.3.5) and subjected to FIS assays. The purpose of this work was firstly to characterise CFTR-mediated HCA7 spheroid swelling in response to known activators and inhibitors of CFTR, and secondly build upon the assay developed in Chapter 3, to produce a fully automated assay suitable for high-throughput screening of compounds potentially beneficial to the restoration of salt and water homeostasis in the CF intestine.

4.3.4.1. Quantification of CFTR-mediated swelling in HCA7 spheroids.

The HCA7 cell line grows as 3D spheroids when seeded into Matrigel and cultured according to the protocol outlined in Section 2.3.5. To determine whether FSK stimulation induced HCA7 spheroid swelling, FIS assays were performed as described in Section 2.6. In brief, spheroids were imaged after 14 days in culture (24 hours before drug treatment) to give a –24 hour time point. Multiple fields of view were selected, and the x and y coordinates and desired z-stack range (7 µm intervals to capture the widest cross section of spheroid) were saved for future use. For I-172 conditions, cells were pre-treated with I-172 (10 µM) 2-hours prior to the addition of 10 µM FSK. At 0 hours, all wells received fresh medium containing final drug conditions. At 2-, 24- and 48- hours post treatment, spheroids were imaged using the x,y coordinates, and z-stack range saved during –24 hour imaging. For initial experiments, image analysis was performed manually using Fiji/ImageJ. Throughout the work presented in Sections 4.3.4.1, 4.3.4.2, 4.3.4.3, .4.3.4.4, 4.3.4.5, and 4.3.4.6 final drug concentrations were FSK (10 µM), and I-172 (10 µM). Figures 4-11, 4-12, and 4-13 illustrate 3 approaches (termed methods 1, 2, and 3) towards quantification of FIS by HCA7 spheroids, from 4 experimental repeats (repeats 1-4 labelled A-D respectively), in response to treatment with FSK, FSK + I-172, I-172, no treatment and control conditions at 2-, 24-, and 48- hours post treatment

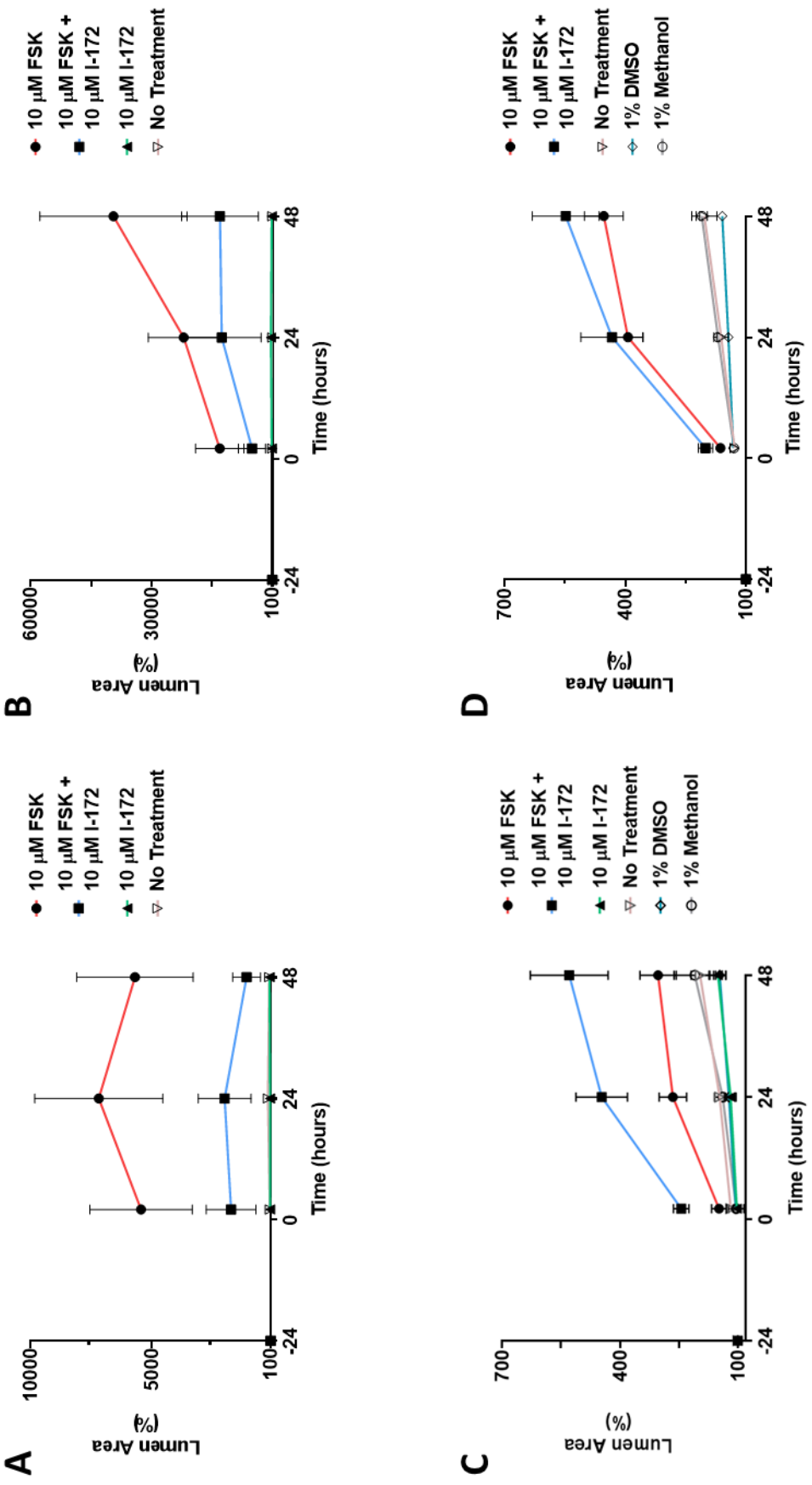

Figure 4-11: HCA7 spheroid lumen area increase in response to FSK stimulation.

Figure 4-11: HCA7 spheroid lumen area increase in response to FSK stimulation.

HCA7 spheroid lumen area was measured in response to 10 µM forskolin (FSK), 10 µM forskolin + 10 µM $CFTR_{inh}$-172 (FSK + I-172), and 10 µM $CFTR_{inh}$-172 (I-172). Untreated spheroids were included as a control for basal lumen area increase corresponding to basal spheroid growth. For conditions involving I-172, spheroids were pre-treated with I-172 2-hours prior to FSK-stimulation. ***A-D*** *represent data from 4 experimental repeats. Lumen area increase was calculated relative to that at –24 hours (100%). Data are means ± S.E.M (****A****, n = 18-24;* ***B****, n = 27-30;* ***C****, n = 17-30 and* ***D****, n = 12-30).*

As demonstrated in Figure 4-11, FSK-stimulation of HCA7 spheroids resulted in luminal swelling, represented as an increase in spheroid lumen area, relative to that at –24 hours in all 4 experimental repeats (A-D). Lumen area was measured (pixels^2) and normalised to that at –24 hours (–24 hours = 100%), and this approach termed method 1. The extent of spheroid lumen swelling from –24 hours varied extensively between repeats with a maximum lumen area increase at 48-hours relative to –24 hours of 39,605% (B), and a minimum increase of 403% (C). With the exception of repeat 1 (Figure 4-11A), lumen area continued to increase over the duration of the assay, although the rate of increase slowed between 24- and 48-hours for repeats 3 and 4 (Figure 4-11C and D). For repeat 1 (Figure 4-11A) lumen area increase peaked 24-hours post FSK addition and decreased thereafter.

Unexpectedly, in repeats 3 and 4 (Figure 4-11C and D) HCA7 spheroids pre-treated with I-172 before FSK-stimulation displayed luminal swelling greater than those stimulated by FSK alone. This contradicts data presented in Section 4.3.3 which show significant inhibition of CFTR-mediated I_{sc} by I-172 (10 µM) by HCA7 epithelia in all Ussing chamber studies. I-172 inhibited FIS swelling of both mouse and human intestinal organoids (Dekkers *et al.*, 2013). For further investigation of this discrepancy, see Section 4.3.4.7.

As for analysis of FIS data with LIM1863 spheroids (please refer to Section 3.3.2), representation of FIS by HCA7 spheroids by method 1 did not consider the variety of spheroid sizes at –24 hours within and between cultures. As such, data from experimental repeats could not be readily compared. To overcome this difficulty, a method of normalisation was sought (method 2).

For the data shown in Figure 4-12, lumen area was normalised to corresponding spheroid area at each time point (lumen area/spheroid area), and these normalised values plotted relative to that at –24 hours (–24 hours = 100%). This approach to FIS

quantification was termed method 2. Although analysis by method 2 accounted for differing spheroid sizes and their continued basal growth over 72-hours (total assay time frame) much variation in swelling was still observed between experimental repeats. A maximum normalised lumen area increase at 48-hours relative to –24 hours of 17,539% was observed for repeat 2 (B), whereas a minimum normalised lumen area increase at 48-hours relative to –24 hours of 139% was recorded for repeat 3 (C). Like data shown in Figure 4-11, for repeats 2, 3 and 4 (Figure 4-12B, C and D) FSK stimulated an increase in normalised lumen area over the duration of the assay. By contrast, for repeat 1 (Figure 4-12A) normalised lumen area decreased between 24- and 48-hours relative to –24 hours. Despite the continued increase in normalised lumen area between 24- and 48-hours observed in repeats 3 and 4 (Figure 4-12C and D), the rate of increase slowed disproportionally to basal levels seen in untreated spheroids. For repeats 3 and 4 (Figure 4-12C and D), HCA7 spheroids pre-treated with I-172 before FSK-stimulation displayed normalised luminal swelling greater than those stimulated by FSK alone.

Quantification of FIS by HCA7 spheroids using method 2 does take into consideration variation in spheroid sizes. However, it would prove difficult and inefficient to automate image analysis using this method. Tracking plugins established for, and tested in, LIM1863 spheroids were able to detect and trace lumen area with several limitations. Attempts to optimise these plugins for use with HCA7 spheroids were unsuccessful because of differences in morphology between spheroids formed by the two cell lines. The epithelium lining HCA7 spheroids was much thinner than that lining LIM1863 spheroids, particularly at later stages of the FIS assay. As a result, differentiation between the lumen area and spheroid area of HCA7 organoids was not feasible with the tracking plugin (see Section 2.6.3 for an example of HCA7 spheroid detection by the tracking plugin). If this method of FIS quantification were to be used, image analysis would be manual, preventing the use of the assay in high-throughput screening. An alternative method to measure spheroid area was therefore investigated to quantify FIS by HCA7 spheroids (method 3).

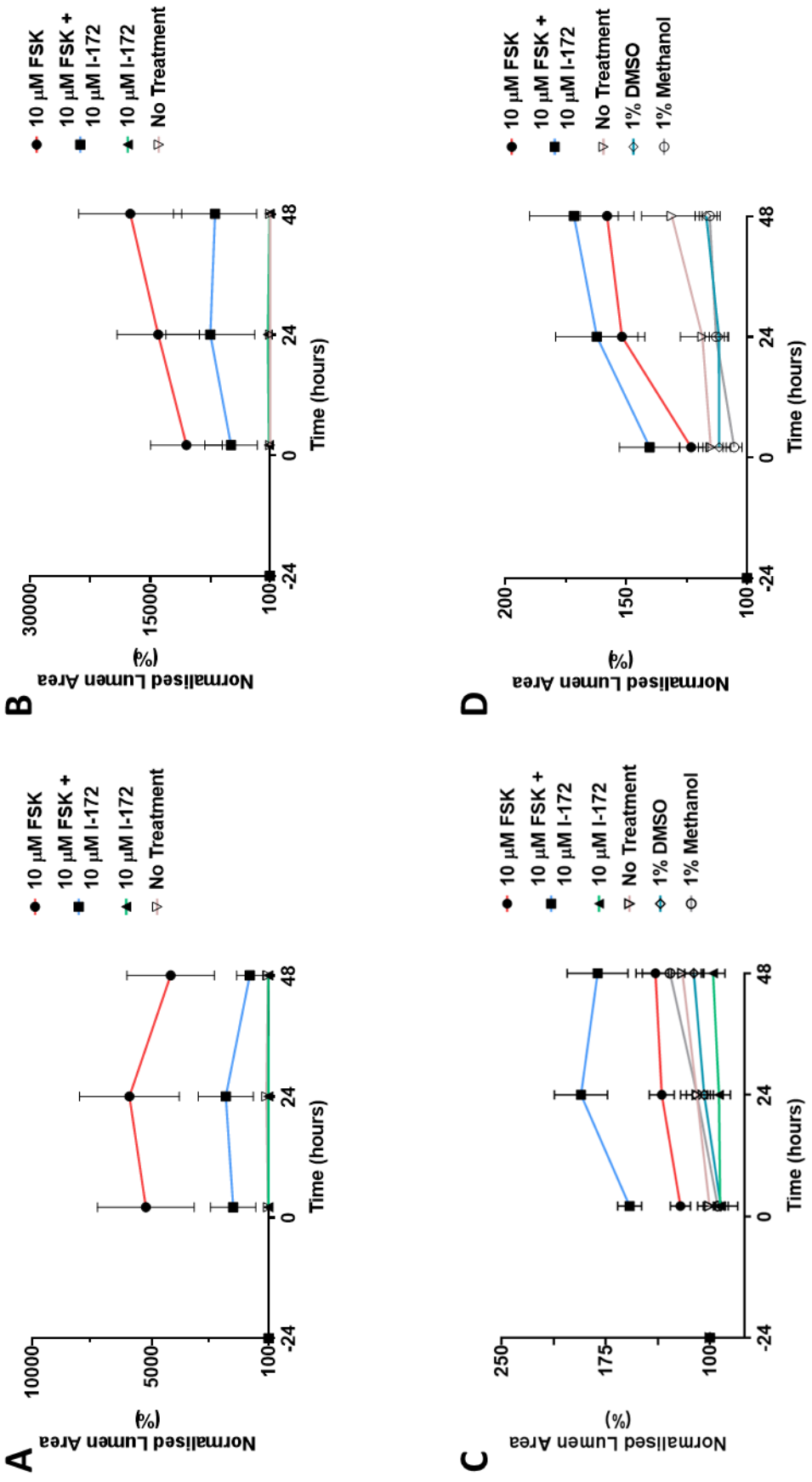

Figure 4-12: HCA7 spheroid normalised lumen area increase in response to FSK stimulation.

Figure 4-12: HCA7 spheroid normalised lumen area increase in response to FSK stimulation.

Normalised HCA7 lumen area increase was measured in response to 10 µM forskolin (FSK), 10 µM forskolin + 10 µM $CFTR_{inh}$-172 (FSK + I-172), and 10 µM $CFTR_{inh}$-172 (I-172). Untreated spheroids were included as a control for basal normalised lumen area increase corresponding to HCA7 spheroid growth. For conditions involving I-172, spheroids were pre-treated with I-172 2-hours prior to FSK-stimulation. ***A-D*** *represent data from 4 experimental repeats. For normalisation, lumen area was divided by spheroid area at each time point and these values calculated relative to that at –24 hours (100%). Data are means ± S.E.M. (**A**, n = 18-24; **B**, n = 27-30; **C**, n = 17-30 and **D**, n = 12-30).*

As illustrated in Figure 4-13, stimulation with FSK induced an increase in total spheroid area relative to that at –24 hours in all 4 experimental repeats (A-D). Here, total spheroid area was normalised to that at –24 hours (–24 hours = 100%). This approach to FIS quantification was termed method 3, and henceforth the resultant measurement will be termed spheroid area. FIS quantification of both mouse and human intestinal organoids has previously been reported using this method (Dekkers *et al.*, 2013; Dekkers, Berkers, *et al.*, 2016). Despite some variation in spheroid area 24- and 48- hours post stimulation with FSK, the variation was much reduced potentially allowing data comparison between experimental repeats. Repeat 2 (B) demonstrated the largest increase in spheroid area at both 24- and 48-hour timepoints relative to that at –24 hours (153% and 188%, respectively), whereas repeat 3 (C) demonstrated the smallest at both 24- and 48-hour timepoints (135% and 139%, respectively). In all 4 experimental repeats, spheroid area continued to increase over the duration of the assay because measurement of total spheroid area included basal spheroid growth over a 78-hour period (basal spheroid area increase over the assay is the same as that of untreated spheroids). Although representation of FIS using method 3 still showed that spheroids pre-treated with I-172 before FSK-stimulation in repeats 3 and 4 (Figure 4-13C and D, respectively) had a greater increase in spheroid area than those treated with FSK alone, the margin of difference was reduced. Large and in some cases overlapping error bars can be observed for FSK-treated and FSK + I-172 spheroids at both 24- and 48-hour timepoints in all 4 experimental repeats.

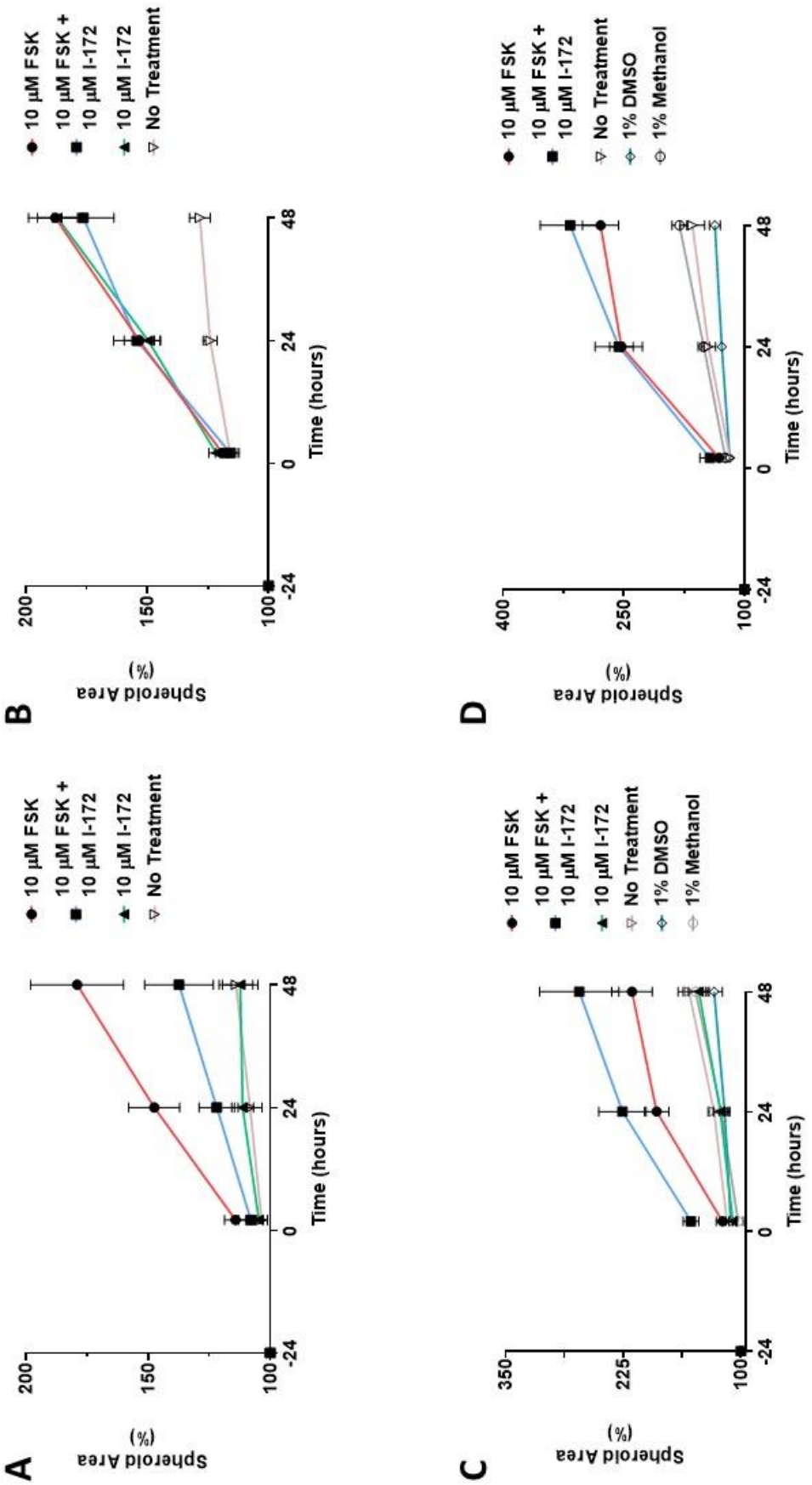

Figure 4-13: HCA7 spheroid area increase in response to FSK stimulation.

Figure 4-13: HCA7 spheroid area increase in response to FSK stimulation.

HCA7 spheroid area was measured in response to 10 µM forskolin (FSK), 10 µM forskolin + 10 µM $CFTR_{inh}$-172 (FSK + I-172), and 10 µM $CFTR_{inh}$-172 (I-172). Untreated spheroids were included as a control for basal spheroid growth. For conditions involving I-172, spheroids were pre-treated with I-172 2-hours prior to FSK stimulation. ***A-D*** *represent data from 4 experimental repeats. Spheroid area increase was calculated relative to that at –24 hours (100%). Data are means ± S.E.M. (**A**, n = 18-24; **B**, n = 27-30; **C**, n = 17-30 and **D**, n = 12-30).*

Based on the data shown in Figures 4-11, 4-12 and 4-13, it was proposed that going forward firstly, total spheroid area would be used to quantify FIS by HCA7 spheroids and secondly, the assay duration would be reduced to 24-hours post FSK addition (i.e. 48-hours total duration). Importantly, this method of quantification has been used previously (Dekkers *et al.*, 2013; Dekkers, Berkers, *et al.*, 2016) and automated analysis plugins for use in Fiji/ImageJ that accurately measured spheroid surface area using phase contrast images were readily available. The possibility of automated analysis of a shorter assay increased the potential use of HCA7 spheroids in a high-throughput screen.

4.3.4.2. Shortening assay duration does not affect assay validity.

To ensure that quantification of FIS based on spheroid area using a shorter assay did not compromise the validity of the results, further data analyses were performed.

Firstly, it was necessary to determine whether shortening the total duration of the FIS assay to 48-hours would affect the outcome of the assay and subsequent data interpretation.

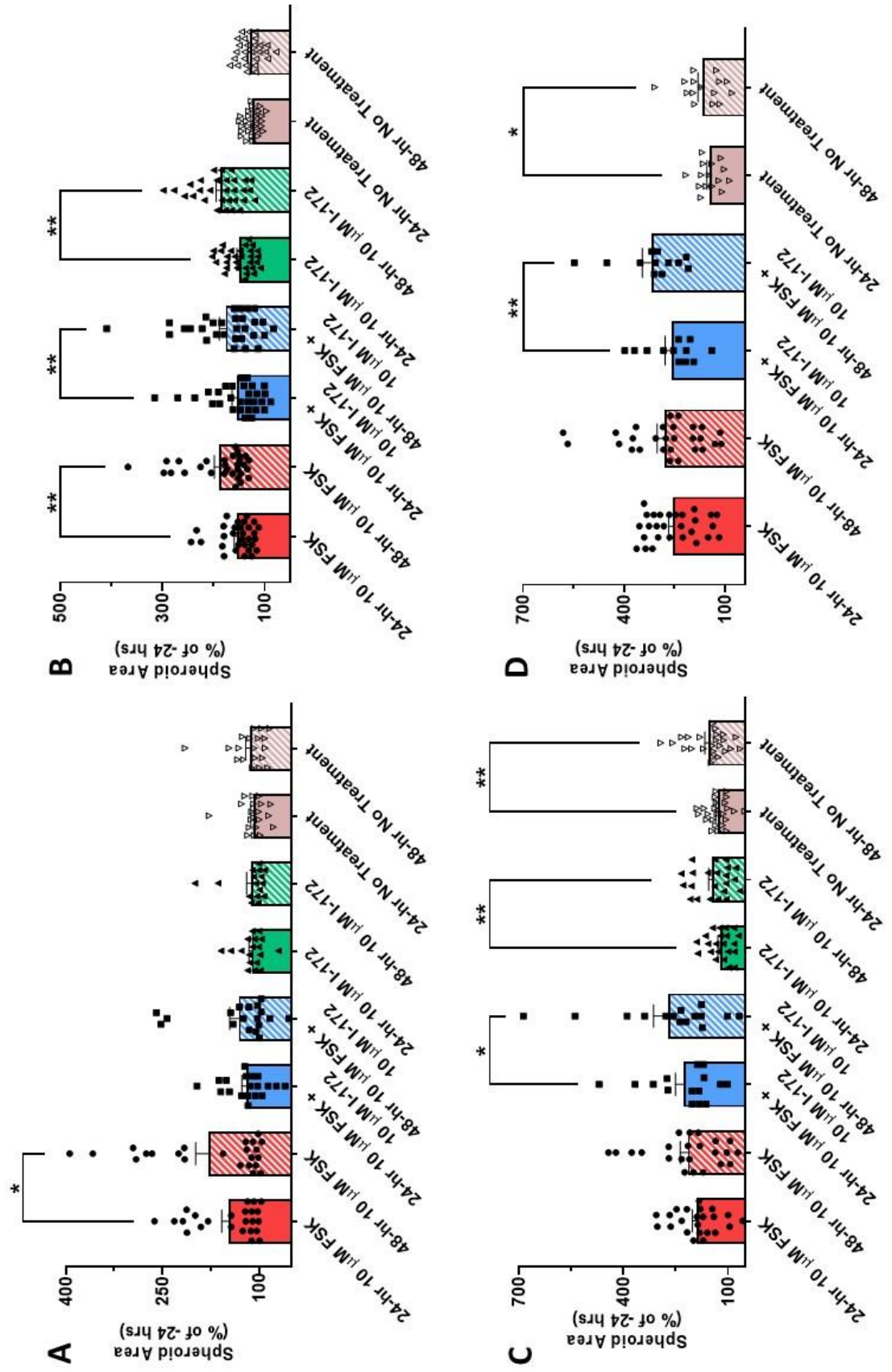

Figure 4-14: Comparison of spheroid area at 24- and 48- hour time points for each experimental condition across 4 experimental repeats.

Figure 4-14: Comparison of spheroid area at 24- and 48- hour time points for each experimental condition across 4 experimental repeats.

HCA7 spheroid area at 24- and 48-hour time points (normalised to –24 hours = 100%) in response to treatment with 10 µM forskolin (FSK), 10 µM forskolin + 10 µM $CFTR_{inh}$-172 (FSK + I-172), and 10 µM $CFTR_{inh}$-172 (I-172). Untreated spheroids were included as a control for basal spheroid growth. For conditions involving I-172, spheroids were pre-treated with I-172 2-hours prior to FSK-stimulation. ***A-D*** *represent data from 4 experimental repeats. Data are means ± S.E.M. (****A****, n = 16-24;* ***B****, n = 27-30;* ***C****, n = 15-34 and* ***D****, n = 15-24.); *, p < 0.05; Wilcoxon matched-pair signed rank test; **, p < 0.01; Wilcoxon matched-pair signed rank test.*

In Figure 4-14 spheroid area for spheroids treated with FSK, FSK + I-172, I-172 alone and untreated spheroids, are compared at 24- and 48-hour time points. In all 4 experimental repeats, a significant increase in spheroid area occurred between 24- and 48-hours post drug addition in at least one experimental condition. In repeats 1 and 2 (Figure 4-14A and B) spheroids treated with FSK demonstrated a significant increase in spheroid area between 24- and 48-hours ($p = 0.02$ and $p < 0.0001$, respectively). However, this was not the case for repeats 3 and 4 (Figure 4-14C and D), despite an increase in mean spheroid area of 26 px^2 following FSK stimulation. For repeat 1 (Figure 4-14A) no significant increase in spheroid area was observed between 24- and 48-hour time points for any other experimental conditions. Spheroids treated with FSK + I-172, and I-172 alone, demonstrated a significant increase in spheroid area between 24- and 48-hours in repeats 2, 3 (both conditions) and 4 (FSK + I-172 only) (Figure 4-14B, C and D respectively; B: FSK + I-172, $p = 0.0016$; I-172, $p < 0.0001$; C: FSK + I-172, $p = 0.0256$; I-172, $p = 0.0001$; D: FSK + I-172, $p = 0.0024$). I-172 treatment alone is not shown for experimental repeat 4 (Figure 4-14D) due to insufficient data. Whilst it could be postulated that the difference in spheroid area observed between 24- and 48-hours in conditions not involving FSK could be a result of basal spheroid area increase over a 24-hour period, only untreated spheroids from repeats 3 and 4 (Figure 4-14C and D, respectively) demonstrated a significant spheroid area increase over this time (C: $p = 0.0001$; D: $p = 0.0103$).

These data show that in many instances a significant increase in spheroid area occurs between the 24- and 48-hour assay time points. This increase occurs both with FSK-stimulation and under control conditions during basal spheroid growth. However, this does not mean that an assay of 48-hours duration would be inappropriate given the purpose of the assay was to quantify spheroid swelling driven by CFTR-mediated ion

and fluid secretion (i.e. between FSK-treated and untreated/control conditions, and not the extent of spheroid area increase over time for each experimental condition).

To determine whether shortening the assay duration to 48-hours would distinguish between FSK stimulated spheroids and all other conditions, spheroid area at 24-hours post FSK treatment was compared to that at 24-hours (Figure 4-15 A-D). This comparison was also made at 48-hours (Figure 4-15 A_i-D_i). Figure 4-15 demonstrates that in all experimental repeats a significant difference in spheroid area was observed between FSK-stimulated and untreated spheroids at both 24- and 48-hours (A, $p = 0.0036$; A_i, $p = 0.0096$; B, $p = 0.0001$; B_i, $p < 0.0001$; C, $p = 0.0002$; C_i, $p = 0.0181$; D, $p < 0.0001$; D_i, $p = 0.0008$). This indicates that a total assay duration of 48-hours detects FIS by HCA7 spheroids. For repeats 1 and 3, a significant difference in spheroid area was observed between FSK-stimulated and I-172-treated spheroids at both 24- and 48-hours (Figure 4-15A and A_i, C and C_i, respectively) (A, $p = 0.0176$; A_i, $p = 0.0022$; C, $p < 0.0001$; C_i, $p = 0.006$). I-172 treatment alone is not shown for experimental repeat 4 (Figure 4-15D and D_i) due to insufficient data. For those repeats that included vehicle controls (1% (v/v) DMSO and 1% (v/v) methanol), there was a significant difference in spheroid area between vehicle-treated spheroids and those stimulated with FSK at both 24- and 48-hours (Figure 4-15). In none of the experimental repeats was a difference in spheroid area observed between FSK-stimulated and FSK + I-172 treated spheroids at either time point (Figure 4-15). This agrees with the data shown in Figure 4-13 where, as discussed, large and often overlapping error bars between FSK and FSK + I-172 treatments were observed at both time points for all 4 repeats.

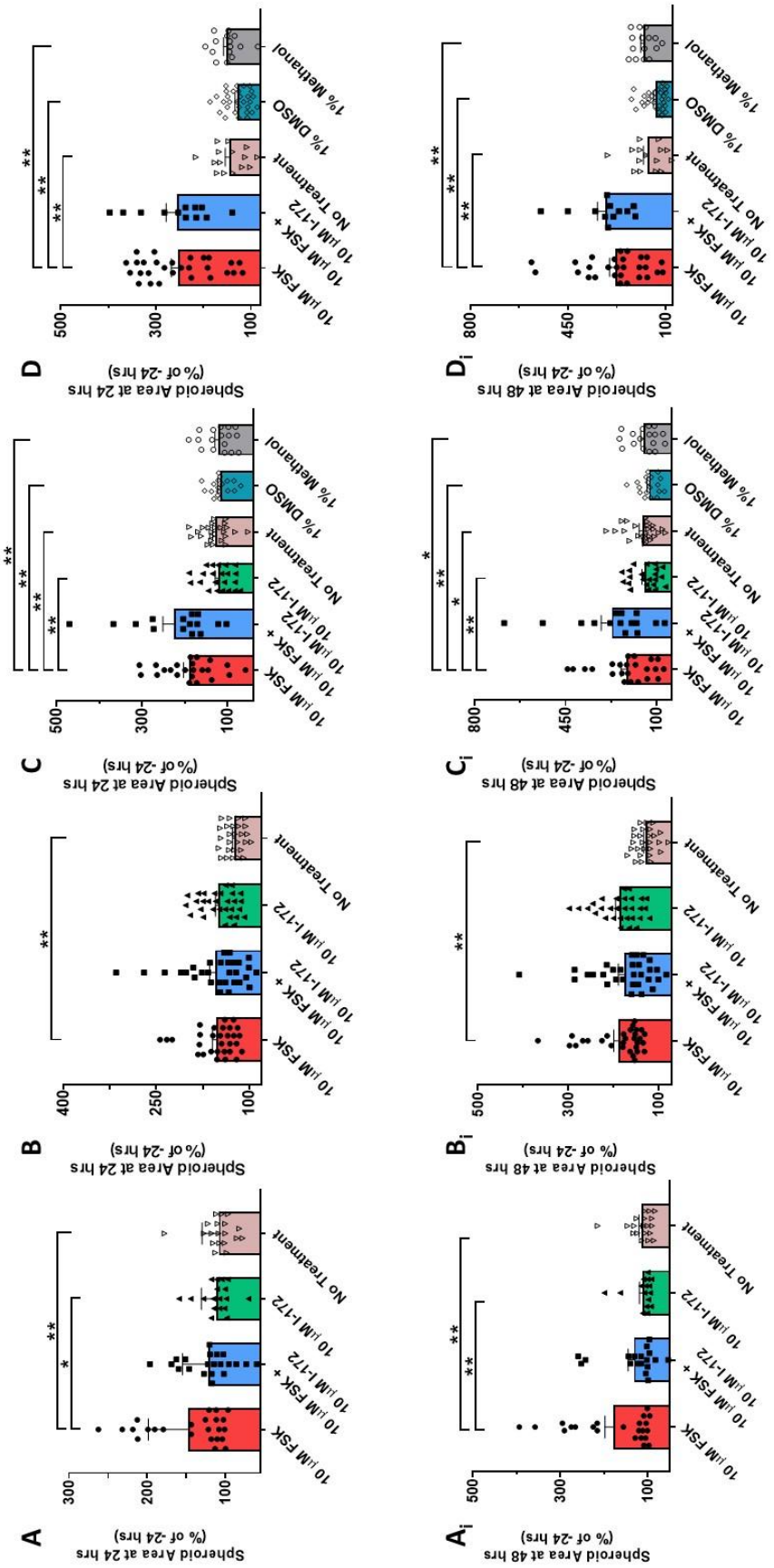

Figure 4-15:Comparison of HCA7 spheroid area between experimental conditions at 24- and 48- hour time points for 4 experimental repeats.

Figure 4-15: Comparison of HCA7 spheroid area between experimental conditions at 24- and 48- hour time points for 4 experimental repeats.

HCA7 spheroid area increase, in response to treatment with 10 µM forskolin (FSK), 10 µM forskolin + 10 µM $CFTR_{inh}$-172 (FSK + I-172), and 10 µM $CFTR_{inh}$-172 (I-172) was compared for 4 experimental repeats, at both 24- and 48-hours. Untreated spheroids were included as a control for basal spheroid growth. For conditions involving I-172, spheroids were pre-treated with I-172 2-hours prior to FSK-stimulation. ***A – D*** *are data from 4 experimental repeats with* ***A – D*** *data at 24-hours and* $\boldsymbol{A_i - D_i}$ *data at 48-hours. Data are means ± S.E.M. (****A + A****$_i$, n = 16-24;* ***B + B****$_i$, n = 27-30;* ***C + C****$_i$, n = 15-34 and* ***D + D****$_i$, n = 15-24); *, p < 0.05; Mann-Whitney test; **, p < 0.01; Mann-Whitney test.*

Despite some variation between repeats, it can be seen that a 48-hour assay differentiates between spheroids treated with FSK and those that are not. Therefore, this period is appropriate for detecting FIS in HCA7 spheroids. Further optimisation of the protocol for the pre-treatment of spheroids with I-172 was required. However, at this stage of assay development the priority was to optimise data acquisition and analysis for full automation, increasing assay throughput and avoiding time consuming manual data analysis. To this end, the data presented above supports the use of a 48-hour assay going forward.

4.3.4.3. HCA7 spheroid area increase in response to forskolin stimulation positively correlates with lumen area increase.

In addition to ensuring that a shorter FIS assay did not compromise assay validity, it was necessary to demonstrate that the increase in spheroid area correlated with the spheroid lumen increase when spheroids were stimulated by FSK. If this were the case, then it would be reasonable to conclude that quantification of FIS using total spheroid area accurately represented CFTR-mediated ion and fluid secretion into the spheroid lumen. As shown in Figure 4-16, spheroid area increase (μm^2) from –24 hours to 24-hours positively correlated with lumen area increase (μm^2) over the same period in all 4 experimental repeats (Spearman's correlation (r) = 0.9, 0.64, 0.98 and 0.99 for repeats 1, 2, 3 and 4; A, B, C and D, respectively).

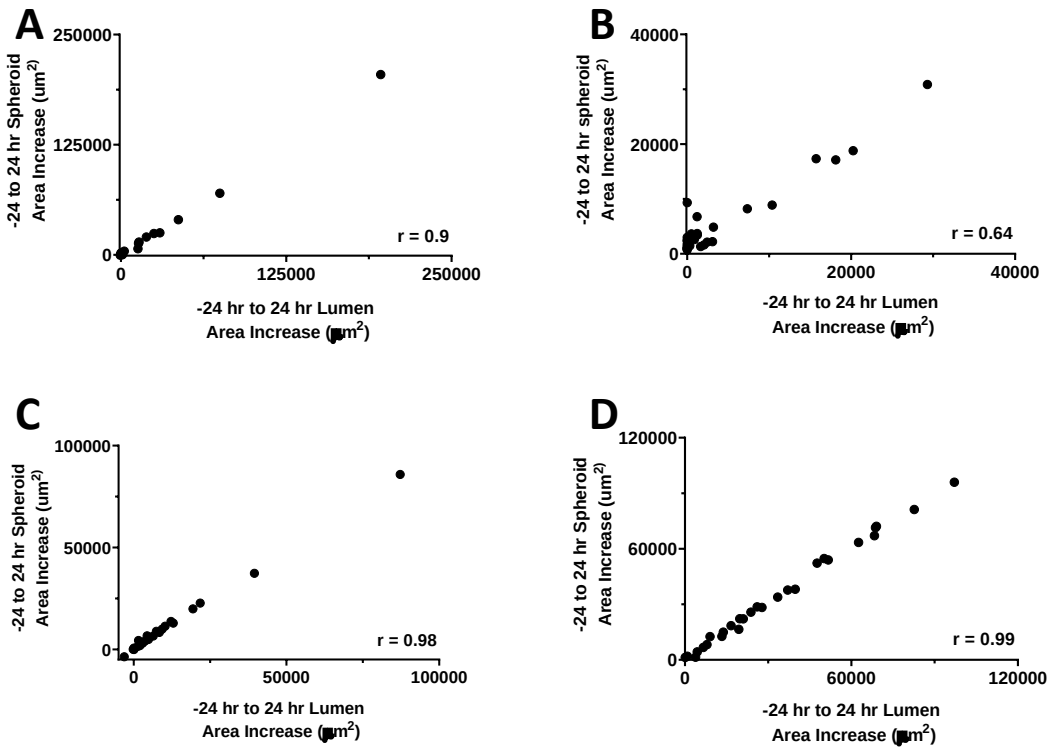

Figure 4-16: Spheroid area increase in response to FSK-stimulation correlates strongly with lumen area increase.

*Increase in HCA7 spheroid area (µm^2) and lumen area (µm^2) between –24 hours and 24 hours in response to forskolin (10 µM) stimulation was calculated and the Spearman's correlation determined (r). For experimental repeats 1-4 (**A-D**), r was 0.9, 0.64, 0.98 and 0.99, respectively. **A-D** are data from 4 experimental repeats (**A**, n = 24; **B**, n = 30; **C**, n = 23 and **D**, n = 28).*

Figure 4-16 demonstrates that for spheroids treated with FSK there was a strong positive correlation between lumen area increase and spheroid area increase over the duration of the assay. Thus, the data presented in Sections 4.3.4.2 and 4.3.4.3 verify that FIS assay quantification based on spheroid area (pixels^2) normalised to that at –24 hours (–24 hours = 100%) for an assay lasting 48-hours accurately assesses CFTR-mediated ion and fluid secretion by HCA7 spheroids. These assay parameters were implemented for subsequent automated image analysis.

4.3.4.4. Automated analysis of forskolin induced swelling by HCA7 spheroids.

An automated Modular Image Analysis (MIA) plugin for use in Fiji/ImageJ, which measured and tracked spheroid growth was provided by the Wolfson Bioimaging Facility (University of Bristol). To determine whether the MIA plugin accurately measured the area of HCA7 spheroids, 3 further independent FIS assays were performed and quantified. These experimental repeats will be referred to as repeats 5, 6 and 7 to distinguish them from repeats 1, 2, 3, and 4 referred to previously.

As shown in Figure 4-17, FIS swelling was detected in all 3 experimental repeats with FSK-stimulated spheroid area increases of 357% for repeat 5 (Figure 4-17A), 249% for repeat 6 (Figure 4-17B) and 305% for repeat 7 (Figure 4-17C). However, the increase was only significant when compared to untreated spheroids in repeats 5 and 7 (Figure 4-18A and C: A, $p < 0.0001$; C, $p < 0.0001$). This was also found to be the case when comparing the extent of swelling in spheroids treated with FSK to those treated with I-172 alone (Figure 4-18A and C: A, $p < 0.0001$; C, $p < 0.0001$).

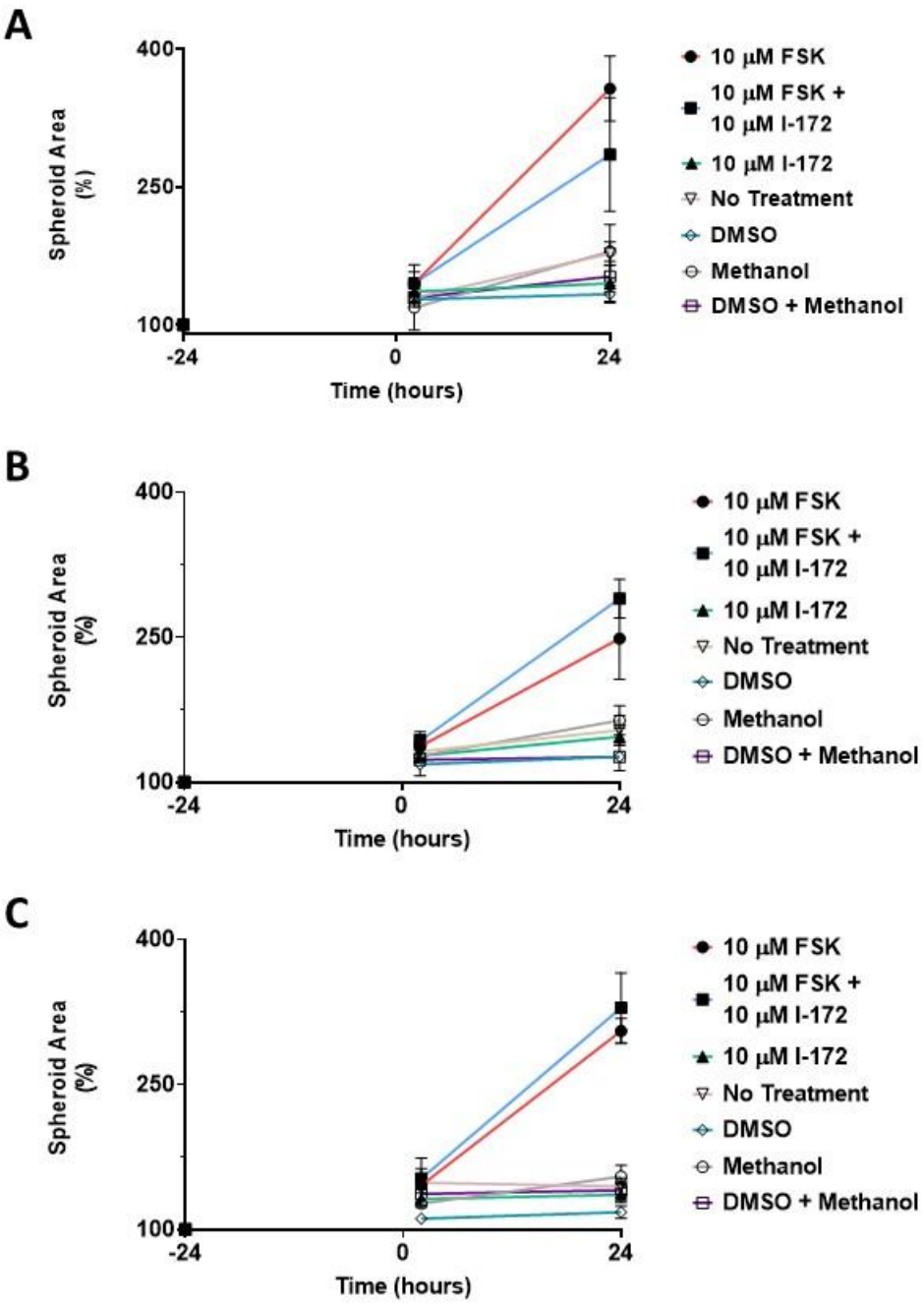

Figure 4-17: Automated image analysis and quantification of HCA7 spheroid area increase stimulated by FSK.

HCA7 spheroid area was measured using a MIA plugin for Fiji/ImageJ and calculated relative to that at –24 hours (100%) in response to 10 µM forskolin (FSK), 10 µM forskolin + 10 µM $CFTR_{inh}$-172 (FSK + I-172), and 10 µM $CFTR_{inh}$-172 (I-172). Untreated spheroids were included as a control for basal spheroid growth. 1% (v/v) DMSO, 1% (v/v) methanol, and 1% (v/v) DMSO + 1% (v/v) methanol were included as vehicle controls. For conditions involving I-172, spheroids were pre-treated with I-172 2-hours prior to FSK-stimulation. ***A-C*** *represent data from 3 experimental repeats. Data are means ± S.E.M. (****A****, n = 5-44;* ***B****, n = 7-35 and* ***C****, n = 19-40).*

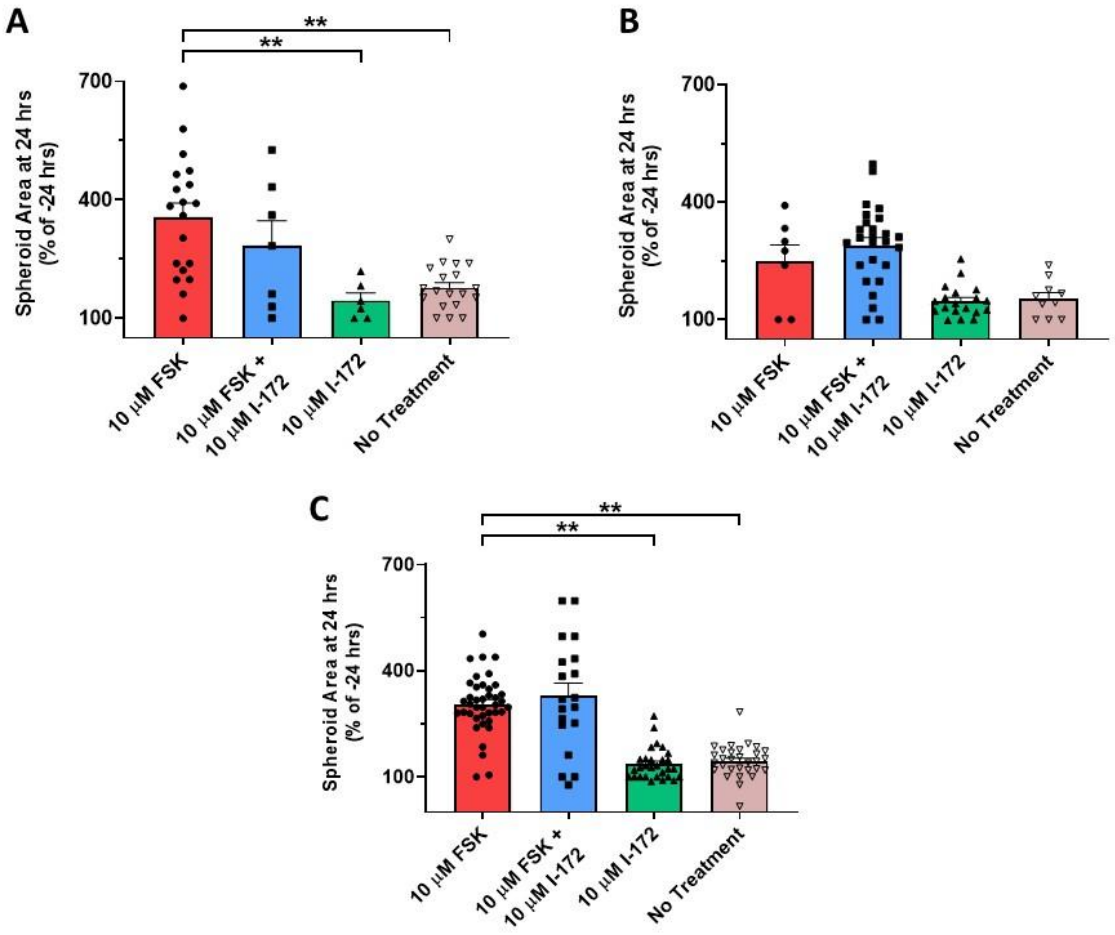

Figure 4-18: Comparison of HCA7 spheroid area between experimental conditions for 3 experimental repeats.

The change in HCA7 spheroid area over 24 hours in response to treatment with 10 μM forskolin (FSK), 10 μM forskolin + 10 μM $CFTR_{inh}$-172 (FSK + I-172), and 10 μM $CFTR_{inh}$-172 (I-172) was compared for 3 experimental repeats. Untreated spheroids were included as a control for basal spheroid growth. For conditions involving I-172, spheroids were pre-treated with I-172 2-hours prior to FSK-stimulation. ***A-C*** *represent data from 3 experimental repeats. Data are means ± S.E.M (****A****, n = 6-19;* ***B****, n = 7-26 and* ***C****, n = 19-40);* ***A*** *and* ***B****: **, p < 0.01; unpaired t-test with Welch's correction;* ***C****: FSK vs I-172: **, p < 0.01; Mann-Whitney test;* ***C****: FSK vs No Treatment: **, p < 0.01; unpaired t-test with Welch's correction.*

The lack of significant spheroid swelling for repeat 6 (B) between spheroids treated with FSK and those treated with either I-172 alone or un-treated spheroids was influenced by both a low number of analysable spheroids that were treated with FSK, and the presence of spheroids that did not swell when stimulated with FSK (Figure 4-18B). Spheroids treated with vehicle controls did not typically exhibit an increase in spheroid area above the basal levels of untreated spheroids (Figure 4-17). As reported for repeats 3 and 4, spheroids in repeats 6 and 7 (Figure 4-17B and C, respectively) treated with FSK + I-172 demonstrated greater FIS than those treated with FSK alone. No significant difference in spheroid area between spheroids treated with FSK and those treated with FSK + I-172 was observed in repeats 5, 6 or 7 after 24-hours, regardless of which condition showed the greater FIS (Figure 4-18A, B and C, respectively).

Despite inconsistencies in the extent of FIS between experimental repeats quantified manually and using automated analysis, it is clear that automated image analysis successfully quantified FIS of HCA7 spheroids. With optimisation of experimental conditions, automated image analysis of FIS by HCA7 spheroids allows the study of CFTR-mediated ion and fluid secretion on a scale whereby screening could be performed to identify compounds with the potential to alleviate gastrointestinal symptoms of CF.

4.3.4.5. HCA7 spheroid area at day 14 varies widely both within and between cultures.

As reported in Sections 4.3.4.1, 4.3.4.2, and 4.3.4.4, the FSK-stimulated spheroid area increase varied both between experimental repeats, and within each experimental repeat (as illustrated in Figure 4-19). Moreover, in over half of the FIS assays, spheroid area increase was greater in spheroids treated with FSK + I-172 than those treated with FSK alone.

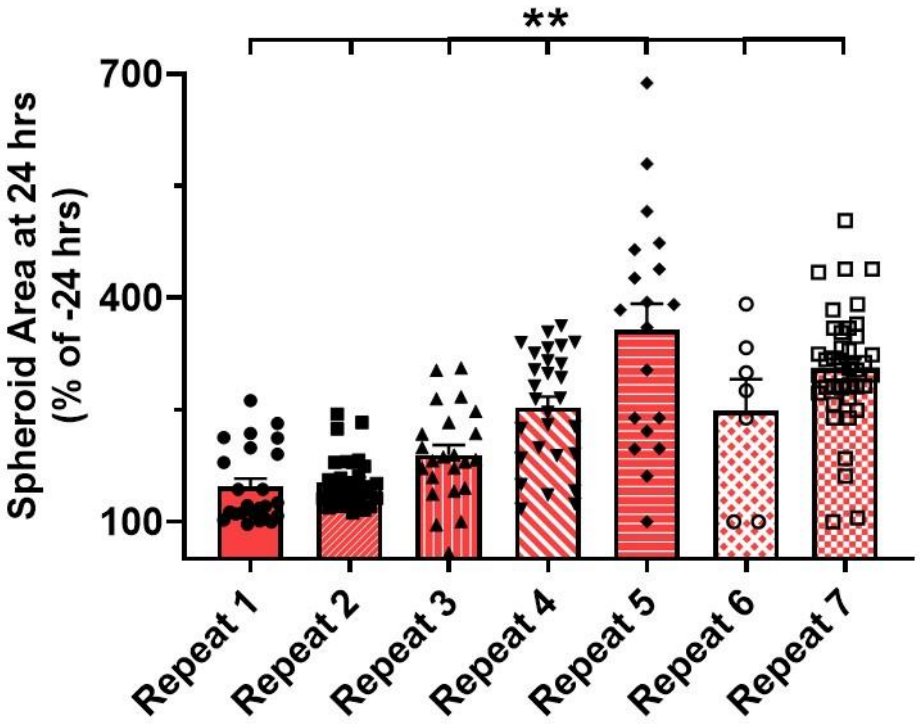

Figure 4-19: HCA7 spheroid area 24-hours post FSK treatment for 7 experimental repeats.

*HCA7 spheroid area 24-hours post FSK treatment [normalised to –24 hours (24-hours = 100%)] was compared for 7 FIS assay repeats. Data are means ± S.E.M. (n = 7-40); **, $p < 0.01$ Kruskal-Wallis test.*

One possible explanation for this variability is that spheroid area at day 14 of culture (corresponding to –24 hour time point) determines the extent of FIS achieved by each spheroid. If this were the case, a condition or experimental repeat with a large proportion of small spheroids on day 14 would appear to demonstrate less FIS. The box and whisker plots in Figure 4-20 illustrate the distribution of spheroid area at day 14 of culture and reveal much variation in spheroid size both within and between experimental repeats. For repeats measured manually (Figure 4-20A), the range of spheroid areas at day 14 were 29,771 μm^2, 7,272 μm^2, 20,304 μm^2, and 19,126 μm^2 (repeats 1, 2, 3, and 4, respectively). For those experiments measured using automated quantification (Figure 4-20B), the range of spheroid areas at day 14 were 85,591 μm^2, 41,895 μm^2, and 85,591 μm^2 (repeat 5, 6, and 7, respectively).

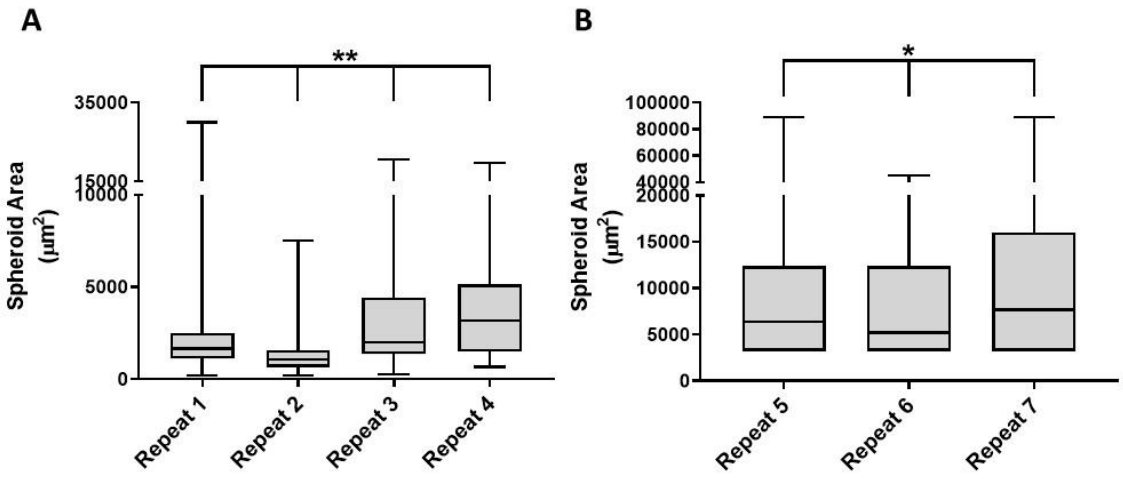

Figure 4-20: Distribution of HCA7 spheroid area at day 14 for all spheroids included in each experimental repeat.

HCA7 spheroid area (µm^2) for all spheroids included in analysis at day 14 (–24 hour time point). Data are medians, first and third quartiles and minimum and maximum values. ***A*** *includes data from repeats 1 - 4 analysed manually, while* ***B*** *includes data from repeats 5 - 7 analysed using automated image analysis (n = 75-565); *, p < 0.05 Kruskal-Wallis test; **, p < 0.01 Kruskal-Wallis test.*

The box and whisker plots in Figure 4-20 demonstrate that on day 14 HCA7 spheroid cultures are not uniform in size (HCA7 spheroids are spheroid in shape, therefore spheroid area corresponds to spheroid size). If spheroid area on day 14 determines spheroid swelling, and therefore extent of FIS exhibited 24-hours post FSK-stimulation, it stands to reason that there will be much variation in spheroid area increase in response to FSK-treatment within repeats. Variation in day 14 spheroid size may also help to explain why for some repeats spheroids treated with FSK + I-172 showed a greater increase in area compared to those treated with FSK alone.

The data presented in Figure 4-20 also highlight a significant difference in median spheroid area between experimental repeats at day 14. The day 14 median spheroid area for repeats 1, 2, 3, and 4 were 1,654 µm^2, 1,079 µm^2, 1,988 µm^2, and 3,167 µm^2, respectively ($p < 0.0001$; Kruskal-Wallis test), and for repeats 5, 6, and 7 6,355 µm^2, 5,193 µm^2, and 7,691 µm^2, respectively ($p = 0.0132$; Kruskal-Wallis test). Presenting spheroid area increase as a percentage normalised to –24 hours (–24 hours = 100%) normalises for difference in spheroid size. However, it does not mitigate for the reduced ability of smaller spheroids to swell when compared with larger spheroids.

4.3.4.6. HCA7 spheroid area on day 14 of culture (–24 hours) does not correlate with extent of forskolin induced swelling.

After establishing that HCA7 spheroid area and therefore size varied at day 14 of culture, its effect on FIS was investigated. For repeats 5, 6, and 7, the area of each spheroid (μm^2) stimulated by FSK was tracked over the FIS assay (Figure 4-21). Figure 4-21 demonstrates that between 2- and 24-hours after FSK stimulation spheroid area increased.

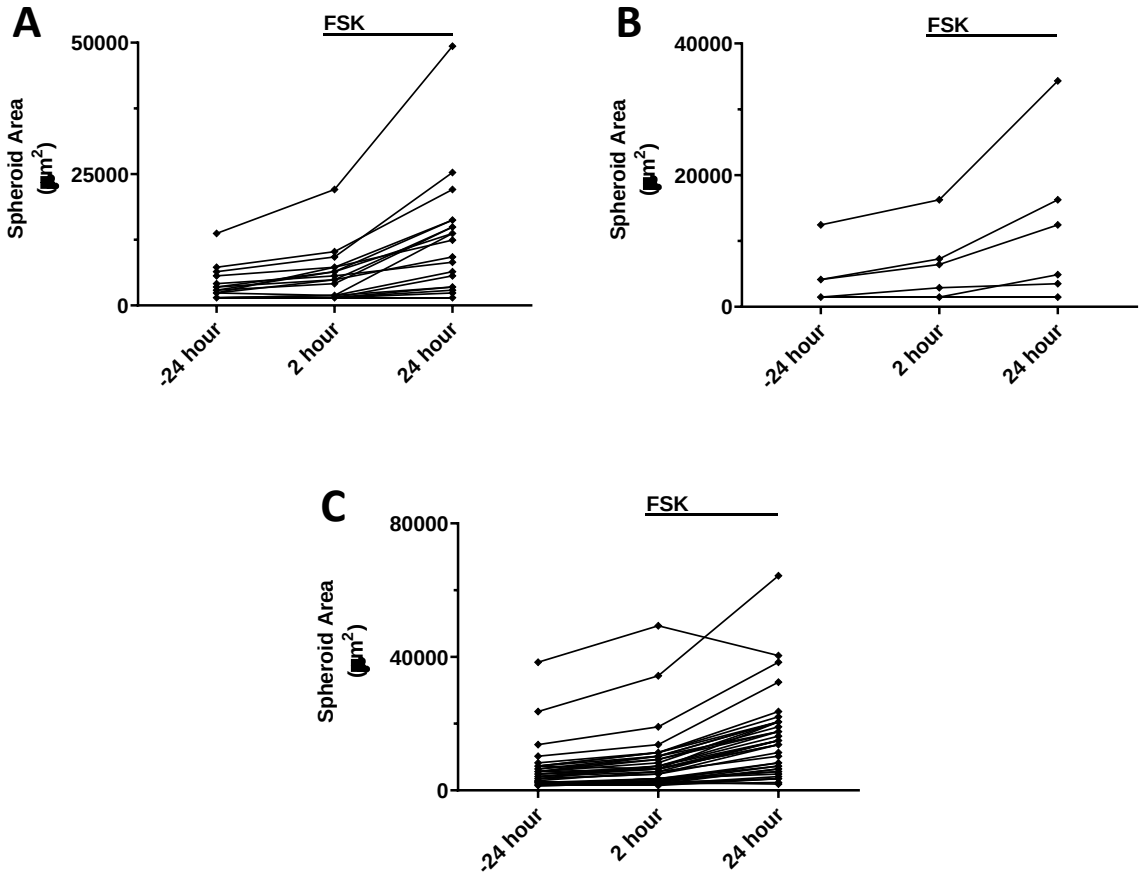

Figure 4-21: Area of individual HCA7 spheroids treated with forskolin over the duration of FIS assays.

Area of individual HCA7 spheroids stimulated by FSK is shown from –24 hours to 24-hours post FSK treatment at T = 0 hours. ***A-C*** *represent data from 3 experimental repeats (****A****, n = 19;* ***B****, n = 7;* ***C****, n = 40). The continuous lines represent the period of FSK treatment.*

In Figure 4-21, the continuous lines linking the –24 and 2- hour time points are for illustrative purposes only to aid the tracking the area change of individual spheroids. These lines do not accurately represent spheroid area increase over this period. Although most spheroids treated with FSK swelled as indicated by an increase in spheroid area between 2- and 24-hours, in all 3 repeats there was a population of spheroids that showed little or no increase in spheroid area during the assay (Figure 4-21). Spheroids belonging to this population were typically those with an area of ~1,463 μm^2, or 665 $pixels^2$, at –24 hours (665 px^2 was manually defined as the minimum spheroid area detected by the automated MIA plugin to avoid artifacts. 665 px^2 converts to 1463 μm^2 for the microscope and lens used to capture images).

Figure 4-22 shows that there was no correlation between day 14 spheroid area (μm^2) and extent of spheroid area increase (normalised to –24 hours) for repeats 5, 6, and 7 (Spearman's correlation (r) = 0.2175, -0.09045, and -0.09826, respectively).

Considered together, the above data suggest that whilst inhibition of FIS by I-172 was not reproducible in all experimental repeats, this cannot be attributed to variation in spheroid size at day 14 limiting FIS. Therefore, an alternative explanation was sought.

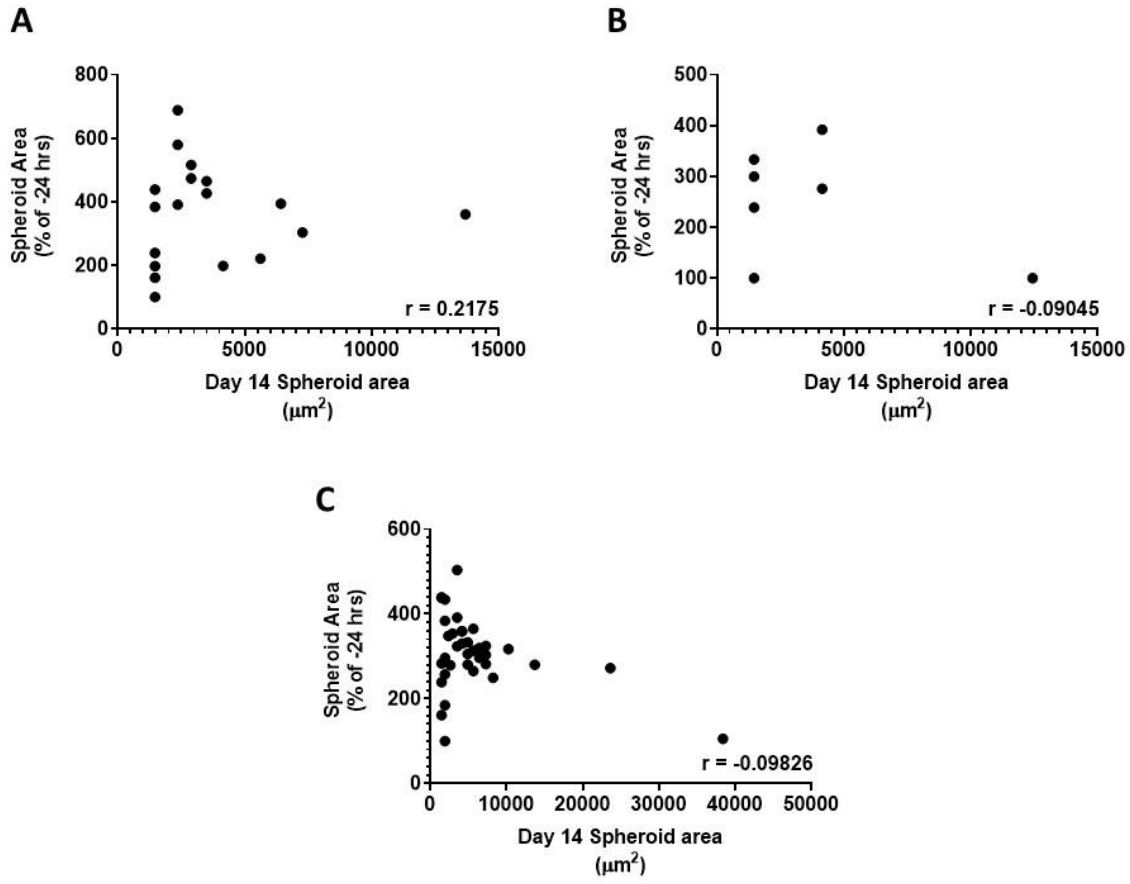

Figure 4-22: Spheroid area at day 14 does not correlate with extent of spheroid area increase stimulated by FSK.

Day 14 spheroid area (µm^2) was plotted against spheroid area (normalised to –24 hours) 24-hours post FSK-stimulation and the Spearman's correlation determined (r). For normalisation, the –24 spheroid area = 100%. ***A-C*** *represent data from experimental repeats 5-7 (****A****, n = 19;* ***B****, n = 7;* ***C****, n = 40); r = 0.2175, -0.09045, and -0.09826, respectively.*

4.3.4.7. Optimisation of FIS inhibition by $CFTR_{inh}$-172 in HCA7 spheroids.

Inhibition of FIS by I-172 in HCA7 spheroids was not reproducible across experimental repeats (Figures 4-13, 4-15, 4-17, and 4-18). As this result was not a result of day 14 spheroid size limiting FIS (Figures 4-21, and 4-22), the effect on FIS of pre-treating spheroids with I-172 was reviewed. In experimental repeats 1-7, for conditions involving I-172, spheroids were pre-treated with I-172 (10 µM) for 2-hours prior to FSK-stimulation. Figures 4-5, 4-7, and 4-10 clearly demonstrate that 10 µM I-172 inhibited CFTR-mediated Cl^- current in Ussing chamber experiments, while Figure 3-7 shows that pre-treatment of LIM1863 spheroids with 10 µM I-172 significantly decreased FSK-stimulated luminal swelling. To determine whether increasing the concentration of I-172 used in HCA7 spheroid FIS assays produced more effective and consistent inhibition of FSK-stimulated spheroid swelling, the FIS assay was repeated using I-172 at final concentrations of 10 µM, 20 µM, and 50 µM. Whilst the reported solubility of I-172 in an aqueous solution is 20 µM (Sonawane and Verkman, 2008), use of I-172 at a concentration of 50 µM was used by Dekkers *et al.* (2013) to inhibit FIS in human primary organoids. Figures 4-23 and 4-24 reveal that FSK stimulation of HCA7 spheroids resulted in significant spheroid swelling at 24-hours when compared with untreated spheroids ($p < 0.0001$), those treated with vehicle controls ($p < 0.0001$), and those treated with I-172 alone (10 µM, $p < 0.0001$; 20 µM, $p < 0.0001$ and 50 µM, $p < 0.0001$). Treatment with I-172 at 10 µM, 20 µM, and 50 µM did not cause spheroid swelling above that of untreated spheroids. An increase in spheroid area was observed in all spheroids pre-treated with I-172 (10 µM, 20 µM, and 50 µM) before FSK-stimulation. Although the extent of swelling at 24-hours for spheroids treated with FSK + I-172 (10 µM, 20 µM, and 50 µM) was less than that observed in spheroids treated with FSK alone, no significant difference was found between FSK treated spheroid area at 24-hours and spheroid area at 24-hours for any FSK + I-172 conditions (Figure 4-24).

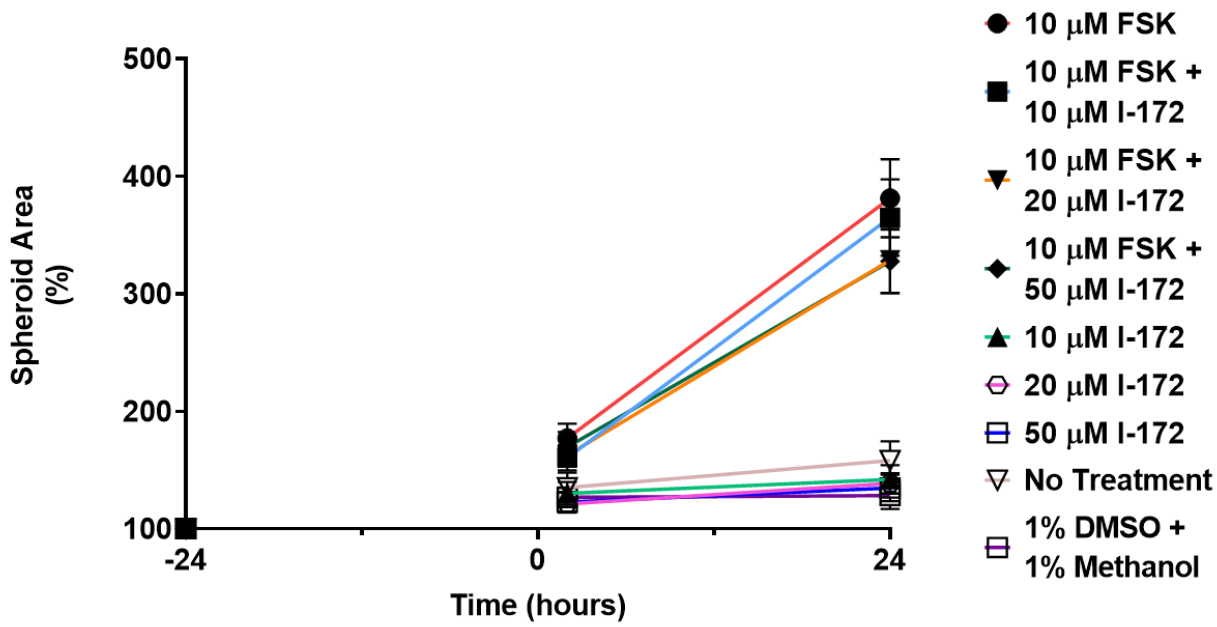

Figure 4-23: Inhibition of FIS in HCA7 spheroids by pre-treatment of spheroids with different concentrations of $CFTR_{inh}$-172.

HCA7 spheroid area was measured using a MIA plugin for Fiji/ImageJ and calculated relative to that at –24 hours (100%), in response to 10 µM forskolin (FSK), 10 µM forskolin + 10 µM $CFTR_{inh}$-172, 10 µM forskolin + 20 µM $CFTR_{inh}$-172, 10 µM forskolin + 50 µM $CFTR_{inh}$-172, 10 µM $CFTR_{inh}$-172, 20 µM $CFTR_{inh}$-172, and 50 µM $CFTR_{inh}$-172. For conditions involving $CFTR_{inh}$-172 (I-172; 10 µM, 20 µM, and 50 µM), spheroids were pre-treated with I-172 2-hours prior to FSK-stimulation. Untreated spheroids were included as a control for basal spheroid growth and 1% (v/v) DMSO + 1% (v/v) methanol was included as a vehicle control. Data are means ± S.E.M. (n = 10 – 28).

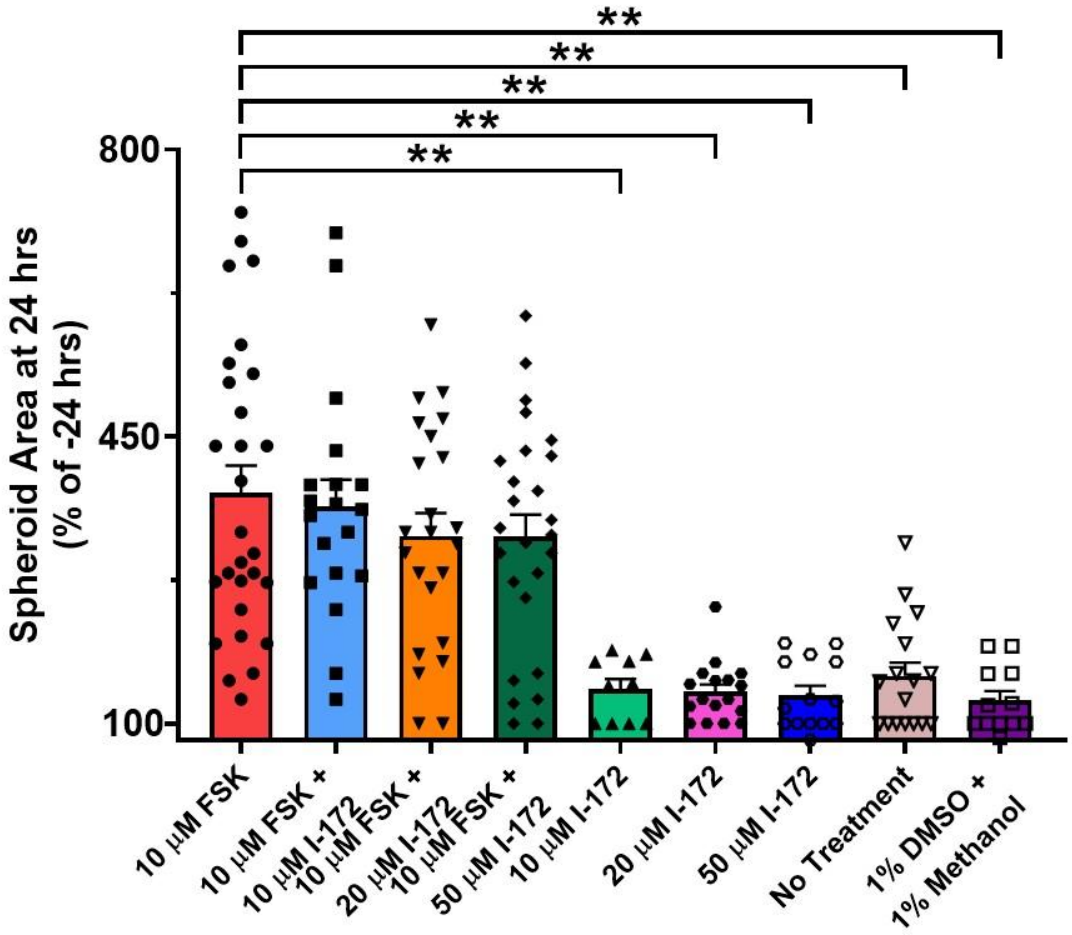

Figure 4-24: Comparison of FIS inhibition in HCA7 spheroids by different concentrations of $CFTR_{inh}$-172 24-hours post FSK-stimulation.

*HCA7 spheroid area, in response to treatment with 10 µM forskolin (FSK), 10 µM forskolin + 10 µM $CFTR_{inh}$-172, 10 µM forskolin + 20 µM $CFTR_{inh}$-172, 10 µM forskolin + 50 µM $CFTR_{inh}$-172, 10 µM $CFTR_{inh}$-172, 20 µM $CFTR_{inh}$-172, and 50 µM $CFTR_{inh}$-172 was compared 24-hours post FSK-stimulation. Untreated spheroids were included as a control for basal spheroid growth and 1% (v/v) DMSO + 1% (v/v) methanol was included as a vehicle control. For conditions involving $CFTR_{inh}$-172 (I-172; 10 µM, 20 µM, and 50 µM), spheroids were pre-treated with I-172 2-hours prior to FSK-stimulation. Data are means ± S.E.M. (n = 10 - 28); **, p < 0.01; unpaired t-test with Welch's correction.*

4.4. Future Work

At this stage, further work was prevented by the COVID-19 pandemic. It is clear from Section 4.3.4.7 that the FIS assay using HCA7 spheroids required further optimisation to ensure that subtle changes in spheroid area could be accurately detected. $CFTR_{inh}$-172 (I-172) is a well-established inhibitor of CFTR activity (Ma *et al.*, 2002), as such inhibition of CFTR activity, and therefore CFTR-mediated spheroid swelling, should be reproducibly reflected in the swelling assays performed, if the FIS observed is indeed CFTR-dependent. It is possible that the reason I-172 fails to significantly prevent HCA7 spheroid swelling is the ineffective penetrance of I-172 through the Matrigel that the spheroids are suspended in. To overcome this possibility, the next stage of assay optimisation would have been to use a higher concentration of I-172 (50 µM), as used by Dekkers *et al.* (2013), combined with an increase in the length of incubation time. An incubation time of 3- to 5-hours would have been tested in line with previous work (Dekkers *et al.*, 2013).

Once confident that HCA7 spheroid FIS is CFTR-dependent and that the assay could be used to detect subtle increases in spheroid area over the duration of the FIS assay, the assay would have been performed using the activators and inhibitors associated with intestinal ion transport used in Ussing chamber studies (Section 4.3.3). FIS assays would also have been performed using the known potentiator of CFTR-activity VX-770 (Ivacaftor) (Van Goor *et al.*, 2009), to assess the degree of CFTR potentiation achieved by this compound in HCA7 spheroids. Together these data would have provided a full characterisation of CFTR-mediated ion transport and fluid secretion in this cell line.

Upon achieving this level of characterisation, it was intended that the HCA7 cell line would be used in 2D Ussing chamber studies, and 3D swelling assay studies to assess the efficacy of new drug therapies, and identify alternative ion channels as therapeutic targets, with the aim of restoring fluidity to the CF intestine.

4.5. Discussion

In this chapter a cell line with potential as a cellular model of CFTR-mediated intestinal ion transport is described. The HCA7 (human colonic adenocarcinoma) cell line was shown to grow as both polarised 2D epithelia suitable for Ussing chamber experiments, and as organised 3D spheroids, or 'mini guts', for use in forskolin-induced swelling (FIS) assays. Moreover, characterisation of this cell line demonstrated the expression and function of several epithelial ion channels, transporters, and pumps key to CFTR-mediated ion transport.

4.5.1. Several cellular models of colorectal adenoma and carcinoma express CFTR

Initial screening of a panel of 15 human colonic adenoma and carcinoma cell lines by Western blotting using the anti-CFTR-596 antibody identified CFTR protein in whole cell lysate of 7 cell lines. Many of the cell lines tested are well established cellular models used in colorectal cancer research (Sekine *et al.*, 2002; Mouradov *et al.*, 2014). Cell lines, including HCT116, Caco-2, LoVo, HT-29, SW480, SW620, and SW1463 have previously been shown to express CFTR either at the mRNA level or functionally with the Ussing chamber or patch-clamp techniques (Kubitz *et al.*, 1992; Tien *et al.*, 1994; Devor *et al.*, 1997; Greger, 2000; Liu *et al.*, 2020). As highlighted in Figure 4-2, those cell lines found to express CFTR protein were AN/C1, RG/C2, HT-29, HCA7/Parental (HCA7), LoVo, LS174T, and SW1463. These cells lines, alongside AA/C1, AA/C1/SB/10C, and Caco-2 cells which were found not to express CFTR protein (Figure 4-2) were analysed for CFTR mRNA expression by Q-RT-PCR (Figure 4-3). Here, quantity of CFTR mRNA was expressed relative to that of the RG/C2 cell line. Both the AA/C1 and AA/C1/SB/10C cell lines were found to express CFTR mRNA, despite the absence of detectable CFTR protein, suggesting that for these cell lines mRNA levels do not correlate with protein expression. If further investigation of CFTR-protein expression were desired, Western blots could be repeated with a larger amount of protein. Surprisingly neither CFTR protein nor mRNA was detected in the Caco-2 cell line, despite previous contradictory reports (Tien *et al.*, 1994; Zhu *et al.*, 2005; Ahsan *et al.*, 2017). This could be a result of incomplete cellular differentiation, or a loss of CFTR expression in culture as passage number increased, an occurrence reported for other CFTR expressing cell lines (Zabner *et al.*, 2003). The AN/C1, RG/C2, HT-29, HCA7, LoVo, LS174T, and SW1463 cell lines were found to express CFTR protein and mRNA (relative to that of RG/C2).

4.5.2. HCA7 grow as epithelial monolayers generating R_t

Cellular models of intestinal ion transport arising from the panel of colorectal cell lines should grow as both 2D epithelia for Ussing chamber studies and 3D spheroids for FIS assays. The Ussing chamber technique allows for the study of transepithelial ion transport. The use of the Ussing chamber technique to characterise ion transport across an epithelium relies on the route of ion transport being restricted to transcellular ion movements, mediated by ion channels, pumps and transporters. This quality of the epithelium is referred to as its tightness, and it is made possible by the formation of tight junction proteins, which securely link adjacent cells together and promote polarisation, whereby the membrane proteins organise asymmetrically to the either apical or basolateral membranes (Zihni *et al.*, 2016). As such, for any cell line to be employed in Ussing chamber studies, they must grow as polarised epithelia with tight junctions between adjacent cells (Li, Sheppard and Hug, 2004). Shown in Figure 4-4 of the 7 intestinal epithelial cell lines tested, only the HCA7 cell line demonstrated an R_t above that of a blank Transwell insert, peaking at 5.3 ± 0.31 kΩ cm^2. Despite lack of detectable CFTR protein and mRNA in the Caco-2 cell line found in this chapter, it was previously reported that these cells express CFTR, grow as polarised epithelia on permeable supports, and form 3D spheroids (Schaar *et al.*, 2004; Sambuy *et al.*, 2005; Anabazhagan *et al.*, 2017). For Caco-2 cells grown on permeable supports generation of an R_t of ≥ 0.2 kΩ cm^2 has previously been used to assess polarisation (Schaar *et al.*, 2004). However, in this work the mean R_t of a blank Transwell insert was 0.32 ± 0.03 kΩ cm^2 and that generated by Caco-2 cells was 0.4 ± 0.02 kΩ cm^2 and as such no discernible R_t was apparent.

The HCA7 (human colonic adenocarcinoma) cell line demonstrates elements of morphological and functional polarity associated with the colonic epithelium (Kirkland, 1985b). When grow in standard 2D culture HCA7 cells form a polarised epithelium with cells linked by tight junctions and desmosomes, and microvilli on the apical membrane (Kirkland, 1985b). When grown on collagen-coated filter supports, HCA7 epithelia generate R_t in the range of 0.55 ± 0.09 kΩ cm^2 (Cuthbert, Kirkland and MacVinish, 1985), and 0.78 ± 0.68 kΩ cm^2 (Cuthbert *et al.*, 1987). The R_t generated by HCA7 epithelia in this work peaked at 5.3 ± 0.31 kΩ cm^2 8-days post seeding onto Transwell inserts, notably higher than that reported by Cuthbert *et al.* (1985), and Cuthbert *et al.* (1987). Possible explanations for this difference include the substrates used to grow the cells as polarised epithelia and changes in properties of the cells over time.

4.5.3. The HCA7 cell line expresses key ion channels and transporters for CFTR-mediated ion transport.

Consistent with previously work (Cuthbert *et al.*, 1985), FSK stimulated an increase in I_{sc} by HCA7 epithelia (Figure 4-5). Forskolin is a secretagogue that raises intracellular concentrations of cAMP, which in turn activates the cAMP-dependent protein kinase (PKA). Activated PKA catalyses the phosphorylation of the regulatory domain (RD) of CFTR (Hwang and Sheppard, 2009). Phosphorylation of the RD initiates channel gating controlled by cycles of ATP binding and hydrolysis at the NBDs (Hwang and Sheppard, 2009; Csanády, Vergani and Gadsby, 2019). The FSK-stimulated I_{sc} of HCA7 epithelia shown in Figure 4-5 peaked at 5.83 μA cm^{-2}, markedly smaller than values reported by Cuthbert *et al.* (1987), where FSK stimulation achieved I_{sc} in the range of 55-65 μA cm^{-2} by HCA7 epithelia. This difference might represent a change in the properties of HCA7 cells over time.

Application of the tyrosine-kinase inhibitor genistein to FSK-stimulated HCA7 epithelia significantly increased I_{sc} above that generated by FSK. All current was inhibited by I-172, a thiazolidinone compound which directly interacts with CFTR (Ma *et al.*, 2002; Caci *et al.*, 2008). Several mechanisms of action have been proposed for how genistein potentiates CFTR activity, including inhibition of serine/threonine phosphatases, inhibition of tyrosine kinases, and direct interaction with CFTR itself (Hwang and Sheppard, 1999; Wang *et al.*, 2002). Later work demonstrated that genistein interacts with the NBDs to potentiate ATP-dependent channel gating (Ai *et al.*, 2004; Moran, Galietta and Zegarra-Moran, 2005; Vergani *et al.*, 2005). Taken together these data show that FSK-stimulated, genistein potentiated and I-172-inhibited I_{sc} occurs across HCA7 epithelium, indicating that the HCA7 cell line, when grown on Transwell supports, demonstrates polarity and functional CFTR protein within the apical membrane. These properties are critical requirements of any cellular model of CFTR-mediated intestinal ion transport.

To further characterise ion transport by HCA7 epithelia, the loop diuretic bumetanide was used to assess the presence of the NKCC1 co-transporter in the basolateral membrane. Bumetanide is a NKCC1 inhibitor that inhibits cation-chloride co-transporters both *in vitro* and *in vivo* (Kahle and Staley, 2008). While the drug has inhibitory actions on both NKCCs and KCCs (potassium-chloride co-transporters), it demonstrates greater affinity for NKCCs over KCCs (Payne *et al.*, 2003). NKCC1 provides the principle route of

intestinal Cl^- uptake into epithelia, across the basolateral membrane, building intracellular Cl^- concentrations above electrochemical equilibrium, for onwards transport into the intestinal lumen via apical Cl^- channels (Anderson *et al.*, 1992). As shown in Figure 4-6 addition of bumetanide to the solution bathing the basolateral membrane of HCA7 epithelia reduced FSK-stimulated, genistein potentiated I_{sc}, providing evidence for the presence of NKCC1 within the HCA7 epithelium. Given bumetanide has greater affinity for NKCCs over KCCs , it is suggested that concentrations of bumetanide in the 2-10 μM range allow for the inhibition of NKCC independent of KCC (Payne *et al.*, 2003; Kahle and Staley, 2008). If further characterisation of basolateral Cl^- uptake by HCA7 epithelia were desired, Ussing chamber experiments could be performed using concentrations of bumetanide in this range.

Routes of apical Cl^- secretion into the intestinal lumen alternative to CFTR exist (Keely and Barrett, 2000), and in pathologies such as CF, where apical CFTR-mediated Cl^- secretion is defective these routes become a target of interest therapeutically (Li *et al.*, 2017). One such alternative route of Cl^- secretion is via calcium-activated chloride channels (CaCC) such as TMEM16A (also known as anoctamin 1) (Caputo *et al.*, 2008; Schroeder *et al.*, 2008; Yang *et al.*, 2008). Secretion of Cl^- by CaCC is stimulated by an increase in intracellular concentrations of Ca^{2+} (Anderson *et al.*, 1992). Activation of CaCC in HCA7 epithelia by the addition of ionomycin and UTP to the solution bathing the apical membrane resulted in a cAMP independent increase in I_{sc}, (Figure 4-7 and Figure 4-8, respectively). In both cases, the increase in I_{sc} was rapid, but transient upon drug addition, characteristic of CaCC-mediated I_{sc} in other epithelia (Li *et al.*, 2017). Pre-treatment of HCA7 epithelia with the CaCC inhibitor, and open channel blocker of CFTR niflumic acid (White and Aylwin, 1990), prevented both cAMP and Ca^{2+} induced Cl^- current across HCA7 epithelia (Figure 4-7B and C). These data indicate the presence of CaCC in the apical membrane of HCA7 epithelia. However, CaCC might be of limited use as therapeutic target to ameliorate intestinal disease in CF as previous research has shown that in the CF intestine CaCC along with CFTR is defective (Taylor *et al.*, 1987; Berschneider *et al.*, 1988).

The Na^{+}/K^+ ATPase was first reported in the 1950s by Skou (1957), work which earned one half of the Nobel prize for chemistry in 1977 (Skou, 1957). Upon hydrolysis of ATP by the basolateral Na^{+}/K^+ ATPase, the pump undergoes a conformational change, allowing for the active transport of 3 Na^+ out of the cell and 2 K^+ into the cell. Cycles of activity by this pump maintain the Na^+ gradient and the inside negative potential across the basolateral membrane of epithelial cells (Charney and Donowitz, 1978; Frizzell and

Hanrahan, 2012). Recycling of K^+ across the basolateral membrane occurs via basolateral K^+ channels, a process which is necessary to preserve the driving force for anion secretion across the apical membrane (Frizzell and Hanrahan, 2012). The endogenous cardiac glycoside ouabain inhibits the $Na^{+/}K^+$ ATPase (Schatzmann and Räss, 1967; Prassas and Diamandis, 2008), disrupting epithelial membrane potential and reducing the driving force for anion secretion across the apical membrane. As shown in Figure 4-9 application of ouabain to the solution bathing the basolateral membrane of HCA7 epithelia resulted in a sharp yet transient decrease in FSK-stimulated Cl^- mediated I_{sc}. Post ouabain treatment, the remaining current was inhibited by I-172. These data suggest the presence of the $Na^{+/}K^+$ ATPase in the basolateral membrane of HCA7 epithelia and highlight the effect of inhibition of $Na^{+/}K^+$ ATPase on cAMP-mediated Cl^- secretion. Further evidence to support both the presence of $Na^{+/}K^+$ ATPase in HCA7 epithelia and its important function was provided by Kirkland (1985a). This author demonstrated that when HCA7 cells are grown on standard tissue culture plastic they form domes as a result of vectorial fluid transport once confluent (Kirkland, 1985a). Dome formation was reduced when HCA7 monolayers were incubated with ouabain for 24-hours (Kirkland, 1985b), similar to its effects on Rama 25 (rat mammary), and MDCK (Madin-Darby canine kidney cells) epithelial domes (Lever, 1979).

HCA7 epithelia are classified as secretory epithelia, demonstrating no Na^+ absorptive properties (Roberts *et al.*, 1991). The epithelial sodium channel (ENaC) and the Na^+/H^+ exchanger (NHE) family of proteins are both important for Na^+ absorption across the apical membrane of epithelial cells (Girardi and di Sole, 2012; Hanukoglu, 2021). In the small intestine, the primary mechanism of Na^+ absorption is via NHE proteins (principally the isoform NHE3), whereas in the colon the primary mediator of Na^+ absorption is ENaC (Yang *et al.*, 2016). A link between impaired CFTR function and upregulated Na^+ conductance via ENaC has been observed in human airway epithelia from individuals with CF (Boucher *et al.*, 1988; Kunzelmann, Kathöfer and Greger, 1995). ENaC inhibitors such as BI1265162 have shown promise, suppressing ENaC activity, decreasing Na^+ and water reabsorption in CF airway (Nickolaus *et al.*, 2020). In this work the ENaC inhibitor amiloride was without effect on baseline and cAMP mediated I_{sc} by HCA7 epithelia (Figure 4-10). Typically addition of amiloride to the solution bathing the apical membrane of ENaC-expressing epithelia results in a prompt decrease in I_{sc} (Mall *et al.*, 1998; Ma *et al.*, 2002; Dekkers, Van Mourik, *et al.*, 2016; Tang *et al.*, 2017). No evidence of ENaC activity was found in HCA7 epithelia, agreeing with previous reports (Roberts *et al.*, 1991).

The proteins investigated in Section 4.3.3 with the Ussing chamber technique are by no means an exhaustive list of the ion channels, pumps and transporters that mediate transepithelial ion transport by secretory epithelia. The discussed Ussing chamber studies do, however, characterise several transport proteins crucial for CFTR-mediated ion transport. It can be concluded from the work presented in this chapter that HCA7 epithelia express CFTR and CaCC in the apical membrane and NKCC1 and the Na^{+}/K^{+} ATPase in the basolateral membrane.

4.5.4. CFTR-mediated swelling in HCA7 spheroids.

To complement Ussing chamber studies of 2D HCA7 epithelia and to determine whether FSK stimulation of 3D HCA7 spheroids results in a quantifiable response, FIS assays were performed. The ability to perform FIS assays with HCA7 spheroids would facilitate use of the HCA7 cell line in screening assays. Unlike FIS with LIM1863 spheroids, where CFTR-mediated Cl^{-} and fluid secretion increased lumen area without increasing spheroid area, FIS with HCA7 spheroids resulted in an increase in both lumen and overall spheroid area (Figures 4-11, 4-12, and 4-13).

Although quantification of FIS as a function of lumen area increase (Figure 4-11) clearly captured the effect of FSK-mediated ion and fluid secretion into the spheroid lumen, there was much variation in the extent of lumen area increase both within and between experimental repeats. Expression of lumen area relative to that at –24 hours provided some normalisation against variation in original spheroid lumen area. However, it did not account for the impact of spheroid size on extent of swelling, nor basal spheroid growth over a 72-hour period. HCA7 spheroid lumen area normalised to spheroid area at each time point, expressed relative to normalised lumen area at –24 hours, provided a method of quantification that incorporates spheroid size and basal spheroid growth over the assay duration (Figure 4-12). Despite this, a large degree of variation was still observed in FIS response both within and between experimental repeats which prevented comparison of data from multiple experimental repeats. Additionally, the tracking plugin developed for use with LIM1863 spheroids was unable to accurately distinguish between HCA7 spheroid lumen and the outer spheroid edge. Whilst the MIA plugin was designed to detect the outer spheroid edge, without a means of automating the quantification of spheroid lumen area, this method of quantification would have to take place manually, precluding use in high-throughput screening.

Quantification of FIS in HCA7 spheroids as a function of spheroid area increase relative to that at –24 hours provided a method of quantification conducive to automation as a plugin for Fiji/ImageJ capable of detecting and tracking spheroid area was available from the Wolfson Bioimaging Facility at the University of Bristol (MIA plugin). Similar to studies using this approach to FIS quantification in mouse and human primary organoids (Dekkers *et al.*, 2013; Dekkers, Berkers, *et al.*, 2016), stimulation of HCA7 spheroids with FSK resulted in an increase in spheroid area compared to untreated and vehicle control treated spheroids (Figure 4-13). This method of quantification resulted in reduced variation in FIS response observed between experimental repeats, although a wide degree of variation in extent of swelling was still observed within repeats, in some cases leading to overlapping error bars between FSK and FSK + I-172 conditions.

Quantification of FIS based on increase in spheroid area relative to –24 hours reproducibly and accurately captured FIS by HCA7 spheroids, and as quantification using this method could be automated with the MIA plugin this approach was deemed most suitable for high-throughput screening. As shown in Figure 4-16, for all experimental repeats spheroid area increase (μm^2) from –24 hours to 24-hours positively correlated with spheroid lumen area increase (μm^2) over the same period. This result confirmed that an increase in spheroid area stimulated by FSK reflected CFTR-mediated ion and fluid secretion into the spheroid lumen.

Automation of quantification alongside a reduction of total assay duration from 72- to 48-hours provided the foundations for a FIS assay in HCA7 spheroids with the capacity for high volume and rapid analysis. Typically FIS assays using human primary colonic or small intestinal organoids have been reported to last 60-minutes with images taken throughout the assay at 10-minute intervals (Dekkers, Berkers, *et al.*, 2016; Dekkers, Van Mourik, *et al.*, 2016; Boj *et al.*, 2017; Vonk *et al.*, 2020), or less frequently to last 40-minutes with image acquisition at 10-miute intervals (Dekkers *et al.*, 2013). Before the FIS assay duration for HCA7 spheroids was reduced to 48-hours (final image acquisition 24-hours post FSK-stimulation), it was necessary to determine whether a reduction would compromise assay validity. Figure 4-14 demonstrates that a significant increase in spheroid area occurred between 24- and 48-hours in at least one treatment condition in all four FIS repeats. No consistent pattern as to which treatment conditions caused spheroids to increase in area beyond 24-hours was identified. Whilst it could be proposed that basal spheroid growth accounted for this increase, a significant increase in basal spheroid size was only observed between 24- and 48- hours in 50% of the FIS

assay repeats. Moreover, unless treatment conditions decreased basal cell proliferation, it is reasonable to assume that basal cell proliferation contributed to spheroid area increase in all treatment conditions and all repeats. It can be seen in Figure 4-14 that at 48-hours data points are more widely spread than at 24-hours, specifically in spheroids that swelled above the mean, demonstrating that some organoids are capable of greater swelling than others. This suggests that each spheroid possesses a maximum amount of swelling that they can achieve, and that the maximum percentage increase in spheroid area increase is not uniform.

Taken together Figures 4-13 and 4-14 show that an assay lasting 72-hours does not allow all spheroids to achieve a maximal increase in area, which plateaus post FSK stimulation. However, the purpose of the assay is the quantification of CFTR-mediated spheroid swelling by test compounds. In FIS assays using primary human CF and non-CF rectal organoids, swelling occurred over a time period when FIS did not plateau (Dekkers *et al.*, 2013; Dekkers, Berkers, *et al.*, 2016; Dekkers, Van Mourik, *et al.*, 2016). Therefore, provided the assay duration distinguishes between those spheroids treated with FSK and those untreated, a shorter assay would be acceptable. Comparison of HCA7 spheroid area increase at 24-hours confirmed that in all four experimental repeats there was a significant difference in spheroid area increase between those treated with FSK and untreated spheroids (Figure 4-15). In all but one repeat, a significant difference in spheroid area increase was also found between those spheroids treated with FSK and those treated with I-172 alone. These data confirmed that a 48-hour assay differentiated the spheroid area increase of FSK stimulated spheroids from untreated spheroids and those treated with either vehicles or I-172 alone. Thus, 24-hours was selected as the final image acquisition point in subsequent FIS assays.

Automated image analysis using the above parameters and the Modular Image Analysis (MIA) plugin designed for use in Fiji/ImageJ was successful. Figures 4-17 and 4-18 demonstrate that the MIA plugin identified FIS in three new experimental repeats. The ability of the MIA plugin to compile z-stack images and identify and measure the widest cross section though spheroids ensured data consistency. The degree of circularity imposed on the plugin is a threshold set by the user. By selecting a higher circularity threshold, the plugin only detects spheroids that are entirely circular. As the circularity threshold is reduced, the plugin will detect spheroids that deviate more and more from uniformity. Cross sections through HCA7 spheroids are typically close to circular, so a high circularity threshold was selected; this prevented the MIA plugin detecting overlapping organoids. A high circularity threshold combined with a defined minimum

spheroid surface area prevented the detection of debris and irregularly shaped spheroids. At the end of image analysis, data output was checked against circle overlay images produced to eliminate the remaining mis-identified spheroids. Unlike similar FIS assays with human and mouse primary intestinal organoids (Dekkers *et al.*, 2013; Dekkers, Van Mourik, *et al.*, 2016), the automated FIS assay analysis presented did not require calcein green staining as the MIA plugin reliably identified HCA7 spheroids using only phase contrast images.

Despite successful automation of image acquisition and analysis in FIS assays with HCA7 spheroids, in over half of the assays performed the extent of spheroid area increase was greater in spheroids treated with FSK + I-172 than FSK alone. It was also noted that variation in spheroid area increase in response to FSK-stimulation existed both within and between experimental repeats. Figure 4-19 shows a significant difference in mean spheroid area 24-hours after FSK-stimulation between all 7 experimental repeats. Moreover, within experimental repeats the extent of spheroid area increase 24-hours post FSK-stimulation varied considerably with some spheroids unchanged in area from the –24 hour time point, others increasing in area >400% and yet others even decreasing in area.

An initial explanation for the variation in spheroid swelling and for the greater swelling of spheroids treated with FSK + I-172 than FSK alone was that the initial spheroid size (–24 hours = day 14 of culture) imposed a limitation on the amount of swelling by individual spheroids. Normalisation of spheroid area to that at –24 hours (–24 hours = 100%) ensured that FIS assay analysis accounted for differences in spheroid size. However, this normalisation did not account for the limited swelling of small spheroids. Box and whisker analysis of day 14 spheroid area distribution for all spheroids studied highlight the variation both between and within cultures (Figure 4-20). Whilst variation in spheroid size was observed when spheroid cultures were visualised under the microscope, and some level of heterogeneity expected, the extent of variation was unanticipated given that all spheroids were derived from single HCA7 cells seeded into Matrigel.

Given that inhibition of FIS by I-172 was inconsistent throughout FIS assays, and not attributed to spheroid size at –24 hours limiting spheroid area increase, it was concluded that FIS inhibition by I-172 was ineffective or sub-optimal during the assays. In electrophysiology studies, 10 µM I-172 effectively inhibits CFTR-mediated current (Ma *et al.*, 2002; Taddei *et al.*, 2004; Hughes, Ju and Sheppard, 2008; Melis *et al.*, 2014). This concentration of I-172 also prevented the enlargement of 3D renal cyst growth (Li,

Findlay and Sheppard, 2004). It is reported that 20 µM is the upper solubility limit of I-172 in aqueous solution (Sonawane and Verkman, 2008), and that use of I-172 at concentrations above 5 µM has an inhibitory effect on volume-sensitive outwardly rectifying Cl^- conductance (VSORC) (Melis *et al.*, 2014). However, studies of CFTR-mediated Cl^- and fluid secretion in 3D intestinal organoids typically utilised 50 µM I-172 to inhibit FIS by about 90% (Dekkers *et al.*, 2013; Okiyoneda *et al.*, 2013). As can be seen in Figures 4-23 and 4-24 where spheroids were pre-treated with 10, 20, and 50 µM I-172 before FSK-stimulation some reduction in FIS was observed compared to spheroids treated with FSK alone. However, this inhibition was not found to be significant for all concentrations of I-172. This result suggests that other anion channels may contribute to FSK-stimulated swelling of HCA7 spheroids. If future studies do not result in effective and consistent inhibition of FSK, it must be considered that cAMP-mediated swelling of HCA7 spheroids is not fully CFTR-dependent, potentially calling into question the use of this cell line as a 3D model of CFTR-mediated intestinal ion and fluid transport.

4.6. Concluding Remarks

From a panel of 15 human colonic adenoma and carcinoma cell lines the HCA7 cell line was shown to express both CFTR mRNA and protein, with the ability to grow as both 2D epithelia and 3D spheroids suitable for Ussing chamber studies and FIS assays of intestinal ion transport. Ussing chamber studies demonstrated that HCA7 cells express CFTR and CaCC in the apical membrane and NKCC1 and $Na^{+/}K^+$ ATPase in the basolateral membrane. FIS assays showed that HCA7 spheroid swelling is stimulated by FSK. However, it is to be confirmed that the observed FIS is completely CFTR-dependent. Full automation of FIS assays with HCA7 spheroids was achieved. As such, it can be concluded that the HCA7 cell line is a potential cellular model of intestinal CFTR-mediated ion and fluid secretion

Chapter 5. Investigating the role of the Na^+/H^+ exchanger, NHE3, in intestinal ion transport.

5.1. Introduction

Within the epithelium of the intestine, the cystic fibrosis transmembrane conductance regulator (CFTR) mediates the majority of Cl^- secretion across the apical membrane into the intestinal lumen (De Lisle and Borowitz, 2013). The regulation of intestinal Cl^- secretion is closely linked to the regulation of Na^+ absorption by Na^+ channels, transporters and pumps in intestinal epithelial cells. In the colon, Na^+ absorption is primarily mediated by the epithelial sodium channel (ENaC), whereas in the small intestine Na^+ absorption is predominantly mediated by the sodium/hydrogen exchanger (NHE) isoform 3 (NHE3) (Zachos, Kovbasnjuk and Donowitz, 2009; Yang *et al.*, 2016). However, these tissue distributions are not exclusive and both proteins (including NHE isoforms 1-3, and 8) are found along the length of the small intestine and colon (Praetorius *et al.*, 2000; He and Yun, 2010).

Some debate exists concerning the location of ion transport in the intestine, specifically the distribution of specialised secretory and absorptive cells along the crypt villus axis. A long-standing idea is that the secretory and absorptive regions of the small intestinal epithelium are spatially distinct, with largely secretory cells located within the crypts, and absorptive cells located at the villi tips (Strong, Boehm and Collins, 1994; Yang *et al.*, 2016). Advances in both molecular biology and 3D tissue culture techniques have challenged this idea in recent years, with new data suggesting that there is an overlap of secretory and absorptive function along the crypt villus axis (Barrett, 2018). Evidence to support this idea comes from multiple sources utilising both undifferentiated (crypt-like) and differentiated (villus-like) enteroids. Foulke-Abel *et al* (2016) detected NHE3 activity in both undifferentiated and differentiated enteroids, alongside NHE3- and NKCC1-inhibition dependent FSK-induced CFTR-mediated enteroid swelling. Yin *et al* (2018) reported that undifferentiated and differentiated enteroids derived from human duodenum demonstrated both cAMP-mediated Cl^- and HCO_3^- secretion, with the capacity for Cl^- secretion but not HCO_3^- secretion decreasing in differentiated enteroids. In addition, the authors found that the expression of ion channels and transporters changed significantly upon enteroid differentiation, namely reduced expression of CFTR, NKCC1, and KCNE3 and increased expression of NHE1, NHE3, DRA (down-regulated-in-adenoma), NBCe1 (electrogenic Na^+/HCO_3^- co-transporter 1), CA2 (carbonic anhydrase 2),and CA4 (Yin *et al.*, 2018).

In the non-CF intestine, cAMP mediates both CFTR activation and NHE3 inhibition, regulating Cl^- secretion and Na^+ absorption across the apical membrane to govern the net movement of NaCl and therefore water into and out of the intestinal lumen (Clarke and Harline, 1996; Saint-Criq and Gray, 2017). NHE3-mediated Na^+ absorption dominates during periods of basal activity. However, during periods of stimulation cAMP-mediated Cl^- secretion via CFTR dominates alongside the concurrent inhibition of NHE3 (Gawenis *et al.*, 2004). The highly coordinated activity of these two proteins also plays an important role in pH buffering within the intestine (Praetorius *et al.*, 2000; Chen, Cai and Sheppard, 2009). HCO_3^- secretion into the intestinal lumen by CFTR occurs alongside that of Cl^- (Song *et al.*, 2006; Riordan, 2008), a process of particular importance in the duodenum where acid from the stomach requires neutralisation (De Lisle and Borowitz, 2013; Borowitz, 2015). Bicarbonate-rich fluid secretion from the pancreas also contributes to duodenal pH buffering (De Lisle and Borowitz, 2013; Wilschanski and Novak, 2013). In addition, group 2 SLC26A (SLC26A6) Cl^-/HCO_3^- exchangers, and group 3 SLC26A (SLC26A9) anion channels contribute to epithelial HCO_3^- secretion, (and in the case of SLC26A9-mediated epithelial Cl^- secretion) and are proposed to account for the large amount of HCO_3^- secretion by the pancreas (Frizzell and Hanrahan, 2012). Reabsorption of HCO_3^- occurs via NHE3-mediated HCO_3^- degradation whereby the binding of H^+ to luminal HCO_3^- gives rise to intermediary H_2CO_3, which is in turn degraded to CO_2 and H_2O (Rector, Carter and Seldin, 1998).

The impact of CF on the intestines is multifactorial and complex. In the CF intestine, regulation of ion and fluid secretion is lost, as is regulation of intestinal pH (Borowitz, 2015). Not only is intestinal Cl^- and HCO_3^- secretion by CFTR impaired, but HCO_3^--rich secretions from the pancreas are reduced (Wilschanski and Novak, 2013). Regulation of coupled Na^+ absorption and H^+ efflux by NHE3, and NHE3-mediated HCO_3^- absorption are also lost. It is the combined effects of loss of channel function and pH regulation that leads to the GI symptoms of CF, namely dehydration and acidification of the intestinal lumen, constipation and intestinal blockage, inflammation, and changes to the gut microbiota (De Lisle and Borowitz, 2013).

Whilst much research has investigated the regulation of NHE3 and CFTR individually (see Section 1.4.3 for further discussion), some evidence suggests their coordinated role in the regulation of cAMP-mediated Cl^- secretion and Na^+ absorption. In the small intestine of NHE3 knockout mice, not only was cAMP-mediated Cl^- secretion decreased, but CFTR mRNA and protein expression were also reduced (Gawenis *et al.*, 2004). Similarly Na^+ absorption and NHE3 protein expression are reduced in the small intestine

of CFTR knockout mice (Clarke and Harline, 1996; Gawenis *et al.*, 2003, 2004). The mechanisms underpinning the coordinated regulation of CFTR and NHE expression and function in the intestine are incompletely understood.

In recent years, NHE3 has become of interest as a mutation-independent target for CF therapy. The importance of NHE3 in intestinal NaCl homeostasis and intestinal pH control is well documented. In the non-CF intestine, inhibition of NHE3 activity by small molecules, targeted gene deletion or reduced protein expression result in secretory diarrhoea (Hayashi *et al.*, 2004). Similarly, in congenital diseases where secretory diarrhoea is characteristic, NHE3 expression is significantly reduced (Ameen and Salas, 2000). Bacterial such as *Vibrio cholerae*, *Clostridium difficile*, and strains of *Escherichia coli* release toxins that ultimately increase either cAMP or cGMP vastly increasing CFTR-mediated Cl^- secretion and inhibiting NHE3-mediated Na^+ absorption, a combination that results in acute diarrhoea (Lencer *et al.*, 1995; Barrett and Keely, 2000; Hayashi *et al.*, 2004; Chen *et al.*, 2019).

Drugs that target NHE3, inducing inhibition of NHE3-mediated Na^+ absorption are attractive as potential therapeutics for the GI complications of CF. As a proof of principle, in *CFTR* null mice, which lacked either one or both copies of the *NHE3* gene, increased intestinal fluidity was observed compared to their *CFTR* null, NHE3 expressing counterparts (Bradford *et al.*, 2009). Tenapanor, linaclotide and lubiprostone are examples of drugs, already licenced for used in humans, that either directly or indirectly inhibit NHE3 (Tan *et al.*, 2021). Tenapanor is a direct inhibitor of NHE3, thought to bind irreversibly to the protein, which has shown promise treating constipation-prominent irritable bowel syndrome (Chey, Lembo and Rosenbaum, 2017; Hayashi, 2019). Linaclotide is a synthetic peptide which increases intracellular levels of cGMP by binding to the transmembrane receptor GCC (guanylyl cyclase C), ultimately inhibiting NHE3 and stimulating CFTR (Steinbrecher, 2014; Ahsan *et al.*, 2017). The synthetic eicosanoid, lubiprostone, which activates ClC-2 chloride channels was originally used to treat chronic constipation (O'Brien, Anderson and Stowe, 2010). Lubiprostone is also a ligand for EP1 (not expressed in intestinal epithelial cells) and EP4 prostaglandin receptors which activates CFTR and inhibits NHE3 via the cAMP/PKA pathway (Bassil *et al.*, 2008; Bijvelds *et al.*, 2009). Studies using these drugs in *CFTR* null and homozygous CFTR-F508del mice concluded that tenapanor, linaclotide and lubiprostone all reduced fluid absorption in the jejunum, and, with the exception of linaclotide, in the colon too (Tan *et al.*, 2021).

It is clear from these studies that restoration of NHE3 regulation using drugs that inhibit NHE3, such as tenapanor, linaclotide and lubiprostone, has much potential as a therapy for intestinal disease in CF. Studies to date have largely been performed in 2D cellular models or animal models. Therefore, assessing the contribution of NHE3 to intestinal ion transport and how its regulation by NHE3 inhibiting drugs, in 3D cellular models could provide new insights into the therapeutic potential of NHE3 inhibition for the CF intestine. Additionally, assessing the absorptive capacity of the HCA7 cell line in terms of expression and activity of NHE3 would be of particular relevance to the work of this thesis which seeks in part to understand and utilise the functional relationship between CFTR and NHE3. Work performed in Chapter 4 of this thesis alongside previous work by Roberts *et al* (1991) failed to demonstrate that the HCA7 cell line has an absorptive phenotype. However, these previous studies examined the Na^* channel ENaC, while the electroneutral activity of NHE3 in this cell line is yet to be fully investigated. If, as emerging evidence suggests, cells of the intestinal epithelium are to varying degrees capable of both the secretion and absorption of fluid and electrolytes, it is possible that further study will reveal NHE3-mediated Na^+ absorption in the HCA7 cell line.

5.2. Aims

The aim of this chapter was to investigate the role of NHE3 in intestinal ion and fluid transport. The drugs tenapanor, linaclotide and lubiprostone will be used in 2D Ussing chamber studies and 3D FIS assays using the HCA7 cell line. Results from these studies will be used to determine how inhibition of NHE3 affects cAMP-stimulated fluid transport in HCA7 spheroids and cAMP-stimulated I_{sc} in HCA7 epithelia.

Initially, NHE3 expression in the HCA7 cell line will be assessed. If it is not expressed, lentiviral transduction will be used to heterologously express NHE3 in the HCA7 cell line. In addition, the expression of GCC, EP1 and EP4, the binding targets of linaclotide and lubiprostone, respectively, will be assessed by Q-RT-PCR and Ussing chamber studies. As both lubiprostone and linaclotide increase the intracellular concentrations of cAMP/cGMP, respectively, treatment of HCA7 epithelia with these compounds should induce CFTR-mediated Cl^- secretion and therefore a change in I_{sc}. Assuming that the HCA7 cell line expresses GCC, EP1 and EP4, dose response curves will be generated using therapeutically relevant drug concentrations to ascertain the optimal concentration of linaclotide and lubiprostone for Ussing chamber studies and FIS assays.

Given the electroneutral nature of Na^+ and H^+ exchange by NHE3 employing the Ussing chamber technique alone to study NHE3 activity is limited. However, the technique is of value to investigate how NHE3 inhibition modulates cAMP/cGMP-mediated Cl^- secretion. If heterologous expression of NHE3 in the HCA7 cell line is required, Ussing chamber experiments will be performed to determine whether this affects FSK-stimulated I_{sc}, compared to control HCA7 cells. cAMP- and cGMP-mediated I_{sc} induced by lubiprostone and linaclotide will be fully characterised.

If NHE3 is expressed exogenously in HCA7 cells, FIS assays will be performed to investigate its effects on FSK-stimulated spheroid swelling. The extent of spheroid swelling induced by linaclotide and lubiprostone will then be assessed. To determine whether inhibition of NHE3 by tenapanor, linaclotide or lubiprostone may be of use in the restoration of intestinal fluid secretion in the CF intestine, the compounds will be used in swelling assays where spheroids have been pre-treated with I-172 to inhibit CFTR-mediated spheroid swelling. Finally, all three compounds will be used in swelling assays alongside CFTR potentiators such as genistein and ivacaftor (VX-770), to determine whether the extent spheroid swelling is increased when CFTR-mediated Cl^- secretion is potentiated and NHE3-mediated Na^+ absorption is inhibited. This combination of compounds should maximise spheroid luminal NaCl concentration and therefore fluid secretion into the spheroid lumen.

Cumulatively, these experiments will illuminate the role NHE3 has in intestinal ion transport in a cellular model expressing wild-type CFTR. These experiments would provide a basis for future work whereby CFTR expression is reduced or mutated CFTR is introduced into the HCA7 cell line, and the extent NHE3 inhibition ‘rescues’ fluid secretion is ascertained. This would go some way to recapitulating the phenotype of the CF-intestine and allow preliminary studies of NHE3 as a mutation-independent therapeutic target before translating these studies to intestinal 2D and 3D epithelium derived from individuals with CF, paving the way for individualised medicines.

5.3. Results

5.3.1. Validation of an NHE3 antibody for use in Western blotting.

Before it could be determined whether the HCA7 cell line expressed NHE3, a suitable antibody to detect NHE3 protein was identified and validated. The initial antibody selected was the Proteintech polyclonal rabbit anti-NHE3 antibody (see Section 2.1.6. for details), reported by Proteintech to react with human NHE3 protein and previously used to identify mouse and pig NHE3 proteins by Western blotting and immunocytochemistry, respectively (Koizumi *et al.*, 2019; Shao *et al.*, 2021; Wang *et al.*, 2021). As no known NHE3 protein positive or negative control cell line was available, a panel of 9 human colonic adenoma and carcinoma cell lines (AA/C1, AA/C1/15B/10C, RG/C2, HT-29, HCA7, LoVo, LS147T, SW1463, and Caco-2) was screened to identify those with anti-NHE3 antibody binding. Western blotting was performed using whole cell lysate corresponding to 64 µg of total protein as determined using the Bio-Rad DC protein assay (see Section 2.8.2). Whilst NHE3 has a calculated molecular weight of 93 kDa, antibody binding during Western blotting was anticipated to occur between 80 - 100 kDa. Figure 5-1 shows that the anti-NHE3 antibody demonstrated much non-specific binding in all cell lines, including in the region where NHE3 protein was anticipated to occur (~85 kDa) particularly in the HCA7, LoVo, LS174T, and Caco-2 cell lines. As LS174T cell line demonstrated particularly strong anti-NHE3 antibody binding at ~85 kDa, it was selected as a likely positive control for NHE3 protein expression and used in subsequent protein expression and antibody specificity validation assays.

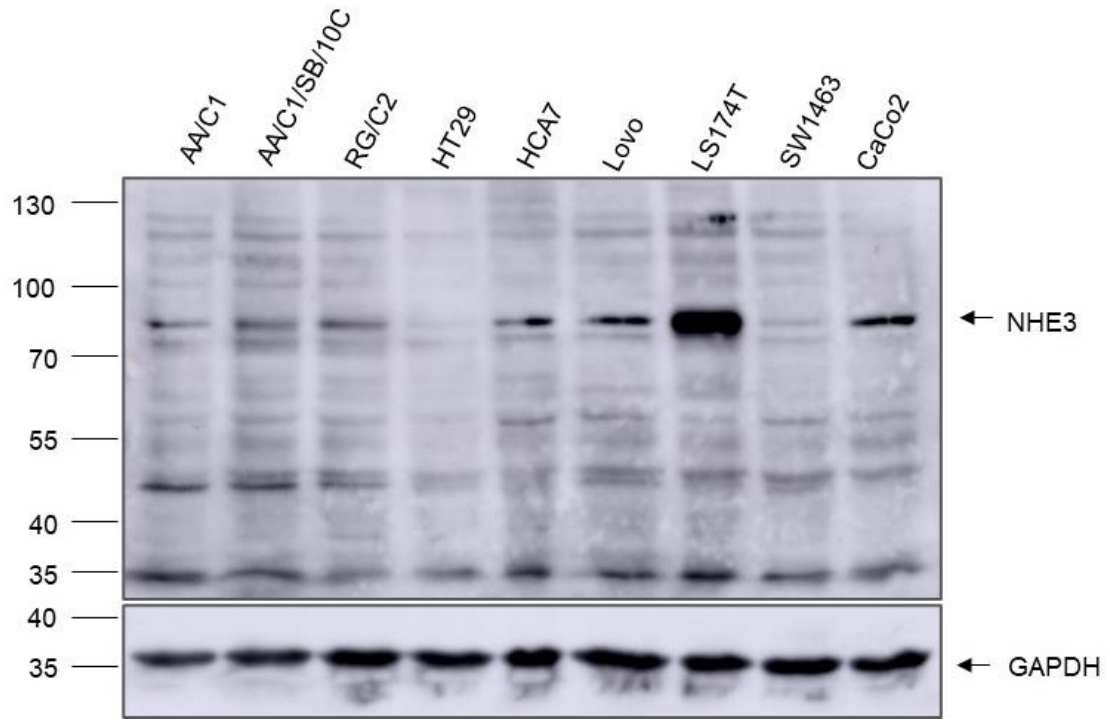

Figure 5-1: Potential NHE3 expression in human colonic adenoma and carcinoma cell lines.

64 µg of protein from human colonic adenoma and carcinoma whole cell lysates were separated by SDS-PAGE and immunoblotted with the Proteintech anti-NHE3 antibody. An anti-GAPDH antibody was used as a loading control. For Western blotting n = 1.

To examine antibody specificity, siRNA-mediated protein depletion was performed. As such, LS174T cells were transfected with SMARTpool ON-TARGETplus human *SLC9A3* siRNA (siNHE3; 100 µM) and non-targeting control siRNA (100 µM) (for protocol see Section 2.4.1). LS174T cell lysates were prepared at 24-, 48-, and 72- hours post transfection, the protein concentration of lysate was determined, and 45 µg of lysate was separated by SDS-PAGE and immunoblotted using the Proteintech anti-NHE3 antibody. Figure 5-2 shows that anti-NHE3 antibody binding occurred at ~85 kDa at all timepoints for LS174T cells transfected with control non-targeting siRNA. For LS174T cells transfected with siNHE3, anti-NHE3 antibody binding decreased over time. It was little changed at 24-hours, greatly reduced at 48-hours and not detected by 72-hours post transfection (Figure 5-2). Interestingly, less non-specific antibody binding occurred in Figure 5-2 than was observed in Figure 5-1. However, this was likely the result of loading the gel with less protein, combined with a shorter exposure time.

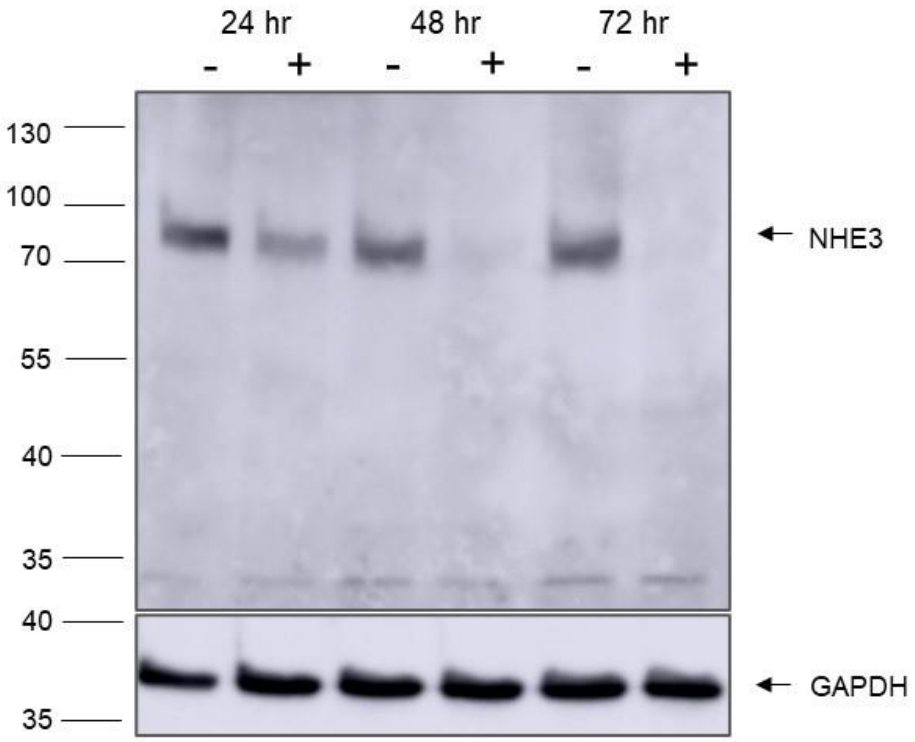

Figure 5-2: siRNA-mediated NHE3 protein depletion in the LS174T cell line.

LS174T cell lysate corresponding to 45 µg of protein from cells transfected with either siRNA targeting NHE3 (+) or control non-targeting siRNA (-), was separated by SDS-PAGE and immunoblotted with the Proteintech anti-NHE3 antibody. Cell lysates were prepared at 24-, 48-, and 72-hours post transfection. An anti-GAPDH antibody was used as a loading control. For Western blotting n = 1.

These results show that siRNA-mediated NHE3 protein depletion begins within 24-hours of transfection, with near complete protein depletion occurring within 48-hours and by 72-hours no detectable NHE3 protein remained. They validate that the Proteintech anti-NHE3 antibody detects human NHE3 protein in colonic cells and identify an siRNA against human NHE3 for use in future experiments.

5.3.2. Characterisation of endogenous NHE3 expression in the HCA7 cell line.

As discussed in Section 4.5.3, the HCA7 cell line has been demonstrated to secrete, but not absorb salt and water. Figure 5-1 shows that the HCA7 cell line produced a weak band at ~85 kDa, corresponding to NHE3 protein. To complement protein detection, Q-RT-PCR was performed on the AA/C1, AA/C1/15B/10C, RG/C2, HT-29, HCA7, LoVo, LS147T, SW1463, and Caco-2 cell lines to identify the presence of NHE3 mRNA. Figure 5-3 quantifies NHE3 mRNA for these cell lines relative to that detected in RG/C2 lysates.

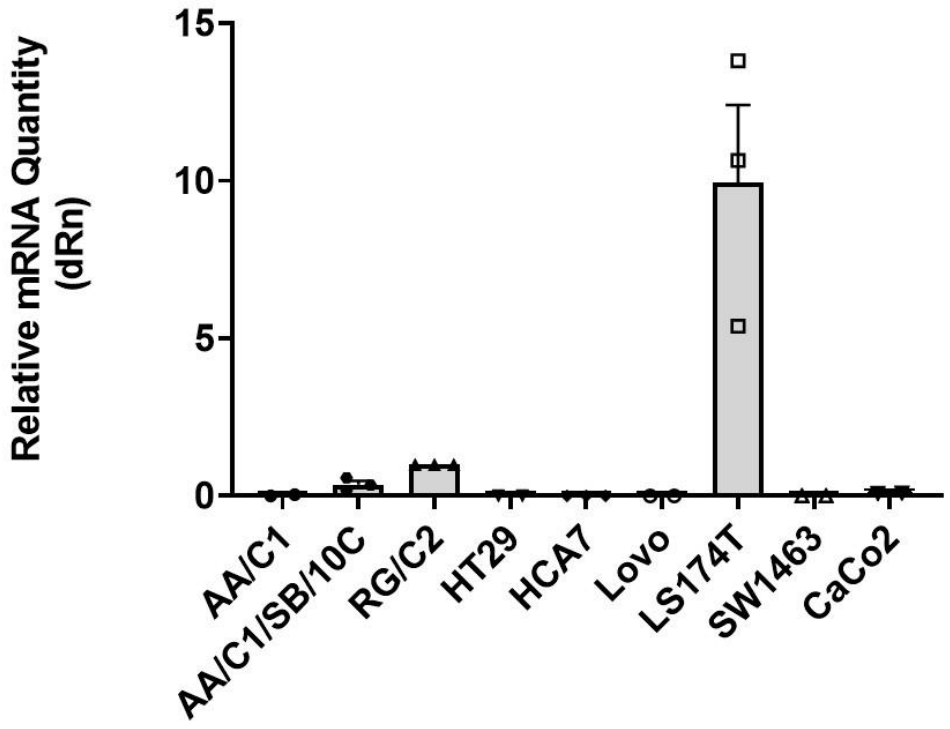

Figure 5-3: NHE3 mRNA expression in human colonic adenoma and carcinoma cell lines.

Q-RT-PCR using an NHE3 primer was performed on 100 ng cDNA synthesised from the cell lines AA/C1, AA/C1/SB/10C, RG/C2, HT-29, HCA7, LoVo, LS174T, SW1463, and Caco-2. Results are presented as fold change in mRNA relative to negative control wells (no reverse transcriptase) and normalised to RG/C2. Data are means ± S.E.M. (n = 3).

No NHE3 mRNA was detected in the AA/C1, HT-29, HCA7, LoVo, SW1463, and Caco-2 cell lines, with negligible NHE3 mRNA detection in the AA/C1/SB/10C cell line (normalised to the RG/C1 cell line). Consistent with Western blotting data (Figure 5-1), the LS174T cell line demonstrated comparatively high levels of NHE3 mRNA. Considered together, these data provide little evidence of either NHE3 mRNA or protein in the HCA7 cell line. Therefore, any future experiments to assess the role of NHE3 in intestinal ion transport using the HCA7 cell line would require heterologous expression of NHE3 in HCA7 cells.

5.3.3. Characterisation of GCC, EP1 and EP4 mRNA expression in HCA7 cells.

Q-RT-PCR was performed to determine the presence of GCC, EP1 and EP4 mRNA in the AA/C1/SB/10C, RG/C2, HCA7, and LS174T cell lines. For consistency, all mRNA expression was normalised to that calculated for the RG/C2 cell line. Figure 5-4A shows that low levels of GCC mRNA were detected in the AA/C1/SB/10C and LS174T cell lines (normalised to the RG/C1 cell line), but none in the HCA7 cell line, suggesting that the HCA7 cell line is unlikely to express the linaclotide binding target GCC. Interestingly, the HCA7 cell line expressed high levels of EP1 mRNA, while AA/C1/SB/10C and LS174T cell lines expressed some (normalised to the RG/C1 cell line) (Figure 5-4B). By contrast, the AA/C1/SB/10C and HCA7 cell lines expressed negligible EP4 mRNA and the LS174T cell line only a little (Figure 5-4C). These data suggest that the HCA7 cell line expresses the EP1, but not the EP4, binding target for the drug lubiprostone.

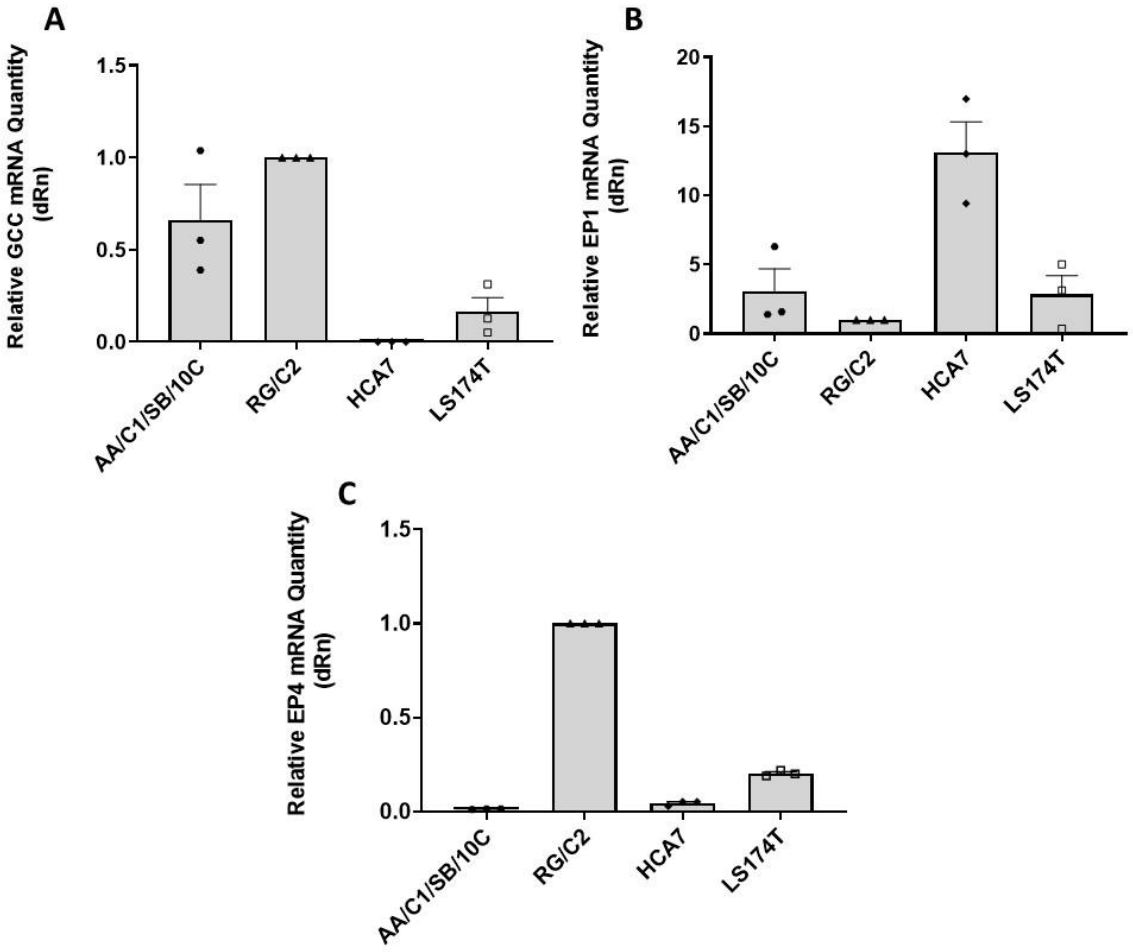

Figure 5-4; GCC, EP1, and EP4 mRNA expression in human colonic adenoma and carcinoma cell lines.

*Q-RT-PCR using primers for (**A**) GCC **(B)** EP1, and **(C)** EP4 was performed on 100 ng cDNA synthesised from cell lines AA/C1/SB/10C, RG/C2, HCA7, and LS174T. Results are presented as fold change in mRNA relative to negative control wells (no reverse transcriptase) and normalised to RG/C2. Data are means ± S.E.M. (n = 3).*

5.3.4. Functional expression of GCC, EP1 and EP4 in HCA7 epithelia.

The exchange of Na^+ and H^+ by NHE3 is an example of electroneutral ion exchange whereby no net charge difference occurs across the apical membrane of the intestinal epithelia (Gawenis *et al.*, 2004). For this reason, the Ussing chamber technique cannot be used to investigate the effects of direct inhibition of NHE3 by tenapanor on basal, or cAMP-generated I_{sc} by HCA7 epithelia. The mechanism of action of linaclotide and lubiprostone on NHE3 involves increases in the intracellular concentrations of cAMP and cGMP, respectively, and subsequent cAMP/cGMP-dependent phosphorylation and inhibition of NHE3. The effects of increased intracellular concentrations of cAMP or cGMP are not specific to NHE3, also promoting CFTR-mediated Cl^- secretion. Therefore, treatment of HCA7 epithelia with either linaclotide or lubiprostone should generate CFTR-mediated I_{sc} in Ussing chamber experiments, assuming the expression of appropriate drug binding targets within the apical membrane of HCA7 cells.

As shown in Figure 5-5A and B, stimulation of HCA7 epithelia with concentrations of linaclotide ranging from 10 nM to 10 µM did not generate I_{sc}. These data support that in Figure 5-4A and provide further evidence that the HCA7 cell line does not express GCC. After stimulation of HCA7 epithelia with the final concentration of linaclotide (10 µM), FSK (10 µM) addition to the solution bathing the apical membrane increased I_{sc}. This I_{sc} was subsequently inhibited by I-172 (10 µM).

Similarly, when HCA7 epithelia were stimulated with concentrations of lubiprostone ranging from 10 nM to 10 µM cAMP mediated I_{sc} was not generated (Figure 5-6A and B). This result contradicts the findings in Figures 5-4B and C as whilst the lubiprostone receptor EP4 mRNA was not detected in the HCA7 cell line, mRNA for EP1 was detected in higher quantities than for all other cell lines tested. The addition of FSK (10 µM) to the solution bathing the apical membrane of HCA7 epithelia generated CFTR-mediated I_{sc} that was inhibited by I-172 (10 µM).

DMSO vehicle control experiments were performed using the concentrations of DMSO (0.1% to 0.73%) tested during linaclotide and lubiprostone experiments. DMSO addition to the solution bathing the apical membrane of HCA7 epithelia did not generate I_{sc} at any concentration tested (data not shown).

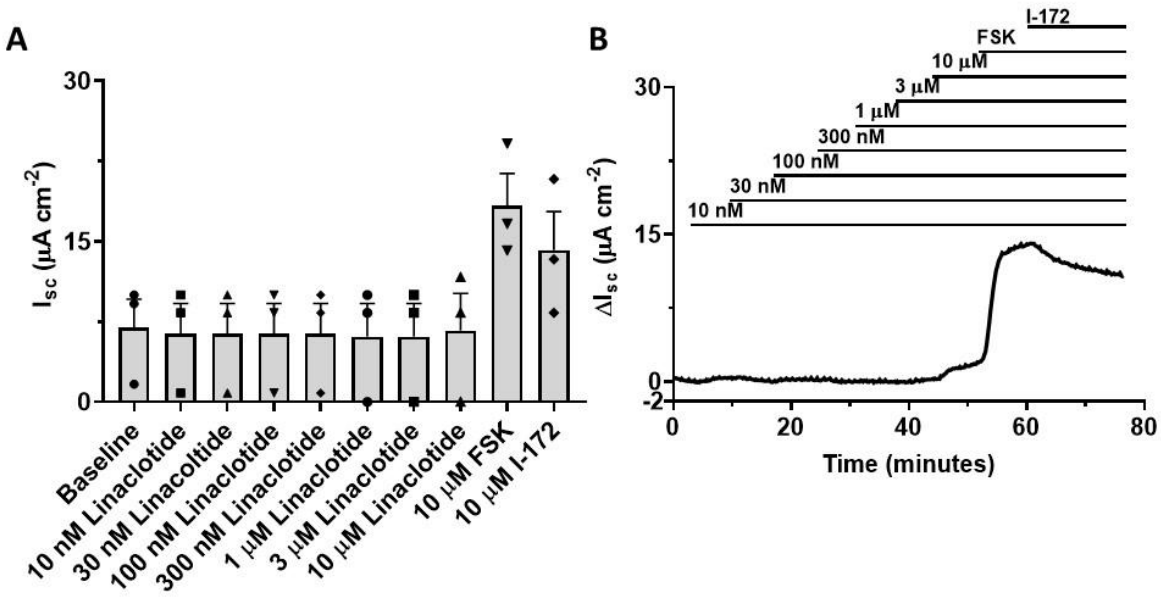

Figure 5-5: Representative Ussing chamber traces characterising the I_{sc} response of HCA7 epithelia to linaclotide treatment.

***A**) Summary I_{sc} data of HCA7 epithelia in response to the GCC ligand linaclotide. Linaclotide was added to the solution bathing the apical membrane in an additive manner to give final concentrations of 10 nM, 30 nM, 100 nM, 300 nM, 1 µM, 3 µM, and 10 µM. Subsequently, the cAMP agonist forskolin (FSK; 10 µM) and the CFTR inhibitor $CFTR_{inh}$-172 (I-172; 10 µM) were added to the apical membrane bathing solution. Data are means ± S.E.M (n = 3). **(B)** Representative Ussing chamber trace for conditions outlined in **(A)**. The continuous lines indicate the presence of different compounds in the apical membrane bathing solution. Data are displayed as transepithelial current (I_{sc}) or change in transepithelial current (ΔI_{sc}) from baseline.*

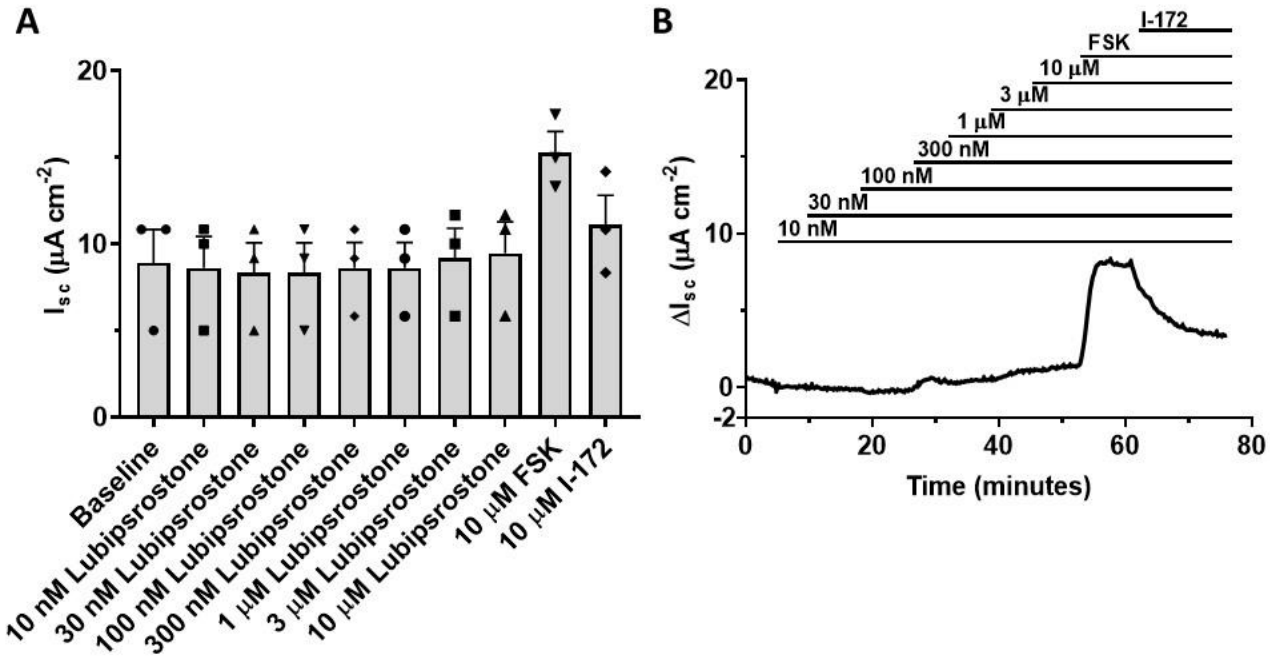

Figure 5-6: Representative Ussing chamber traces characterising the I_{sc} response of HCA7 epithelia to lubiprostone treatment.

(A) *Summary I_{sc} data of HCA7 epithelia in response to the EP1 and EP4 ligand lubiprostone. Lubiprostone was added to the solution bathing the apical membrane in an additive manner to give final concentrations of 10 nM, 30 nM, 100 nM, 300 nM, 1 µM, 3 µM, and 10 µM. Subsequently, the cAMP agonist forskolin (FSK; 10 µM) and the CFTR inhibitor $CFTR_{inh}$-172 (I-172; 10 µM) were added to the solution bathing the apical membrane. Data are means ± S.E. (n = 3).* ***(B)*** *Representative Ussing chamber trace for conditions outlined for* ***(A)****. The continuous lines indicate the presence of different compounds in the apical membrane bathing solution. Data are displayed as transepithelial current (I_{sc}) or change in transepithelial current (ΔI_{sc}) from baseline.*

5.4. Future Work

The work presented in this chapter was in its infancy when it was stopped by the COVID-19 pandemic. Whilst initial work to characterise NHE3 protein expression in the HCA7 cell line strongly suggested that the cell line expressed little or no NHE3 protein, further work to confirm this would have taken place. Repetition of Western blotting of the cell lines included in Figure 5-1, with the exception of the LS174T cell line, would have allowed longer exposure without saturation of the digital signal detected by the Amersham Imager. Similarly, siRNA-mediated depletion of NHE3 protein in the HCA7 cell line, as performed in the LS174T cell line, would have further investigated the expression of NHE3 in HCA7 cells.

The data gathered to date suggest that the HCA7 cell line does not express NHE3 and so it was intended to use lentiviral transduction to express NHE3 in HCA7 cells. The lentiviral vector XLG3-NHE3 (modified XLG3eGFP with NHE3 cDNA) was produced by GenScript and used to transfect HEK cells to generate recombinant lentivirus. Western blotting using the Proteintech anti-NHE3 antibody validated in Section 5.3.1, alongside siRNA-mediated depletion of NHE3 protein would have been performed to confirm successful heterologous expression of NHE3 in the HCA7 cell line.

Assuming work to stably express NHE3 in the HCA7 cell line was successful (referred to as HCA7-NHE3 going forward), HCA7-NHE3 epithelia and spheroids would be used in Ussing chamber experiments and FIS assays. Q-RT-PCR data and Ussing chamber experiments strongly suggested that the HCA7 cell line would not be suitable for studying cAMP- or cGMP-mediated NHE3 inhibition by lubiprostone or linaclotide. However, future experiments utilising HCA7-NHE3 cells and the direct NHE3 inhibitor tenapanor would have been performed.

Firstly it would have been of interest to determine whether the heterologous expression of NHE3 affects the endogenous expression of CFTR in the HCA7 cell line, as it has previously been reported that expression of these two proteins is closely linked (Clarke and Harline, 1996; Gawenis *et al.*, 2003). Interestingly, intestinal NHE3 has been reported to regulate R_t with inhibition of NHE3 activity linked to an increase in R_t (Turner *et al.*, 2000). Measurement of R_t across HCA7-NHE3 and HCA7 epithelia before and after tenapanor treatment would further investigate this possibility. Ussing chamber studies would be performed to compare FSK-stimulated I_{sc} by HCA7 and HCA7-NHE3

epithelia. This would demonstrate whether heterologous expression of NHE3 affects endogenous cAMP-mediated I_{sc}. Then, NHE3 activity would be inhibited using tenapanor and any change in cAMP-mediated I_{sc} assessed. Combined, these studies would reveal how heterologous expression of NHE3 affects cAMP-mediated Cl^- secretion, and by extension CFTR function. Further experiments using HCA7-NHE3 epithelia treated with I-172 would investigate alternative routes to stimulate transepithelial ion transport. CaCC activation by ionomycin or UTP in the absence and presence of NHE3 inhibition by tenapanor would reveal whether tenapanor used in conjunction with stimulation of an alternative route of Cl^- secretion could compensate for loss of CFTR activity.

Complementary studies would be performed in spheroids derived from HCA7 and HCA7-NHE3 cells. Extent of FIS would be assessed in both sets of spheroids with further characterisation of FIS using tenapanor and pharmacological modulators of intestinal CFTR-mediated ion and fluid secretion. Together Ussing chamber experiments and FIS assays would provide a detailed picture of the role NHE3 plays in intestinal ion transport.

5.5. Discussion

This chapter describes the initial characterisation of NHE3 expression in the HCA7 cell line, with the intention of using this cell line to investigate the role of NHE3 in intestinal ion transport. The expression of binding targets for drugs known to inhibit NHE3 activity and approved for use in humans were also investigated. These were guanylyl cyclase C (GCC), the binding target of linaclotide, and the prostaglandin receptors EP1 and EP4, binding targets for the drug lubiprostone.

Initial screening of a panel of 9 adenoma and carcinoma cell lines using the Proteintech anti-NHE3 antibody served the dual purpose of indicating which cell lines might express NHE3 protein and providing initial antibody validation (Figure 5-1). Whilst the calculated molecular weight of NHE3 is 93 kDa, antibody binding to NHE3 protein during immunoblotting was anticipated to occur between 80 - 100 kDa. Discrepancy between observed and calculated molecular weights is not uncommon during protein separation by SDS-PAGE with factors such as net charge; glycosylation, phosphorylation and ubiquitination status; incomplete denaturation of protein complexes; different isoforms of a protein and the occurrence of protein precursors all contributing towards this difference. Of the cell lines screened, the anti-NHE3 antibody detected bands corresponding to ~85 kDa in the HCA7, LoVo, LS174T, and Caco-2 cell lines. However, the intensity of antibody staining in this region was similar to non-specific antibody binding in other regions of the blot. As such, visible protein bands in this region were not conclusive evidence of NHE3 expression in the cell lines studied. The Caco-2 cell line has previously been reported to express functional NHE3 protein (Turner *et al.*, 2000; Hecht *et al.*, 2004). However, the Caco-2 cell line used throughout this thesis demonstrated characteristics atypical of those reported previously (no detectable CFTR mRNA nor protein, and failure to generate R_t when cultured on Transwell inserts). For this reason, the Caco-2 cells used in Figure 5-1 were not assumed to be a positive control for NHE3 expression.

Strong anti-NHE3 antibody binding at ~85 kDa, clearly distinguishable from non-specific antibody binding in all other regions of the blot, was observed in the LS174T cell line. As a result, this cell line was used to determine the specificity of the Proteintech anti-NHE3 antibody. First described in 1976, the LS174T cell line originates from a moderately differentiated colonic adenocarcinoma (Tom *et al.*, 1976; Klinkspoor *et al.*, 1999; Bu *et al.*, 2011). siRNA-mediated depletion of NHE3 protein in LS174T cells followed by SDS-

PAGE separation and Western blotting of lysates taken 24-, 48-, and 72- hours post transfection revealed time dependent depletion of antibody binding at ~85 kDa (Figure 5-2). These results authenticate use of the Proteintech anti-NHE3 antibody to detect human NHE3 protein. They also validate an siRNA for use in siRNA-mediated depletion of NHE3. This would be of use in future experiments to confirm heterologous expression of NHE3 in the HCA7 cell line.

In agreement with Figure 5-1, Q-RT-PCR data revealed that LS174T cells expressed considerably higher levels of NHE3 mRNA than other screened cell lines (Figure 5-3). However, contrary to previous reports (Sambuy *et al.*, 2005), the Caco-2 cell line demonstrated no NHE3 mRNA. This was also the case for the AA/C1, AA/C1/SB/10C, HT-29, HCA7, LoVo, and SW1463 cell lines where little or no NHE3 mRNA was detected. Combined, the data in Figures 5-1 and 5-3 strongly suggest that the HCA7 cell line does not express NHE3 protein or mRNA. They also argue that the ~85 kDa protein band observed in Figure 5-1 in the HCA7, LoVo, LS174T, and Caco-2 cell lines represented non-specific antibody binding.

It could be argued that the LS174T cell line would make a more suitable model for studying the role of NHE3 in intestinal ion transport. This cell line demonstrated the highest expression of NHE3 mRNA and protein and also expressed both CFTR mRNA and protein, albeit to a lesser degree than the HCA7 cell line (Figures 4-2 and 4-3). However, the LS174T cell line failed to generate a R_t when seeded onto Transwell inserts and so was unsuitable for Ussing chamber experiments. Therefore, the HCA7 cell line was pursued as the cellular model of choice for investigating the role of NHE3 in intestinal ion transport by heterologous expression of NHE3 in the cell line using lentiviral-mediated transduction of NHE3 cDNA.

Both Q-RT-PCR and Ussing chamber studies were used to confirm the expression of GCC, EP1 and EP4 in HCA7 cells. Figure 5-4A and Figure 5-5 demonstrate that no GCC mRNA was detected in HCA7 cells and stimulation of HCA7 epithelia with linaclotide did not generate cGMP-mediated I_{sc}. Considered together, these data strongly suggest that the HCA7 cell line does not express the linaclotide binding target GCC and would therefore not be of use in linaclotide-mediated NHE3 inhibition studies. Whilst only negligible amounts of EP4 mRNA was detected in the HCA7 cell line, the quantity of EP1 mRNA detected was considerably higher (Figure 5-4B and C). This result was somewhat surprising given previous reports suggesting EP1 is not expressed in the intestine (Bassil *et al.*, 2008; Bijvelds *et al.*, 2009). Despite the potential for

prostaglandin receptor binding and therefore cAMP-mediated I_{sc} generation by lubiprostone, no increase in I_{sc} was observed in HCA7 epithelia treated with lubiprostone at concentrations ranging from 10 nM to 10 μM (Figure 5-6). By contrast, lubiprostone stimulated a dose-dependent increase in CFTR-mediated I_{sc} by T84 epithelia at concentrations of lubiprostone ranging from 0.05 μmol/L to 1 μmol/L (Bijvelds *et al.*, 2009).

The findings discussed above highlight several limitations of the HCA7 cell line both for the study of NHE3 in intestinal ion transport, and as a potential mutation-independent therapeutic target in the CF intestine. However, the heterologous expression of NHE3 in this cell line would go some way to overcoming these limitations.

5.6. Concluding Remarks

The work performed to date, and presented in this chapter, identify several limitations concerning the use of the HCA7 cell line as a model for studying the role of NHE3 in intestinal ion transport. These limitations become particularly relevant when considering the use of the HCA7 cell line to investigate the effect of NHE3 inhibition by linaclotide or lubiprostone on net fluid secretion across the intestinal epithelium. Not only were the HCA7 cell line shown not to express endogenous NHE3, both Q-RT-PCR and Ussing chamber studies suggest that the HCA7 cell line does not express functional receptors for linaclotide nor lubiprostone (GCC, and EP1 and EP4, respectively). That said, HCA7 cells heterologously expressing NHE3 would not only allow for the contribution of NHE3 to intestinal ion transport to be fully investigated, they would also provide a model whereby the inhibition of NHE3 by tenapanor could be assessed as a potential mutation-independent therapeutic agent in the CF intestine.

Chapter 6. General Discussion

6.1. Key Findings

In this thesis, two epithelial cell lines have been characterised, and their suitability as cellular models for both 2D and 3D studies of intestinal ion transport assessed. Firstly, the human colonic carcinoma cell line LIM1863, known to express CFTR and grow as 3D spheroids (Currid, Ortega and Valverde, 2004), and secondly, the human colonic adenocarcinoma cell line HCA7, shown to demonstrate vectorial fluid transport (Cuthbert, Kirkland and MacVinish, 1985; Kirkland, 1985b; Henderson *et al.*, 1992). This thesis also sought to repurpose and optimise the FIS assay developed for use with primary intestinal organoids (Dekkers *et al.*, 2013), with the aim of establishing a cost effective and high-throughput screening assay to identify novel therapeutic compounds for the treatment of gastrointestinal (GI) disease in CF.

As a summary it was found that **A:** Both LIM1863 and HCA7 cell lines form 3D spheroids that demonstrate CFTR-mediated swelling stimulated by forskolin (FSK). **B:** FIS of both LIM1863 and HCA7 spheroids was reduced by the CFTR inhibitor $CFTR_{inh}$-172, and FIS was also reduced in LIM1863 spheroids by the NKCC1 inhibitor, bumetanide. **C:** Unlike the HCA7 cell line, the LIM1863 cell line did not generate a transepithelial resistance (R_t) when grown on permeable membrane supports, and therefore was unsuitable for Ussing chamber studies. **D:** In Ussing chamber studies, HCA7 epithelia were shown to express CFTR and CaCC in the apical membrane, and NKCC1 and Na^+/K^+ ATPase in the basolateral membrane. **E:** Western blotting and Q-RT-PCR confirmed that the HCA7 cell line does not express endogenous NHE3. **F:** Similarly, Q-RT-PCR and Ussing chamber studies demonstrated that the HCA7 cell line does not express the receptors GCC, EP1, and EP4.

6.2. Intestinal cell lines as models for studying intestinal ion transport

The LIM1863 cell line showed promise as a potential model for both 2D, and 3D studies of intestinal ion transport. As discussed in Sections 3.3.1 and 3.3.4, it was possible to reproduce the early work of Currid *et al.* (2004) and achieve FIS with LIM1863 spheroids, a secretory response that was decreased by bumetanide. Development of this work confirmed that FIS was CFTR-dependent, as incubation of spheroids with I-172 before FSK-stimulation significantly decreased swelling. Attempts to stain LIM1863 spheroids with calcein green for FIS quantification as used by Dekkers *et al.* (2013, 2016, 2016)

were unsuccessful. However, methods to quantify FIS using automated analysis of phase contrast images were developed and successfully implemented, saving the time associated with an additional incubation step, and the cost of purchasing an additional reagent, both important considerations when developing a screening assay.

Unlike colonic adenocarcinoma cells lines such as Caco-2, HT-29, and T84 cells, the LIM1863 cell line did not generate a R_t when grown on permeable membrane supports (McCool *et al.*, 1990; Sambuy *et al.*, 2005; Simon-Assmann *et al.*, 2007). To date, there is no literature on the use of the LIM1863 cell line in Ussing chamber studies, or indeed growth as a 2D epithelium. The growth of populations of LIM1863 cells as adherent monolayers linked by adherens junctions was reported by Vincan *et al*. (2007). However, the population of LIM1863 cells used were found to be undergoing spontaneous epithelial-mesenchymal transition, and therefore loosing qualities associated with differentiated epithelia (Vincan *et al.*, 2007).

The HCA7 cell line was identified as one of 7 adenocarcinoma cell lines that expressed CFTR. However, it was the only cell line to form both 3D spheroids and generate a R_t when grown on Transwell inserts. Although the HCA7 cell line was suitable for use in FIS assays and Ussing chamber studies, inhibition of CFTR-mediated Cl^- transport by I-172 was often not statistically significant, raising the question, to what extent is FSK-induced Cl^- secretion CFTR-dependent in this cell line?

Considered together, this research challenges the aim to identify a single cell line that can perform both 2D and 3D studies of epithelial ion transport and suggests that it is perhaps more appropriate to utilise a combination of cell lines and assay methods to gain deeper understanding of intestinal ion transport. One exception is the Caco-2 cell line, known to retain features of cellular differentiation, express CFTR, be suitable for Ussing chamber studies, and more recently successfully cultured as 3D spheroids (Schaar *et al.*, 2004; Sambuy *et al.*, 2005; Simon-Assmann *et al.*, 2007; Rainaldi, Boe and Gessani, 2016; Gheytanchi *et al.*, 2021). Whether Caco-2 spheroids are capable of FIS remains to be seen. Although the Caco-2 cells used in this thesis did not exhibit previously reported characteristics, future work to optimise the differentiation of Caco-2 cells would reveal whether this cell line is both a 2D and 3D model of intestinal ion transport.

6.3. Applications of the FIS assay as a tool to identify novel treatments for GI diseases.

Advances in primary intestinal organoid technology has had much positive impact for individuals with CF, particularly those with rare mutations against which current licenced drugs are ineffective, and for whom large scale clinical trials are unfeasible (Boj *et al.*, 2017). The FIS assay developed by Dekkers *et al.* (2013) provides a method to quantify and compare CFTR function, and as such is a pre-trial screening tool to identify new therapeutic strategies as well as establish which therapies are effective for rare mutations (Dekkers *et al.*, 2013; Dekkers, Berkers, *et al.*, 2016; de Poel, Lefferts and Beekman, 2020). The FIS assay in primary intestinal organoids lends itself to high-throughput screening as experiments can be performed in bulk in multi-well tissue culture plates. Steps towards its use with intestinal organoids, derived from individuals with rare *CFTR* mutations to assess the efficacy of experimental CF drugs in restoring CFTR function are currently underway as part of the European HIT-CF project (HIT-CF-Europe press release, February 2020).

The application of the FIS assay could reach beyond CF research and be utilised to screen for therapeutic compounds to alleviate other GI diseases. Secretory diarrhoea (SD) is an entirely preventable and treatable disease, largely caused by contaminated food and water, or poor hygiene practices, and yet is the second leading cause of death in the under 5's, accounting for 525,000 childhood deaths per year (WHO diarrhoeal disease fact-sheet; available at https://www.who.int/en/news-room/fact-sheets/detail/diarrhoeal-disease). Many bacterial enterotoxins responsible for causing SD make use of the cAMP and cGMP signalling pathways to cause acute and excessive NaCl and fluid secretion (de Jonge *et al.*, 2020). Pathogenic strains of *Vibrio cholerae* release AB_5 enterotoxin, termed cholera toxin (CT). Localisation of the A and B subunits of CT to their respective host cell targets (cell surface gangliosides for B subunits, and the endoplasmic reticulum for A subunits), ultimately results in ongoing increased cAMP and PKA concentrations, and unchecked CFTR activity and NHE3 inhibition (de Jonge *et al.*, 2020). For a comprehensive review of the pathophysiology of enterotoxin-mediated SD, the Reader is directed to de Jonge *et al.* (2020). Potential strategies for the small molecule treatment of SD include molecules that inhibit CFTR, target accessory channels and transporters (e.g. NKCC1, NHE3, KCNQ1 and KCNN4), and inhibit the cAMP and cGMP signalling pathways, (McGahan, Yorio and Bentley, 1977; Greger, 2000; Wulff and Castle, 2010; Singh *et al.*, 2014; Bijvelds *et al.*, 2015, 2018; Zomer-Van

Ommen *et al.*, 2016; de Jonge *et al.*, 2020). Utilising the FIS assay for high-throughput screening could facilitate the identification of effective therapeutic molecules for SD, saving many lives in the future.

The inflammatory autoimmune condition coeliac disease (CD) illustrates a second example of a GI disease where FIS assay screening of small molecules could be applied to identify those with therapeutic benefit. CD is a relatively common intestinal disease whereby the proteolysis resistant peptide gliadin, found in gluten, instigates a disproportional immune response in the intestine, made worse by an already damaged and stressed intestinal epithelium (Vachel and Muallem, 2019; Escudero-Hernández, 2021). Increased incidence of CD in individuals with CF is well documented (Pop *et al.*, 2008; Hjelm and Shaikhkhalil, 2020). Recent work to understand the role of CFTR in CD revealed that gliadin reduces CFTR function in the small intestine of gluten intolerant mouse models and demonstrated that the specific α gliadin peptide (P31-43) blocks CFTR function by direct interaction with NBD1 (Villella *et al.*, 2019). Furthermore, CFTR inhibition was prevented by VX-770, suggesting competition for CFTR binding between VX-770, and P31-43 (Villella *et al.*, 2019), and highlighting a role for small molecule modulators of CFTR in the treatment of CD. FIS assays using primary organoids derived from individuals with CD could prove to be of great use in the screening of such compounds.

6.4. Inhibition of Na^+ absorption as a mutation-independent approach to CF therapy.

The potential of NHE3 as a mutation-independent therapeutic target in the treatment of CF intestinal disease was not fully explored in this thesis as a result of COVID-19 restrictions. However, given the importance of regulated Na^+ absorption for intestinal ion and fluid homeostasis, inhibition of Na^+ absorption holds great promise as a mutation-independent therapy for individuals with CF, especially those with rare *CFTR* mutations.

Like NHE3 in the intestine, ENaC plays a significant role in epithelial fluid homeostasis in the lungs, colon, kidney, and sweat duct, contributing to airway surface liquid (ASL) dehydration and reduced mucociliary clearance (MCC) in CF lung disease (Mall, 2020). ENaC is therefore an exciting target for mutation-independent therapy (Boucher *et al.*, 1988; Jaques, Shakeel and Hoyle, 2020). Several studies have investigated the efficacy of the ENaC blocker amiloride, taken in an aerosolised form, to restore ASL and MCC in

CF. However, the benefits of inhaled amiloride were limited and variable, perhaps due to the compound's short half-life and lack of potency (Knowles *et al.*, 1990; Pons *et al.*, 2000; Mall, 2020). A more potent derivative of amiloride, GS-9411, reached Phase I clinical trials as an inhaled treatment (Mall, 2020). However, further trials were not conducted as the compound caused inhibition of ENaC in the kidneys leading to hyperkalaemia (O'Riordan *et al.*, 2014).

Despite the initial lack of success of ENaC inhibitors as a therapy for CF, work to identity a novel method of ENaC inhibition continues. New compounds designed to target ENaC activity have varied mechanisms of action, some are designed to inhibit the channel pore, some inhibit the proteases required to activate ENaC, while others prevent expression of ENaC itself using siRNA-mediated protein deletion (Hirsh *et al.*, 2004; Reihill *et al.*, 2016; Mall, 2020, clinicaltrials.gov NCT04375514). Currently, the only ENaC inhibiting compound in Phase II clinical trials is the direct ENaC blocker BI 1265162 (Goss *et al.*, 2020), having shown promise in preclinical work, a higher potency than amiloride, yet no undesirable effects on the kidney, and proving safe in Phase I clinical trials (Gordat *et al.*, 2019; Nickolaus *et al.*, 2020).

The emerging approaches to inhibiting Na^+ absorption discussed above and throughout this thesis highlight NHE3 and ENaC as promising mutation independent targets for CF therapy. These could be used independently in individuals for whom current licenced small molecule modulators of CFTR are ineffective or unavailable, and synergistically in those who already benefit from CFTR modulator therapy.

6.5. Limitations of this Work

Despite the potential of the work presented in this thesis, it is not without limitations.

Investigation of protein expression was performed using Western blotting of whole cell lysates. Whilst this approach can provide a sound indication of the presence or absence of a protein, it does not inform subcellular localisation including the proportion of said protein associated with the plasma membrane. This said, in the case of CFTR, Ussing chamber studies were used to complement analyses of protein expression. This approach allowed the detection of functional and presumably membrane associated CFTR protein. In subsequent chapters, similar to CFTR, Western blotting of whole cell lysates was used to study NHE3 protein expression. Whilst the Ussing chamber technique did not permit the detection of electroneutral NHE3-mediated ion exchange,

proposed future work to elucidate NHE3 activity within the plasma membrane would have adopted alternate techniques as discussed below. If further investigation of membrane associated CFTR and NHE3 protein were desired techniques such as the immunofluorescent labelling of proteins, and the isolation of surface proteins using biotin tagging and subsequent magnetic streptavidin bead pull-down could be utilised.

As highlighted previously the Ussing chamber technique is unsuitable for the study of electrogenic NHE3-mediated Na^+ and H^+ exchange. Instead, pH-sensitive fluorochromes could be used to determine NHE3 activity by monitoring intracellular pH (pH_i). The steady-state pH_i of intestinal epithelial cells is maintained by the balance of acid loaders (CFTR and SLC26A3) which facilitate the movement of HCO_3^- into the intestinal lumen, and acid extruders such as members of the NHE family of proteins (NHE2, NHE3, and NHE8) which facilitate the movement of H^+ into the intestinal lumen (Amiri, Seidler and Nikolovska, 2021). Inhibition or promotion of either acid loader or acid extruder function would cause a deviation in steady-state pH_i, detectable by intracellular pH-sensitive fluorochromes. Evidence to support this principle comes from Simpson *et al* (2005) who demonstrated a decrease in the pH_i of duodenal epithelial cells from *CFTR*$^{-/-}$ mice compared to duodenal epithelial cells from mice expressing wild-type CFTR. For the study of extracellular pH changes, such as those occurring across 2D epithelial monolayers upon manipulation of ion transporter and channel activity, pH-sensitive fluorochromes could also be of use. The pH indicator SNARF-1 has been used successfully to assess pH changes of airway surface liquid associated with impaired CFTR function and associated pH buffering (Shah *et al.*, 2016; Rehman *et al.*, 2020), and as such could be used to study changes of extracellular pH by 2D intestinal epithelium.

Whilst the compounds used throughout this thesis have been widely used in the study of epithelial ion transport, it is of importance to highlight potential limitations in their specificity as well as potentially conflicting downstream signalling events. For example, the use of genistein as a CFTR potentiator is well documented (Wang *et al.*, 2002; Ai *et al.*, 2004; French *et al.*, 2017). This effect, however, is concentration-dependent with concentrations of genistein in the low µM range increasing the open probability of CFTR, but higher concentrations of genistein (>35 µM) inhibiting CFTR activity (Wang *et al.*, 2002). The mechanisms by which genistein influences CFTR channel activity are not yet fully understood. It is proposed that potentiation occurs via both the direct interaction of genistein with NBD2 preventing channel closure, alongside inhibition by genistein of serine/threonine protein phosphatases which dephosphorylate CFTR (Hwang *et al.*,

1997; Randak *et al.*, 1999). A suggested mechanism for the inhibitory effect of genistein on CFTR channel activity is obstruction of the ATP binding site of NBD1 (or interaction with a near site) to prevent channel opening (Lansdell *et al.*, 2000). The cAMP agonist forskolin promotes the phosphorylation of CFTR via the activation of adenylyl cyclase, and subsequent intracellular increase of cAMP and activation of PKA. However, the effect of forskolin on cells is not limited to CFTR activation as the second messenger cAMP is known to mediate many intracellular processes, including the phosphorylation and activation or inhibition of several epithelial ion channels and transporters.

The use of intestinal cells lines derived from adenocarcinomas for the study of normal intestinal physiology has limitations to be considered when determining suitability for experiments. The HCA7 cell is reported to contain mutations in genes associated with but not limited to chromatin remodelling, histone methylation, the p53 pathway, the mitogen-activated protein kinase (MAPK) pathway, and the mismatch repair (MMR) pathway (Mouradov *et al.*, 2014). Arguably the most relevant HCA7 cell line mutations to this thesis are those associated with the WNT-signalling pathway, such as mutations in the tumour suppressor adenomatous polyposis coli (APC) which has a significant role in determining cell polarity and integrity of epithelial tightness (Lesko *et al.*, 2015). Despite the emergence of primary intestinal organoids, intestinal cell lines derived from cancerous tissue provide an invaluable model of the intestinal epithelium and possess advantageous qualities in the context of this work seeking to identify a cell line for initial drug screening.

6.6. Final Conclusion

Epithelial cell lines demonstrate potential as 3D models for the study of intestinal ion transport. While several cell lines mentioned in this study have previously been employed for Ussing chamber studies, their use in 3D FIS assays is under explored. With further optimisation both the LIM1863 and HCA7 cell lines characterised in this thesis, demonstrate potential as both 3D models of intestinal ion transport and as screening tools to identify new therapeutics for not only CF, but also other GI diseases.

Chapter 7. References

Accurso, F. J. and Sontag, M. K. (2008) ‘Gene modifiers in cystic fibrosis’, *Journal of Clinical Investigation*, 118(3), pp. 839–841.

Ahn, W. *et al*. (2001) ‘Regulatory Interaction between the Cystic Fibrosis Transmembrane Conductance Regulator and HCO_3^- Salvage Mechanisms in Model Systems and the Mouse Pancreatic Duct’, *American Society for Biochemistry and Molecular Biology*., 276(20), pp. 17236–17243.

Ahsan, M. K. *et al*. (2017) ‘Linaclotide activates guanylate cyclase-C/cGMP/protein kinase-II-dependent trafficking of CFTR in the intestine’, *Physiological Reports*, 5(11),

Ai, T. *et al*. (2004) ‘Capsaicin potentiates wild-type and mutant cystic fibrosis transmembrane conductance regulator chloride-channel currents’, *Molecular Pharmacology*, 65(6), pp. 1415–1426.

Alton, E. W. F. W. *et al*. (2015) ‘Repeated nebulisation of non-viral CFTR gene therapy in patients with cystic fibrosis: a randomised, double-blind, placebo-controlled, phase 2b trial’, *The Lancet Respiratory Medicine*, 3(9), pp. 684–691.

Amaral, M. D. (2004) ‘CFTR and chaperones: Processing and degradation’, *Journal of Molecular Neuroscience,* 23(1–2), pp. 41–48.

Ameen, N. A. *et al*. (1995) ‘A unique subset of rat and human intestinal villus cells express the cystic fibrosis transmembrane conductance regulator’, *Gastroenterology*, 108(4), pp. 1016–1023.

Ameen, N. A. and Salas, P. J. I. (2000) ‘Microvillus inclusion disease: A genetic defect affecting apical membrane protein traffic in intestinal epithelium’, *Traffic*, 1(1), pp. 76–83.

Amiri, M., Seidler, U. E. and Nikolovska, K. (2021) ‘The Role of pHi in Intestinal Epithelial Proliferation–Transport Mechanisms, Regulatory Pathways, and Consequences’, *Frontiers in Cell and Developmental Biology*, 9 (1), pp. 1–7.

Anabazhagan, A. N. *et al*. (2017) ‘Methods to study epithelial transport protein function and expression in native intestine and caco-2 cells grown in 3D’, *Journal of Visualized Experiments*, 2017(121), pp. 1–8.

Anderson, M. P. *et al*. (1992) ‘Chloride channels in the apical membrane of normal and cystic fibrosis airway and intestinal epithelia’, American Journal of Physiology - *Lung Cellular and Molecular Physiology,* 263(1 7-1).

Anthony, H. *et al*. (1999) ‘Pancreatic enzyme replacement therapy in cystic fibrosis: Australian guidelines’, *Journal of Paediatrics and Child Health*, 35(2), pp. 125–129.

St. Aubin, C. and Linsdell, P. (2006) ‘Positive charges at the intracellular mouth of the pore regulate anion conduction in the CFTR chloride channel’, *Journal of General Physiology*, 128(5), pp. 535–545.

Aurora, M. and Spence, J. R. (2016) ‘hPSC-derived lung and intestinal organoids as models of human fetal tissue’, *Developmental Biology*, 420(2), pp. 230–238.

Bachmann, A., Quast, U. and Russ, U. (2001) 'Chromanol 293b, a blocker of the slow delayed rectifier K^+ current (IKs), inhibits the CFTR Cl^- current', *Naunyn-Schmiedeberg's Archives of Pharmacology*, 363(6), pp. 590–596.

Bachmann, O. *et al*. (2003) 'Expression and regulation of the Na+-K+-2Cl- contransporter NKCC1 in the normal and CFTR-deficient murine colon', *Journal of Physiology*, 549(2), pp. 525–536.

Bagorda, A. *et al*. (2002) 'Reciprocal protein kinase A regulatory interactions between cystic fibrosis transmembrane conductance regulator and Na^+/H^+ exchanger isoform 3 in a renal polarized epithelial cell model.', *The Journal of biological chemistry*, 277(24), pp. 21480–21488.

Bai, Y., Li, M. and Hwang, T. C. (2010) 'Dual roles of the sixth transmembrane segment of the CFTR chloride channel in gating and permeation', *Journal of General Physiology*, 136(3), pp. 293–309.

Banerjee, A., Coffey, R. J. and Lau, K. S. (2018) 'Interpreting heterogeneity in intestinal tuft cell structure and function', *The Journal of Clinical Investigation*, 128(5), pp. 1711–1719.

Barker, N. *et al*. (2007) 'Identification of stem cells in small intestine and colon by marker gene Lgr5', Nature, 449, pp. 10003-1007.

Barker, N. (2008) 'The Canonical Wnt/β-Catenin Signalling Pathway', *Methods in Molecular Biology*, 468. pp. 5–15.

Barker, N., Van Oudenaarden, A. and Clevers, H. (2012) 'Identifying the stem cell of the intestinal crypt: Strategies and pitfalls', *Cell Stem Cell*, 11(4), pp. 452–460.

Barrett, K. E. and Keely, S. J. (2000) 'Chloride secretion by the intestinal epithelium: molecular basis and regulatory aspects.', *Annual review of physiology*, 62(1), pp. 535–572.

Bassil, A. K. *et al*. (2008) 'Activation of prostaglandin EP receptors by lubiprostone in rat and human stomach and colon', *British Journal of Pharmacology*, 154(1), pp. 126–135.

Beck, E. J. *et al*. (2008) 'Conformational changes in a pore-lining helix coupled to cystic fibrosis transmembrane conductance regulator channel gating', *Journal of Biological Chemistry*, 283(8), pp. 4957–4966.

Becq, F. *et al*. (2011) 'Pharmacological therapy for cystic fibrosis: From bench to bedside', *Journal of Cystic Fibrosis,* 10, pp. S129–S145.

Becq, F. *et al*. (2021) 'The rescue of F508del-CFTR by elexacaftor/tezacaftor/ivacaftor (Trikafta) in human airway epithelial cells is underestimated due to the presence of ivacaftor', *European Respiratory Journal*, 58(3), p. 2100671.

Benharouga, M. *et al*. (2003) 'The role of the C terminus and Na+/H+ exchanger regulatory factor in the functional expression of cystic fibrosis transmembrane

conductance regulator in nonpolarized cells and epithelia', *Journal of Biological Chemistry*, 278(24), pp. 22079–22089.

Berschneider, H. M. *et al*. (1988) 'Altered intestinal chloride transport in cystic fibrosis', *The FASEB Journal,* 2(10), pp. 2625–2629.

Bezprozvanny, I. and Maximov, A. (2001) 'PDZ domains: More than just a glue', *Proceedings of the National Academy of Sciences of the United States of America,* 98(3), pp. 787–789.

Bijvelds, M. J. C. *et al*. (2009) 'Activation of Intestinal Cl- Secretion by Lubiprostone Requires the Cystic Fibrosis Transmembrane Conductance Regulator', *Gastroenterology*, 137(3), pp. 976–985.

Bijvelds, M. J. C. *et al*. (2015) 'Inhibition of Heat-Stable Toxin-Induced Intestinal Salt and Water Secretion by a Novel Class of Guanylyl Cyclase C Inhibitors', *Journal of Infectious Diseases*, 212(10), pp. 1806–1815.

Bijvelds, M. J. C. *et al*. (2018) 'Selective inhibition of intestinal guanosine 3,5-cyclic monophosphate signaling by small-molecule protein kinase inhibitors', Journal of Biological Chemistry, 293(21), pp. 8173–8181.

Birchenough, G. M. H. *et al*. (2015) 'New developments in goblet cell mucus secretion and function'*, Mucosal Immunolog*y, 8(4), pp. 712–719.

Blackman, S. M. *et al*. (2006) 'Relative Contribution of Genetic and Nongenetic Modifiers to Intestinal Obstruction in Cystic Fibrosis', Gastroenterology, 131(4), pp. 1030–1039.

Boj, S. F. *et al*. (2017) 'Forskolin-induced Swelling in Intestinal Organoids: An *In Vitro* Assay for Assessing Drug Response in Cystic Fibrosis Patients', *Journal of Visualized Experiments*, (120), pp. 1–12.

Bombieri, C. *et al*. (2011) 'Recommendations for the classification of diseases as CFTR-related disorders', *Journal of Cystic Fibrosis*, 10(Suppl. 2), pp. 86–102.

Bompadre, S. G. *et al*. (2007) 'G551D and G1349D, two CF-associated mutations in the signature sequences of CFTR, exhibit distinct gating defects', *Journal of General Physiology*, 129(4), pp. 285–298.

Borowitz, D. *et al*. (2013) 'Maximal daily dose of pancreatic enzyme replacement therapy in infants with cystic fibrosis: A reconsideration', *Journal of Cystic Fibrosis. European Cystic Fibrosis Society*., 12(6), pp. 784–785.

Borowitz, D. (2015) 'CFTR, bicarbonate, and the pathophysiology of cystic fibrosis', *Pediatric Pulmonology,* Suppl 40, S24–S30.

Bosanquet, D. C. *et al*. (2014) 'FERM family proteins and their importance in cellular movements and wound healing', *International Journal of Molecular Medicine*, 34(1), pp. 3–12.

Boucher, R. C. *et al*. (1988) 'Evidence for reduced Cl^- and increased Na^+ permeability in cystic fibrosis human primary cell cultures.', *The Journal of Physiology*, 405(1), pp. 77–103.

Bradford, E. M. *et al*. (2009) 'Reduced NHE3-mediated Na^+ absorption increases survival and decreases the incidence of intestinal obstructions in cystic fibrosis mice', *Gastrointestinal and Liver Physiology*, 296(4), pp. G886–G898.

Bratosin, D. *et al*. (2005) 'Novel fluorescence assay using calcein-AM for the determination of human erythrocyte viability and aging', *Cytometry Part A*, 66(1), pp. 78–84.

Bu, X. D. *et al*. (2011) 'Caco-2 and LS174T cell lines provide different models for studying mucin expression in colon cancer', *Tissue and Cell*, 43(3), pp. 201–206.

Buczacki, S. J. A. *et al*. (2013) 'Intestinal label-retaining cells are secretory precursors expressing lgr5', *Nature*, 495(7439), pp. 65–69.

Burgel, P. *et al*. (2015) 'Future trends in cystic fibrosis demography in 34 European countries', *European Respiratory Journal*, 46(1), pp. 133–141.

Caci, E. *et al*. (2008) 'Evidence for direct CFTR inhibition by $CFTR_{inh}$-172 based on Arg347 mutagenesis', *Biochemical Journal*, 413(1), pp. 135–142.

Callebaut, I. *et al*. (2004) 'Nucleotide-binding domains of human cystic fibrosis transmembrane conductance regulator: Detailed sequence analysis and three-dimensional modeling of the heterodimer', *Cellular and Molecular Life Sciences*, 61(2), pp. 230–242.

Cammack, R. *et al*. (2008) Oxford Dictionary of Biochemistry and Moecular Biology.

Caputo, A. *et al*. (2008) 'TMEM16A, A Membrane Protein Associated with Calcium-Dependent Chloride Channel Activity', *Science*, 322(5901), pp. 590–594.

Chang, B. H. *et al*. (2011) 'A systematic family-wide investigation reveals that ~30% of mammalian PDZ domains engage in PDZ-PDZ interactions', *Chemistry and Biology*, 18(9), pp. 1143–1152.

Charman, S. *et al*. (2018) 'UK Cystic Fibrosis Registry Annual data report 2018'.

Charney, A. N. and Donowitz, M. (1978) 'Functional significance of intestinal Na^+-K^+-ATPase: *In vivo* ouabain inhibition', *American Journal of Physiology Endocrinology Metabolism and Gastrointestinal Physiology,* 3(6).

Chen, J. H., Cai, Z. and Sheppard, D. N. (2009) 'Direct sensing of intracellular pH by the cystic fibrosis transmembrane conductance regulator (CFTR) Cl^- channel', *Journal of Biological Chemistry,* 284(51), pp. 35495–35506.

Chen, T. *et al*. (2015) 'Cyclic GMP kinase II (cGKII) inhibits NHE3 by altering its trafficking and phosphorylating NHE3 at three required sites: Identification of a multifunctional phosphorylation site', *Journal of Biological Chemistry*, 290(4), pp. 1952–1965.

Chen, T. *et al*. (2019) 'NHERF3 is necessary for Escherichia coli heat-stable enterotoxin-induced inhibition of NHE3: Differences in signaling in mouse small intestine and Caco-2 cells', *American Journal of Physiology*, 317(4), pp. C737–C748.

Cheng, H. and Leblond, C. P. (1974) 'Origin, differentiation and renewal of the four main epithelial cell types in the mouse small intestine I. Columnar cell', *American Journal of Anatomy*, 141(4), pp. 461–479.

Cheng, S. H. *et al*. (1990) 'Defective intracellular transport and processing of CFTR is the molecular basis of most cystic fibrosis', *Cell*, 63(4), pp. 827–834.

Chey, W. D. *et al*. (2021) 'Efficacy of Tenapanor in Treating Patients With Irritable Bowel Syndrome With Constipation: A 26-Week, Placebo-Controlled Phase 3 Trial (T3MPO-2)', *American Journal of Gastroenterology,* 116(6), pp. 1294–1303.

Chey, W. D., Lembo, A. J. and Rosenbaum, D. P. (2017) 'Tenapanor Treatment of Patients With Constipation-Predominant Irritable Bowel Syndrome: A Phase 2, Randomized, Placebo-Controlled Efficacy and Safety Trial', *American Journal of Gastroenterology*, 112(5), pp. 763–774.

Chong, P. A. *et al*. (2013) 'Dynamics intrinsic to cystic fibrosis transmembrane conductance regulator function and stability', *Cold Spring Harbor Perspectives in Medicine*, 3(3), pp. 1–17.

Clancy, J. P. *et al*. (2012) 'Results of a phase IIa study of VX-809, an investigational CFTR corrector compound, in subjects with cystic fibrosis homozygous for the F508del-CFTR mutation', *Thorax*, 67(1), pp. 12–18.

Clarke, L. (2009) 'A guide to Ussing chamber studies of mouse intestine', *AJP: Gastrointestinal and Liver Physiology*, 296(6), pp. G1151–G1166.

Clarke, L. and Harline, M. (1996) 'CFTR is required for cAMP inhibition of intestinal Na^+ absorption in a cystic fibrosis mouse model', *American Journal of Physiology - Gastrointestinal and Liver Physiology,* 270(2 33-2).

Clausen, M, Hilbers, F. and Poulsen, H. (2017) 'The Structure and Function of the Na,K-ATPase Isoforms in Health and Disease', *Frontiers in Physiology*, 8, pp. 1–16.

Clevers, H. (2013) 'The Intestinal Crypt, A Prototype Stem Cell Compartment', *Cell*., 154(2), pp. 274–284

Clevers, H. and Bevins, C. (2013) 'Paneth Cells: Maestros of the Small Intestinal Crypts', *Annual Review of Physiology,* 75(1), pp. 289–311.

Colemeadow, J., Joyce, H. and Turcanu, V. (2016) 'Precise treatment of cystic fibrosis – current treatments and perspectives for using CRISPR', *Expert Review of Precision Medicine and Drug Development*, 1(2), pp. 169–180.

Corradi, V., Vergani, P. and Tieleman, D. P. (2015) 'Cystic fibrosis transmembrane conductance regulator (CFTR): closed and open state channel models', *Journal of Biological Chemistry*, 290(38), pp. 22891–22906

Costa, J. and Ahluwalia, A. (2019) 'Advances and Current Challenges in Intestinal in vitro Model Engineering: A Digest', *Frontiers in Bioengineering and Biotechnology*, 7, pp. 1–14.

Csanády, L., Vergani, P. and Gadsby, D. C. (2019) 'Structure, Gating, and Regulation of the CFTR Anion Channel', *Physiological Reviews*, 99(1), pp. 707–738.

Cui, L. *et al*. (2007) 'Domain Interdependence in the Biosynthetic Assembly of CFTR', *Journal of Molecular Biology*, 365(4), pp. 981–994.

Cuppoletti, J. *et al*. (2004) 'SPI-0211 activates T84 cell chloride transport and recombinant human ClC-2 chloride currents.', *American journal of physiology. Cell physiology*, 287(5), pp. C1173–C1183.

Currid, A., Ortega, B. and Valverde, M. A. (2004) 'Chloride secretion in a morphologically differentiated human colonic cell line that expresses the epithelial Na^+ channel', *The Journal of Physiology*, 555(1), pp. 241–250.

Cuthbert, A. W. *et al*. (1987) 'Calcium-and cyclic AMP-dependent chloride secretion in human colonic epithelia', *British Journal of Pharmacology*, 91(3), pp. 503–515.

Cuthbert, A. W., Kirkland, S. and MacVinish, L. (1985) 'Kinin effects on ion transport in monolayers of HCA-7 cells, a line from a human colonic adenocarcinoma', *British Journal of Pharmacology*, 86(1), pp. 3–5.

Cutting, G. (2015) 'Cystic fibrosis genetics: From molecular understanding to clinical application', *Nature Reviews Genetics*,16(1), pp. 45–56.

Cystic Fibrosis Trust UK (2019) UK cystic fibrosis registry annual data report 2019.

Czerwinski, M., Shroyer, N. F. and Spence, J. R. (2018) 'WNT Signaling in the Intestine: Development, Homeostasis, Disease', *Physiology of the Gastrointestinal Tract*: Sixth Edition, 1–2, pp. 185–196.

Date, S. and Sato, T. (2015) 'Mini-Gut Organoids: Reconstitution of the Stem Cell Niche', *Annual Review of Cell and Developmental Biology*, 31(1), pp. 269–289.

Dedkova, E., Sigova, A. and Zinchenko, V. (2000) 'Mechanism of action of calcium ionophores on intact cells: Ionophore-resistant cells', *Membrane & Cell Biology*, 13(3), pp. 357–368.

Dekkers, J., Berkers, G., *et al*. (2016) 'Characterizing responses to CFTR-modulating drugs using rectal organoids derived from subjects with cystic fibrosis', Science Translational Medicine, 8(344), p. 344-84.

Dekkers, J., Van Mourik, P., *et al*. (2016) 'Potentiator synergy in rectal organoids carrying S1251N, G551D, or F508del CFTR mutations', *Journal of Cystic Fibrosis*, 15(5), pp. 568–578.

Dekkers, J. *et al*. (2013) 'A functional CFTR assay using primary cystic fibrosis intestinal organoids', *Nature Medicine*, 19(7), pp. 939–945.

Devor, D. *et al*. (1997) 'Inhibition of intestinal Cl- secretion by clotrimazole: Direct effect on basolateral membrane K+ channels', *Cell Physiology*, 273(2 Pt 1), C531-C540.

Donowitz, M. and Li, X. (2007) 'Regulatory binding partners and complexes of NHE3', *Physiological Reviews*, 87(3), pp. 825–872.

Dransfield, D. T. *et al*. (1997) 'Ezrin is a cyclic AMP-dependent protein kinase anchoring protein', *EMBO Journal*, 16(1), pp. 35–43.

Drumm, M. L. *et al*. (1990) 'Correction of the cystic fibrosis defect in vitro by retrovirus-mediated gene transfer', *Cell*, 62(6), pp. 1227–1233.

Dulhanty, A. M. and Riordan, J. R. (1994) 'Phosphorylation by cAMP-Dependent Protein Kinase Causes a Conformational Change in the R Domain of the Cystic Fibrosis Transmembrane Conductance Regulator', Biochemistry, 33(13), pp. 4072–4079.

Eggermont, J. (2004) 'Calcium-activated chloride channels: (un)known, (un)loved?', *Proceedings of the American Thoracic Society*, 1(1), pp. 22–27.

Elborn, J. S. *et al*. (2016) 'Efficacy and safety of lumacaftor/ivacaftor combination therapy in patients with cystic fibrosis homozygous for Phe508del CFTR by pulmonary function subgroup: a pooled analysis', *The Lancet Respiratory Medicine*, 4(8), pp. 617–626.

Erb, L. and Weisman, G. A. (2012) 'Coupling of P2Y receptors to G proteins and other signaling pathways', *Wiley Interdisciplinary Reviews: Membrane Transport and Signaling,* 1(6), pp. 789–803.

Escudero-Hernández, C. (2021) Epithelial cell dysfunction in coeliac disease, *International Review of Cell and Molecular Biology*, 358, pp.133-164.

Farinha, C. M. *et al*. (2002) 'The human Dnaj homologue (Hdj)-1/heat-shock protein (Hsp) 40 co-chaperone is required for the in vivo stabilization of the cystic fibrosis transmembrane conductance regulator by Hsp70', *Biochemical Journal,* 366(3), pp. 797–806.

Farinha, C. M., Matos, P. and Amaral, M. D. (2013) 'Control of cystic fibrosis transmembrane conductance regulator membrane trafficking: Not just from the endoplasmic reticulum to the Golgi', *FEBS Journal*, 280(18), pp. 4396–4406.

Flagella, M. *et al*. (1999) 'Mice lacking the basolateral Na-K-2Cl cotransporter have impaired epithelial chloride secretion and are profoundly deaf', *Journal of Biological Chemistry*, 274(38), pp. 26946–26955.

van der Flier, L. G. and Clevers, H. (2009) 'Stem Cells, Self-Renewal, and Differentiation in the Intestinal Epithelium', *Annual Review of Physiology, 71*(1), pp. 241–260.

Flume, P. A. *et al*. (2012) 'Ivacaftor in Subjects With Cystic Fibrosis Who Are Homozygous for the F508del-CFTR Mutation', *Chest*, 142(3), pp. 718–724.

Foroni, L. *et al*. (2017) 'Molecular and Cytogenetic Analysis', *Dacie and Lewis Practical Haematology,* pp. 126–164.

Fre, S. (2015) 'Intestinal stem cells', *Stem Cell Biology and Regenerative Medicine*, 12(5), pp. 455–475.

Frizzell, R. A., Field, M. and Schultz, S. G. (1979) 'Sodium-coupled chloride transport by epithelial tissues', *American Journal of Physiology-Renal Physiology*, 236(1), pp. F1–F8.

Frizzell, R. A. and Hanrahan, J. W. (2012) 'Physiology of epithelial chloride and fluid secretion', *Cold Spring Harbor Perspectives in Medicine*, 2(6), pp. a009563–a009563.

Gao, X., Bai, Y. and Hwang, T. C. (2013) 'Cysteine scanning of CFTR's first transmembrane segment reveals its plausible roles in gating and permeation', *Biophysical Journal. Biophysical Society*, 104(4), pp. 786–797.

Gassler, N. (2017) 'Paneth cells in intestinal physiology and pathophysiology', *World Journal of Gastrointestinal Pathophysiology*, 8(4), pp. 150–160.

Gawenis, L. R. *et al*. (2002) 'Intestinal NaCl transport in NHE2 and NHE3 knockout mice', *Gastrointestinal and Liver Physiology*, 282(5 45-5), pp. 776–784.

Gawenis, L. R. *et al*. (2003) 'cAMP inhibition of murine intestinal Na+/H+ exchange requires CFTR-mediated cell shrinkage of villus epithelium', *Gastroenterology,* 125(4), pp. 1148–1163.

Gawenis, L. R. *et al*. (2004) 'Electroneutral sodium absorption and electrogenic anion secretion across murine small intestine are regulated in parallel', *American Journal of Physiology - Gastrointestinal and Liver Physiology*, 287(6 50-6), pp. 1140–1149.

Gawenis, L. R. *et al*. (2010) 'AE2 Cl^-/HCO_3^- exchanger is required for normal cAMP-stimulated anion secretion in murine proximal colon.', *American journal of physiology. Gastrointestinal and liver physiology,* 298(4), pp. G493-503.

Gelfond, D. *et al*. (2017) 'Impact of CFTR Modulation on Intestinal pH, Motility, and Clinical Outcomes in Patients With Cystic Fibrosis and the G551D Mutation', *Clinical and Translational Gastroenterology,* 8(3), p.81.

Geurts, M. H. *et al*. (2020) 'CRISPR-Based Adenine Editors Correct Nonsense Mutations in a Cystic Fibrosis Organoid Biobank', *Cell Stem Cell*, 26(4), pp. 503-510.e7.

Gheytanchi, E. *et al*. (2021) ‘Morphological and molecular characteristics of spheroid formation in HT-29 and Caco-2 colorectal cancer cell lines’, *Cancer Cell International*, 21(1), pp. 1–16.

Gillie, D. J. *et al*. (2001) ‘Liquid and ion transport by fetal airway and lung epithelia of mice deficient in sodium-potassium-2-chloride transporter’, *American Journal of Respiratory Cell and Molecular Biology*, 25(1), pp. 14–20.

Girardi, A. and di Sole, F. (2012) ‘Deciphering the mechanisms of the Na^+/H^+ exchanger-3 regulation in organ dysfunction’, American Journal of Physiology - *Cell Physiology,* 302(11), pp. 1569–1587.

Van Goor, F. *et al*. (2009) ‘Rescue of CF airway epithelial cell function in vitro by a CFTR potentiator, VX-770’, *Proceedings of the National Academy of Sciences*, 106(44), pp. 18825–18830.

Van Goor, F. *et al*. (2011) ‘Correction of the F508del-CFTR protein processing defect in vitro by the investigational drug VX-809’, *Proceedings of the National Academy of Sciences*, 108(46), pp. 18843–18848.

Gordat, M. *et al*. (2019) ‘Single and multiples doses of the inhaled ENaC inhibitor BI 443651 are well tolerated in healthy males’, *Journal of Cystic Fibrosis*, 18, p. S133.

Goss, C. H. *et al*. (2020) ‘An innovative phase II trial to establish proof of efficacy and optimal dose of a new inhaled epithelial sodium channel inhibitor BI 1265162 in adults and adolescents with cystic fibrosis: BALANCE-CF TM 1’, *ERJ Open Research*, 6(4), pp. 00395–02020.

Greger, R. (2000) ‘Role of CFTR in the Colon’, *Annual Review of Physiology*, 62, pp. 467–491.

Gribble, F. M. and Reimann, F. (2019) ‘Function and mechanisms of enteroendocrine cells and gut hormones in metabolism’, *Nature Reviews Endocrinology*, 15(4), pp. 226–237.

Groves, T. *et al*. (2017) ‘Question 8: How should distal intestinal obstruction syndrome [DIOS] be managed?’, *Paediatric Respiratory Reviews,* 21, pp. 68–71.

Guigui, S., Wang, J. and Cohen, R. I. (2016) ‘The use of ivacaftor in CFTR mutations resulting in residual functioning protein’, *Respiratory Medicine Case Reports*, 19, pp. 193–195.

Gustafsson, J. K. *et al*. (2012) ‘Bicarbonate and functional CFTR channel are required for proper mucin secretion and link cystic fibrosis with its mucus phenotype’, *The Journal of Experimental Medicine*, 209(7), pp. 1263–1272.

Haardt, M. *et al*. (1999) ‘C-terminal truncations destabilize the cystic fibrosis transmembrane conductance regulator without impairing its biogenesis. A novel class of mutation’, *Journal of Biological Chemistry*, 274(31), pp. 21873–21877.

Hadida, S. *et al*. (2014) 'Discovery of N -(2,4-Di- tert -butyl-5-hydroxyphenyl)-4-oxo-1,4-dihydroquinoline-3-carboxamide (VX-770, Ivacaftor), a Potent and Orally Bioavailable CFTR Potentiator', *Journal of Medicinal Chemistry,* 57(23), pp. 9776–9795.

Haggie, P. M. *et al*. (2006) 'Tracking of Quantum Dot-labeled CFTR Shows Near Immobilization by C-Terminal PDZ Interactions', *Molecular Biology of the Cell*, 17(12), pp. 4937–4945.

Haggie, P. M. *et al*. (2017) 'Correctors and potentiators rescue function of the truncated W1282X-Cystic Fibrosis Transmembrane Regulator (CFTR) translation product', *Journal of Biological Chemistry*, 292(3), pp. 771–785.

Hanrahan, J. W. *et al*. (2017) 'Corrector combination therapies for F508del-CFTR', *Current Opinion in Pharmacology*, 34, pp. 105–111.

Hanukoglu, I. (2021) 'Epithelial sodium channel (ENaC) in guidetopharmacology.org v.2021.2', *IUPHAR/BPS Guide to Pharmacology*, 2021(2).

Harris, B. Z. and Lim, W. A. (2001) 'Mechanism and role of PDZ domains in signaling complex assembly', *Journal of Cell Science,* 114(18), pp. 3219–3231.

Harvey, B. G. *et al*. (1999) 'Airway epithelial CFTR mRNA expression in cystic fibrosis patients after repetitive administration of a recombinant adenovirus.', *The Journal of Clinical Investigation*, 104(9), pp. 1245–55.

Hayashi, H. *et al*. (2004) 'Inhibition and redistribution of NHE3, the apical Na^+/H^+ exchanger, by Clostridium difficile toxin B.', *The Journal of General Physiology,* 123(5), pp. 491–504.

Hayashi, H. (2019) 'The Mode of Action of NHE3 Inhibitors in Intestinal Na^+ Absorption', *Gastroenterology: Medicine & Research*, 4(1), pp. 2–5.

Hayee, B. *et al*. (2019) 'A high prevalence of chronic gastrointestinal symptoms in adults with cystic fibrosis is detected using tools already validated in other GI disorders', *United European Gastroenterology Journal,* 7(7), pp. 881–888.

Hayward, I. P. and Whitehead, R. H. (1992) 'Patterns of growth and differentiation in the colon carcinoma cell line LIM1863', *International Journal of Cancer*, 50(5), pp. 752–759.

He, P. and Yun, C. C. (2010) 'Mechanisms of the Regulation of the Intestinal Na^+/H^+ Exchanger NHE3', *Journal of Biomedicine and Biotechnology*, 2010(2010), pp. 1–10.

Hecht, G. *et al*. (2004) 'Differential regulation of Na^+/H^+ exchange isoform activities by enteropathogenic E. coli in human intestinal epithelial cells', *American Journal of Physiology - Gastrointestinal and Liver Physiology*, 287(2 50-2), pp. 370–378.

Hegedus, T. *et al*. (2009) 'Role of individual R domain phosphorylation sites in CFTR regulation by protein kinase A', *Biochimica et Biophysica Acta - Biomembranes*, 1788(6), pp. 1341–1349.

Henderson, R. M. *et al*. (1992) ‘Chloride channels and anion fluxes in a human colonic epithelium (HCA-7)’, British Journal of Pharmacology, 106, pp. 109–114.

El Hiani, Y. and Linsdell, P. (2015) ‘Functional architecture of the cytoplasmic entrance to the cystic fibrosis transmembrane conductance regulator chloride channel pore’, *Journal of Biological Chemistry,* 290(25), pp. 15855–15865.

El Hiani, Y., Negoda, A. and Linsdell, P. (2016) ‘Cytoplasmic pathway followed by chloride ions to enter the CFTR channel pore’, *Cellular and Molecular Life Sciences*. 73(9), pp. 1917–1925.

Hirsh, A. J. *et al*. (2004) ‘Evaluation of Second Generation Amiloride Analogs as Therapy for Cystic Fibrosis Lung Disease’, *Journal of Pharmacology and Experimental Therapeutics*, 311(3), pp. 929–938.

Hjelm, M. and Shaikhkhalil, A. K. (2020) ‘Celiac Disease in Patients With Cystic Fibrosis on Ivacaftor: A Case Series’, *Journal of Pediatric Gastroenterology and Nutrition,* 71(2), pp. 257–260.

Hoelen, H. *et al*. (2010) ‘The primary folding defect and rescue of ΔF508 CFTR emerge during translation of the mutant domain’, *PLoS ONE*, 5(11), pp. 1–10.

Hoover, B. *et al*. (2017) ‘The intestinal tuft cell nanostructure in 3D’, *Scientific Reports*, 7(1), pp. 1–8.

Houwen, R. H. *et al*. (2010) ‘Defining DIOS and constipation in cystic fibrosis with a multicentre study on the incidence, characteristics, and treatment of DIOS’, *Journal of Pediatric Gastroenterology and Nutrition,* 50(1), pp. 38–42.

Hughes, L. K., Ju, M. and Sheppard, D. N. (2008) ‘Potentiation of cystic fibrosis transmembrane conductance regulator (CFTR) Cl^- currents by the chemical solvent tetrahydrofuran’, *Molecular Membrane Biology,* 25(6–7), pp. 528–538.

Hung, A. Y. and Sheng, M. (2002) ‘PDZ domains: Structural modules for protein complex assembly’, *Journal of Biological Chemistry*, 277(8), pp. 5699–5702.

Hwang, T.-C. and Kirk, K. L. (2013) ‘The CFTR Ion Channel: Gating, Regulation, and Anion Permeation’, *Cold Spring Harbor Perspectives in Medicine*, 3(1), pp. a009498–a009498.

Hwang, T. C. *et al*. (1994) ‘Regulation of the gating of cystic fibrosis transmembrane conductance regulator Cl channels by phosphorylation and ATP hydrolysis’, *Proceedings of the National Academy of Sciences of the United States of America*, 91(11), pp. 4698–4702.

Hwang, T. C. *et al.* (1997) ‘Genistein potentiates wild-type and delta F508-CFTR channel activity’, *American Journal of Physiology-Cell Physiology*, 273(3), pp. C988–C998.

Hwang, T. C. *et al*. (2018) 'Structural mechanisms of CFTR function and dysfunction', *Journal of General Physiology*, 150(4), pp. 539–570.

Hwang, T. C. and Sheppard, D. N. (1999) 'Molecular pharmacology of the CFTR Cl^- channel', Trends in Pharmacological Sciences, 20(11), pp. 448–453. doi: 10.1016/S0165-6147(99)01386-3.

Hwang, T. C. and Sheppard, D. N. (2009) 'Gating of the CFTR Cl^- channel by ATP-driven nucleotide-binding domain dimerisation', *Journal of Physiology,* 587(10), pp. 2151–2161.

Ikpa, P. T. *et al*. (2016) 'Guanylin and uroguanylin are produced by mouse intestinal epithelial cells of columnar and secretory lineage', *Histochemistry and Cell Biology*, 146(4), pp. 445–455.

Jansson, K. *et al*. (2015) 'Ouabain Regulates CFTR-Mediated Anion Secretion and Na,K-ATPase Transport in ADPKD Cells', *The Journal of Membrane Biology*, 248(6), pp. 1145–1157.

Jantarajit, W. *et al*. (2017) 'CFTR-mediated anion secretion across intestinal epithelium-like Caco-2 monolayer under PTH stimulation is dependent on intermediate conductance K^+ channels', *American Journal of Physiology - Cell Physiology*, 313(1), pp. C118–C129.

Jaques, R., Shakeel, A. and Hoyle, C. (2020) 'Novel therapeutic approaches for the management of cystic fibrosis', *Multidisciplinary Respiratory Medicine*, 15(1), pp.690.

Jih, K.-Y. *et al*. (2017) 'CFTR potentiators: from bench to bedside', *Current Opinion in Pharmacology,* 34(12), pp. 98–104.

Johns, T. *et al*. (2013) 'Defining the disease liability of variants in the cystic fibrosis transmembrane conductance regulator gene', *Nature genetics,* 45(10), pp. 1160–1167.

de Jonge, H. R. *et al*. (2020) 'Strategies for cystic fibrosis transmembrane conductance regulator inhibition: from molecular mechanisms to treatment for secretory diarrhoeas', *FEBS Letters*, 594(23), pp. 4085–4108.

Julio-Kalajzić, F. *et al*. (2018) 'K 2P TASK-2 and KCNQ1-KCNE3 K^+ channels are major players contributing to intestinal anion and fluid secretion', *The Journal of Physiology*, 596(3), pp. 393–407.

Kahle, K. T. and Staley, K. J. (2008) 'The bumetanide-sensitive Na-K-2Cl cotransporter NKCC1 as a potential target of a novel mechanism-based treatment strategy for neonatal seizures', *Neurosurgical Focus*, 25(3), pp. 1–8.

Keating, D. *et al*. (2018) 'VX-445–Tezacaftor–Ivacaftor in Patients with Cystic Fibrosis and One or Two Phe508del Alleles', *New England Journal of Medicine,* 379(17), pp. 1612–1620.

Keely, S. J. and Barrett, K. E. (2000) 'Regulation of chloride secretion. Novel pathways and messengers.', *Annals of the New York Academy of Sciences*, 915, pp. 67–76.

Khamsi, R. (2020) ‘Chasing an inclusive cure’, *Nature Outlook*, 583, s 12-14

Kim, J., Koo, B. K. and Knoblich, J. A. (2020) ‘Human organoids: model systems for human biology and medicine’, *Nature Reviews Molecular Cell Biology*, 21(10), pp. 571–584.

Kirkland, S. C. (1985a) ‘*Dome Formation by a Human Colonic Adenocarcinoma Cell Line (HCA-7)’, Cancer Research*, 45(August), pp. 3790–3795.

Klinkspoor, J. H. *et al*. (1999) ‘Mucin secretion by the human colon cell line LS174T is regulated by bile salts’, *Glycobiology,* 9(1), pp. 13–19.

Knowles, M. R. *et al*. (1990) ‘A Pilot Study of Aerosolized Amiloride for the Treatment of Lung Disease in Cystic Fibrosis’, *New England Journal of Medicine,* 322(17), pp. 1189–1194.

Ko, S. B. H. *et al*. (2002) ‘A molecular mechanism for aberrant CFTR-dependent HCO_3^- transport in cystic fibrosis’, *EMBO Journal*, 21(21), pp. 5662–5672.

Koizumi, M. *et al*. (2019) ‘Podocyte Injury Augments Intrarenal Angiotensin II Generation and Sodium Retention in a Megalin-Dependent Manner’, *Hypertension*, 74(3), pp. 509–517.

Konstan, M. W. *et al*. (2017) ‘Assessment of safety and efficacy of long-term treatment with combination lumacaftor and ivacaftor therapy in patients with cystic fibrosis homozygous for the F508del-CFTR mutation (PROGRESS): a phase 3, extension study’, *The Lancet Respiratory Medicine,* 5(2), pp. 107–118.

Kubitz, R. *et al*. (1992) ‘Small-conductance chloride channels induced by cAMP, $Ca2^+$, and hypotonicity in HT29 cells: ion selectivity, additivity and stilbene sensitivity’, *Pflügers Archiv European Journal of Physiology*, 421(5), pp. 447–454.

Kuk, K. and Taylor-Cousar, J. L. (2015) ‘Lumacaftor and ivacaftor in the management of patients with cystic fibrosis: Current evidence and future prospects’, *Therapeutic Advances in Respiratory Disease,* 9(6), pp. 313–326.

Kunzelmann, K., Kathöfer, S. and Greger, R. (1995) ‘Na^+ and Cl^- conductances in airway epithelial cells: increased Na^+ conductance in cystic fibrosis’, *Pflügers Archiv European Journal of Physiology,* 431(1), pp. 1–9.

Lamprecht, G., Weinman, E. J. and Yun, C. H. C. (1998) ‘The role of NHERF and E3KARP in the cAMP-mediated inhibition of NHE3’, Journal of Biological Chemistry, 273(45), pp. 29972–29978.

Lansdell, K. A. *et al.* (2000) ‘Two mechanisms of genistein inhibition of cystic fibrosis transmembrane conductance regulator Cl- channels expressed in murine cell line’, *Journal of Physiology*, 524(2), pp. 317–330.

Lencer, W. I. *et al*. (1995) ‘Transcytosis of cholera toxin subunits across model human intestinal epithelia’, *Proceedings of the National Academy of Sciences of the United States of America*, 92(22), pp. 10094–10098.

Lesko, A. C. *et al.* (2015) ‘The APC tumor suppressor is required for epithelial cell polarization and three-dimensional morphogenesis’, *Biochimica et Biophysica Acta (BBA) - Molecular Cell Research*, 1853(3), pp. 711–723.

Lever, J. E. (1979) ‘Differentiated Epithelial Cell Cultures’, 272, pp. 259–272.

Lewis, H. A. *et al*. (2004) ‘Structure of nucleotide-binding domain 1 of the cystic fibrosis transmembrane conductance regulator’, EMBO Journal, 23(2), pp. 282–293.

Li, B., Rietmeijer, R. A. and Brohawn, S. G. (2020) ‘Structural basis for pH gating of the two-pore domain K^+ channel TASK2’, *Nature*, 586(7829), pp. 457–462.

Li, C. and Naren, A. P. (2010) ‘CFTR chloride channel in the apical compartments: Spatiotemporal coupling to its interacting partners’, *Integrative Biology*, 2(4), pp. 161–177.

Li, H. *et al*. (2017) ‘Bypassing CFTR dysfunction in cystic fibrosis with alternative pathways for anion transport’, *Current Opinion in Pharmacology*, 34, pp. 91–97.

Li, H., Findlay, I. A. and Sheppard, D. N. (2004) ‘The relationship between cell proliferation, Cl^- secretion, and renal cyst growth: A study using CFTR inhibitors’, *Kidney International,* 66(5), pp. 1926–1938.

Li, H., Sheppard, D. N. and Hug, M. J. (2004) ‘Transepithelial electrical measurements with the Ussing chamber’, *Journal of Cystic Fibrosis*, 3(suppl. 2), pp. 123–126.

Li, L. and Clevers, H. (2010) ‘Coexistence of Quiescent and Active Adult Stem Cells in Mammals’, *Science*, 327(5965), pp. 542–545.

Li, N. *et al*. (2016) ‘Mouse Label-Retaining Cells Are Molecularly and Functionally Distinct From Reserve Intestinal Stem Cells’, *Gastroenterology*, 151(2), pp. 298-310.e7.

Linsdell, P. (2017) ‘Architecture and functional properties of the CFTR channel pore’, Cellular and Molecular Life Sciences. *Springer International Publishing*, 74(1), pp. 67–83.

Linsdell, P., Evagelidis, A. and Hanrahan, J. W. (2000) ‘Molecular determinants of anion selectivity in the cystic fibrosis transmembrane conductance regulator chloride channel pore’, *Biophysical Journal*, 78(6), pp. 2973–2982.

Linsdell, P., Tabcharani, J. A. and Hanrahan, J. W. (1997) ‘Multi-ion mechanism for ion permeation and block in the cystic fibrosis transmembrane conductance regulator chloride channel’, *Journal of General Physiology*, 110(4), pp. 365–377.

Linsdell, P., Zheng, S. X. and Hanrahan, J. W. (1998) 'Non-pore lining amino acid side chains influence anion selectivity of the human CFTR Cl^- channel expressed in mammalian cell lines', *Journal of Physiology*, 512(1), pp. 1–16.

De Lisle, R. C. and Borowitz, D. (2013) 'The cystic fibrosis intestine.', *Cold Spring Harbor perspectives in medicine*, 3(9), pp. 1–17.

Liu, C. *et al*. (2020) 'CFTR functions as a tumor suppressor and is regulated by DNA methylation in colorectal cancer', *Cancer Management and Research*, 12, pp. 4261–4270.

Liu, F. *et al*. (2017) 'Molecular Structure of the Human CFTR Ion Channel', *Cell*, 169(1), pp. 85–92.

Liu, F. *et al*. (2019) 'Structural identification of a hotspot on CFTR for potentiation', *Science,* 364(6446), pp. 1184–1188.

Loo, M. A. *et al*. (1998) 'Perturbation of Hsp90 interaction with nascent CFTR prevents its maturation and accelerates its degradation by the proteasome', *EMBO Journal*, 17(23), pp. 6879–6887.

Ma, T. *et al*. (2002) 'Thiazolidinone CFTR inhibitor identified by high-throughput screening blocks cholera toxin-induced intestinal fluid secretion', *Journal of Clinical Investigation*, 110(11), pp. 1651–1658.

Mall, M. *et al*. (1998) 'The amiloride-inhibitable Na^+ conductance is reduced by the cystic fibrosis transmembrane conductance regulator in normal but not in cystic fibrosis airways', *Journal of Clinical Investigation*, 102(1), pp. 15–21.

Mall, M. A. (2020) 'ENaC inhibition in cystic fibrosis: potential role in the new era of CFTR modulator therapies', *European Respiratory Journal*, 56(6), p. 2000946.

Mall, M. A. and Galietta, L. J. V. (2015) 'Targeting ion channels in cystic fibrosis', *Journal of Cystic Fibrosis,* 14(5), pp. 561–570.

Maule, G. *et al*. (2019) 'Allele specific repair of splicing mutations in cystic fibrosis through AsCas12a genome editing', *Nature Communications,* 10(1), p. 3556.

McCool, D. J. *et al*. (1990) 'The T84 human colonic adenocarcinoma cell line produces mucin in culture and releases it in response to various secretagogues', *Biochemical Journal*, 267(2), pp. 491–500.

McCracken, K. W. *et al*. (2011) 'Generating human intestinal tissue from pluripotent stem cells in vitro', Nature Protocols. Nature Publishing Group, 6(12), pp. 1920–1928.

McDonough, S. *et al*. (1994) 'Novel pore-lining residues in CFTR that govern permeation and open-channel block', *Neuron*, 13(3), pp. 623–634.

McGahan, M. C., Yorio, T. and Bentley, P. J. (1977) ‘The mode of action of bumetanide: inhibition of chloride transport across the amphibian cornea.’, *Journal of Pharmacology and Experimental Therapeutics*, 203(1), pp. 97–102.

McNamara, J. J. *et al*. (2019) ‘Safety, pharmacokinetics, and pharmacodynamics of lumacaftor and ivacaftor combination therapy in children aged 2–5 years with cystic fibrosis homozygous for F508del-CFTR: an open-label phase 3 study’, *The Lancet Respiratory Medicine*, 7(4), pp. 325–335.

Meacham, G. C. (1999) ‘The Hdj-2/Hsc70 chaperone pair facilitates early steps in CFTR biogenesis’, The EMBO Journal, 18(6), pp. 1492–1505.

Melis, N. *et al*. (2014) ‘Revisiting CFTR inhibition: a comparative study of CFTR $_{inh}$ -172 and GlyH -101 inhibitors’, *British Journal of Pharmacology*, 171(15), pp. 3716–3727.

Middleton, P. G. *et al*. (2019) ‘Elexacaftor–Tezacaftor–Ivacaftor for Cystic Fibrosis with a Single Phe508del Allele’, *New England Journal of Medicine*, 381(19), pp. 1809–1819.

Mijnders, M., Kleizen, B. and Braakman, I. (2017) ‘Correcting CFTR folding defects by small-molecule correctors to cure cystic fibrosis’, *Current Opinion in Pharmacology*, 34, pp. 83–90.

Milla, C. E. *et al*. (2017) ‘Lumacaftor/Ivacaftor in Patients Aged 6–11 Years with Cystic Fibrosis and Homozygous for F508del-CFTR’, *American Journal of Respiratory and Critical Care Medicine*, 195(7), pp. 912–920.

Moe, O. W., Amemiya, M. and Yamaji, Y. (1995) ‘Activation of protein kinase A acutely inhibits and phosphorylates Na/H exchanger NHE-3’, *Journal of Clinical Investigation*, 96(5), pp. 2187–2194.

Montoro, D. T. *et al*. (2018) ‘A revised airway epithelial hierarchy includes CFTR-expressing ionocytes’, *Nature*, 560(7718), pp. 319–324.

Montoro, D. T. *et al*. (2020) ‘A Synthesis Concerning Conservation and Divergence of Cell Types across Epithelia’, *Cold Spring Harbor Perspectives in Biology*, p. a035733.

Moran, O., Galietta, L. J. V. and Zegarra-Moran, O. (2005) ‘Binding site of activators of the cystic fibrosis transmembrane conductance regulator in the nucleotide binding domains’, *Cellular and Molecular Life Sciences,* 62(4), pp. 446–460.

Moran, O. and Zegarra-Moran, O. (2008) ‘On the measurement of the functional properties of the CFTR’, *Journal of Cystic Fibrosis. European Cystic Fibrosis Society*, 7(6), pp. 483–494.

Morgan, R. G. *et al*. (2018) ‘Optimized delivery of siRNA into 3D tumor spheroid cultures in situ’, *Scientific Reports*, 8(1), pp. 1–10.

Mornon, J. P. *et al*. (2015) ‘Full-open and closed CFTR channels, with lateral tunnels from the cytoplasm and an alternative position of the F508 region, as revealed by molecular dynamics’, *Cellular and Molecular Life Sciences*, 72(7), pp. 1377–1403.

Mornon, J. P., Lehn, P. and Callebaut, I. (2008) 'Atomic model of human cystic fibrosis transmembrane conductance regulator: Membrane-spanning domains and coupling interfaces', *Cellular and Molecular Life Sciences*, 65(16), pp. 2594–2612.

Mouradov, D. *et al*. (2014) 'Colorectal cancer cell lines are representative models of the main molecular subtypes of primary cancer', *Cancer Research*, 74(12), pp. 3238–3247.

Nickolaus, P. *et al*. (2020) 'Preclinical evaluation of the epithelial sodium channel inhibitor BI 1265162 for treatment of cystic fibrosis', *ERJ Open Research*, 6(4), pp. 00429–02020.

O'Brien, C. E., Anderson, P. J. and Stowe, C. D. (2010) 'Use of the chloride channel activator lubiprostone for constipation in adults with cystic fibrosis: A case series', *Annals of Pharmacotherapy*, 44(3), pp. 577–581.

O'Riordan, T. G. *et al*. (2014) 'Acute Hyperkalemia Associated with Inhalation of a Potent ENaC Antagonist: Phase 1 Trial of GS-9411', *Journal of Aerosol Medicine and Pulmonary Drug Delivery,* 27(3), pp. 200–208.

Okiyoneda, T. *et al*. (2013) 'Mechanism-based corrector combination restores ΔF508-CFTR folding and function', *Nature Chemical Biology*, 9(7), pp. 444–454.

Oldham, M. L., Davidson, A. L. and Chen, J. (2008) 'Structural insights into ABC transporter mechanism', *Current Opinion in Structural Biology*, 18(6), pp. 726–733.

Ostedgaard, L. S. *et al*. (2000) 'A functional R domain from cystic fibrosis transmembrane conductance regulator is predominantly unstructured in solution', *Proceedings of the National Academy of Sciences of the United States of America*, 97(10), pp. 5657–5662.

Ostedgaard, L. S. *et al*. (2003) 'Effects of C-terminal deletions on cystic fibrosis transmembrane conductance regulator function in cystic fibrosis airway epithelia', *Proceedings of the National Academy of Sciences of the United States of America,* 100(4), pp. 1937–1942.

Ousingsawat, J. *et al*. (2009) 'Loss of TMEM16A causes a defect in epithelial Ca^{2+} -dependent chloride transport', *Journal of Biological Chemistry*, 284(42), pp. 28698–28703.

Pawel, B. R., de Chadarévian, J.-P. and Franco, M. E. (1997) 'The pathology of fibrosing colonopathy of cystic fibrosis: A study of 12 cases and review of the literature', *Human Pathology,* 28(4), pp. 395–399.

Payne, J. A. *et al*. (2003) 'Cation-chloride co-transporters in neuronal communication, development and trauma', Trends in Neurosciences, 26(4), pp. 199–206. doi: 10.1016/S0166-2236(03)00068-7.

Pedemonte, N. and Galietta, L. J. V. (2014) 'Structure and Function of TMEM16 Proteins (Anoctamins)', *Physiological Reviews*, 94(2), pp. 419–459.

Phuan, P. W. *et al*. (2019) ‘Nanomolar-potency “co-potentiator” therapy for cystic fibrosis caused by a defined subset of minimal function CFTR mutants’, *Scientific Reports*, 9(1), pp. 1–12.

Pind, S., Riordan, J. R. and Williams, D. B. (1994) ‘Participation of the endoplasmic reticulum chaperone calnexin (p88, IP90) in the biogenesis of the cystic fibrosis transmembrane conductance regulator’, Journal of Biological Chemistry, 269(17), pp. 12784–12788.

Plasschaert, L. W. *et al*. (2018) ‘A single-cell atlas of the airway epithelium reveals the CFTR-rich pulmonary ionocyte’, *Nature*, 560(7718), pp. 377–381.

Playford, R. J. (1997) ‘Trefoil peptides: What are they and what do they do?’, *Journal of the Royal College of Physicians of London,* 31(1), pp. 37–41.

de Poel, E., Lefferts, J. W. and Beekman, J. M. (2020) ‘Intestinal organoids for Cystic Fibrosis research’, *Journal of Cystic Fibrosis*, 19(1), pp. S60–S64.

Pons, G. *et al*. (2000) ‘French multicenter randomized double-blind placebo-controlled trial on nebulized amiloride in cystic fibrosis patients’, *Pediatric Pulmonology*, 30(1), pp. 25–31.

Pop, L. *et al*. (2008) ‘Cystic Fibrosis and Coeliac Disease’, *Archives of Disease in Childhood*, 93(Suppl 2),

Potten, C. S., Kovacs, L. and Hamilton, E. (1974) ‘Labelling Studies on Mouse Skin and Intestine’, *Cell Proliferation*, 7(3), pp. 271–283.

Praetorius, J. *et al*. (2000) ‘NHE1, NHE2, and NHE3 contribute to regulation of intracellular pH in murine duodenal epithelial cells’, *American Journal of Physiology - Gastrointestinal and Liver Physiology*, 278(2 41-2), pp. 197–206.

Prassas, I. and Diamandis, E. P. (2008) ‘Novel therapeutic applications of cardiac glycosides’, *Nature Reviews Drug Discovery*, 7(11), pp. 926–935.

Rahmani, S. *et al*. (2019) ‘Intestinal organoids: A new paradigm for engineering intestinal epithelium in vitro’, *Biomaterials*, 194(August 2018), pp. 195–214.

Rainaldi, G., Boe, A. and Gessani, S. (2016) ‘3D (Three-Dimensional) Caco-2 Spheroids: Optimized in vitro Protocols to Favor Their Differentiation Process and to Analyze Their Cell Growth Behavior’, *Journal of Pharmacy and Pharmacology*, 4(7), pp. 341–350.

Ramsey, B. W. *et al*. (2011) ‘A CFTR potentiator in patients with cystic fibrosis and the G551D mutation’, *New England Journal of Medicine*, 365(18), pp. 1663–1672.

Randak, C. *et al.* (1999) ‘Inhibition of ATPase, GTPase and adenylate kinase activities of the second nucleotide-binding fold of the cystic fibrosis transmembrane conductance regulator by genistein’, *Biochemical Journal*, 340(1), pp. 227–235.

Ratjen, F. *et al*. (2015) ‘Cystic fibrosis’, *Nature Reviews Disease Primers,* 1(1), p. 15010.

Ratjen, F. *et al*. (2017) 'Efficacy and safety of lumacaftor and ivacaftor in patients aged 6–11 years with cystic fibrosis homozygous for F508del-CFTR : a randomised, placebo-controlled phase 3 trial', *The Lancet Respiratory Medicine*, 5(7), pp. 557–567.

Rector, F. C., Carter, N. W. and Seldin, D. W. (1998) 'The mechanism of bicarbonate reabsorption in the proximal and distal tubules of the kidney. 1965.', *Journal of the American Society of Nephrology,* 9(6), pp. 1134–1145.

Rehman, T. *et al.* (2020) 'TNF and IL-17 alkalinize airway surface liquid through CFTR and pendrin', *American Journal of Physiology - Cell Physiology*, 319(2), pp. C331–C344.

Reihill, J. A. *et al*. (2016) 'Inhibition of Protease–Epithelial Sodium Channel Signaling Improves Mucociliary Function in Cystic Fibrosis Airways', *American Journal of Respiratory and Critical Care Medicine*, 194(6), pp. 701–710.

Reynolds, A. *et al*. (2007) 'Dynamic and differential regulation of NKCC1 by calcium and cAMP in the native human colonic epithelium', *Journal of Physiology*, 582(2), pp. 507–524.

Rich, D. P. *et al*. (1990) 'Expression of cystic fibrosis transmembrane conductance regulator corrects defective chloride channel regulation in cystic fibrosis airway epithelial cells', *Nature*, 347(6291), pp. 358–363..

Riordan, J. R. *et al*. (1989) 'Identification of the cystic fibrosis gene: Cloning and characterization of complementary DNA', *Science*, 245(4922), pp. 1066–1073.

Riordan, J. R. (2008) 'CFTR Function and Prospects for Therapy', *Annual Review of Biochemistry,* 77(1), pp. 701–726.

Roberts, M. *et al*. (1991) 'Stimulation of Sodium Transport by Duramycin in Cultured Human Colonic Epithelium', The Journal of pharmacology and experimental Treatments, 259(3), pp. 1050–1058.

Rommens, J. M. *et al*. (1989) 'Identification of the cystic fibrosis gene: Chromosome walking and jumping', *Science*, 245(4922), pp. 1059-65.

Rowe, S. M. *et al*. (2017) 'Tezacaftor–Ivacaftor in Residual-Function Heterozygotes with Cystic Fibrosis', *New England Journal of Medicine*, 377(21), pp. 2024–2035.

Rowe, S. M., Miller, S. and Sorscher, E. J. (2005) 'Cystic Fibrosis', New England Journal of Medicine, 352(19), pp. 1992–2001. doi: 10.1056/NEJMra043184.

Sabharwal, S. (2016) 'Gastrointestinal manifestations of cystic fibrosis', *Gastroenterology and Hepatology,* 12(1), pp. 43–47.

Saint-Criq, V. and Gray, M. A. (2017) 'Role of CFTR in epithelial physiology', *Cellular and Molecular Life Sciences*, 74(1), pp. 93–115.

MK Al Salmani, E Sondo, C Balut, DN Sheppard, AK Singh, N Pedemonte. Molecular Physiology and Pharmacology of the Cystic Fibrosis Transmembrane Conductance

Regulator. In: *Studies of Epithelial Transporters and Ion Channels, Physiology in Health and Disease*, Second Edition, Eds KL Hamilton and DC Devor, American Physiological Society / Springer-Verlag. (2020) Volume 3, Chapter 16, pages 605-670, ISBN#978-3-030-55453-8; doi.org/10.1007/978-3-030-55454-5_16.

Sambuy, Y. *et al*. (2005) 'The Caco-2 cell line as a model of the intestinal barrier: influence of cell and culture-related factors on Caco-2 cell functional characteristics', *Cell Biology and Toxicology*, 21(1), pp. 1–26.

Samy, K. E. *et al*. (2019) 'Human intestinal spheroids cultured using Sacrificial Micromolding as a model system for studying drug transport', *Scientific Reports,* 9(1), pp. 1–12.

Sato, T. *et al*. (2009) 'Single Lgr5 stem cells build crypt-villus structures in vitro without a mesenchymal niche', *Nature*, 459(7244), pp. 262–265.

Sato, T. *et al*. (2011) 'Long-term Expansion of Epithelial Organoids From Human Colon, Adenoma, Adenocarcinoma, and Barrett's Epithelium', *Gastroenterology*, 141(5), pp. 1762–1772.

Schaar, S. *et al*. (2004) 'Caco-2 Cells on Snapwell ® Membranes and the Ussing Chamber System as a Model for Cadmium Transport In Vitro', *Instrumentation Science & Technology*, 32(6), pp. 627–639.

Schatzmann, H. and Räss, B. (1967) 'Inhibition of the active Na-K-transport and Na-K-activated membrane ATP-ase of erythrocyte stroma by ouabain', *Angewandte Chemie International Edition,* 65(1), pp. 47–9.

Schroeder, B. C. *et al*. (2000) 'A constitutively open potassium channel formed by KCNQ1 and KCNE3', *Nature*, 403(6766), pp. 196–199.

Schroeder, B. C. *et al*. (2008) 'Expression Cloning of TMEM16A as a Calcium-Activated Chloride Channel Subunit', *Cell,* 134(6), pp. 1019–1029.

Schwank, G. *et al*. (2013) 'Functional Repair of CFTR by CRISPR/Cas9 in Intestinal Stem Cell Organoids of Cystic Fibrosis Patients', *Cell Stem Cell*, 13(6), pp. 653–658.

Scott-Ward, T. S. *et al.* (2004) 'Direct block of the cystic fibrosis transmembrane conductance regulator Cl (-) channel by niflumic acid', *Molecular Membrane Biology*, 21(1), pp. 27-38.

Seidler, U. *et al*. (2009) 'The role of the NHERF family of PDZ scaffolding proteins in the regulation of salt and water transport: Lessons learned from knockout mice', *Annals of the New York Academy of Sciences*, 1165, pp. 249–260.

Sekine, S. *et al*. (2002) 'Target disruption of the mutant β-catenin gene in colon cancer cell line HCT116: Preservation of its malignant phenotype', *Oncogene*, 21(38), pp. 5906–5911.

Serohijos, A. W. R. *et al*. (2008) 'Phenylalanine-508 mediates a cytoplasmic-membrane domain contact in the CFTR 3D structure crucial to assembly and channel function', *Proceedings of the National Academy of Sciences of the United States of America,* 105(9), pp. 3256–3261.

Shao, S. *et al*. (2021) 'Renal Natriuretic Peptide Receptor-C Deficiency Attenuates NaCl Cotransporter Activity in Angiotensin II-Induced Hypertension', *Hypertension*, (March), pp. 868–881.

Shah, V. S. *et al.* (2016) 'Airway acidification initiates host defense abnormalities in cystic fibrosis mice', *Science*, 351(6272), pp. 503–507.

Shen, C.-H. (2019) 'Quantification and Analysis of Proteins', *Diagnostic Molecular Biology*, pp. 187–214.

Sheppard, D. N. *et al*. (1993) 'Mutations in CFTR associated with mild-disease-form Cl^- channels with altered pore properties', *Nature,* 362(6416), pp. 160–164.

Sheppard, D. N. *et al*. (1994) 'Expression of cystic fibrosis transmembrane conductance regulator in a model epithelium', *American Journal of Physiology-Lung Cellular and Molecular Physiology*, 266(4), pp. 405–413.

Sheppard, D. N. *et al*. (1995) 'Mechanism of dysfunction of two nucleotide binding domain mutations in cystic fibrosis transmembrane conductance regulator that are associated with pancreatic sufficiency.', *The EMBO Journal,* 14(5), pp. 876–883.

Sheppard, D. and Welsh, M. (1999) 'Structure and Function of the CFTR Chloride Channel', *Physiological Reviews*, 79(1), pp. S23–S45.

Shirazi-Beechey, S. P. *et al*. (2011) 'Glucose sensing and signalling; regulation of intestinal glucose transport', *Proceedings of the Nutrition Society*, 70(2), pp. 185–193.

Short, D. B. *et al*. (1998) 'An apical PDZ protein anchors the cystic fibrosis transmembrane conductance regulator to the cytoskeleton', *Journal of Biological Chemistry*, (31), pp. 19797–19801.

Shoshani, T. *et al*. (1992) 'Association of a nonsense mutation (W1282X), the most common mutation in the Ashkenazi Jewish cystic fibrosis patients in Israel, with presentation of severe disease', *American Journal of Human Genetics,* 50(1), pp. 222–228.

Simon-Assmann, P. *et al*. (2007) 'In vitro models of intestinal epithelial cell differentiation', *Cell Biology and Toxicology,* 23(4), pp. 241–256.

Singh, V. *et al*. (2014) 'Translating molecular physiology of intestinal transport into pharmacologic treatment of diarrhea: Stimulation of Na^+ absorption', *Clinical Gastroenterology and Hepatology*, 12(1), pp. 27–31.

Skou, J. C. (1957) 'The influence of some cations on an adenosine triphosphatase from peripheral nerves', *Biochimica et Biophysica Acta,* 23(C), pp. 394–401.

Smith, S. *et al*. (2020) ‘How can we relieve gastrointestinal symptoms in people with cystic fibrosis? An international qualitative survey’, *BMJ Open Respiratory Research*, 7(1).

Smith, S. *et al*. (2001) ‘CFTR: Covalent and noncovalent modification suggests a role for fixed charges in anion conduction’, *Journal of General Physiology*, 118(4), pp. 407–431.

Smyth, R. L. *et al*. (1994) ‘Strictures of ascending colon in cystic fibrosis and high-strength pancreatic enzymes’, *The Lancet*, 343(8889), pp. 85–86.

Snoeck, V., Goddeeris, B. and Cox, E. (2005) ‘The role of enterocytes in the intestinal barrier function and antigen uptake’, *Microbes and Infection*, 7(7–8), pp. 997–1004.

Sonawane, N. D. and Verkman, A. S. (2008) ‘Thiazolidinone CFTR inhibitors with improved water solubility identified by structure-activity analysis’, *Bioorganic and Medicinal Chemistry*, 16(17), pp. 8187–8195.

Song, Y. *et al*. (2006) ‘Hyperacidity of secreted fluid from submucosal glands in early cystic fibrosis.’, *American Journal of Physiology. Cell Physiology*, 290(3), pp. 741–749.

Stallings, V. A. *et al*. (2008) ‘Evidence-Based Practice Recommendations for Nutrition-Related Management of Children and Adults with Cystic Fibrosis and Pancreatic Insufficiency: Results of a Systematic Review’, *Journal of the American Dietetic Association*, 108(5), pp. 832–839.

Steinbrecher, K. A. (2014) ‘The multiple roles of guanylate cyclase C, a heat stable enterotoxin receptor’, *Current Opinion in Gastroenterology*, 30(1), pp. 1–6.

Stevens, J. C. *et al*. (1998) ‘Pancreatic Enzyme Supplementation in Cystic Fibrosis Patients Before and After Fibrosing Colonopathy’, *Journal of Pediatric Gastroenterology & Nutrition*, 26(1), pp. 80–84.

Strong, T. V., Boehm, K. and Collins, F. S. (1994) ‘Localization of cystic fibrosis transmembrane conductance regulator mRNA in the human gastrointestinal tract by in situ hybridization’, *Journal of Clinical Investigation*, 93(1), pp. 347–354.

Stutts, M. *et al*. (1995) ‘CFTR as a cAMP-dependent regulator of sodium channels’, *Science*, 269(5225), pp. 847–850.

Subhi, R. *et al*. (2014) ‘Distal intestinal obstruction syndrome in cystic fibrosis: presentation, outcome and management in a tertiary hospital (2007-2012)’, *ANZ Journal of Surgery*, 84(10), pp. 740–744.

Sun, F., Hug, M. J., Lewarchik, C. M., *et al*. (2000) ‘E3KARP mediates the association of ezrin and protein kinase A with the cystic fibrosis transmembrane conductance regulator in airway cells’, *Journal of Biological Chemistry*, 275(38), pp. 29539–29546.

Sun, F., Hug, M. J., Bradbury, N. A., *et al*. (2000) ‘Protein kinase A associates with cystic fibrosis transmembrane conductance regulator via an interaction with ezrin’, *Journal of Biological Chemistry*, 275(19), pp. 14360–14366.

Sun, H. *et al*. (2008) 'The Caco-2 cell monolayer: Usefulness and limitations', *Expert Opinion on Drug Metabolism and Toxicology*, 4(4), pp. 395–411.

Taddei, A. *et al*. (2004) 'Altered channel gating mechanism for CFTR inhibition by a high-affinity thiazolidinone blocker', *FEBS Letters*, 558(1–3), pp. 52–56.

Takahashi, T. and Shiraishi, A. (2020) 'Stem Cell Signaling Pathways in the Small Intestine', *International Journal of Molecular Sciences*, 21(6), p. 2032.

Takeda, N. *et al*. (2011) 'Interconversion between intestinal stem cell populations in distinct niches', *Science*, 334(6061), pp. 1420–1424.

Tan, Q. *et al*. (2021) 'Inhibition of Na^+/H^+ exchanger isoform 3 improves gut fluidity and alkalinity in cystic fibrosis transmembrane conductance regulator-deficient and F508del mutant mice', *British Journal of Pharmacology,* 178(5), pp. 1018–1036. doi: 10.1111/bph.15323.

Tang, L. *et al*. (2017) 'Bumetanide increases Cl^- dependent short-circuit current in late distal colon: Evidence for the presence of active electrogenic Cl^- absorption', *PLoS ONE*, 12(2), pp. 1–23.

Taylor-Cousar, J. L. *et al*. (2017) 'Tezacaftor–Ivacaftor in Patients with Cystic Fibrosis Homozygous for Phe508del', *New England Journal of Medicine*, 377(21), pp. 2013–2023.

Taylor, C. J. *et al*. (1987) 'Absence of Secretory response in Jejunal Biopsy Samples from Children with Cystic Fibrosis', *The Lancet*, 330(8550), pp. 107–108.

Thorne, C. A. *et al*. (2018) 'Enteroid Monolayers Reveal an Autonomous WNT and BMP Circuit Controlling Intestinal Epithelial Growth and Organization', *Developmental Cell,* 44(5), pp. 624-633.

Tien, X. Y. *et al*. (1994) 'Activation of the cystic fibrosis transmembrane conductance regulator by cGMP in the human colonic cancer cell line, Caco-2', *Journal of Biological Chemistry*, 269(1), pp. 51–54.

Ting, H.-A. and von Moltke, J. (2019) 'The Immune Function of Tuft Cells at Gut Mucosal Surfaces and Beyond', *The Journal of Immunology*, 202(5), pp. 1321–1329.

Tom, B. H. *et al*. (1976) 'Human colonic adenocarcinoma cells', *In Vitro*, 12(3), pp. 180–191.

Travis, S. M., Berger, H. A. and Welsh, M. J. (1997) 'Protein phosphatase 2C dephosphorylates and inactivates cystic fibrosis transmembrane conductance regulator', *Proceedings of the National Academy of Sciences of the United States of America*, 94(20), pp. 11055–11060.

Turner, J. R. *et al*. (2000) 'Transepithelial resistance can be regulated by the intestinal brush-border Na^+/H^+ exchanger NHE3', *American Journal of Physiology - Cell Physiology*, 279(6 48-6), pp. 1918–1924.

Ussing, H. and Zerahn, K. (1951) ‘Active Transport of Sodium as the Source of Electric Current in the Short-circuited Isolated Frog Skin.’, *Acta Physiologica Scandinavica,* 23(2–3), pp. 110–127.

Vaandrager, A. B. *et al*. (1997) ‘cGMP stimulation of cystic fibrosis transmembrane conductance regulator Cl^- channels co-expressed with cGMP-dependent protein kinase type II but not type Ib’, *Journal of Biological Chemistry*, 272(7), pp. 4195–4200.

Vachel, L. and Muallem, S. (2019) ‘CFTR is not a gluten lover either’, *The EMBO Journal*, 38(2), pp. 2018–2020.

Valentine, C. D. *et al*. (2012) ‘Reduced PDZ interactions of rescued ΔF508CFTR increases its cell surface mobility’, *Journal of Biological Chemistry*, 287(52), pp. 43630–43638.

Veit, G. *et al*. (2016) ‘From CFTR biology toward combinatorial pharmacotherapy: Expanded classification of cystic fibrosis mutations’, *Molecular Biology of the Cell*, 27(3), pp. 424–433.

Vergani, P. *et al*. (2005) ‘CFTR channel opening by ATP-driven tight dimerization of its nucleotide-binding domains’, *Nature*, 433(7028), pp. 876–880.

Villella, V. R. *et al*. (2019) ‘A pathogenic role for cystic fibrosis transmembrane conductance regulator in celiac disease’, *The EMBO Journal*, 38(2), pp. 1–22.

Vincan, E. *et al*. (2007) ‘Frizzled-7 dictates three-dimensional organization of colorectal cancer cell carcinoids’, *Oncogene*, 26(16), pp. 2340–2352.

Vonk, A. M. *et al*. (2020) ‘Protocol for Application, Standardization and Validation of the Forskolin-Induced Swelling Assay in Cystic Fibrosis Human Colon Organoids’, *STAR Protocols*, 1(1), p. 100019.

Wang, D. *et al*. (2021) ‘Effects of Guava (Psidium guajava L.) Leaf Extract on the Metabolomics of Serum and Feces in Weaned Piglets Challenged by Escherichia coli’, *Frontiers in Veterinary Science,* 8(May), pp. 1–13.

Wang, F. *et al*. (1998) ‘Actions of Genistein on Cystic Fibrosis Transmembrane Conductance Regulator Channel Gating. Evidence for two binding sites with opposite effects’, *The Journal of General Physiology*, 111(3), pp. 477–490.

Wang, W. *et al*. (2014) ‘Relative contribution of different transmembrane segments to the CFTR chloride channel pore’, *Pflugers Archiv European Journal of Physiology*, 466(3), pp. 477–490.

Wang, Y. *et al*. (2014) ‘Understanding how cystic fibrosis mutations disrupt CFTR function: From single molecules to animal models’, *International Journal of Biochemistry and Cell Biology*. Elsevier Ltd, 52, pp. 47–57.

Watson, M. S. *et al*. (2004) 'Cystic fibrosis population carrier screening: 2004 Revision of American College of Medical Genetics mutation panel', *Genetics in Medicine*, 6(5), pp. 387–391.

Wei, L. *et al*. (2001) 'The C-terminal part of the R-domain, but not the PDZ binding motif, of CFTR is involved in interaction with Ca^{2+}-activated Cl^- channels', *Pflugers Archiv - European Journal of Physiology,* 442(2), pp. 280–285.

Weinman, E. J., Steplock, D. and Shenolikar, S. (2001) 'Acute regulation of NHE3 by protein kinase A requires a multiprotein signal complex', *Kidney International*, 60(2), pp. 450–454.

Welsh, M. J. and Smith, A. E. (1993) 'Molecular mechanisms of CFTR chloride channel dysfunction in cystic fibrosis', *Cell*, 73(7), pp. 1251–1254.

White, M. M. and Aylwin, M. (1990) 'Niflumic and flufenamic acids are potent reversible blockers of Ca^{2+}-activated Cl^- channels in Xenopus oocytes', *Molecular Pharmacology*, 37(5), pp. 720–724.

Whitehead, R. H. *et al*. (1987) 'A New Colon Carcinoma Cell Line (LIM1863) That Grows as Organoids with Spontaneous Differentiation into Crypt-like Structures in Vitro', *Cancer Research*, 47, pp. 2683–2689.

Widdicombe, J. H., Welsh, M. J. and Finkbeiner, W. E. (1985) 'Cystic fibrosis decreases the apical membrane chloride permeability of monolayers cultured from cells of tracheal epithelium', *Proceedings of the National Academy of Sciences of the United States of America*, 82(18), pp. 6167–6171.

Wilschanski, M. and Novak, I. (2013) 'The cystic fibrosis of exocrine pancreas', *Cold Spring Harbor Perspectives in Medicine*, 3(5), pp. 1–17.

Winter, M. C. and Welsh, M. J. (1997) 'Stimulation of CFTR activity by its phosphorylated R domain', *Nature*, 389(6648), pp. 294–296.

Wulff, H. and Castle, N. A. (2010) 'Therapeutic potential of KCa3.1 blockers: Recent advances and promising trends', *Expert Review of Clinical Pharmacology*, 3(3), pp. 385–396.

Xu, P. *et al*. (2018) 'Current knowledge on the nucleotide agonists for the P2Y2 receptor', *Bioorganic and Medicinal Chemistry.* Elsevier Ltd, 26(2), pp. 366–375.

Yang, G. *et al*. (2016) 'Physiology of Intestinal Absorption and Secretion', *Best Practice & Research Clinical Gastroenterology,* 30(2), pp. 145–159.

Yang, Y. *et al*. (1993) 'The common variant of cystic fibrosis transmembrane conductance regulator is recognized by hsp70 and degraded in a pre-Golgi nonlysosomal compartment', *Proceedings of the National Academy of Sciences of the United States of America*, 90(20), pp. 9480–9484.

Yang, Y. D. *et al*. (2008) 'TMEM16A confers receptor-activated calcium-dependent chloride conductance', *Nature*, 455(7217), pp. 1210–1215.

Yin, J. *et al.* (2018) 'Molecular Basis and Differentiation-Associated Alterations of Anion Secretion in Human Duodenal Enteroid Monolayers', *Cellular and Molecular Gastroenterology and Hepatology*, 5(4), pp. 591–609.

Yun, C. H. C. *et al*. (1997) 'cAMP-mediated inhibition of the epithelial brush border Na^+/H^+ exchanger, NHE3, requires an associated regulatory protein', *Proceedings of the National Academy of Sciences of the United States of America*, 94(7), pp. 3010–3015.

Zabner, J. *et al*. (1993) 'Adenovirus-mediated gene transfer transiently corrects the chloride transport defect in nasal epithelia of patients with cystic fibrosis', *Cell*, 75(2), pp. 207–216.

Zabner, J. *et al*. (2003) 'Development of cystic fibrosis and noncystic fibrosis airway cell lines', *American Journal of Physiology - Lung Cellular and Molecular Physiology*, 284(5 28-5), pp. 844–854.

Zachos, N. C., Kovbasnjuk, O. and Donowitz, M. (2009) 'Regulation of intestinal electroneutral sodium absorption and the brush border Na^+/H^+ exchanger by intracellular calcium', *Annals of the New York Academy of Sciences,* 1165, pp. 240–248.

Zhang, Z. and Chen, J. (2016) 'Atomic Structure of the Cystic Fibrosis Transmembrane Conductance Regulator', *Cell. Elsevier*, 167(6), pp. 1586-1597.

Zhang, Z., Liu, F. and Chen, J. (2018) 'Molecular structure of the ATP-bound, phosphorylated human CFTR', *Proceedings of the National Academy of Sciences*, 115(50), pp. 12757–12762.

Zhao, H. *et al*. (1999) 'Acute inhibition of Na/H exchanger NHE-3 by cAMP: Role of protein kinase A and NHE-3 phosphoserines 552 and 605', *Journal of Biological Chemistry*, 274(7), pp. 3978–3987.

Zhou, J. *et al*. (2010) 'Regulation of conductance by the number of fixed positive charges in the intracellular vestibule of the CFTR chloride channel pore', *Journal of General Physiology*, 135(3), pp. 229–245.

Zhou, Q. and Melton, D. A. (2018) 'Pancreas regeneration', *Nature*, 557(7705), pp. 351–358.

Zhu, J. X. *et al*. (2005) 'Activation of apical CFTR and basolateral Ca^{2+}-activated K^+ channels by tetramethylpyrazine in Caco-2 cell line', *European Journal of Pharmacology*, 510(3), pp. 187–195.

Zielenski, J. (1995) 'Cystic Fibrosis: Genotypic and Phenotypic Variations', *Annual Review of Genetics*, 29(1), pp. 777–807.

Zihni, C. *et al*. (2016) 'Tight junctions: From simple barriers to multifunctional molecular gates', *Nature Reviews Molecular Cell Biology*, 17(9), pp. 564–580.

Zomer-Van Ommen, D. D. *et al*. (2016) ‘Functional characterization of cholera toxin inhibitors using human intestinal organoids’, *Journal of Medicinal Chemistry*, 59(14), pp. 6968–6972.